

Designing Fibrin Microthread Scaffolds for Skeletal Muscle Regeneration

A Dissertation
Submitted to the Faculty of

WORCESTER POLYTECHNIC INSTITUTE


in partial fulfillment of the requirements for the
Degree of Doctor of Philosophy in
Biomedical Engineering


December 3rd, 2014


By

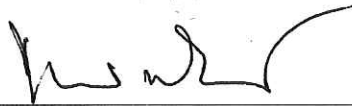

Jonathan Mark Grasman

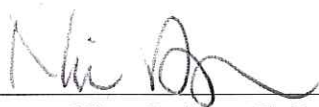
Approved by:

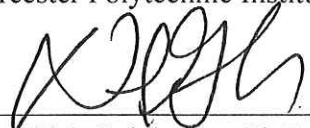

George D. Pins, Ph.D.
Associate Professor, Advisor
Biomedical Engineering
Worcester Polytechnic Institute


Raymond L. Page, Ph.D.
Professor of Practice, Co-Advisor
Biomedical Engineering
Worcester Polytechnic Institute


Marsha W. Rolle, Ph.D.
Associate Professor
Biomedical Engineering
Worcester Polytechnic Institute


Tanja Dominko, D.V.M., Ph.D.
Associate Professor
Biology and Biotechnology
Worcester Polytechnic Institute


Nima Rahbar, Ph.D.
Assistant Professor
Civil and Environmental Engineering
Worcester Polytechnic Institute


David J. Goldhamer, Ph.D.
Professor
Molecular and Cell Biology
University of Connecticut

Acknowledgements

First and foremost, I would like to thank my advisor, George Pins, Ph.D., for all of his guidance and support over the years. By allowing me to work in the lab and giving me the freedom to explore new ideas, he has provided me with tremendous opportunities to perform high-impact research, cultivate my own mentoring style, develop some much needed writing skills, and have fun. You have been a fantastic mentor; thank you for all of your advice.

In addition to George, I owe a great deal of gratitude to my co-advisor, Ray Page, Ph.D. for teaching me how to perform microsurgery, and for always having time to talk about data or discuss new experiments or ideas. Your guidance and assistance have been invaluable.

To my dissertation committee: Tanja Dominko D.V.M., Ph.D., Marsha Rolle, Ph.D., Nima Rahbar, Ph.D., and David Goldhamer, Ph.D., your guidance and encouragement have played a pivotal role in my development as a scientist. Thank you for all of the time and feedback that you have given me.

I would also like to thank the rest of the faculty of the Biomedical Engineering Department at WPI, as well as the lab staff at Gateway Park. You have all spent time providing me knowledge and technical assistance, and your assistance has been instrumental.

Beyond the help of advisors, committee members, faculty, and staff, there are countless people I would like to thank who have worked “in the trenches” with me. Special thanks to my “lab spouse”, Zoë Reidinger, for her advice, support, and costume ideas. To my lab mates in Pins lab, past and present, thank you so much for your support, feedback, and unofficial meetings. To my fellow graduated students in BME (and Dominko lab), I took full advantage of your varying skill sets and you were all gracious enough to help me. A big thank you to all of the undergraduate volunteers who spent so much time assisting me; without you I would still be working to complete this project.

Last but certainly not least, I could not be here today without my family and friends. Special thanks to my mother and father, Susan and Mark, for your unfailing support and love throughout the years. To Michael Chrin, thank you so much for supporting and putting up with me throughout this journey. Thank you as well to all of my friends from Pitt and home. You have kept me going through the good and the bad, and your support has been appreciated.

I have learned so much during my journey through graduate school, and words cannot begin to express how grateful I am to all of you for your guidance, support, and advice throughout the years. Thank you.

Table of Contents

| | Page |
|---|-------------|
| Acknowledgements | i |
| Table of Contents | ii |
| Table of Figures | vii |
| Table of Tables | ix |
| Abbreviations | x |
| Abstract | xii |
| Chapter 1: Overview | 1 |
| 1.1 Introduction | 1 |
| 1.2 Overall Goal and Hypothesis | 3 |
| 1.3 Specific Aim 1: Develop Microthreads with Tunable Structural Properties While Maintaining Cellular Viability | 3 |
| 1.4 Specific Aim 2: Quantify the Effects of Incorporating HGF onto Fibrin Microthreads to Increase Satellite Cell Recruitment | 5 |
| 1.5 Specific Aim 3: Assess Microthreads' Enhancement of Skeletal Muscle Regeneration <i>In Vivo</i> | 6 |
| 1.6 References | 7 |
| Chapter 2: Background | 9 |
| 2.1 Clinical Need for Scaffolds to Regenerate Skeletal Muscle | 9 |
| 2.2 Skeletal Muscle Anatomy | 10 |
| 2.3 Native Regenerative Pathway of Skeletal Muscle Repair | 11 |
| 2.3.1 Destruction/Inflammatory Phase | 13 |
| 2.3.2 Repair Phase | 13 |
| 2.3.3 Remodeling Phase | 15 |
| 2.3.4 Cell Types Involved in Skeletal Muscle Regeneration | 16 |
| 2.4 Current Tissue Engineering Strategies and Limitations | 17 |
| 2.4.1 <i>In Vitro</i> Skeletal Muscle Development | 18 |
| 2.4.2 Biomaterials for Skeletal Muscle Regeneration | 19 |
| 2.4.2.1 Synthetic Polymers | 19 |
| 2.4.2.2 Natural Polymers | 20 |
| 2.4.2.3 Decellularized ECM | 23 |
| 2.4.3 Limitations | 24 |
| 2.5 Microthreads for Use in Skeletal Muscle Regeneration | 25 |
| 2.5.1 Tuning Mechanical Cues | 26 |

| | | |
|--|---|-----------|
| 2.5.2 | Tuning Biochemical Cues | 27 |
| 2.5.3 | Tuning Cellular Microniches | 28 |
| 2.6 | Conclusions and Future Directions | 29 |
| 2.7 | References | 31 |
| Chapter 3: Crosslinking Strategies Facilitate Tunable Structural Properties of Fibrin Microthreads | | 41 |
| 3.1 | Introduction | 41 |
| 3.2 | Materials and Methods | 43 |
| 3.2.1 | Fibrin Microthread Preparation | 43 |
| 3.2.1.1 | Microthread Extrusion | 43 |
| 3.2.1.2 | EDC Crosslinking Procedure | 44 |
| 3.2.2 | Mechanical Characterization of Crosslinked Microthreads | 44 |
| 3.2.3 | Structural Characterization of Crosslinked Microthreads | 45 |
| 3.2.3.1 | Microthread Swelling | 45 |
| 3.2.3.2 | Degradation Assay | 45 |
| 3.2.4 | Cell Culture | 46 |
| 3.2.5 | Cell Attachment Assay | 46 |
| 3.2.5.1 | Microthread Bundling and Seeding | 46 |
| 3.2.5.2 | Analysis of Cell Viability | 47 |
| 3.2.5.3 | Analysis of Cell Number | 47 |
| 3.2.6 | Statistical Analyses | 48 |
| 3.3 | Results | 48 |
| 3.3.1 | Crosslinking Enhances the Ultimate Tensile Strength of Fibrin Microthreads | 48 |
| 3.3.2 | Crosslinking Decreases the Swelling Ratio of Fibrin Microthreads | 51 |
| 3.3.3 | Crosslinking Increases Fibrin Microthread Resistance to Proteolytic Degradation | 52 |
| 3.3.4 | EDC Crosslinking Enhances Cell Attachment to Fibrin Microthreads | 54 |
| 3.4 | Discussion | 58 |
| 3.5 | Conclusions | 60 |
| 3.6 | Acknowledgements | 61 |
| 3.7 | References | 61 |
| Chapter 4: Static Axial Stretching Enhances the Mechanical Properties and Cellular Responses of Fibrin Microthreads | | 64 |
| 4.1 | Introduction | 64 |
| 4.2 | Materials and Methods | 66 |
| 4.2.1 | Fibrin Microthread Preparation | 66 |
| 4.2.1.1 | Microthread Extrusion | 66 |
| 4.2.1.2 | Static Axial Stretching with and without a Drying Phase | 66 |
| 4.2.2 | Mechanical Characterization of Stretched Fibrin Microthreads | 67 |
| 4.2.3 | Structural Characterization of Stretched Fibrin Microthreads | 69 |
| 4.2.3.1 | Scanning Electron Microscopy | 69 |
| 4.2.3.2 | Microthread Swelling | 69 |
| 4.2.3.3 | Transverse Strain and Poisson Ratio Calculations | 69 |

| | |
|--|-----------|
| 4.2.3.4 Degradation Assay | 69 |
| 4.2.4 Cell Culture | 70 |
| 4.2.5 Cell Attachment and Alignment Assay | 70 |
| 4.2.6 Statistical Analyses | 71 |
| 4.3 Results | 72 |
| 4.3.1 Stretching Increases the Ultimate Tensile Strength of Fibrin Microthreads | 72 |
| 4.3.2 Stretching Decreases the Diameters and Swelling Ratios of Fibrin Microthreads, but does not Affect Poisson's Ratio | 75 |
| 4.3.3 A Drying Phase is Necessary for the Increase in Ultimate Tensile Strength of Stretched Fibrin Microthreads | 77 |
| 4.3.4 Stretch Does Not Affect the Proteolytic Degradation of Fibrin Microthreads | 78 |
| 4.3.5 Stretch Enhances Cell Alignment along the Longitudinal Axis of Fibrin Microthreads | 79 |
| 4.4 Discussion | 80 |
| 4.5 Conclusions | 83 |
| 4.6 Acknowledgements | 84 |
| 4.7 References | 84 |
| Chapter 5: Adsorbed Hepatocyte Growth Factor on Crosslinked Fibrin Microthreads Enhances Cell Recruitment | 86 |
| 5.1 Introduction | 86 |
| 5.2 Materials and Methods | 88 |
| 5.2.1 Fibrin Microthread Preparation | 88 |
| 5.2.1.1 Microthread Extrusion | 88 |
| 5.2.1.2 Fibrin Microthread Crosslinking | 88 |
| 5.2.2 Adsorption of HGF to Microthreads | 89 |
| 5.2.3 Cell Culture | 89 |
| 5.2.4 Quantifying Release of HGF from Microthreads | 89 |
| 5.2.5 Two-dimensional Motogenic Response from HGF-loaded Microthreads | 90 |
| 5.2.6 Three-dimensional Motogenic Outgrowth from HGF-loaded Microthreads | 91 |
| 5.2.7 Statistical Analyses | 93 |
| 5.3 Results | 93 |
| 5.3.1 Adsorbed HGF is Rapidly Released from Fibrin Microthreads | 93 |
| 5.3.2 HGF Released from Fibrin Microthreads is a Motogenic Factor for Myoblasts | 95 |
| 5.3.3 HGF Adsorbed onto Fibrin Microthreads Enhances Myoblast Outgrowth | 96 |
| 5.3.4 Fibrin Microthreads Enhance Myoblast Proliferation | 97 |
| 5.4 Discussion | 99 |
| 5.5 Conclusions | 102 |
| 5.6 Acknowledgements | 103 |
| 5.7 References | 103 |

| | |
|--|-----|
| Chapter 6: Hepatocyte Growth Factor Adsorbed onto EDC Crosslinked Microthreads Restores Mechanical Function in Mouse Model of VML | 106 |
| 6.1 Introduction | 106 |
| 6.2 Materials and Methods | 108 |
| 6.2.1 Fibrin Microthread Preparation | 108 |
| 6.2.1.1 Microthread Extrusion | 108 |
| 6.2.1.2 Fibrin Microthread Crosslinking | 109 |
| 6.2.1.3 Adsorption of HGF to Microthreads | 109 |
| 6.2.2 Animals and Surgical Procedures | 110 |
| 6.2.3 Histological and Immunohistochemical Analysis | 111 |
| 6.2.3.1 Estimation of Wound Size | 113 |
| 6.2.3.2 Collagen Quantification | 113 |
| 6.2.4 Contractile Force Measurements | 114 |
| 6.2.5 Statistical Analyses | 115 |
| 6.3 Results | 115 |
| 6.3.1 Gross Morphology of No Intervention and Fibrin Gel Implants Show Loss of Muscle Volume | 115 |
| 6.3.2 Fourteen Days Post-Injury, Microthread Implants Support Myoblast Infiltration | 117 |
| 6.3.3 Sixty Days Post-Injury, EDCn-HGF Microthreads Support Robust Regeneration of Muscular Tissue | 120 |
| 6.3.4 Microthread Implants Reduce the Size of the Defect Site, but do not Affect Collagen Deposition | 123 |
| 6.3.5 Crosslinked Microthreads Enhance Recruitment of Satellite Cells | 124 |
| 6.3.6 HGF Delivery Promotes Increased Number of Myogenin Positive Nuclei | 126 |
| 6.3.7 Microthread Implant Groups Support Early Angiogenesis in VML Defects | 129 |
| 6.3.8 EDCn-HGF Microthreads Restore Mechanical Function of TA Muscles after VML Injuries | 132 |
| 6.4 Discussion | 135 |
| 6.5 Conclusions | 139 |
| 6.6 Acknowledgements | 139 |
| 6.7 References | 140 |

| | |
|---|-----|
| Chapter 7: Conclusions and Future Work | 143 |
| 7.1 Overview | 143 |
| 7.2 Results and Conclusions | 143 |
| 7.2.1 Specific Aim 1: Develop Microthreads with Tunable Structural Properties While Maintaining Cellular Viability | 143 |
| 7.2.2 Specific Aim 2: Quantify the Effects of Incorporating HGF onto Fibrin Microthreads to Increase Satellite Cell Recruitment | 146 |
| 7.2.3 Specific Aim 3: Assess Microthreads' Enhancement of Skeletal Muscle Regeneration <i>In Vivo</i> | 148 |
| 7.3 Future Work | 151 |
| 7.3.1 Complete Analysis of our <i>In Vivo</i> Model to Assess Long-Term Remodeling | 151 |
| 7.3.2 Next Generation of Fibrin Microthreads: Alternative Post-Modification Methods for Fibrin Microthreads | 153 |
| 7.3.3 Development of an <i>In Vitro</i> Model System for Skeletal Muscle Tissue | 156 |
| 7.4 Final Conclusions | 157 |
| 7.5 References | 158 |

Table of Figures

| | Page |
|--|-------------|
| Figure 2.1. Anatomy of skeletal muscle tissue | 10 |
| Figure 2.2. Schematic representation of native skeletal muscle regeneration | 12 |
| Figure 2.3. Schematic representation of repair of VML injuries | 16 |
| Figure 2.4. Our approach to skeletal muscle regeneration | 30 |
| Figure 3.1. Experimental configuration of the degradation assay | 46 |
| Figure 3.2. Mechanical properties of microthreads as a function of crosslinking time and buffer | 49 |
| Figure 3.3. Mechanical properties of microthreads crosslinked for 2 hours | 50 |
| Figure 3.4. Swelling ratio of microthreads crosslinked as a function of time and buffer pH | 51 |
| Figure 3.5. Representative images of microthreads in a degradation assay | 53 |
| Figure 3.6. Degradation profiles of microthreads treated with plasmin | 54 |
| Figure 3.7. Representative images of microthreads seeded with 10,000 C2C12 cells | 55 |
| Figure 3.8. Density of C2C12 cells seeded on fibrin microthreads for 1 or 3 days | 56 |
| Figure 3.9. Representative images of C2C12 cell viability on crosslinked microthreads | 57 |
| Figure 4.1. Flow-chart of the experimental setup for microthread fabrication with and without a drying phase | 67 |
| Figure 4.2. A representative stress-strain curve showing how each mechanical parameter was calculated in our MATLAB script | 68 |
| Figure 4.3. Method to determine nuclear alignment on fibrin microthreads | 71 |
| Figure 4.4. Characteristic stress-strain curves for fibrin microthreads fabricated with a drying phase | 72 |
| Figure 4.5. Mechanical properties of fibrin microthreads as a function of stretch percentage | 73 |
| Figure 4.6. Scanning electron micrographs of stretched fibrin microthreads | 75 |
| Figure 4.7. Structural properties of fibrin microthreads as a function of stretch | 76 |
| Figure 4.8. Comparison of the UTS of fibrin microthreads stretched with or without a drying phase. | 77 |
| Figure 4.9. Degradation profiles of microthreads static axially stretched with a drying phase | 78 |
| Figure 4.10. C2C12 myoblast alignment on static axially stretched fibrin microthreads | 79 |

| | |
|--|-----|
| Figure 5.1. Two dimensional assay developed to quantify the migration of myoblasts towards HGF-loaded microthreads | 91 |
| Figure 5.2. Myoblast outgrowth assay schematic | 92 |
| Figure 5.3. Representative images of microthreads loaded with FITC-labeled BSA | 94 |
| Figure 5.4. Percentage of C2C12 myoblasts expressing Ki67 stimulated from fibrin microthread C-SFM | 95 |
| Figure 5.5. Two-dimensional myoblast migration towards HGF-loaded microthreads | 96 |
| Figure 5.6. Cell outgrowth of C2C12 myoblasts from fibrin gels | 97 |
| Figure 5.7. Representative images of the outgrowth assay at day 4 with Ki67 staining | 98 |
| Figure 5.8. Percentage of Ki67 positive myoblasts in the migration front of the outgrowth assay at day 4 | 99 |
| Figure 6.1. Schematic representation of study performed in Chapter 6 | 111 |
| Figure 6.2. Cartoon denoting location of proximal and distal ends of TA muscle | 112 |
| Figure 6.3. Definition of VML defect dimensions | 113 |
| Figure 6.4. Collagen quantification method for VML defects | 114 |
| Figure 6.5. Gross morphology of TA muscle defects | 116 |
| Figure 6.6. Low magnification images of entire VML defect sites 14 days post-injury | 118 |
| Figure 6.7. Morphology of the distal end of VML defect sites 14 days post-injury | 119 |
| Figure 6.8. Low magnification images of entire VML defect sites 60 days post-injury | 121 |
| Figure 6.9. Morphology of the distal end of VML defect sites 60 days post-injury | 122 |
| Figure 6.10. Change in muscle defect length and width from 14 to 60 days post-injury | 123 |
| Figure 6.11. Percent collagen content within VML defect sites 60 days post-injury | 124 |
| Figure 6.12. IHC staining of Pax7 positive cells in VML defects 14 days post-injury | 125 |
| Figure 6.13. IHC staining of Pax7 positive cells in VML defects 60 days post-injury | 125 |
| Figure 6.14. Number of Pax7 positive cells in VML defects | 126 |
| Figure 6.15. IHC staining of myogenin positive nuclei in VML defects 14 days post-injury | 127 |
| Figure 6.16. IHC staining of myogenin positive nuclei in VML defects 60 days post-injury | 128 |
| Figure 6.17. Number of myogenin positive nuclei in VML defects | 128 |
| Figure 6.18. IHC staining of PECAM in VML defects 14 days post-injury | 130 |
| Figure 6.19. IHC staining of PECAM in VML defects 60 days post-injury | 131 |
| Figure 6.20. Number of blood vessels in VML defects | 131 |
| Figure 6.21. Isometric twitch force of TA muscles 60 days post-injury | 132 |
| Figure 6.22. Force at tetanic contraction of TA muscles 60 days post-injury | 133 |
| Figure 7.1. Scanning electron micrographs of EDC crosslinked microthreads | 154 |

Table of Tables

| | Page |
|---|-------------|
| Table 3.1. The mechanical and structural properties of EDC crosslinked fibrin microthreads | 50 |
| Table 4.1. Percent yield for fabrication of static axially stretched microthreads | 72 |
| Table 4.2. The mechanical and structural properties of fibrin microthreads stretched after a drying phase | 74 |
| Table 4.3. Strain hardening behavior of static uniaxially stretched fibrin microthreads | 74 |
| Table 4.4. The mechanical properties of fibrin microthreads stretched with and without a drying phase | 78 |
| Table 6.1. Animal weight at time of sacrifice | 115 |
| Table 6.2. Length and width of VML defects 14 and 60 days post-injury | 123 |
| Table 6.3. Summary of the functional characteristics of TA muscles before and immediately after the generation of a VML defect, and 60 days post-injury | 134 |

Abbreviations

2D – Two-dimensional
3D – Three dimensional
ANOVA – Analysis of variance
BSA – Bovine serum albumin
C-SFM – Conditioned serum free medium
DHT – Dehydrothermal
DI – Deionized
DMEM – Dulbecco’s Modified Eagle medium
DPBS – Dulbecco’s phosphate buffered saline
ECM – Extracellular matrix
EDC – 1-ethyl-3-(3-dimethylaminopropyl) carbodiimide
EDCa – Microthreads crosslinked in acidic buffer
EDCn – Microthreads crosslinked in neutral buffer
EDCn-HGF – HGF loaded EDCn microthreads
FBS – Fetal bovine serum
FGF2 – Fibroblast growth factor 2
FGF6 – Fibroblast growth factor 6
FITC – Fluorescein isothiocyanate
FTIR – Fourier transform infrared spectroscopy
HBS – HEPES buffered saline
HEPES – N-[2-Hydroxyethyl]piperazine-N’-[2-ethanesulfonic acid]
HGF – Hepatocyte growth factor
IGF1 – Insulin-like growth factor 1
IGF2 – Insulin-like growth factor 2
IGFBP – Insulin-like growth factor binding protein
IGFR1 – Insulin-like growth factor receptor-I
IHC – Immunohistochemistry
i.p. – intra-peritoneal
IQR – Inner quartile range
M-ECM – Skeletal muscle extracellular matrix
MES – 2-(N-morpholino)ethanesulfonic acid
MRI – Magnetic resonance imaging
MSC – Mesenchymal stem cell
MTM – Maximum tangent modulus
Myf5 – Myogenic factor 5

MyoD – Myogenic differentiation factor-1
NHS – N-hydroxysuccinimide
Pax7 – Paired box gene 7
PBS – Phosphate buffered saline
PCL – Poly(ϵ -caprolactone)
PDGFR α – Platelet derived growth factor α
PDMS – Polydimethylsiloxane
PECAM – Platelet endothelial cell adhesion molecule
PEG – polyethylene glycol
PGA – Poly(glycolic acid)
PLA – Poly(lactic acid)
PLLA/PLGA – Copolymer of poly(L-Lactic acid) and poly(L-glycolic acid)
RGB – Red, green, blue
RICE – Rest, ice, compression, and elevation
SAF – Strain at failure
SC – Satellite cell
SEM – Scanning electron microscope
SF – Silk fibroin
SFM – Serum free medium
SHO – SCID hairless outbred
SIS – Small intestine submucosa
SMU – Skeletal muscle unit
TA – *Tibialis anterior*
TBS – Tris buffered saline
UBM – Urinary bladder matrix
UNX – Uncrosslinked
UNXa – Uncrosslinked microthreads hydrated with acidic buffer
UNXdi – Uncrosslinked microthreads hydrated with distilled water
UNXn – Uncrosslinked microthreads hydrated with neutral buffer
UTS – Ultimate tensile strength
UV – Ultraviolet
VEGF – Vascular endothelial growth factor
VML – Volumetric muscle loss

Abstract

Volumetric muscle loss (VML) typically results from traumatic incidents; such as those presented from combat missions, where soft-tissue extremity injuries account for approximately 63% of diagnoses. These injuries lead to a devastating loss of function due to the complete destruction of large amounts of tissue and its native basement membrane, removing important biochemical cues such as hepatocyte growth factor (HGF), which initiates endogenous muscle regeneration by recruiting progenitor cells. Clinical strategies to treat these injuries consist of autologous tissue transfer techniques, requiring large amounts of healthy donor tissue and extensive surgical procedures that can result in donor site morbidity and limited functional recovery. As such, there is a clinical need for an off-the-shelf, bioactive scaffold that directs patient's cells to align and differentiate into muscle tissue *in situ*. In this thesis, we developed fibrin microthreads, scaffolds composed of aligned fibrin material that direct cell alignment along the longitudinal axis of the microthread structure, with specific structural and biochemical properties to recreate structural cues lost in VML injuries. We hypothesized that fibrin microthreads with an increased resistance to proteolytic degradation and loaded with HGF would enhance the functional, mechanical regeneration of skeletal muscle tissue in a VML injury. We developed a crosslinking strategy to increase fibrin microthread resistance to enzymatic degradation, and increased their tensile strength and stiffness two- to three-fold. This crosslinking strategy enhanced the adsorption of HGF, facilitated its rapid release from microthreads for 2 to 3 days, and increased the chemotactic response of myoblasts twofold in 2D and 3D assays. Finally, we implanted HGF-loaded, crosslinked (EDCn-HGF) microthreads into a mouse model of VML to evaluate tissue regeneration and functional recovery. Fourteen days post-injury, we observed more muscle ingrowth along EDCn-HGF microthreads than untreated controls, suggesting that released HGF recruited additional progenitor cells to the injury site. Sixty days post-injury, EDCn-HGF microthreads guided mature, organized muscle to replace the microthreads in the wound site. Further, EDCn-HGF microthreads restored the contractile mechanical strength of the tissue to pre-injured values. In summary, we designed fibrin microthreads that recapitulate regenerative cues lost in VML injuries and enhance the functional regeneration of skeletal muscle.

Chapter 1: Overview

1.1 INTRODUCTION

Skeletal muscle injuries typically result from traumatic incidents, such as combat injuries, where soft-tissue extremity injuries account for 63% of diagnoses.^{1,2} Additionally, about 4.5 million reconstructive surgical procedures are performed annually as a result of car accidents, cancer ablation, or cosmetic procedures.^{3,4} These combat- and trauma-induced skeletal muscle injuries are characterized by volumetric muscle loss (VML), where large amounts of tissue and its native basement membrane is removed or destroyed, profoundly impacting the quality of life of patients.⁵ While skeletal muscle has an innate repair mechanism, it is unable to compensate for VML injuries, resulting in the formation of scar tissue to fill the void created by the muscle defect, and ultimately leading to a loss of mechanical function and disfigurement. The current standard of care for large volume skeletal muscle injury is an autologous tissue transfer from an uninjured site.⁴ This complicated surgical procedure yields limited restoration of muscle function and can result in complications such as donor site morbidity, infection, and graft failure due to necrosis in as many as 10% of these surgeries.^{4,6,7} Thus, there is a need to develop an off-the-shelf, biomimetic scaffold that directs functional skeletal muscle tissue regeneration within VML injuries.

Skeletal muscle regeneration is mediated by local progenitor cells known as satellite cells (SCs), which reside between the sarcolemma and basal lamina of muscle fibers.⁸ Typically quiescent, SCs enter the cell cycle after an injury, proliferate, and fuse into new myofibers to repair the injury.⁹ Upon mechanical injury of a muscle fiber, hepatocyte growth factor (HGF) is rapidly released from the extracellular matrix (ECM) of the muscle fiber itself in the first 48-72 hours after injury, stimulating the activation and proliferation of SCs as well as the chemotaxis of SCs to migrate towards the wound site.¹⁰⁻¹³ Because it inhibits SC differentiation, HGF will inhibit muscle regeneration if present for more than 4 days.^{9,13,14} Traumatic loss of the basal

lamina in VML injuries eliminates this HGF reservoir that recruits SCs; therefore, we hypothesize that the addition of HGF to an intervention in these large defects will promote the endogenous skeletal muscle regeneration pathway by facilitating the recruitment of SCs to the injury site.

Two of the most important criteria for the design of materials to guide skeletal muscle regeneration are that scaffolds must facilitate uniaxial alignment of myoblasts,¹⁵ and that the scaffolding material must remain mechanically stable throughout the regenerative process to ensure that the regenerating tissue does not rupture or become damaged due to premature degradation of the scaffold.^{16,17} A variety of materials have been investigated for use as a scaffold for skeletal muscle regeneration including poly(glycolic acid) (PGA),^{18,19} alginate,^{20,21} decellularized ECM,²²⁻²⁴ and fibrin.²⁵⁻²⁷ Synthetic materials such as PGA or poly(ϵ -caprolactone) (PCL) can be fabricated with tuned mechanical and structural properties and, due to their fibrous structure, readily direct myoblast alignment.²⁸ Decellularized ECM scaffolds have demonstrated some success in enhancing skeletal muscle regeneration when the decellularization process conserves the bioactivity of the material.²⁴ A limitation of many of these materials is that their bulk structure and randomly polymerized internal fibrillar networks do not consistently promote uniaxial alignment of myoblasts, generating disorganized regenerated tissue which will impair the muscle's ability to efficiently contract. As such, there is a need to create biomimetic materials that are capable of aligning myoblasts within an injury site to promote skeletal muscle regeneration.

Our laboratory has developed a method to control the polymerization process of fibrin to create microthreads, discrete cylindrical structures that direct cell alignment.²⁹ These fibrin microthreads can bind growth factors, such as fibroblast growth factor 2 (FGF2), using the protein-binding domains present on fibrin.³⁰ When implanted into a mouse model of VML, fibrin microthreads, as well as cell-seeded fibrin microthreads, increased the functional recovery of the defect.²⁷ However, these studies showed that the fibrin microthreads completely degrade within two weeks *in vivo*,²⁷ suggesting that their degradation rate would need to be decreased for use as a scaffold for skeletal muscle regeneration to facilitate increased organized regeneration of muscle tissue.

1.2 OVERALL GOAL and HYPOTHESIS

The ultimate goal of this project was to develop a scaffold material that was mechanically stable *in situ* to guide aligned, myoblast ingrowth and that will incorporate growth factors, delivered at clinically relevant times, to direct mechanically functional skeletal muscle tissue regeneration of VML injuries.

We hypothesize that fibrin microthreads with an increased resistance to proteolytic degradation and loaded with HGF will enhance the functional regeneration of skeletal muscle tissue in a VML injury model.

To systematically test this hypothesis, this dissertation was separated into three specific aims. We investigated crosslinking and post-polymerization processing conditions in Specific Aim 1 to develop fibrin microthreads with increased resistance to proteolytic degradation. In Specific Aim 2, we developed strategies to incorporate HGF onto fibrin microthreads. Finally, in Specific Aim 3, we investigated the restoration of mechanical function of the mouse *tibialis anterior* (TA) muscle after the generation of a critically sized VML defect. The expected outcome of this dissertation was the identification of post-fabrication modifications such as chemical crosslinking, controlled uniaxial stretching, and growth factor adsorption to fibrin microthreads to match scaffolds with known structural and biochemical properties to site-specific tissue properties (e.g. skeletal muscle) to recapitulate regenerative cues lost in traumatic injuries.

1.3 SPECIFIC AIM 1: DEVELOP MICROTHREADS WITH TUNABLE STRUCTURAL PROPERTIES WHILE MAINTAINING CELLULAR VIABILITY

A significant challenge in the design of biomimetic scaffolds is combining morphological, mechanical, and biochemical cues into a single construct to promote tissue regeneration. The goal of this study was to develop fibrin microthreads with controlled degradation rates to decrease the rate of proteolytic degradation to generate scaffolds designed for directional cell guidance with increased mechanical stability. In Chapter 3 of this thesis, we analyzed the effects of different crosslinking conditions on fibrin biopolymer microthreads to create scaffolds with tunable mechanical and structural properties to increase *in vivo* scaffold persistence. Fibrin microthreads were crosslinked using carbodiimides in either acidic (EDCa)

or neutral (EDCn) buffer, and changes in the mechanical, structural, and biochemical properties of the microthreads were investigated. EDCa microthreads had significantly higher tensile strengths and moduli than all other microthreads, and failed at lower strains than all other microthreads. EDCn microthreads were also significantly stronger and stiffer than uncrosslinked (UNX) microthreads and were comparable to contracting muscle in stiffness. Swelling ratios of crosslinked microthreads were significantly different from each other and uncrosslinked controls, suggesting a difference in the internal organization and compaction of the microthreads. Using an *in vitro* degradation assay, we observed that EDCn microthreads degraded within 24 hours, six times slower than UNX control microthreads, but EDCa microthreads did not show any significant indication of degradation within the 7 day assay period. Microthreads with higher stiffnesses supported significantly increased attachment of C2C12 myoblasts, as well as increases in myoblast proliferation without a decrease in viability. Taken together, these data demonstrate the ability to create microthreads with tunable mechanical and structural properties that differentially direct cell functions. Ultimately, we anticipate that we can strategically exploit these properties to promote site-specific tissue regeneration. *Grasman JM, Page RL, Dominko T, Pins GD. Crosslinking strategies facilitate tunable structural properties of fibrin microthreads. Acta Biomaterialia 2012;8(11):4020-30.*

As an alternate to exogenous crosslinking agents, we analyzed fibrin microthread processing conditions in Chapter 4 of this thesis to determine the effects of static axial stretching on the proteolytic degradation of these materials. Our hypothesis was that increased amounts of stretch on fibrin microthreads would decrease the rate of proteolytic degradation, which was based upon previous work demonstrating that stretched fibrin clots had increased resistance to proteolytic degradation.³¹ Fibrin microthreads were extruded, dried, rehydrated, and static axially stretched 0-200% of their original lengths; then the mechanical and structural properties of the microthreads were assessed. Stretching significantly increased the tensile strength of microthreads threefold, yielding scaffolds with tensile strengths and stiffnesses that equaled or exceeded values reported in Chapter 3 for EDCa and EDCn microthreads without affecting intrinsic material properties such as strain hardening or Poisson's ratio. Interestingly, these stretching conditions did not affect the rate of proteolytic degradation of the microthreads. The swelling ratios of stretched microthreads decreased, and scanning electron micrographs showed

increases in grooved topography with increased stretch, suggesting that stretching may increase the fibrillar alignment of fibrin fibrils. The average myoblast alignment with respect to the longitudinal axis of the microthreads increased twofold with increased stretch, further supporting the hypothesis that stretching microthreads increases the alignment of fibrin fibrils on the surfaces of the scaffolds. Together, these data suggest that stretching fibrin microthreads generates stronger materials without affecting their proteolytic stability, making stretched microthreads ideal for use as implantable scaffolds that require short degradation times and large initial loading properties, as opposed to use in long term implantation. Further modifications to stretched microthreads, such as carbodiimide crosslinking, could generate microthreads to direct cell orientation and align tissue deposition, with additional resistance to degradation for use as a long-term scaffold for tissue regeneration. *Grasman JM, Pumphrey LM, Dunphy M, Perez-Rogers J, Pins GD. Static axial stretching enhances the mechanical properties and cellular responses of fibrin microthreads. Acta Biomaterialia 2014;10(10):4367-76.*

1.4 SPECIFIC AIM 2: QUANTIFY THE EFFECTS OF INCORPORATING HGF ONTO FIBRIN MICROTHREADS TO INCREASE SATELLITE CELL RECRUITMENT

There are almost 100,000 reconstructive maxillofacial surgical procedures performed annually as a result of traumatic injury, cancer ablation, or cosmetic procedures, profoundly impacting the quality of life of patients. These procedures result in the destruction of the basal lamina, which removes important biochemical cues such as the release of HGF, which initiates endogenous skeletal muscle regeneration. The goal of this study was to develop a system to rapidly release HGF from fibrin microthreads to mimic the rapid release of HGF in minor muscle injuries. In Chapter 5 of this thesis, we investigated the effect of adsorbing HGF onto UNX, EDCn, or EDCa microthreads on myoblast proliferation and recruitment in an *in vitro* model designed to mimic *in vivo* SC recruitment. EDCn microthreads facilitated the most HGF adsorption, the release of which was able to significantly elevate the number of proliferating myoblasts for at least 2 days. This active release also increased the two-dimensional migration and three-dimensional outgrowth of myoblasts twofold. UNX microthreads supported HGF adsorption as well; however, it was completely released within 24 hours and only enhanced myoblast proliferation, not migration, possibly due to low concentrations of HGF adsorbed to the

surface. While EDCa microthreads did not facilitate the adsorption of HGF, medium conditioned from these microthreads stimulated myoblast proliferation, possibly due to the release of fibrin degradation products that resulted from the crosslinking procedure. Regardless of the amount of HGF adsorbed on the microthreads, significantly more myoblasts were proliferating on crosslinked, stiffer microthreads 4 days after myoblasts migrated along the microthreads. The ability of EDCn microthreads to adsorb HGF in a way that facilitated its rapid, active release is ideal for VML injuries, and we hypothesize that these HGF-loaded EDCn microthreads will enhance the functional regeneration of these injuries. *Grasman JM, Page RL, Dominko T, Pins GD. Adsorbed Hepatocyte Growth Factor on Crosslinked Fibrin Microthreads Enhances Cell Recruitment. In preparation 2014.*

1.5 SPECIFIC AIM 3: ASSESS MICROTHREADS' ENHANCEMENT OF SKELETAL MUSCLE REGENERATION *IN VIVO*

VML injuries typically result from traumatic incidents; such as those presented from combat missions, where soft-tissue extremity injuries account for 63% of diagnoses.^{1,2} These injuries can result in muscle loss, which lead to cosmetic deformities and devastating loss of function. In Chapter 6 of this thesis, we evaluated the ability of HGF adsorbed, EDCn microthreads to guide functional regeneration in VML-sized defects in an *in vivo* animal model created by excising approximately 40-50% of the TA muscle, reducing the force output of the muscle by 50%. Fourteen days post-injury, there were significantly more myogenin positive nuclei present in the defect site of HGF-loaded EDCn microthreads, suggesting an increased number of myoblasts were differentiating into myotubes. There was also a significantly higher number of blood vessels present in microthread (UNX, EDCn, and HGF-loaded EDCn) implants. Sixty days post-injury, HGF-loaded EDCn (EDCn-HGF) microthreads facilitated significant functional recovery of the skeletal muscle defect that approached pre-injury values. Histomorphometrically, EDCn and EDCn-HGF microthreads persisted 60 days post-injury, and mature, organized muscle tissue replaced the microthreads in areas of the injury site instead of disorganized muscle, or adipose infiltration observed within the injury site of negative controls. The amount of Pax7 positive SCs and myogenin positive nuclei present in the injury site returned to values similar to uninjured muscle, suggesting that much of the injury site has resolved at this

time. Together, these data suggest that the scaffold materials are being remodeled with functional muscle tissue, and that we designed fibrin biopolymer microthreads that recapitulate several of the regenerative cues lost in VML injuries and enhance the functional regeneration of skeletal muscle. *Grasman JM, Do DM, Page RL, Pins GD. Hepatocyte Growth Factor Adsorbed onto EDC Crosslinked Microthreads Restores Mechanical Function in Mouse Model of VML. In preparation 2014.*

1.6 REFERENCES

1. Masini BD, Waterman SM, Wenke JC, Owens BD, Hsu JR, Ficke JR. Resource utilization and disability outcome assessment of combat casualties from Operation Iraqi Freedom and Operation Enduring Freedom. *J Orthop Trauma* 2009;23(4):261-6.
2. Owens BD, Kragh JF, Jr., Macaitis J, Svoboda SJ, Wenke JC. Characterization of extremity wounds in Operation Iraqi Freedom and Operation Enduring Freedom. *J Orthop Trauma* 2007;21(4):254-7.
3. 2009 report of the 2008 statistics of plastic surgery statistics. American Society of Plastic Surgeons 2009.
4. Eckardt A. Microsurgical reconstruction in the head and neck region: an 18-year experience with 500 consecutive cases. *Journal of Cranio-Maxillofacial Surgery* 2003;31(4):197-201.
5. Heemskerk J, Kitslaar P. Acute compartment syndrome of the lower leg: retrospective study on prevalence, technique, and outcome of fasciotomies. *World Journal of Surgery* 2003;27(6):744-7.
6. Bianchi B, Copelli C, Ferrari S, Ferri A, Sesenna E. Free flaps: outcomes and complications in head and neck reconstructions. *Journal of cranio-maxillo-facial surgery : official publication of the European Association for Cranio-Maxillo-Facial Surgery* 2009;37(8):438-42.
7. Floriano R, Peral B, Alvarez R, Verrier A. Microvascular free flaps in head and neck reconstruction. Report of 71 cases. *Journal of Cranio-Maxillofacial Surgery* 2006;34:90-90.
8. Zammit PS, Partridge TA, Yablonka-Reuveni Z. The skeletal muscle satellite cell: the stem cell that came in from the cold. *The journal of histochemistry and cytochemistry : official journal of the Histochemistry Society* 2006;54(11):1177-91.
9. Charge SB, Rudnicki MA. Cellular and molecular regulation of muscle regeneration. *Physiol Rev* 2004;84(1):209-38.
10. Tatsumi R, Anderson JE, Nevoret CJ, Halevy O, Allen RE. HGF/SF is present in normal adult skeletal muscle and is capable of activating satellite cells. *Developmental biology* 1998;194(1):114-128.
11. Tatsumi R, Hattori A, Ikeuchi Y, Anderson JE, Allen RE. Release of hepatocyte growth factor from mechanically stretched skeletal muscle satellite cells and role of pH and nitric oxide. *Mol Biol Cell* 2002;13(8):2909-18.
12. Tatsumi R, Liu X, Pulido A, Morales M, Sakata T, Dial S, Hattori A, Ikeuchi Y, Allen RE. Satellite cell activation in stretched skeletal muscle and the role of nitric oxide and hepatocyte growth factor. *Am J Physiol Cell Physiol* 2006;290(6):C1487-94.
13. Gal-Levi R, Leshem Y, Aoki S, Nakamura T, Halevy O. Hepatocyte growth factor plays a dual role in regulating skeletal muscle satellite cell proliferation and differentiation. *Biochim Biophys Acta* 1998;1402(1):39-51.
14. Miller KJ, Thaloor D, Matteson S, Pavlath GK. Hepatocyte growth factor affects satellite cell activation and differentiation in regenerating skeletal muscle. *Am J Physiol Cell Physiol* 2000;278(1):174-181.
15. Yamamoto DL, Csikasz RI, Li Y, Sharma G, Hjort K, Karlsson R, Bengtsson T. Myotube formation on micro-patterned glass: intracellular organization and protein distribution in C2C12 skeletal muscle cells. *The Journal of Histochemistry and Cytochemistry : Official Journal of the Histochemistry Society* 2008;56(10):881-92.

16. Koning M, Harmsen MC, van Luyn MJ, Werker PM. Current opportunities and challenges in skeletal muscle tissue engineering. *J Tissue Eng Regen Med* 2009;3(6):407-15.
17. Shah R, Sinanan AC, Knowles JC, Hunt NP, Lewis MP. Craniofacial muscle engineering using a 3-dimensional phosphate glass fibre construct. *Biomaterials* 2005;26(13):1497-505.
18. Saxena AK, Marler J, Benvenuto M, Willital GH, Vacanti JP. Skeletal muscle tissue engineering using isolated myoblasts on synthetic biodegradable polymers: Preliminary studies. *Tissue Eng* 1999;5(6):525-531.
19. Lesman A, Koffler J, Atlas R, Blinder YJ, Kam Z, Levenberg S. Engineering vessel-like networks within multicellular fibrin-based constructs. *Biomaterials* 2011;32(31):7856-69.
20. Borselli C, Storrle H, Benesch-Lee F, Shvartsman D, Cezar C, Lichtman JW, Vandenberg HH, Mooney DJ. Functional muscle regeneration with combined delivery of angiogenesis and myogenesis factors. *Proc Natl Acad Sci U S A* 2010;107(8):3287-92.
21. Shvartsman D, Storrle-White H, Lee K, Kearney C, Brudno Y, Ho N, Cezar C, McCann C, Anderson E, Koullias J and others. Sustained delivery of VEGF maintains innervation and promotes reperfusion in ischemic skeletal muscles via NGF/GDNF signaling. *Molecular therapy : the journal of the American Society of Gene Therapy* 2014;22(7):1243-53.
22. Valentin JE, Turner NJ, Gilbert TW, Badylak SF. Functional skeletal muscle formation with a biologic scaffold. *Biomaterials* 2010;31(29):7475-84.
23. Corona BT, Ward CL, Baker HB, Walters TJ, Christ GJ. Implantation of in vitro tissue engineered muscle repair constructs and bladder acellular matrices partially restore in vivo skeletal muscle function in a rat model of volumetric muscle loss injury. *Tissue Eng Part A* 2014;20(3-4):705-15.
24. Sicari BM, Rubin JP, Dearth CL, Wolf MT, Ambrosio F, Boninger M, Turner NJ, Weber DJ, Simpson TW, Wyse A and others. An acellular biologic scaffold promotes skeletal muscle formation in mice and humans with volumetric muscle loss. *Science translational medicine* 2014;6(234):234ra58.
25. Huang YC, Dennis RG, Larkin L, Baar K. Rapid formation of functional muscle in vitro using fibrin gels. *Journal of Applied Physiology* 2005;98(2):706-713.
26. Hammers DW, Sarathy A, Pham CB, Drinnan CT, Farrar RP, Suggs LJ. Controlled release of IGF-I from a biodegradable matrix improves functional recovery of skeletal muscle from ischemia/reperfusion. *Biotechnology and bioengineering* 2012;109(4):1051-9.
27. Page RL, Malcuit C, Vilner L, Vojtic I, Shaw S, Hedblom E, Hu J, Pins GD, Rolle MW, Dominko T. Restoration of skeletal muscle defects with adult human cells delivered on fibrin microthreads. *Tissue engineering. Part A* 2011;17(21-22):2629-40.
28. Guex AG, Birrer DL, Fortunato G, Tevaeai HT, Giraud MN. Anisotropically oriented electrospun matrices with an imprinted periodic micropattern: a new scaffold for engineered muscle constructs. *Biomed Mater* 2013;8(2):021001.
29. Cornwell KG, Pins GD. Discrete crosslinked fibrin microthread scaffolds for tissue regeneration. *J Biomed Mater Res A* 2007;82(1):104-12.
30. Cornwell KG, Pins GD. Enhanced proliferation and migration of fibroblasts on the surface of fibroblast growth factor-2-loaded fibrin microthreads. *Tissue Eng Part A* 2010;16(12):3669-77.
31. Varju I, Sotonyi P, Machovich R, Szabo L, Tenekedjiev K, Silva MM, Longstaff C, Kolev K. Hindered dissolution of fibrin formed under mechanical stress. *J Thromb Haemost* 2011;9(5):979-86.

Chapter 2: Background

2.1 CLINICAL NEED FOR SCAFFOLDS TO REGENERATE SKELETAL MUSCLE

Large skeletal muscle defects, while not life threatening, profoundly impact the quality of life of patients. Skeletal muscle injuries typically result from traumatic incidents; such as those presented from excessive exercise, contusions, lacerations, surgical resection or reconstruction, or combat injuries.¹⁻³ Approximately 35-55% of all sports injuries are due to skeletal muscle damage, typically as a result of myofiber and/or connective tissue damage.⁴ Further, there are about 4.5 million reconstructive surgical procedures performed annually as a result of traumatic injury, car accidents, cancer ablation, or cosmetic procedures.^{5,6} On the battlefield, extremity injuries account for 63% of diagnoses, with most of these wounds involving soft tissue damage.^{7,8} Many of these injuries involve the loss of at least 20% of a given muscle's mass, which is termed volumetric muscle loss (VML).^{9,10} These injuries result in billions of dollars in health care expenses, as well as the development of different surgical techniques and medical devices, to repair them,¹¹⁻¹⁴ and are characterized by a significant loss of muscle volume and mechanical function.^{9,15}

While skeletal muscle has an innate repair mechanism that can repair small wounds such as those incurred through exercise, VML defects and injuries are beyond the ability of this mechanism.¹ Further, there are no treatments available that attempt to harness or direct this endogenous regenerative pathway. There are several established protocols for the treatment of small-scale skeletal muscle injuries, such as RICE (resting the wound with a combination of ice, compression, and elevation),^{13,14,16} however, larger-scale injuries such as those presented by VML often require more specialized surgical solutions.¹⁷ The current standard of care for large-scale VML injuries is an autologous tissue transfer from an uninjured site, where surgeons remove the damaged muscle tissue and graft healthy muscle from a donor site unaffected by the traumatic incident.^{6,18} While autologous tissue transfers are the best available treatment option,

as many as 10% of these surgeries undergo complete graft failure, due to complications such as infection and necrosis, demonstrating the need for an alternative treatment.^{18,19} Regardless of the level of success of these procedures, there is always a loss of muscle strength and function, usually due to the formation of scar tissue.^{10,15,17} Additionally, in the case of extensive traumatic injuries such as those presented by military personnel, there may be limited donor site availability.^{15,20} In the case of extensive traumatic injury to a limb, amputation is the standard of care, requiring the use of a prosthetic device to regain limited functionality.¹⁰ As such, there is a significant need to develop off-the-shelf biomimetic materials that can direct skeletal muscle tissue formation within these large defect sites to facilitate functional tissue regeneration.

2.2 SKELETAL MUSCLE ANATOMY

Skeletal muscle is one of the most abundant tissues in the human body, accounting for 40% to 45% of the total body mass.²¹ It induces coordinated locomotion through attachment points to the skeleton, and its macroscopic structure consists of organized networks of myofibers, blood vessels, nerves, and connective tissue. The working contractile unit of skeletal muscle is the sarcomere, which consists of interposing filaments of actin and myosin.²² Multiple myoblasts fuse together to form myofibrils, which are structures with repeating sarcomeres along the length of the myofibril.

A bundle of myofibrils form the basic structural element of muscle: the myofiber (Figure 2.1). Myofibers range between 20-100 μm in size, and are the conglomeration of multiple myofibrils.^{21,22} Ultimately, the nuclei of these myoblasts translocate to the periphery of the myofibers, residing just beneath the sarcolemma,

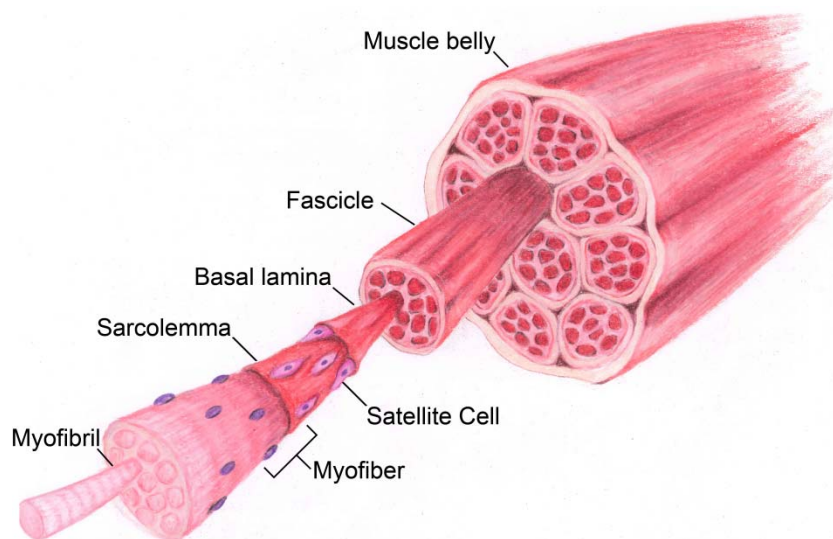


Figure 2.1. Anatomy of skeletal muscle tissue. Skeletal muscle tissue is a highly organized series of cable like structures, with the smallest functional unit referred to as a myofibril. Bundles of myofibrils form myofibers, which in turn are grouped together to form fascicles, which are bundled to form the muscle belly. Image courtesy of M Zayas.

or cell membrane of myofibers. Myofibers organize into larger structures referred to as fascicles,²¹ and in general, the anatomical structure of skeletal muscle can be thought of as a series of self-contracting cables that organize into a complex hierarchical structure.

Each myofiber is surrounded by a basement membrane referred to as the basal lamina (Figure 2.1). This dense structure is composed of a variety of basement membrane proteins such as type IV collagen and laminin-2, and is essential for guiding the endogenous regenerative pathway of skeletal muscle.^{23,24} Skeletal muscle progenitor cells, termed satellite cells (SCs), reside in the interstitial space between the sarcolemma of myofibers and the basal lamina. These cells are identified by expressing paired box gene 7 (Pax7), and are typically quiescent in mature, healthy tissue.^{1,25,26} Satellite cells account for 2-7% of all myofiber nuclei, but they are the primary cell type responsible for the regeneration of skeletal muscle tissue.²⁷

2.3 NATIVE REGENERATIVE PATHWAY OF SKELETAL MUSCLE

Skeletal muscle regeneration is a complex process that involves an inflammatory response, growth factor signaling, SC repair of the injury, and fibroblast infiltration, ultimately leading to either functional regeneration, or scar tissue formation. These processes have been loosely classified into three phases: (1) the destruction/inflammatory phase, (2) the repair phase, and (3) the remodeling phase (Figure 2.2).^{10,13,21,28,29}

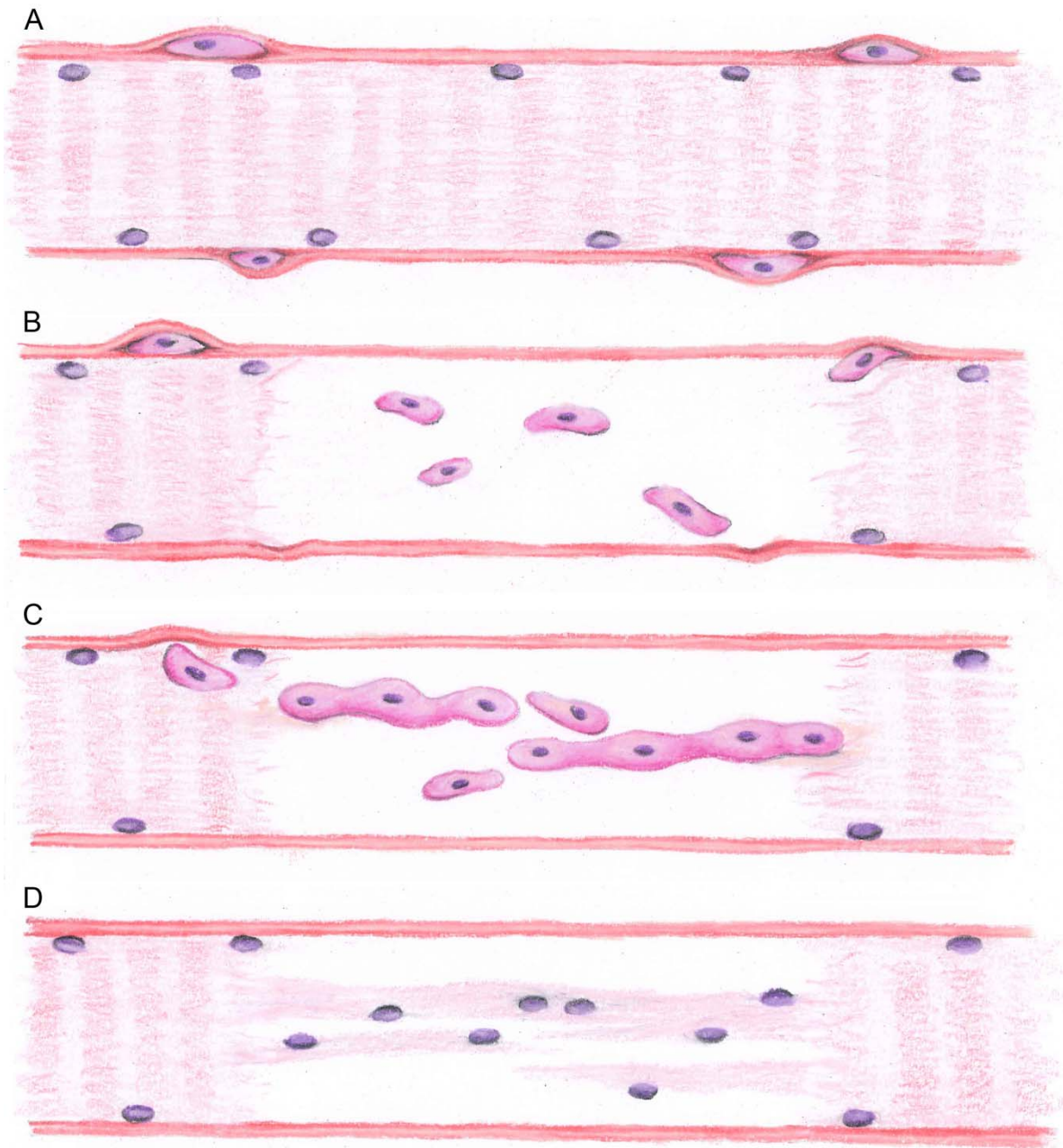


Figure 2.2. Schematic representation of native skeletal muscle regeneration. SCs can be identified by their position between the sarcolemma and basal lamina of mature skeletal muscle (A). Upon injury, SCs are recruited to the wound site and begin to proliferate (B). These proliferating SCs will eventually begin to fuse together to form immature myofibers (C), which will fuse with the existing healthy myofibers, and will then mature by expressing more contractile proteins to regenerate functional tissue (D). Image courtesy of M Zayas.

2.3.1 Destruction/Inflammatory Phase

Traumatic injury to skeletal muscle leads to the rupture of the sarcolemma, which exposes the intracellular contents of the myofiber to large amounts of extracellular calcium. This triggers the activation of calcium-dependent proteases, initiating myofiber necrosis.^{21,29} Necrosis occurs along the length of the damaged myofiber until it reaches a contraction band, a dense band of cytoskeletal material that is designed to halt the necrosis of injured myofibers.^{13,30,31} Almost immediately after injury, neutrophils migrate to the injury site and assist in the degradation of damaged myofibers. Macrophages quickly migrate to the injury site and become the predominate cell type present in as little as two days post-injury.³² One of the most critical cytokines secreted from the inflammatory cells is nitric oxide, whose functions include: (1) the facilitation of further degradation of myofibers present in the wound environment,^{28,32} (2) the facilitation of the release of growth factors such as hepatocyte growth factor (HGF) from the surrounding matrix,^{28,33-35} and (3) the induction of vasodilation of nearby blood vessels to recruit additional inflammatory cells.^{13,36} While macrophages migrate to the wound site within two days of injury, they also modulate the cytokines they release over time. Initially, pro-inflammatory M1 phenotype macrophages assist in the phagocytosis of necrotic myofibers, and also support satellite cell survival and proliferation.^{28,32} Over the next 3-7 days, M1 macrophages are replaced by M2 macrophages, which are believed to enhance the regenerative response of tissues by promoting myoblast proliferation, growth, and differentiation.^{10,28,32}

2.3.2 Repair Phase

The repair phase of skeletal muscle regeneration is comprised of two sub-phases: the recruitment and proliferation of SCs (Figure 2.2B), and the differentiation of SCs into mature muscle tissue (Figure 2.2C). The recruitment/proliferation phase is initiated upon mechanical injury of muscle fibers, when HGF is rapidly released from the extracellular matrix (ECM) of the muscle fiber itself, stimulating the activation and proliferation of SCs as well as the chemotaxis of SCs to migrate to the injury site.^{34,35,37,38} HGF has been found to be the sole growth factor capable of bringing SCs back into the cell cycle.³⁹⁻⁴¹ Other factors, such as fibroblast growth factor 2 (FGF2) and fibroblast growth factor 6 (FGF6), are also released from the ECM, and also stimulate SC proliferation to gather enough progenitor cells to repair the injury.^{13,38,42-46} Because

of their location between the sarcolemma and the basal lamina, SCs typically migrate longitudinally from the same myofiber to the injury site, rather than laterally from other, intact fibers.^{1,25,47} However, once injuries result in the rupture of the basal lamina, lateral migration of SCs to the injury site does occur.^{48,49} SCs are extremely efficient at repairing muscle, and are capable of generating thousands of myoblasts from a small number of satellite cells.^{50,51} Once SCs reenter the cell cycle (i.e. activate), they begin to express myogenic factor 5 (Myf5), and will express myogenic differentiation factor-1 (MyoD) when they are committed to myogenic differentiation.^{1,52-55} Additionally, once SCs are committed to differentiation they are referred to as myoblasts, and begin to lose Pax7 expression.⁵⁶

The second sub-phase of regeneration, the differentiation phase, occurs when myoblasts begin to express myogenin, fuse with other myoblasts, and mature into myofibers (Figure 2.2C).^{53,56} This process is inhibited by the growth factors associated with the proliferation phase of muscle regeneration, mainly HGF, FGF2, and FGF6, highlighting the importance of the temporal expression of growth factors in skeletal muscle regeneration.^{1,38,57,58} Specifically, there is evidence that prolonged, systemic supplementation of HGF will inhibit healing, showing a need for the growth factor to be present for no longer than 48-72 hours.^{38,59,60} Instead, the process of myoblast differentiation is stimulated by the insulin-like growth factor (IGF) family.^{61,62} This family (consisting of members IGF1 and IGF2) is unique in that each growth factor will stimulate both the proliferation, and subsequent differentiation, of myoblasts.⁶³⁻⁶⁶ Both *in vitro* and *in vivo* studies have suggested that IGF1 is more potent in skeletal muscle regeneration than IGF2, either due to growth factor activity or the increased availability of its receptor, insulin-like growth factor receptor-I (IGFR1).^{67,68} Neutralizing the function of IGF1 was found to inhibit skeletal muscle regeneration, highlighting the importance of this factor in the regenerative response.⁶⁹ Further, injections of exogenous IGF1 into skeletal muscle injuries in aged animals have been shown to restore the proliferative ability of SCs, marking it as a potent factor in skeletal muscle regeneration, and indeed a necessary factor for use in enhancing the endogenous regenerative response of skeletal muscle.⁷⁰⁻⁷² IGF-mediated cell-fusion events occur after the initiation of myogenin expression, which also terminates MyoD/Myf5 expression.^{1,26,56} Nascent myofibers are characterized by centrally aligned nuclei, and as these cells mature and generate more contractile proteins the nuclei gradually translocate to the periphery of the myofiber.^{1,13,26,54}

2.3.3 Remodeling Phase

The final stage of muscle regeneration is the remodeling phase and is a balance between the culmination of the differentiation sub-phase of muscle regeneration and the infiltration of fibroblasts into the injury site. Regenerating myoblasts will fuse with the existing musculature at the interface of the injury, or to the ECM (Figure 2.2D).¹⁰ The infiltration of fibroblasts, which can begin as early as the inflammatory phase, supports regeneration by repairing and replacing connective tissue that was damaged by the injury.¹³ While the connective tissue synthesized by fibroblasts is important in providing stability for the regenerating tissue and replacing damaged or lost ECM, collagen deposition often remodels into scar tissue and limits the organization of the regenerated tissue (Figure 2.3).^{10,13,73} The balance between these two antagonistic responses dictates the functional outcome from the regenerative pathway. In general, small injuries remodel without the presence of scar tissue, but as the injury becomes larger the fibroblast infiltration increases such that there begins to be a significant amount of collagen deposition, ultimately impeding the functional regeneration of skeletal muscle tissue.

In injuries resulting from VML, there are no regenerative cues present due to the complete destruction, or removal, of the basal lamina and surrounding connective tissue (Figure 2.3). This results in a loss of traditional signaling that indicates the need for SCs to migrate into the injury site; therefore, there does not appear to be a large influx of myoblasts into these injuries.^{13,74} Because of the lack of SC infiltration into the injury site, the infiltrating fibroblasts dominate this stage of regeneration, resulting in large amounts of collagen deposition.^{75,76} Ultimately, the deposition of collagen I into the wound site results in the formation of scar tissue, limiting the ability of the muscle to uniformly contract, which results in a loss of function as observed from the patient.^{10,73,77} In addition to the loss of mechanical function observed in patients with VML injuries, these injuries also result in significant losses in muscle volume, which can generate physical deformities that may impact the psychological health of the patient.

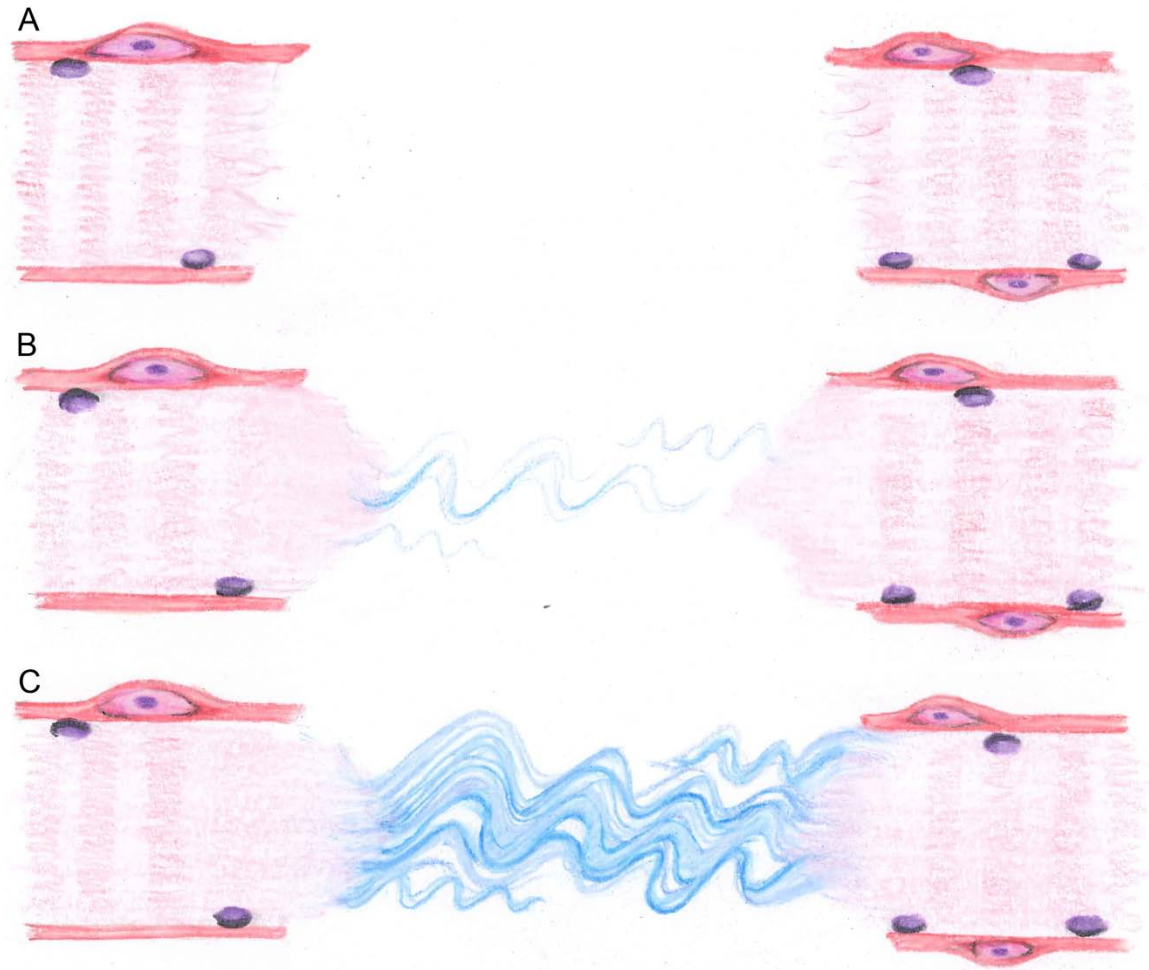


Figure 2.3. Schematic representation of repair of VML injuries. The basal lamina is typically destroyed or removed in large muscle injuries, eliminating important signaling cues that recruit SCs to the injury (A). Instead, fibroblasts migrate into the injury site and deposit collagen (B), ultimately leading to massive scar tissue formation (C). Image courtesy of M Zayas.

2.3.4 Cell Types Involved in Skeletal Muscle Regeneration

Concurrent with the repair phase of skeletal muscle regeneration, blood vessels, nerves, and fibroblasts are infiltrating the injury site.^{1,10,29} Skeletal muscle is a highly vascularized tissue, and as such its revascularization is vital for successful regeneration.^{78,79} The close proximity of SCs and endothelial cells in skeletal muscle facilitates paracrine signaling between these cell types to support both angiogenesis and myogenesis.^{80,81} Muscle is not only highly vascularized, but also heavily innervated to facilitate the cooperative contraction of myofibers to conduct uniaxial force.²⁹ Factors such as IGF1 have been shown to induce nerve sprouting, and

HGF and FGF2 have been shown to be potent angiogenic factors, suggesting that the growth factor cascade in skeletal muscle regeneration affects a variety of cell types in addition to myoblasts.⁸²⁻⁸⁷ The infiltration of fibroblasts coincides with SC infiltration to support regeneration by repairing and replacing connective tissue that was damaged by the injury.¹³ However, as stated earlier, the deposition of connective tissue often leads to scar tissue formation as well as functionally impaired regeneration.^{12,13,30,88}

2.4 CURRENT TISSUE ENGINEERING STRATEGIES AND LIMITATIONS

There are two main approaches to develop materials for skeletal muscle regeneration: the development of *in vitro* skeletal muscle constructs to augment, and the development of scaffolds to regenerate, damaged skeletal muscle tissue *in vivo*.⁸⁹⁻⁹² Materials designed to guide regeneration of skeletal muscle can be further defined as either acellular or cellular; incorporating myoblasts or stem cells into their matrix. The utilization of the scaffolding material as a delivery vehicle of progenitor cells attempts to address the limitation of needing sufficient numbers of cells to regenerate large scale injuries, while acellular strategies attempt to address this same limitation by delivering sustained amounts of growth factors to stimulate local progenitor cells into the injury site. To direct skeletal muscle growth, biomimetic scaffolds must facilitate cell alignment, promote skeletal muscle formation, and stimulate vascularization and innervation. Cell alignment is one of the most critical factors in skeletal muscle regeneration due to the unique geometric organization of muscle fibers.^{21,93-96} Fibrous elements within scaffolding materials have been shown to direct cell alignment along the length of the scaffold's surface.⁹⁷⁻¹⁰⁰ Strategies to promote skeletal muscle formation and angiogenesis include the incorporation of growth factors and peptide sequences within the scaffolding material.^{78,101,102} Sustained delivery of growth factors improves skeletal muscle regeneration compared to single bolus dosing, suggesting that the controlled release of growth factors from scaffold materials is an efficient delivery method for these molecules.^{61,71,78} Finally, scaffolds need to balance degradation with structural and mechanical support of the injury site such that enough structural stability is present within the scaffold material to support mechanical loading until the regenerated tissue is stable enough to withstand loading independently.^{3,76,103}

2.4.1 *In Vitro* Skeletal Muscle Development

Engineered skeletal muscle constructs have been developed to study skeletal muscle formation *in vitro*, to develop high throughput models for drug screening applications, and ultimately to replace or augment damaged tissue *in vivo*.^{21,92,93} These tissues are typically prepared by seeding myoblasts onto a protein surface, commonly fibrin, which is remodeled into muscle tissue.^{68,104-108} Vandenburg and colleagues developed a platform technology that could generate muscle constructs in the bottom of 96 well plates between two polydimethylsiloxane (PDMS) posts as a high throughput model for drug screening applications. Each individual well was capable of being mechanically stimulated and assessed for force production.¹⁰⁹⁻¹¹¹ *In vitro* skeletal muscle constructs designed for implantation to replace damaged muscle tissue or to model skeletal muscle formation can spontaneously contract, and have been electrically stimulated to induce tetanic contractions, demonstrating that these constructs can accurately mimic skeletal muscle function.¹⁰⁷ One of the limitations of these skeletal muscle constructs is the inability of nutrients to diffuse to the innermost layers of the tissue. While this is not a problem for small skeletal muscle constructs used in drug screening applications, constructs approaching 0.4 mm in thickness result in the formation of a necrotic core, making it unsuitable for implantation.^{107,112} Recently, a study using a heterogeneous population of cells isolated from the muscles in mice hind limbs demonstrated that vascular networks could be formed *in vitro* to support the survival of these constructs for at least 40 days in culture.¹¹³

Larger skeletal muscle constructs, ranging between 1 and 4 cm in length, have been implanted to observe engraftment, vascularization, and functional recovery of VML injuries. Implanting *in vitro* skeletal muscle constructs near existing blood vessels greatly enhances their vascularization.¹¹⁴ Successful *in vivo* engraftment significantly increases the force output of these constructs, demonstrating that these constructs are capable of integrating with the surrounding tissue to remain viable and enhance their force production.¹¹⁵ Finally, *in vitro* skeletal muscle constructs approximately 4 cm in length, termed “skeletal muscle units” (SMUs), were implanted into a rat VML model where 33% of the *tibialis anterior* (TA) muscle was removed. While these SMU constructs supported some vascular and nervous tissue integration as well as a significant increase in TA force production after 28 days, the forces generated in these muscles remained significantly below baseline force values.¹¹⁶

The major limitation of these methods is the lack of vascularization of *in vitro* skeletal muscle constructs. Dennis and Kosnik showed that myoblasts need to be within 150 μm of a source of oxygen to proliferate or differentiate, limiting the size of viable constructs without a functional vascular network.¹¹² Further, these constructs are generated by seeding myoblasts and fibroblasts on protein surfaces and then they are differentiated into functional tissue. This requires 3-4 weeks of culture time for the formation of a robust ECM to support construct contractility.⁹² The ability to generate contractile constructs from a patient's own cells is an attractive possibility;^{92,111} however, nearly a month would pass between obtaining the biopsy and implantation. Therefore, these constructs might be better suited for chronic reconstruction rather than the repair of traumatic VML injuries.

2.4.2 Biomaterials for Skeletal Muscle Regeneration

Scaffolds for skeletal muscle regeneration have been made from a variety of materials, ranging from synthetic polymers such as poly(glycolic acid) (PGA)¹¹⁷ and poly- ϵ -caprolactone (PCL);⁹⁴ to natural polymers such as alginate,⁷⁸ collagen,⁹⁸ and fibrin;⁷⁶ to decellularized ECM materials.¹¹⁸ In addition to the use of a variety of materials as acellular scaffolds, strategies for skeletal muscle regeneration have utilized a variety of cell sources.^{90,93} The incorporation of cells into scaffolds has significantly increased the survival of implanted cells in the injury site, which has previously been below 5%.^{119,120} While the source of these cells can vary with different scaffolds, in general, SCs, or myoblasts derived from satellite cells in culture, have been investigated to regenerate skeletal muscle injuries.^{90,121} The sections below discuss recent advances in the design of scaffolds for the regeneration of VML injuries, and are organized based on the composition of their scaffolding materials.

2.4.2.1 Synthetic Polymers

A variety of synthetic materials have been used as scaffolds for skeletal muscle regeneration such as PGA,^{117,122} poly(lactic acid) (PLA),¹²³ their copolymers (PLLA/PLGA),¹²⁴ and PCL.^{94,125} Synthetic materials offer several advantages to natural polymers, such as their ability to have precisely tuned mechanical and structural properties that can be tailored to each tissue engineering application.^{100,126,127} Synthetic polymers can be fabricated into a variety of

geometries such as individual fibers or electrospun meshes with aligned, or random, nanofiber orientation.¹²⁸⁻¹³⁰ Myoblasts seeded on electrospun meshes with aligned nanofiber orientation generate highly aligned cultures that, when cultured in differentiation medium, readily fuse into aligned myotubes.^{94,131} Incorporating electrically conductive materials within synthetic scaffolding materials facilitated more efficient electrical stimulation of myoblast cultures, further improving myoblast differentiation compared to aligned fibers without stimulation.¹³²⁻¹³⁴ Synthetic scaffolds can easily be fabricated with multiple growth factors incorporated into their bulk structure to facilitate the controlled release of these factors into a potential injury site.¹³⁵

The mechanical stability of synthetic polymer scaffolds that have been used for skeletal muscle applications,¹³⁶⁻¹³⁸ have previously demonstrated successful outcomes as structural support in the abdomen to repair hernias.^{139,140} In these applications, several studies noted the beginning of a vascular network forming in as little as 6 weeks after implantation of PGA meshes, suggesting that these scaffold materials have a modest ability to stimulate angiogenesis.^{122,141} However, a common criticism of synthetic materials is that their surfaces do not always readily support cell attachment.¹⁴² Due to their inherent suboptimal bioactivity, many strategies exist to functionalize the surfaces of synthetic polymer scaffolds, such as the addition of collagen or decellularized ECM, to modulate tissue responses.^{94,136} The limited bioactivity of scaffolds made from synthetic polymers limit their utility for treating VML injuries because of the need for the scaffolds to guide functional tissue regeneration.

2.4.2.2 Natural Polymers

Naturally occurring polymers, such as alginate,^{78,83,143} collagen,^{98,144,145} and fibrin^{20,76,124} have been used extensively in skeletal muscle engineering. Unlike synthetic polymers, natural polymers possess intrinsic bioactive signaling cues, and can form complexes with proteins, such as heparan sulfate, and growth factors to enhance cell migration, proliferation, or differentiation.¹⁴⁶⁻¹⁴⁹ Alginate is derived from seaweed and was originally used as an encapsulation agent for a variety of cell types,¹⁵⁰ but due to its amenability to chemical alterations to promote cell adhesion,¹⁵¹ as well as its tunable mechanical and structural properties,¹⁵²⁻¹⁵⁴ it has become increasingly used as a scaffold for skeletal muscle regeneration. Alginate gels with stiffnesses between 13 and 45 kPa were found to maximize myoblast

proliferation and differentiation.¹⁵⁵ Additionally, alginate facilitates the controlled release of a variety of growth factors important to skeletal muscle regeneration, such as HGF,^{120,143} FGF2,^{120,143} IGF1,^{78,156} and vascular endothelial growth factor (VEGF).^{78,156-158} Alginate gels loaded with HGF and FGF2 significantly increased myoblast viability within, as well as the migration of myoblasts out of, these scaffolds, demonstrating that alginate can deliver myoblasts to skeletal muscle.¹²⁰ When translated to a mouse TA laceration model, myoblast-seeded gels loaded with HGF and FGF2 almost completely resolved the muscular injury. It was found that the combination of growth factors and the myoblasts produced this effect, as each condition individually only elicited a modest regenerative response.¹⁴³ More recently, alginate gels incorporating VEGF and IGF1 have been implanted into ischemia-induced skeletal muscle injuries to address skeletal muscle regeneration by improving the early vascularization and myoblast survival within the injury sites.^{78,157} While this model of injury is not as severe as VML injuries, bulk alginate scaffolds loaded with multiple growth factors can dramatically improve the regeneration of skeletal muscle injuries by improving the overall vascularization and myoblast differentiation *in situ*. However, these alginate gels have only been implanted on the surface of the injury site,¹⁵⁹ and therefore their ability to direct skeletal muscle regeneration without the presence of the existing skeletal muscle ECM is not known.

Collagen, particularly type I, belongs to a family of ECM proteins found in connective tissue, particularly in the dermis, tendons, and blood vessels.¹⁶⁰ Scaffolds made from type I collagen have been used in a wide variety of tissue engineering applications including skin, cartilage, bone, tendon, skeletal muscle, and nerve.^{148,161} Collagen gels have been frequently used in skeletal muscle regeneration as a cell delivery vehicle, as intramuscular injections of myoblasts results in the rapid death of these injected cells.¹¹⁹ Myoblasts implanted within a collagen gel have been shown to migrate out of the scaffold and fuse with the existing myofibers present at the periphery of the injury site.^{162,163} Disorganized myofibers form as a result of the amorphous polymerization process of the collagen lattices, resulting in less optimal healing of muscle injuries.¹⁶⁴ Acellular collagen sponges also supported disorganized repair of large muscle defects; however, a large amount of adipose tissue was observed 12 to 24 weeks post-injury, which further limited the amount of organized, functional recovery.¹⁶⁵ To improve the alignment of regenerating myofibers, collagen gels can be fabricated with aligned pore structures

through controlled freeze-drying processes. These modified scaffolds facilitated aligned myotubes along the direction of the pores, which, when integrated into a large muscle defect, were capable of producing force upon electrical stimulation.⁹⁸ However, because of the lack of a robust regenerative response observed with implanted collagen scaffolds, collagen materials were customized with molecules such as heparin to achieve controlled release of growth factors into the injury site.^{166,167} In fact, the functional recovery of muscles damaged by acute ischemia was significantly increased by adding a VEGF-loaded collagen scaffold, demonstrating that scaffolds can contribute to regeneration by supplying necessary growth factors to the wound site.¹⁶⁸ Other growth factors, such as HGF, IGF1, and FGF2 have been added to denatured collagen gels to increase SC recruitment into the injury site;¹⁶⁹ however, no functional measurements were performed on these regenerating muscles and data was obtained only at early time points.

Fibrin has been used extensively as a scaffold material in tissue engineering because of its intrinsic bioactivity and role as a provisional matrix during the initial stages of wound healing.^{149,170} Fibrin is a branched, microfibrillar polymer, formed when activated thrombin cleaves two small peptides from fibrinogen, allowing fibrinogen to self-assemble into a complex fibrillar network. Fibrin gels have been used as the provisional seeding matrix for many *in vitro* skeletal muscle constructs, as described above in section 2.4.1.¹⁷¹⁻¹⁷³ Despite completely degrading within 3 weeks post-injury, fibrin gels promote myoblast survival and differentiation into myofibers that can integrate with uninjured tissue.^{20,174,175} Implanting a myoblast populated fibrin gel near an existing blood vessel greatly enhances the vascular perfusion of these constructs. These primary myoblasts formed vascularized functional mature skeletal muscle tissue three weeks after implantation.¹¹⁴ In a different approach to vascularization of skeletal muscle constructs, endothelial cells were seeded into fibrin-PLLA/PLGA constructs in addition to fibroblasts and myoblasts. This tri-culture supported a complex vascular network, suggesting the need for multiple cell types to be present in cell constructs for skeletal muscle regeneration.¹²⁴ The addition of PLLA/PLGA to these tri-culture scaffolds was done in part to augment the stability of fibrin constructs, as uncrosslinked fibrin is rapidly remodeled. Another strategy to decrease the rate of proteolytic degradation of fibrin has been to add polyethylene glycol (PEG) groups to the bulk structure of fibrin. In addition to modulating the structural

properties of the material, PEGylation can also be a loading mechanism for a variety of growth factors, such as IGF1, to facilitate a controlled release of the factor to enhance skeletal muscle regeneration.¹⁷⁶

2.4.2.3 Decellularized ECM

Decellularized ECM has been harvested from a variety of tissues such as the small intestine, urinary bladder, dermis, and pericardium.¹⁷⁷⁻¹⁷⁹ This scaffolding material serves as an excellent “top-down” approach to biomaterial construction, meaning that the entire regenerative environment is provided at the start of regeneration, as it contains many matrix proteins and growth factors in their native configuration. In contrast, a “bottom-up” approach combines discrete functional units with tissue-specific properties designed for specific functions, and will be further described in section 2.5. While ECM-derived scaffolds are thought to contain all of the proteins and growth factors necessary to direct tissue regeneration, care needs to be taken with the decellularization process, as the types of detergents used could have a dramatic effect on the protein and growth factor content within the scaffold.¹⁸⁰ Interestingly, there does not appear to be site-specific advantages between the decellularized ECM source site and the site of implantation in skeletal muscle applications. The regenerative response in a rodent partial thickness abdominal wall defect due to skeletal muscle derived ECM (M-ECM) was equivalent to the regenerative response using a small intestine submucosa (SIS) scaffold.¹⁸¹ One advantage of using ECM derived scaffolds is that they are angiogenic and serve to promote vascularization of skeletal muscle injury sites.^{17,182} However, there are conflicting reports regarding the efficacy of a variety of acellular ECM scaffolds, including M-ECM, dermal ECM, and SIS, to enhance the functional recovery of a large muscle defect. Investigations looking at remodeling events 1-2 months post-injury reported modest myoblast infiltration into the injury site, although it appears to be somewhat disorganized.¹⁸³⁻¹⁸⁶ There is no consensus whether these additional myofibers contribute to the functional recovery of the muscle 2 months post-injury, as some studies report no improvements in force generation,¹⁸⁷ while other studies report a significant improvement in functional recovery.¹⁸⁸ The addition of bone-marrow derived mesenchymal stem cells (MSCs) to ECM scaffolds significantly improved functional recovery and blood vessel formation. However, MSCs have not been shown to engraft into skeletal muscle tissue, so the exact

mechanism of MSC-mediated increases in recovery are not clear.¹⁸⁹ M-ECM scaffolds seeded with muscle derived cells that were differentiated prior to implantation also significantly increased the functional recovery of VML injuries 2 months post-injury by engrafting into the uninjured tissue.^{74,190} Long term remodeling, between 3-6 months post-injury, is required for acellular urinary bladder matrix (UBM) and SIS scaffold mediated functional recovery.^{191,192} Interestingly, Corona *et al.* observed an increase in the force production of their negative control groups (i.e. the creation of a VML injury with no treatment) over time, suggesting that the scar tissue deposited in the injury site may be reorganizing over time to facilitate some amount of contractility.^{75,192} In human clinical trials, there have been several accounts of successful partial restoration of mechanical function using SIS and UBM ECM scaffolds to treat VML defects.^{15,118} While ECM scaffolds have been shown to significantly enhance skeletal muscle repair in VML defects, there remains a significant reduction in mechanical function compared to uninjured muscle. As ECM based scaffolds are derived from complex tissue environments, the exact composition of these materials is not known, and while they have the ability to direct a regenerative response after longer time points, how these materials do so remains an active area of research.

2.4.3 Limitations

There have been many significant successes in developing materials to guide skeletal muscle regeneration. One of the strengths of synthetic materials is the ease in which they are fabricated, as well as the flexibility to construct scaffolds in a variety of controlled geometries to control myoblast growth and differentiation,⁹⁴ despite needing functionalization with natural materials to improve myoblast attachment or tissue outcomes.¹³⁶ While natural scaffolds are typically more bioactive than unmodified synthetic materials, bulk scaffolds that form through random protein polymerization do not generate uniform cell alignment. Applying static axial stretching techniques to natural polymers may facilitate the alignment of protein fibrils within the bulk scaffold, which will direct uniaxial alignment of cells; however, these materials have not yet been applied to VML injuries.^{193,194}

Further, many of the models of skeletal muscle injury utilize ischemia,^{78,176} toxin,¹⁵⁶ or crush induced¹⁹⁵ injuries. These methods of muscle injury leave the basal lamina intact, which

allows SC recruitment to the injury site due to chemotactic factors being released by the basal lamina.^{9,42,76} The combination of the early recruitment of SCs to the injury site, as well as the persistence of the regenerative template of the basal lamina, allows these injuries to quickly, and completely regenerate in 3-4 weeks.^{1,13,21,23} VML injuries, on the other hand, result in the complete destruction or removal of the basal lamina, providing no regenerative template for SCs to facilitate regeneration.^{9,76} By definition, these massive injuries do not spontaneously regenerate, and are instead characterized by a loss of muscle tissue and function, as well as an increase in the amount of scar tissue within the skeletal muscle ECM.^{9,183,196} Decellularized ECM materials have been shown to significantly improve functional outcomes in VML defects; however, despite their similarities to native tissue, they also do not appear to achieve complete alignment between healthy and regenerating tissue, likely due to the sheer volume of defect space. Future scaffolds must be able to direct cell alignment within the defect sites to facilitate seamless integration between healthy and regenerating tissue, and likely will be required to enhance SC recruitment to the defect site, as the matrix cues present in injured muscle are destroyed in VML injuries. Additionally, care must be taken to select a clinically relevant animal model to appropriately draw conclusions on effects of a given treatment on VML injuries.

2.5 MICROTHREADS FOR USE IN SKELETAL MUSCLE REGENERATION

Integration of the engineered tissue with the wound site can be mediated by creating a scaffold that is morphologically similar to the tissue itself, thereby controlling the scaffold-tissue interface to facilitate a robust integration of surrounding progenitor cells onto, or into, the scaffold.¹⁹⁷ This approach of starting with a similar macroscopic structure as native tissue can be thought of as a “bottom-up” approach to tissue engineering, where scientists begin with basic, bioactive materials and subsequently modify these materials to enhance the regenerative response of the host tissue. We, and others, have exploited the native properties of several proteins, including silk fibroin (SF), collagen, and fibrin, to polymerize into discrete biopolymer microthreads.¹⁹⁸⁻²⁰⁰ SF fibers are isolated by reeling and collecting the individual fibers found in domesticated silkworm (*Bombyx mori*) cocoons or spider draglines (*Nephila clavipes* or *Araneus diadematus*).²⁰⁰⁻²⁰² Silk fibers typically are fabricated in this way with a gumming protein called sericin, which serves to strengthen and bundle the individual fibers.^{203,204} These microthreads

can be organized as series of fiber-like cables in increasingly complex hierarchal structures mimicking the organization of a variety of functional tissue systems such as muscle, tendon, or ligament.^{21,205} Further, these scaffolds can be tailored to meet specific tissue engineering applications through changes in the manufacturing processes. By creating scaffolds from the bottom-up, there is more flexibility and control in creating a tunable, biomimetic scaffold that is instructive in facilitating and directing tissue regeneration.

Recently, our lab developed a method to control the polymerization process of fibrin to create microthreads, which have been shown to facilitate cell alignment along the longitudinal axis of the material.¹⁹⁸ These fibrin microthreads have been implanted into a mouse model of VML injury seeded with human myoblasts, and the combination of a morphologically relevant scaffold material and highly myogenic cell line allowed for more complete endogenous muscle regeneration.⁷⁶ While we observed a reduction in the deposition of scar tissue 3-4 months post-injury, histological analyses of tissue harvested at early time points suggested that the microthreads were largely degraded within 2 weeks of implantation and many of the regenerated myofibers in the wound site at later time points exhibited some degree of misalignment with respect to the native muscle tissue.⁷⁶ Fibrin is rapidly degraded by proteinases, such as plasmin, within the wound site,^{206,207} which suggests that the rate of proteolytic degradation of fibrin microthreads needs to be decreased to be used as a scaffold for skeletal muscle regeneration.

2.5.1 Tuning Mechanical Cues

While the goal of a scaffold is not to replace the intended function of a tissue, it must be mechanically stable in its intended environment to successfully direct regeneration and degrade at an appropriate, tissue-specific rate.^{197,208} The mechanical properties of biopolymer microthreads vary significantly depending on the protein being considered. SF is one of the strongest protein structures that has been described, and often the mechanical and structural properties of SF are regulated at the scaffold fabrication level, such as by changing the concentration of SF within a scaffold, rather than the post-processing level, such as through chemical crosslinking, to tune the mechanical properties to that of the tissue of interest. One such modification is the removal of the gumming protein sericin through incubations in salt

and/or detergent solutions, which lowers the tensile strength as well as improves the immunologic response *in vivo*.^{203,204}

On the other hand, biopolymer microthreads constructed of proteins commonly found *in vivo*, such as collagen or fibrin, are not as mechanically robust as SF. To this end, various crosslinking methods have been described for biopolymer microthreads.^{198,209-211} These methods span a variety of methodologies of crosslinking, such as physical (dehydrothermal (DHT)),^{209,211} irradiative (ultraviolet (UV) light exposure),^{198,211} chemical (carbodiimide or glutaraldehyde incubation),²⁰⁹⁻²¹² or biochemical (transglutaminase).²¹¹ As expected, these methods increase the ultimate tensile strength (UTS), as well as the stiffness of biopolymer microthreads. Interestingly, discrete mechanical properties were developed by modifying the pH environment of the carbodiimide crosslinking reaction for fibrin microthreads.²¹⁰ This suggests that, similar to saturation of transglutaminase crosslinking,²¹³ the efficiency of carbodiimide crosslinking can be regulated both through controlling the pH environment of the crosslinking reaction as well as the total crosslinking time. These crosslinking procedures were also found to significantly increase the stiffness of biopolymer microthreads.²¹⁰ Substrate stiffness is known to have a significant effect on cell behavior.²¹⁴ In the case of skeletal muscle, softer substrates trigger a proliferative phenotype in myoblasts, while stiffer substrates trigger the differentiation and subsequent maturation of new myofibers.¹⁵⁵ Such cell-specific responses to varying substrate stiffnesses highlight the need to closely match both the mechanical and biochemical environment of the scaffold with native muscle tissue to promote tissue regeneration.

2.5.2 Tuning Biochemical Cues

Biochemical cues and receptors are the primary way that cells communicate with each other and their surroundings. Altering the ECM ligands present on a material modulates the cellular response to the material. Matrix cues are known to elicit very specific cellular responses and changing the availability of different matrix molecules will alter the cell phenotype.^{215,216} Additionally, growth factors or cytokines can also be incorporated into scaffolds to enhance cell responses. For example, FGF2 was incorporated into fibrin microthreads to significantly increase fibroblast migration and proliferation, while the initial attachment of the fibroblasts was not affected by FGF2 incorporation.²¹⁷ An advantage to using fibrin as a scaffolding material is

that this fibrin-FGF2 system did not require any intermediate molecules, such as heparin, to facilitate growth factor binding, rather, fibrin itself has an affinity for a large array of growth factors.²¹⁸ Further, a variety of peptide sequences have been identified that can be crosslinked into the fibrin matrix with Factor XIII and will serve as tethering agents to facilitate the controlled release of a specific growth factor as the fibrin scaffold is degraded.^{102,219-221} Other molecules such as heparin sulfate and heparin are commonly used as intermediate molecules for materials such as collagen, SF, or synthetic polymers due to their high binding efficiency to a large number of growth factors.²²² These intermediaries are often tethered using common crosslinking methods such as 1-ethyl-3-(3-dimethylaminopropyl) carbodiimide (EDC), a chemical crosslinking agent that joins primary amine groups to free carboxylic acid groups, to increase bioactivity by conjugating different growth factors or peptides to scaffolds.^{167,223-225}

2.5.3. Tuning Cellular Microniches

Biopolymer fibers made from materials such as collagen, fibrin, or silk have inherent biochemical properties that support cell growth. In particular, fibrin is an essential part of the native provisional matrix that modulates the wound healing response and directs tissue regeneration.^{170,206} Unmodified biopolymer microthreads have been shown to support cell growth and outgrowth along the length of these fibers through a combination of factors including the radius of curvature of the microthreads, biochemical signaling, and integrin receptors present on the surface of the biopolymer microthreads.^{97,198} Additionally, MSCs maintain their multipotency while being cultured on fibrin microthreads, demonstrating that the cell microniche on fibrin microthreads is capable of supporting cells in a more plastic state.²²⁶ By altering the surface chemistry of fibrin microthreads with chemical or irradiative crosslinking, the microniche of the microthreads can be modified to direct cells to proliferate in greater number than without these surface modifications.^{210,217} Further, chemical crosslinking can also be used to alter the biochemical environment to induce enhanced fibroblast proliferation on braided collagen microthreads.¹⁶⁷ By altering the structural organization of the microthreads with static axial stretching, the surface fibrillar structure of fibrin microthreads is modified to incorporate aligned topographic grooves, which direct increased cell alignment along the longitudinal axis of the microthread.¹⁹⁴ Combined, these findings suggest that the microniche of fibrin microthreads

is itself able to support a variety of cell functions including growth, differentiation, and higher-order functions such as complete tissue regeneration.⁷⁶ Further, these scaffolds represent a dynamic platform technology that can be tuned both mechanically and biochemically to elicit specific, controlled cell functions to further guide tissue regeneration.

2.6 CONCLUSIONS AND FUTURE DIRECTIONS

Tissue engineering scaffolds for VML injuries have advanced from passive materials implanted that provide structural support to inductive scaffolds that direct endogenous tissue regeneration. In addition to developing SMUs designed to directly replace lost skeletal muscle tissue, *in vitro* skeletal muscle constructs are a powerful model system to investigate biological questions regarding skeletal muscle formation and regeneration *ex vivo*. Novel strategies have been developed to incorporate essential growth factors, and sophisticated materials have been created to direct skeletal muscle regeneration, and these materials have expanded our knowledge on how VML injuries repair *in situ*. However, scaffolds could support more efficient regeneration by enhancing SC recruitment (i.e. migration) to the defect site to recruit more progenitor cells, as the matrix cues present in traditional muscle regeneration are destroyed or missing in VML injuries. These recruited SCs must be aligned in the direction of the native muscle, so that nascent myofibers can fuse with existing healthy tissue at the wound margin. Finally, controlled structural and mechanical properties are necessary to ensure that scaffolds persist long enough to support organized, functional skeletal muscle regeneration.

In this thesis, we propose to address the limitation of organizing tissue ingrowth to facilitate aligned muscle regeneration by implanting discrete fibrin microthreads into the void created by VML injuries (Figure 2.4 A-B). The resistance to proteolytic degradation of fibrin microthreads will be increased through post-production crosslinking methods to ensure that the microthreads persist long enough to guide functional regeneration *in vivo*. We will load fibrin microthreads with HGF to increase the recruitment of SCs onto fibrin microthreads and into the void space created by VML injuries (Figure 2.4C). We hypothesize that fibrin microthreads with an increased resistance to proteolytic degradation and loaded with HGF will enhance the functional, regeneration of skeletal muscle tissue (Figure 2.5 D-E).

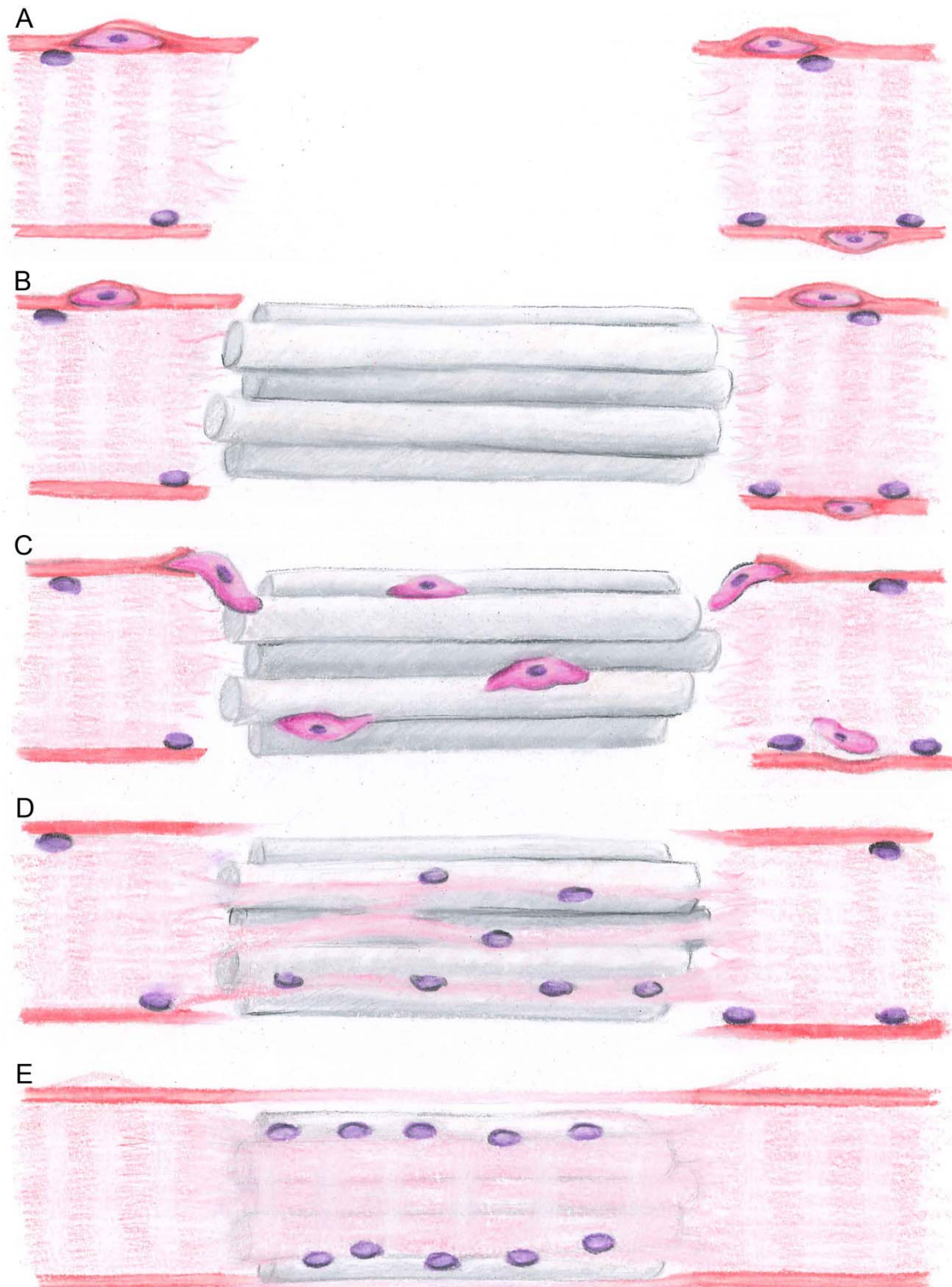


Figure 2.4. Our approach to skeletal muscle regeneration. To regenerate muscle tissue from VML defects (A), fibrin microthreads will be implanted in plane with undamaged muscle (B). Microthreads will be loaded with HGF to recruit SCs to the wound site and begin to proliferate (C) and fuse (D) to regenerate large volumes of muscle tissue (D). Image courtesy of M Zayas.

2.7 REFERENCES

1. Charge SB, Rudnicki MA. Cellular and molecular regulation of muscle regeneration. *Physiol Rev* 2004;84(1):209-38.
2. Quintero AJ, Wright VJ, Fu FH, Huard J. Stem cells for the treatment of skeletal muscle injury. *Clin Sports Med* 2009;28(1):1-11.
3. Bian W, Bursac N. Tissue engineering of functional skeletal muscle: challenges and recent advances. *IEEE Eng Med Biol Mag* 2008;27(5):109-13.
4. Counsel P, Breidahl W. Muscle injuries of the lower leg. *Seminars in musculoskeletal radiology* 2010;14(2):162-75.
5. 2009 report of the 2008 statistics of plastic surgery statistics. American Society of Plastic Surgeons 2009.
6. Eckardt A. Microsurgical reconstruction in the head and neck region: an 18-year experience with 500 consecutive cases. *Journal of Cranio-Maxillofacial Surgery* 2003;31(4):197-201.
7. Masini BD, Waterman SM, Wenke JC, Owens BD, Hsu JR, Ficke JR. Resource utilization and disability outcome assessment of combat casualties from Operation Iraqi Freedom and Operation Enduring Freedom. *J Orthop Trauma* 2009;23(4):261-6.
8. Owens BD, Kragh JF, Jr., Macaitis J, Svoboda SJ, Wenke JC. Characterization of extremity wounds in Operation Iraqi Freedom and Operation Enduring Freedom. *J Orthop Trauma* 2007;21(4):254-7.
9. Grogan BF, Hsu JR. Volumetric muscle loss. *The Journal of the American Academy of Orthopaedic Surgeons* 2011;19 Suppl 1:S35-7.
10. Turner NJ, Badylak SF. Regeneration of skeletal muscle. *Cell and tissue research* 2012;347(3):759-74.
11. Lynch GS, Schertzer JD, Ryall JG. Anabolic agents for improving muscle regeneration and function after injury. *Clin Exp Pharmacol Physiol* 2008;35(7):852-8.
12. Jarvinen TA, Jarvinen TL, Kaariainen M, Aarimaa V, Vaittinen S, Kalimo H, Jarvinen M. Muscle injuries: optimising recovery. *Best practice & research. Clinical rheumatology* 2007;21(2):317-31.
13. Jarvinen TA, Jarvinen TL, Kaariainen M, Kalimo H, Jarvinen M. Muscle injuries: biology and treatment. *Am J Sports Med* 2005;33(5):745-64.
14. Jarvinen TA, Kaariainen M, Jarvinen M, Kalimo H. Muscle strain injuries. *Curr Opin Rheumatol* 2000;12(2):155-61.
15. Mase VJ, Jr., Hsu JR, Wolf SE, Wenke JC, Baer DG, Owens J, Badylak SF, Walters TJ. Clinical application of an acellular biologic scaffold for surgical repair of a large, traumatic quadriceps femoris muscle defect. *Orthopedics* 2010;33(7):511.
16. Kannus P, Parkkari J, Jarvinen TL, Jarvinen TA, Jarvinen M. Basic science and clinical studies coincide: active treatment approach is needed after a sports injury. *Scand J Med Sci Sports* 2003;13(3):150-4.
17. De Coppi P, Bellini S, Conconi MT, Sabatti M, Simonato E, Gamba PG, Nussdorfer GG, Parnigotto PP. Myoblast-acellular skeletal muscle matrix constructs guarantee a long-term repair of experimental full-thickness abdominal wall defects. *Tissue Eng* 2006;12(7):1929-36.
18. Bianchi B, Copelli C, Ferrari S, Ferri A, Sesenna E. Free flaps: outcomes and complications in head and neck reconstructions. *Journal of cranio-maxillo-facial surgery : official publication of the European Association for Cranio-Maxillo-Facial Surgery* 2009;37(8):438-42.
19. Floriano R, Peral B, Alvarez R, Verrier A. Microvascular free flaps in head and neck reconstruction. Report of 71 cases. *Journal of Cranio-Maxillofacial Surgery* 2006;34:90-90.
20. Beier JP, Stern-Straeter J, Foerster VT, Kneser U, Stark GB, Bach AD. Tissue engineering of injectable muscle: three-dimensional myoblast-fibrin injection in the syngeneic rat animal model. *Plast Reconstr Surg* 2006;118(5):1113-21; discussion 1122-4.
21. Huard J, Li Y, Fu FH. Muscle injuries and repair: current trends in research. *J Bone Joint Surg Am* 2002;84-A(5):822-32.
22. Grefte S, Kuijpers-Jagtman AM, Torensma R, Von den Hoff JW. Skeletal muscle development and regeneration. *Stem Cells Dev* 2007;16(5):857-68.
23. Sanes JR. The basement membrane/basal lamina of skeletal muscle. *The Journal of Biological Chemistry* 2003;278(15):12601-4.
24. Cassano M, Quattrocelli M, Crippa S, Perini I, Ronzoni F, Sampaolesi M. Cellular mechanisms and local progenitor activation to regulate skeletal muscle mass. *J Muscle Res Cell Motil* 2009;30(7-8):243-53.

25. Morgan JE, Partridge TA. Muscle satellite cells. *The International Journal of Biochemistry and Cell Biology* 2003;35:1151-1156.
26. Zammit PS, Partridge TA, Yablonka-Reuveni Z. The skeletal muscle satellite cell: the stem cell that came in from the cold. *The Journal of Histochemistry and Cytochemistry : Official Journal of the Histochemistry Society* 2006;54(11):1177-91.
27. Cosgrove BD, Sacco A, Gilbert PM, Blau HM. A home away from home: challenges and opportunities in engineering in vitro muscle satellite cell niches. *Differentiation; research in biological diversity* 2009;78(2-3):185-94.
28. Tidball JG. Mechanisms of muscle injury, repair, and regeneration. *Compr Physiol* 2011;1(4):2029-62.
29. Bodine-Fowler S. Skeletal muscle regeneration after injury: an overview. *J Voice* 1994;8(1):53-62.
30. Hurme T, Kalimo H, Lehto M, Jarvinen M. Healing of skeletal muscle injury: an ultrastructural and immunohistochemical study. *Med Sci Sports Exerc* 1991;23(7):801-10.
31. Carpenter S, Karpati G. Segmental necrosis and its demarcation in experimental micropuncture injury of skeletal muscle fibers. *J Neuropathol Exp Neurol* 1989;48(2):154-70.
32. Tidball JG, Villalta SA. Regulatory interactions between muscle and the immune system during muscle regeneration. *American journal of physiology. Regulatory, integrative and comparative physiology* 2010;298(5):R1173-87.
33. Tatsumi R. Mechano-biology of skeletal muscle hypertrophy and regeneration: possible mechanism of stretch-induced activation of resident myogenic stem cells. *Anim Sci J* 2010;81(1):11-20.
34. Tatsumi R, Hattori A, Ikeuchi Y, Anderson JE, Allen RE. Release of hepatocyte growth factor from mechanically stretched skeletal muscle satellite cells and role of pH and nitric oxide. *Mol Biol Cell* 2002;13(8):2909-18.
35. Tatsumi R, Liu X, Pulido A, Morales M, Sakata T, Dial S, Hattori A, Ikeuchi Y, Allen RE. Satellite cell activation in stretched skeletal muscle and the role of nitric oxide and hepatocyte growth factor. *Am J Physiol Cell Physiol* 2006;290(6):C1487-94.
36. Cannon JG, St Pierre BA. Cytokines in exertion-induced skeletal muscle injury. *Mol Cell Biochem* 1998;179(1-2):159-67.
37. Tatsumi R, Sheehan SM, Iwasaki H, Hattori A, Allen RE. Mechanical stretch induces activation of skeletal muscle satellite cells in vitro. *Experimental Cell Research* 2001;267(1):107-14.
38. Gal-Levi R, Leshem Y, Aoki S, Nakamura T, Halevy O. Hepatocyte growth factor plays a dual role in regulating skeletal muscle satellite cell proliferation and differentiation. *Biochim Biophys Acta* 1998;1402(1):39-51.
39. Tatsumi R, Allen RE. Active hepatocyte growth factor is present in skeletal muscle extracellular matrix. *Muscle Nerve* 2004;30(5):654-8.
40. Tatsumi R, Anderson JE, Nevoret CJ, Halevy O, Allen RE. HGF/SF is present in normal adult skeletal muscle and is capable of activating satellite cells. *Developmental biology* 1998;194(1):114-128.
41. Anderson JE, Wozniak AC. Satellite cell activation on fibers: modeling events in vivo--an invited review. *Can J Physiol Pharmacol* 2004;82(5):300-10.
42. Hayashi S, Aso H, Watanabe K, Nara H, Rose MT, Ohwada S, Yamaguchi T. Sequence of IGF-I, IGF-II, and HGF expression in regenerating skeletal muscle. *Histochemistry and cell biology* 2004;122(5):427-34.
43. deLapeyriere O, Ollendorff V, Planche J, Ott MO, Pizette S, Coulier F, Birnbaum D. Expression of the Fgf6 gene is restricted to developing skeletal muscle in the mouse embryo. *Development* 1993;118:601-611.
44. Floss T, Arnold HH, Braun T. A role for FGF-6 in skeletal muscle regeneration. *Genes Dev* 1997;11(16):2040-51.
45. Cornelison DD, Filla MS, Stanley HM, Rapraeger AC, Olwin BB. Syndecan-3 and syndecan-4 specifically mark skeletal muscle satellite cells and are implicated in satellite cell maintenance and muscle regeneration. *Dev Biol* 2001;239(1):79-94.
46. Sheehan SM, Tatsumi R, Temm-Grove CJ, Allen RE. HGF is an autocrine growth factor for skeletal muscle satellite cells in vitro. *Muscle Nerve* 2000;23(2):239-245.
47. Montarras D, Morgan J, Collins C, Relaix F, Zaffran S, Cumano A, Partridge T, Buckingham M. Direct isolation of satellite cells for skeletal muscle regeneration. *Science* 2005;309(5743):2064-7.
48. Watt DJ, Morgan JE, Clifford MA, Partridge TA. The movement of muscle precursor cells between adjacent regenerating muscles in the mouse. *Anat Embryol* 1987;175(4):527-536.

49. Rosenblatt JD, Yong D, Parry DJ. Satellite cell activity is required for hypertrophy of overloaded adult rat muscle. *Muscle Nerve* 1994;17(6):608-13.
50. Sacco A, Doyonnas R, Kraft P, Vitorovic S, Blau HM. Self-renewal and expansion of single transplanted muscle stem cells. *Nature* 2008;456(7221):502-6.
51. Collins CA, Olsen I, Zammit PS, Heslop L, Petrie A, Partridge TA, Morgan JE. Stem cell function, self-renewal, and behavioral heterogeneity of cells from the adult muscle satellite cell niche. *Cell* 2005;122(2):289-301.
52. Cooper RN, Tajbakhsh S, Mouly V, Cossu G, Buckingham M, Butler-Browne GS. In vivo satellite cell activation via Myf5 and MyoD in regenerating mouse skeletal muscle. *Journal of cell science* 1999;112 (Pt 17):2895-901.
53. Cornelison DD, Wold BJ. Single-cell analysis of regulatory gene expression in quiescent and activated mouse skeletal muscle satellite cells. *Dev Biol* 1997;191(2):270-83.
54. Yablonka-Reuveni Z, Day K, Vine A, Shefer G. Defining the transcriptional signature of skeletal muscle stem cells. *J Anim Sci* 2008;86(14 Suppl):E207-16.
55. Zammit P. Kinetics of Myoblast Proliferation Show That Resident Satellite Cells Are Competent to Fully Regenerate Skeletal Muscle Fibers. *Exp Cell Res* 2002;281(1):39-49.
56. Yablonka-Reuveni Z, Rivera AJ. Temporal expression of regulatory and structural muscle proteins during myogenesis of satellite cells on isolated adult rat fibers. *Dev Biol* 1994;164(2):588-603.
57. Leshem Y, Spicer DB, Gal-Levi R, Halevy O. Hepatocyte growth factor (HGF) inhibits skeletal muscle cell differentiation: a role for the bHLH protein twist and the cdk inhibitor p27. *J Cell Physiol* 2000;184(1):101-9.
58. Kastner S, Elias MC, Rivera AJ, Yablonka-Reuveni Z. Gene Expression Patterns of the Fibroblast Growth Factors and Their Receptors During Myogenesis of Rat Satellite Cells. *Journal of Histochemistry & Cytochemistry* 2000;48(8):1079-1096.
59. O'Reilly C, McKay B, Phillips S, Tarnopolsky M, Parise G. Hepatocyte growth factor (HGF) and the satellite cell response following muscle lengthening contractions in humans. *Muscle Nerve* 2008;38(5):1434-42.
60. Suzuki S, Yamanouchi K, Soeta C, Katakai Y, Harada R, Naito K, Tojo H. Skeletal muscle injury induces hepatocyte growth factor expression in spleen. *Biochem Biophys Res Commun* 2002;292(3):709-14.
61. Menetrey J, Kasemkijwattana C, Day CS, Bosch P, Vogt M, Fu FH, Moreland MS, Huard J. Growth factors improve muscle healing in vivo. *J Bone Joint Surg Br* 2000;82(1):131-7.
62. Pelosi L, Giacinti C, Nardis C, Borsellino G, Rizzuto E, Nicoletti C, Wannenes F, Battistini L, Rosenthal N, Molinaro M and others. Local expression of IGF-1 accelerates muscle regeneration by rapidly modulating inflammatory cytokines and chemokines. *The FASEB journal : official publication of the Federation of American Societies for Experimental Biology* 2007;21(7):1393-402.
63. Engert JC, Berglund EB, Rosenthal N. Proliferation precedes differentiation in IGF-I-stimulated myogenesis. *J Cell Biol* 1996;135(2):431-40.
64. Florini JR, Ewton DZ, Coolican SA. Growth hormone and the insulin-like growth factor system in myogenesis. *Endocr Rev* 1996;17(5):481-517.
65. Florini JR, Ewton DZ, Magri KA. Hormones, growth factors, and myogenic differentiation. *Annu Rev Physiol* 1991;53:201-16.
66. Coolican SA, Samuel DS, Ewton DZ, McWade FJ, Florini JR. The mitogenic and myogenic actions of insulin-like growth factors utilize distinct signaling pathways. *J Biol Chem* 1997;272(10):6653-62.
67. Smith CW, Klaasmeyer JG, Woods TL, Jones SJ. Effects of IGF-I, IGF-II, bFGF and PDGF on the initiation of mRNA translation in C2C12 myoblasts and differentiating myoblasts. *Tissue Cell* 1999;31(4):403-12.
68. Vandeburgh HH, Karlisch P, Shansky J, Feldstein R. Insulin and IGF-I induce pronounced hypertrophy of skeletal myofibers in tissue culture. *Am J Physiol* 1991;260(3 Pt 1):C475-84.
69. Lefaucheur JP, Sebille A. Muscle regeneration following injury can be modified in vivo by immune neutralization of basic fibroblast growth factor, transforming growth factor beta 1 or insulin-like growth factor I. *J Neuroimmunol* 1995;57(1-2):85-91.
70. Keller HL, St Pierre Schneider B, Eppihimer LA, Cannon JG. Association of IGF-I and IGF-II with myofiber regeneration in vivo. *Muscle Nerve* 1999;22(3):347-54.

71. Chakravarthy MV, Davis BS, Booth FW. IGF-I restores satellite cell proliferative potential in immobilized old skeletal muscle. *J Appl Physiol* 2000;89(4):1365-79.
72. Hawke TJ, Garry DJ. Myogenic satellite cells: physiology to molecular biology. *J Appl Physiol* 2001;91:534-551.
73. Lehto M, Jarvinen M, Nelimarkka O. Scar formation after skeletal muscle injury. A histological and autoradiographical study in rats. *Arch Orthop Trauma Surg* 1986;104(6):366-70.
74. Machingal MA, Corona BT, Walters TJ, Kesireddy V, Koval CN, Dannahower A, Zhao W, Yoo JJ, Christ GJ. A tissue-engineered muscle repair construct for functional restoration of an irrecoverable muscle injury in a murine model. *Tissue Eng Part A* 2011;17(17-18):2291-303.
75. Corona BT, Wu X, Ward CL, McDaniel JS, Rathbone CR, Walters TJ. The promotion of a functional fibrosis in skeletal muscle with volumetric muscle loss injury following the transplantation of muscle-ECM. *Biomaterials* 2013;34(13):3324-35.
76. Page RL, Malcuit C, Vilner L, Vojtic I, Shaw S, Hedblom E, Hu J, Pins GD, Rolle MW, Dominko T. Restoration of skeletal muscle defects with adult human cells delivered on fibrin microthreads. *Tissue engineering. Part A* 2011;17(21-22):2629-40.
77. Lehto M, Duance VC, Restall D. Collagen and fibronectin in a healing skeletal muscle injury. An immunohistological study of the effects of physical activity on the repair of injured gastrocnemius muscle in the rat. *J Bone Joint Surg Br* 1985;67(5):820-8.
78. Borselli C, Storie H, Benesch-Lee F, Shvartsman D, Cezar C, Lichtman JW, Vandenburg HH, Mooney DJ. Functional muscle regeneration with combined delivery of angiogenesis and myogenesis factors. *Proc Natl Acad Sci U S A* 2010;107(8):3287-92.
79. Springer ML, Chen AS, Kraft PE, Bednarski M, Blau HM. VEGF gene delivery to muscle: potential role for vasculogenesis in adults. *Mol Cell* 1998;2(5):549-58.
80. Christov C, Chretien F, Abou-Khalil R, Bassez G, Vallet G, Authier FJ, Bassaglia Y, Shinin V, Tajbakhsh S, Chazaud B and others. Muscle satellite cells and endothelial cells: close neighbors and privileged partners. *Molecular biology of the cell* 2007;18(4):1397-409.
81. Mounier R, Chretien F, Chazaud B. Blood vessels and the satellite cell niche. *Curr Top Dev Biol* 2011;96:121-38.
82. Caroni P, Schneider C, Kiefer MC, Zapf J. Role of muscle insulin-like growth factors in nerve sprouting: suppression of terminal sprouting in paralyzed muscle by IGF-binding protein 4. *J Cell Biol* 1994;125(4):893-902.
83. Liu G, Pareta RA, Wu R, Shi Y, Zhou X, Liu H, Deng C, Sun X, Atala A, Opara EC and others. Skeletal myogenic differentiation of urine-derived stem cells and angiogenesis using microbeads loaded with growth factors. *Biomaterials* 2013;34(4):1311-26.
84. Kim MS, Bhang SH, Yang HS, Rim NG, Jun I, Kim SI, Kim BS, Shin H. Development of functional fibrous matrices for the controlled release of basic fibroblast growth factor to improve therapeutic angiogenesis. *Tissue engineering. Part A* 2010;16(10):2999-3010.
85. Fathi E, Nassiri SM, Atyabi N, Ahmadi SH, Imani M, Farahzadi R, Rabbani S, Akhlaghpour S, Sahebjam M, Taheri M. Induction of angiogenesis via topical delivery of basic-fibroblast growth factor from polyvinyl alcohol-dextran blend hydrogel in an ovine model of acute myocardial infarction. *J Tissue Eng Regen Med* 2013;7(9):697-707.
86. Nakamura T, Mizuno S. The discovery of hepatocyte growth factor (HGF) and its significance for cell biology, life sciences and clinical medicine. *Proc Jpn Acad Ser B Phys Biol Sci* 2010;86(6):588-610.
87. Madonna R, Cevik C, Nasser M, De Caterina R. Hepatocyte growth factor: molecular biomarker and player in cardioprotection and cardiovascular regeneration. *Thromb Haemost* 2012;107(4):656-61.
88. Jarvinen TA, Jarvinen M, Kalimo H. Regeneration of injured skeletal muscle after the injury. *Muscles Ligaments Tendons J* 2013;3(4):337-345.
89. Stern-Straeter J, Riedel F, Bran G, Hormann K, Goessler UR. Advances in skeletal muscle tissue engineering. *In Vivo* 2007;21(3):435-44.
90. Koning M, Harmsen MC, van Luyn MJ, Werker PM. Current opportunities and challenges in skeletal muscle tissue engineering. *J Tissue Eng Regen Med* 2009;3(6):407-15.
91. Wolf MT, Dearth CL, Sonnenberg SB, Lobo EG, Badylak SF. Naturally derived and synthetic scaffolds for skeletal muscle reconstruction. *Advanced drug delivery reviews* 2014.

92. Mertens JP, Sugg KB, Lee JD, Larkin LM. Engineering muscle constructs for the creation of functional engineered musculoskeletal tissue. *Regen Med* 2014;9(1):89-100.
93. Liao H, Zhou GQ. Development and progress of engineering of skeletal muscle tissue. *Tissue Eng Part B Rev* 2009;15(3):319-31.
94. Choi JS, Lee SJ, Christ GJ, Atala A, Yoo JJ. The influence of electrospun aligned poly(epsilon-caprolactone)/collagen nanofiber meshes on the formation of self-aligned skeletal muscle myotubes. *Biomaterials* 2008;29(19):2899-906.
95. Shah R, Sinanan AC, Knowles JC, Hunt NP, Lewis MP. Craniofacial muscle engineering using a 3-dimensional phosphate glass fibre construct. *Biomaterials* 2005;26(13):1497-505.
96. Beier JP, Klumpp D, Rudisile M, Dersch R, Wendorff JH, Bleiziffer O, Arkudas A, Polykandriotis E, Horch RE, Kneser U. Collagen matrices from sponge to nano: new perspectives for tissue engineering of skeletal muscle. *BMC Biotechnol* 2009;9:34.
97. Cornwell KG, Downing BR, Pins GD. Characterizing fibroblast migration on discrete collagen threads for applications in tissue regeneration. *J Biomed Mater Res A* 2004;71(1):55-62.
98. Kroehne V, Heschel I, Schugner F, Lasrich D, Bartsch JW, Jockusch H. Use of a novel collagen matrix with oriented pore structure for muscle cell differentiation in cell culture and in grafts. *J Cell Mol Med* 2008;12(5A):1640-8.
99. Norman JJ, Desai TA. Control of cellular organization in three dimensions using a microfabricated polydimethylsiloxane-collagen composite tissue scaffold. *Tissue Eng* 2005;11(3-4):378-86.
100. Williamson MR, Adams EF, Coombes AG. Gravity spun polycaprolactone fibres for soft tissue engineering: interaction with fibroblasts and myoblasts in cell culture. *Biomaterials* 2006;27(7):1019-26.
101. Lutolf MP, Hubbell JA. Synthetic biomaterials as instructive extracellular microenvironments for morphogenesis in tissue engineering. *Nat Biotechnol* 2005;23(1):47-55.
102. Geer DJ, Swartz DD, Andreadis ST. Biomimetic delivery of keratinocyte growth factor upon cellular demand for accelerated wound healing in vitro and in vivo. *American Journal of Pathology* 2005;167(6):1575-1586.
103. Hutmacher DW. Scaffold design and fabrication technologies for engineering tissues--state of the art and future perspectives. *J Biomater Sci Polym Ed* 2001;12(1):107-24.
104. Vandenburg H, Del Tatto M, Shansky J, Lemaire J, Chang A, Payumo F, Lee P, Goodyear A, Raven L. Tissue-engineered skeletal muscle organoids for reversible gene therapy. *Hum Gene Ther* 1996;7(17):2195-200.
105. Vandenburg HH, Hatfaludy S, Karlisch P, Shansky J. Mechanically induced alterations in cultured skeletal muscle growth. *Journal of biomechanics* 1991;24 Suppl 1:91-9.
106. Dennis RG, Kosnik PE, 2nd, Gilbert ME, Faulkner JA. Excitability and contractility of skeletal muscle engineered from primary cultures and cell lines. *Am J Physiol Cell Physiol* 2001;280(2):C288-95.
107. Huang YC, Dennis RG, Larkin L, Baar K. Rapid formation of functional muscle in vitro using fibrin gels. *Journal of Applied Physiology* 2005;98(2):706-713.
108. Kosnik PE, Faulkner JA, Dennis RG. Functional development of engineered skeletal muscle from adult and neonatal rats. *Tissue Eng* 2001;7(5):573-84.
109. Vandenburg H. High-content drug screening with engineered musculoskeletal tissues. *Tissue Eng Part B Rev* 2010;16(1):55-64.
110. Vandenburg H, Shansky J, Benesch-Lee F, Barbata V, Reid J, Thorrez L, Valentini R, Crawford G. Drug-screening platform based on the contractility of tissue-engineered muscle. *Muscle & nerve* 2008;37(4):438-47.
111. Vandenburg H, Shansky J, Benesch-Lee F, Skelly K, Spinazzola JM, Saponjian Y, Tseng BS. Automated drug screening with contractile muscle tissue engineered from dystrophic myoblasts. *FASEB J* 2009;23(10):3325-34.
112. Dennis RG, Kosnik PE, 2nd. Excitability and isometric contractile properties of mammalian skeletal muscle constructs engineered in vitro. *In vitro cellular & developmental biology. Animal* 2000;36(5):327-35.
113. Carosio S, Barberi L, Rizzuto E, Nicoletti C, Del Prete Z, Musaro A. Generation of eX vivo-vascularized Muscle Engineered Tissue (X-MET). *Sci Rep* 2013;3:1420.
114. Borschel GH, Dow DE, Dennis RG, Brown DL. Tissue-engineered axially vascularized contractile skeletal muscle. *Plastic and Reconstructive Surgery* 2006;117(7):2235-42.

115. Williams ML, Kostrominova TY, Arruda EM, Larkin LM. Effect of implantation on engineered skeletal muscle constructs. *J Tissue Eng Regen Med* 2013;7(6):434-42.
116. VanDusen KW, Syverud BC, Williams ML, Lee JD, Larkin LM. Engineered Skeletal Muscle Units for Repair of Volumetric Muscle Loss in the Tibialis Anterior Muscle of a Rat. *Tissue Eng Part A* 2014;20(21-22):2920-2930.
117. Saxena AK, Marler J, Benvenuto M, Willital GH, Vacanti JP. Skeletal muscle tissue engineering using isolated myoblasts on synthetic biodegradable polymers: Preliminary studies. *Tissue Eng* 1999;5(6):525-531.
118. Sicari BM, Rubin JP, Dearth CL, Wolf MT, Ambrosio F, Boninger M, Turner NJ, Weber DJ, Simpson TW, Wyse A and others. An acellular biologic scaffold promotes skeletal muscle formation in mice and humans with volumetric muscle loss. *Science translational medicine* 2014;6(234):234ra58.
119. Thorrez L, Shansky J, Wang L, Fast L, VandenDriessche T, Chuah M, Mooney D, Vandenberg H. Growth, differentiation, transplantation and survival of human skeletal myofibers on biodegradable scaffolds. *Biomaterials* 2008;29(1):75-84.
120. Hill E, Boontheekul T, Mooney DJ. Designing scaffolds to enhance transplanted myoblast survival and migration. *Tissue Eng* 2006;12(5):1295-304.
121. Stern-Straeter J, Bran G, Riedel F, Sauter A, Hormann K, Goessler UR. Characterization of human myoblast cultures for tissue engineering. *Int J Mol Med* 2008;21(1):49-56.
122. Saxena AK, Willital GH, Vacanti JP. Vascularized three-dimensional skeletal muscle tissue-engineering. *Biomed Mater Eng* 2001;11(4):275-81.
123. Cronin EM, Thurmond FA, Bassel-Duby R, Williams RS, Wright WE, Nelson KD, Garner HR. Protein-coated poly(L-lactic acid) fibers provide a substrate for differentiation of human skeletal muscle cells. *J Biomed Mater Res A* 2004;69(3):373-81.
124. Lesman A, Koffler J, Atlas R, Blinder YJ, Kam Z, Levenberg S. Engineering vessel-like networks within multicellular fibrin-based constructs. *Biomaterials* 2011;32(31):7856-69.
125. Hoque ME, San WY, Wei F, Li S, Huang MH, Vert M, Hutmacher DW. Processing of polycaprolactone and polycaprolactone-based copolymers into 3D scaffolds, and their cellular responses. *Tissue Eng Part A* 2009;15(10):3013-24.
126. Grizzi I, Garreau H, Li S, Vert M. Hydrolytic degradation of devices based on poly(DL-lactic acid) size-dependence. *Biomaterials* 1995;16(4):305-11.
127. Li S. Hydrolytic degradation characteristics of aliphatic polyesters derived from lactic and glycolic acids. *J Biomed Mater Res* 1999;48(3):342-53.
128. Ostrovidov S, Hosseini V, Ahadian S, Fujie T, Parthiban SP, Ramalingam M, Bae H, Kaji H, Khademhosseini A. Skeletal muscle tissue engineering: methods to form skeletal myotubes and their applications. *Tissue Eng Part B Rev* 2014;20(5):403-36.
129. Tamayol A, Akbari M, Annabi N, Paul A, Khademhosseini A, Juncker D. Fiber-based tissue engineering: Progress, challenges, and opportunities. *Biotechnol Adv* 2013;31(5):669-87.
130. Neumann T, Hauschka SD, Sanders JE. Tissue engineering of skeletal muscle using polymer fiber arrays. *Tissue Eng* 2003;9(5):995-1003.
131. Guex AG, Birrer DL, Fortunato G, Tevaearai HT, Giraud MN. Anisotropically oriented electrospun matrices with an imprinted periodic micropattern: a new scaffold for engineered muscle constructs. *Biomed Mater* 2013;8(2):021001.
132. Sirivisoot S, Pareta R, Harrison BS. Protocol and cell responses in three-dimensional conductive collagen gel scaffolds with conductive polymer nanofibres for tissue regeneration. *Interface Focus* 2014;4(1):20130050.
133. Ku SH, Lee SH, Park CB. Synergic effects of nanofiber alignment and electroactivity on myoblast differentiation. *Biomaterials* 2012;33(26):6098-104.
134. Chen MC, Sun YC, Chen YH. Electrically conductive nanofibers with highly oriented structures and their potential application in skeletal muscle tissue engineering. *Acta biomaterialia* 2013;9(3):5562-72.
135. Nelson DM, Baraniak PR, Ma Z, Guan J, Mason NS, Wagner WR. Controlled release of IGF-1 and HGF from a biodegradable polyurethane scaffold. *Pharm Res* 2011;28(6):1282-93.
136. Wolf MT, Carruthers CA, Dearth CL, Crapo PM, Huber A, Burns OA, Londono R, Johnson SA, Daly KA, Stahl EC and others. Polypropylene surgical mesh coated with extracellular matrix mitigates the host foreign body response. *J Biomed Mater Res A* 2013.

137. Lam CX, Hutmacher DW, Schantz JT, Woodruff MA, Teoh SH. Evaluation of polycaprolactone scaffold degradation for 6 months in vitro and in vivo. *J Biomed Mater Res A* 2009;90(3):906-19.
138. Zhao W, Ju YM, Christ G, Atala A, Yoo JJ, Lee SJ. Diaphragmatic muscle reconstruction with an aligned electrospun poly(epsilon-caprolactone)/collagen hybrid scaffold. *Biomaterials* 2013;34(33):8235-40.
139. Cobb WS, Kercher KW, Heniford BT. The argument for lightweight polypropylene mesh in hernia repair. *Surg Innov* 2005;12(1):63-9.
140. Klosterhalfen B, Junge K, Klinge U. The lightweight and large porous mesh concept for hernia repair. *Expert Rev Med Devices* 2005;2(1):103-17.
141. Kamelger FS, Marksteiner R, Margreiter E, Klima G, Wechselberger G, Hering S, Piza H. A comparative study of three different biomaterials in the engineering of skeletal muscle using a rat animal model. *Biomaterials* 2004;25(9):1649-55.
142. Kim MS, Jun I, Shin YM, Jang W, Kim SI, Shin H. The development of genipin-crosslinked poly(caprolactone) (PCL)/gelatin nanofibers for tissue engineering applications. *Macromolecular bioscience* 2010;10(1):91-100.
143. Hill E, Boontheekul T, Mooney DJ. Regulating activation of transplanted cells controls tissue regeneration. *Proceedings of the National Academy of Sciences of the United States of America* 2006;103(8):2494-9.
144. Moon du G, Christ G, Stitzel JD, Atala A, Yoo JJ. Cyclic mechanical preconditioning improves engineered muscle contraction. *Tissue engineering. Part A* 2008;14(4):473-82.
145. Rhim C, Lowell DA, Reedy MC, Slentz DH, Zhang SJ, Kraus WE, Truskey GA. Morphology and ultrastructure of differentiating three-dimensional mammalian skeletal muscle in a collagen gel. *Muscle Nerve* 2007;36(1):71-80.
146. Bidarra SJ, Barrias CC, Granja PL. Injectable alginate hydrogels for cell delivery in tissue engineering. *Acta biomaterialia* 2014;10(4):1646-62.
147. Walters BD, Stegemann JP. Strategies for directing the structure and function of three-dimensional collagen biomaterials across length scales. *Acta biomaterialia* 2014;10(4):1488-501.
148. Chattopadhyay S, Raines RT. Review collagen-based biomaterials for wound healing. *Biopolymers* 2014;101(8):821-33.
149. Brown AC, Barker TH. Fibrin-based biomaterials: modulation of macroscopic properties through rational design at the molecular level. *Acta biomaterialia* 2014;10(4):1502-14.
150. Andrejcsk JW, Cui J, Chang WG, Devalliere J, Pober JS, Saltzman WM. Paracrine exchanges of molecular signals between alginate-encapsulated pericytes and freely suspended endothelial cells within a 3D protein gel. *Biomaterials* 2013;34(35):8899-908.
151. Rowley JA, Madlambayan G, Mooney DJ. Alginate hydrogels as synthetic extracellular matrix materials. *Biomaterials* 1999;20(1):45-53.
152. Boontheekul T, Kong HJ, Mooney DJ. Controlling alginate gel degradation utilizing partial oxidation and bimodal molecular weight distribution. *Biomaterials* 2005;26(15):2455-65.
153. Drury JL, Boontheekul T, Mooney DJ. Cellular cross-linking of peptide modified hydrogels. *Journal of Biomechanical Engineering* 2005;127(2):220-8.
154. Wang L, Shansky J, Borselli C, Mooney D, Vandenburg H. Design and fabrication of a biodegradable, covalently crosslinked shape-memory alginate scaffold for cell and growth factor delivery. *Tissue Eng Part A* 2012;18(19-20):2000-7.
155. Boontheekul T, Hill EE, Kong HJ, Mooney DJ. Regulating myoblast phenotype through controlled gel stiffness and degradation. *Tissue Engineering* 2007;13(7):1431-42.
156. Wang L, Cao L, Shansky J, Wang Z, Mooney D, Vandenburg H. Minimally Invasive Approach to the Repair of Injured Skeletal Muscle With a Shape-memory Scaffold. *Molecular therapy : the journal of the American Society of Gene Therapy* 2014;22(8):1441-9.
157. Shvartsman D, Storrer-White H, Lee K, Kearney C, Brudno Y, Ho N, Cezar C, McCann C, Anderson E, Koullias J and others. Sustained delivery of VEGF maintains innervation and promotes reperfusion in ischemic skeletal muscles via NGF/GDNF signaling. *Molecular therapy : the journal of the American Society of Gene Therapy* 2014;22(7):1243-53.
158. Smith MK, Peters MC, Richardson TP, Garbern JC, Mooney DJ. Locally enhanced angiogenesis promotes transplanted cell survival. *Tissue Eng* 2004;10(1-2):63-71.

159. Borselli C, Cezar CA, Shvartsman D, Vandeburgh HH, Mooney DJ. The role of multifunctional delivery scaffold in the ability of cultured myoblasts to promote muscle regeneration. *Biomaterials* 2011;32(34):8905-14.
160. Chevally B, Herbage D. Collagen-based biomaterials as 3D scaffold for cell cultures: applications for tissue engineering and gene therapy. *Med Biol Eng Comput* 2000;38(2):211-8.
161. Parenteau-Bareil R, Gauvin R, Berthod F. Collagen-Based Biomaterials for Tissue Engineering Applications. *Materials* 2010;3(3):1863-1887.
162. Carnio S, Serena E, Rossi CA, De Coppi P, Elvassore N, Vitiello L. Three-dimensional porous scaffold allows long-term wild-type cell delivery in dystrophic muscle. *J Tissue Eng Regen Med* 2011;5(1):1-10.
163. Serena E, Flaibani M, Carnio S, Boldrin L, Vitiello L, De Coppi P, Elvassore N. Electrophysiologic stimulation improves myogenic potential of muscle precursor cells grown in a 3D collagen scaffold. *Neurol Res* 2008;30(2):207-14.
164. van Wachem PB, Brouwer LA, van Luyn MJ. Absence of muscle regeneration after implantation of a collagen matrix seeded with myoblasts. *Biomaterials* 1999;20(5):419-26.
165. Kin S, Hagiwara A, Nakase Y, Kuriu Y, Nakashima S, Yoshikawa T, Sakakura C, Otsuji E, Nakamura T, Yamagishi H. Regeneration of skeletal muscle using in situ tissue engineering on an acellular collagen sponge scaffold in a rabbit model. *ASAIO journal* 2007;53(4):506-13.
166. van Wachem PB, Plantinga JA, Wissink MJ, Beernink R, Poot AA, Engbers GH, Beugeling T, van Aken WG, Feijen J, van Luyn MJ. In vivo biocompatibility of carbodiimide-crosslinked collagen matrices: Effects of crosslink density, heparin immobilization, and bFGF loading. *J Biomed Mater Res* 2001;55(3):368-78.
167. Makridakis JL, Pins GD, Dominko T, Page RL. Design of a novel engineered muscle construct using muscle derived fibroblastic cells seeded onto braided collagen threads. 2009 3-5 April 2009. p 1-2.
168. Frey SP, Jansen H, Raschke MJ, Meffert RH, Ochman S. VEGF improves skeletal muscle regeneration after acute trauma and reconstruction of the limb in a rabbit model. *Clin Orthop Relat Res* 2012;470(12):3607-14.
169. Ju YM, Atala A, Yoo JJ, Lee SJ. In situ regeneration of skeletal muscle tissue through host cell recruitment. *Acta biomaterialia* 2014;10(10):4332-9.
170. Clark RA. Fibrin and wound healing. *Ann N Y Acad Sci* 2001;936:355-67.
171. Chiron S, Tomczak C, Duperray A, Laine J, Bonne G, Eder A, Hansen A, Eschenhagen T, Verdier C, Coirault C. Complex Interactions between Human Myoblasts and the Surrounding 3D Fibrin-Based Matrix. *PLoS ONE* 2012;7(4).
172. Bian W, Bursac N. Engineered skeletal muscle tissue networks with controllable architecture. *Biomaterials* 2009;30(7):1401-12.
173. Martin NR, Passey SL, Player DJ, Khodabakus A, Ferguson RA, Sharples AP, Mudera V, Baar K, Lewis MP. Factors affecting the structure and maturation of human tissue engineered skeletal muscle. *Biomaterials* 2013;34(23):5759-65.
174. Beier JP, Kneser U, Stern-Strater J, Stark GB, Bach AD. Y chromosome detection of three-dimensional tissue-engineered skeletal muscle constructs in a syngeneic rat animal model. *Cell Transplant* 2004;13(1):45-53.
175. Gerard C, Forest MA, Beauregard G, Skuk D, Tremblay JP. Fibrin gel improves the survival of transplanted myoblasts. *Cell Transplant* 2012;21(1):127-37.
176. Hammers DW, Sarathy A, Pham CB, Drinnan CT, Farrar RP, Suggs LJ. Controlled release of IGF-I from a biodegradable matrix improves functional recovery of skeletal muscle from ischemia/reperfusion. *Biotechnology and bioengineering* 2012;109(4):1051-9.
177. Badylak SF. The extracellular matrix as a biologic scaffold material. *Biomaterials* 2007;28(25):3587-93.
178. Badylak SF, Freytes DO, Gilbert TW. Extracellular matrix as a biological scaffold material: Structure and function. *Acta biomaterialia* 2009;5(1):1-13.
179. Brown BN, Badylak SF. Extracellular matrix as an inductive scaffold for functional tissue reconstruction. *Transl Res* 2014;163(4):268-85.
180. Faulk DM, Carruthers CA, Warner HJ, Kramer CR, Reing JE, Zhang L, D'Amore A, Badylak SF. The effect of detergents on the basement membrane complex of a biologic scaffold material. *Acta biomaterialia* 2013.

181. Wolf MT, Daly KA, Reing JE, Badylak SF. Biologic scaffold composed of skeletal muscle extracellular matrix. *Biomaterials* 2012;33(10):2916-25.
182. Conconi MT, De Coppi P, Bellini S, Zara G, Sabatti M, Marzaro M, Zanon GF, Gamba PG, Parnigotto PP, Nussdorfer GG. Homologous muscle acellular matrix seeded with autologous myoblasts as a tissue-engineering approach to abdominal wall-defect repair. *Biomaterials* 2005;26(15):2567-74.
183. Sicari BM, Agrawal V, Siu BF, Medberry CJ, Dearth CL, Turner NJ, Badylak SF. A murine model of volumetric muscle loss and a regenerative medicine approach for tissue replacement. *Tissue Eng Part A* 2012;18(19-20):1941-8.
184. Perniconi B, Costa A, Aulino P, Teodori L, Adamo S, Coletti D. The pro-myogenic environment provided by whole organ scale acellular scaffolds from skeletal muscle. *Biomaterials* 2011;32(31):7870-82.
185. Wolf MT, Daly KA, Brennan-Pierce EP, Johnson SA, Carruthers CA, D'Amore A, Nagarkar SP, Velankar SS, Badylak SF. A hydrogel derived from decellularized dermal extracellular matrix. *Biomaterials* 2012;33(29):7028-38.
186. Wang L, Johnson JA, Chang DW, Zhang Q. Decellularized musculofascial extracellular matrix for tissue engineering. *Biomaterials* 2013;34(11):2641-54.
187. Merritt EK, Hammers DW, Tierney M, Suggs LJ, Walters TJ, Farrar RP. Functional assessment of skeletal muscle regeneration utilizing homologous extracellular matrix as scaffolding. *Tissue Eng Part A* 2010;16(4):1395-405.
188. Chen XK, Walters TJ. Muscle-derived decellularised extracellular matrix improves functional recovery in a rat latissimus dorsi muscle defect model. *J Plast Reconstr Aesthet Surg* 2013;66(12):1750-8.
189. Merritt EK, Cannon MV, Hammers DW, Le LN, Gokhale R, Sarathy A, Song TJ, Tierney MT, Suggs LJ, Walters TJ and others. Repair of traumatic skeletal muscle injury with bone-marrow-derived mesenchymal stem cells seeded on extracellular matrix. *Tissue Eng Part A* 2010;16(9):2871-81.
190. Corona BT, Machingal MA, Criswell T, Vadhavkar M, Dannahower AC, Bergman C, Zhao W, Christ GJ. Further development of a tissue engineered muscle repair construct in vitro for enhanced functional recovery following implantation in vivo in a murine model of volumetric muscle loss injury. *Tissue Eng Part A* 2012;18(11-12):1213-28.
191. Valentin JE, Turner NJ, Gilbert TW, Badylak SF. Functional skeletal muscle formation with a biologic scaffold. *Biomaterials* 2010;31(29):7475-84.
192. Corona BT, Ward CL, Baker HB, Walters TJ, Christ GJ. Implantation of in vitro tissue engineered muscle repair constructs and bladder acellular matrices partially restore in vivo skeletal muscle function in a rat model of volumetric muscle loss injury. *Tissue Eng Part A* 2014;20(3-4):705-15.
193. Matsumoto T, Sasaki J, Alsberg E, Egusa H, Yatani H, Sohmura T. Three-dimensional cell and tissue patterning in a strained fibrin gel system. *PLoS ONE* 2007;2(11):e1211.
194. Grasman JM, Pumphrey LM, Dunphy M, Perez-Rogers J, Pins GD. Static axial stretching enhances the mechanical properties and cellular responses of fibrin microthreads. *Acta biomaterialia* 2014;10(10):4367-76.
195. Stratos I, Graff J, Rotter R, Mittlmeier T, Vollmar B. Open blunt crush injury of different severity determines nature and extent of local tissue regeneration and repair. *Journal of orthopaedic research : official publication of the Orthopaedic Research Society* 2010;28(7):950-7.
196. Wu X, Corona BT, Chen X, Walters TJ. A Standardized Rat Model of Volumetric Muscle Loss Injury for the Development of Tissue Engineering Therapies. *BioResearch Open Access* 2012;1(6):280-290.
197. Laurencin CT, Freeman JW. Ligament tissue engineering: an evolutionary materials science approach. *Biomaterials* 2005;26(36):7530-6.
198. Cornwell KG, Pins GD. Discrete crosslinked fibrin microthread scaffolds for tissue regeneration. *J Biomed Mater Res A* 2007;82(1):104-12.
199. Pins GD, Christiansen DL, Patel R, Silver FH. Self-assembly of collagen fibers. Influence of fibrillar alignment and decorin on mechanical properties. *Biophysical Journal* 1997;73:2164-2172.
200. Vepari C, Kaplan DL. Silk as a Biomaterial. *Prog Polym Sci* 2007;32(8-9):991-1007.
201. Kluge JA, Rabotyagova O, Leisk GG, Kaplan DL. Spider silks and their applications. *Trends Biotechnol* 2008;26(5):244-51.
202. Altman GH, Horan RL, Lu HH, Moreau J, Martin I, Richmond JC, Kaplan DL. Silk matrix for tissue engineered anterior cruciate ligaments. *Biomaterials* 2002;23(20):4131-41.

203. Altman GH, Diaz F, Jakuba C, Calabro T, Horan RL, Chen J, Lu H, Richmond J, Kaplan DL. Silk-based biomaterials. *Biomaterials* 2003;24(3):401-16.
204. Perez-Rigueiro J, Viney C, Llorca J, Elices M. Mechanical properties of single-brin silkworm silk. *Journal of Applied Polymer Science* 2000;75(10):1270-1277.
205. Rodrigues MT, Reis RL, Gomes ME. Engineering tendon and ligament tissues: present developments towards successful clinical products. *J Tissue Eng Regen Med* 2013;7(9):673-86.
206. Mosesson MW. Fibrinogen and fibrin structure and functions. *J Thromb Haemost* 2005;3(8):1894-904.
207. Ahmann KA, Weinbaum JS, Johnson SL, Tranquillo RT. Fibrin degradation enhances vascular smooth muscle cell proliferation and matrix deposition in fibrin-based tissue constructs fabricated in vitro. *Tissue Eng Part A* 2010;16(10):3261-70.
208. Lu HH, Cooper JA, Jr., Manuel S, Freeman JW, Attawia MA, Ko FK, Laurencin CT. Anterior cruciate ligament regeneration using braided biodegradable scaffolds: in vitro optimization studies. *Biomaterials* 2005;26(23):4805-16.
209. Cornwell KG, Lei P, Andreadis ST, Pins GD. Crosslinking of discrete self-assembled collagen threads: Effects on mechanical strength and cell-matrix interactions. *J Biomed Mater Res A* 2007;80(2):362-71.
210. Grasman JM, Page RL, Dominko T, Pins GD. Crosslinking strategies facilitate tunable structural properties of fibrin microthreads. *Acta Biomaterialia* 2012;8(11):4020-30.
211. Zeugolis DI, Paul GR, Attenburrow G. Cross-linking of extruded collagen fibers--a biomimetic three-dimensional scaffold for tissue engineering applications. *Journal of biomedical materials research. Part A* 2009;89(4):895-908.
212. Walters VI, Kwansa AL, Freeman JW. Design and analysis of braid-twist collagen scaffolds. *Connect Tissue Res* 2012;53(3):255-66.
213. Orban JM, Wilson LB, Kofroth JA, El-Kurdi MS, Maul TM, Vorp DA. Crosslinking of collagen gels by transglutaminase. *J Biomed Mater Res A* 2004;68(4):756-62.
214. Engler AJ, Sen S, Sweeney HL, Discher DE. Matrix elasticity directs stem cell lineage specification. *Cell* 2006;126(4):677-89.
215. Eckes B, Nischt R, Krieg T. Cell-matrix interactions in dermal repair and scarring. *Fibrogenesis Tissue Repair* 2010;3:4.
216. Reilly GC, Engler AJ. Intrinsic extracellular matrix properties regulate stem cell differentiation. *Journal of biomechanics* 2010;43(1):55-62.
217. Cornwell KG, Pins GD. Enhanced proliferation and migration of fibroblasts on the surface of fibroblast growth factor-2-loaded fibrin microthreads. *Tissue Eng Part A* 2010;16(12):3669-77.
218. Martino MM, Briquez PS, Ranga A, Lutolf MP, Hubbell JA. Heparin-binding domain of fibrin(ogen) binds growth factors and promotes tissue repair when incorporated within a synthetic matrix. *Proc Natl Acad Sci U S A* 2013;110(12):4563-8.
219. Sakiyama SE, Schense JC, Hubbell JA. Incorporation of heparin-binding peptides into fibrin gels enhances neurite extension: an example of designer matrices in tissue engineering. *FASEB J* 1999;13(15):2214-24.
220. Sakiyama-Elbert SE, Hubbell JA. Controlled release of nerve growth factor from a heparin-containing fibrin-based cell ingrowth matrix. *J Control Release* 2000;69(1):149-58.
221. Liang MS, Andreadis ST. Engineering fibrin-binding TGF-beta1 for sustained signaling and contractile function of MSC based vascular constructs. *Biomaterials* 2011;32(33):8684-93.
222. Sakiyama-Elbert SE. Incorporation of heparin into biomaterials. *Acta biomaterialia* 2014;10(4):1581-7.
223. Pieper JS, Hafmans T, Veerkamp JH, van Kuppevelt TH. Development of tailor-made collagen-glycosaminoglycan matrices: EDC/NHS crosslinking, and ultrastructural aspects. *Biomaterials* 2000;21(6):581-93.
224. Wissink MJ, Beernink R, Pieper JS, Poot AA, Engbers GH, Beugeling T, van Aken WG, Feijen J. Binding and release of basic fibroblast growth factor from heparinized collagen matrices. *Biomaterials* 2001;22(16):2291-9.
225. Wissink MJ, Beernink R, Pieper JS, Poot AA, Engbers GH, Beugeling T, van Aken WG, Feijen J. Immobilization of heparin to EDC/NHS-crosslinked collagen. Characterization and in vitro evaluation. *Biomaterials* 2001;22(2):151-63.
226. Proulx MK, Carey SP, Ditroia LM, Jones CM, Fakhrazadeh M, Guyette JP, Clement AL, Orr RG, Rolle MW, Pins GD and others. Fibrin microthreads support mesenchymal stem cell growth while maintaining differentiation potential. *J Biomed Mater Res A* 2011;96(2):301-12.

Chapter 3: Crosslinking Strategies Facilitate Tunable Structural Properties of Fibrin Microthreads¹

3.1 INTRODUCTION

Scaffolds that direct skeletal muscle regeneration must facilitate alignment and organization of newly forming muscle fibers parallel to the uniaxial force conduction pathway.^{2,3} To best promote *de novo* muscle regeneration in a large defect, the scaffold must also be biocompatible, support cell ingrowth from the surrounding musculature, and ultimately degrade as new tissue forms.^{2,4} Several studies have investigated synthetic materials and natural polymers, such as a copolymer of poly(L-Lactic acid) and poly(L-glycolic acid)polyglycolic/polylactic acid (PLLA/PLGA),⁵ poly(ϵ -caprolactone) (PCL),^{6,7} alginate,^{8,9} Matrigel,¹⁰ decellularized muscle tissue,¹¹⁻¹³ collagen,¹⁴⁻¹⁷ and fibrin,^{4,5,18,19} as scaffolds to facilitate muscle regeneration. While synthetic scaffolds are advantageous for generating materials with aligned fibrillar morphology, they are commonly modified with bioactive signaling molecules, such as collagen, to direct cell-mediated tissue regeneration.⁶ Biopolymer scaffolds that are fabricated from extracellular matrix molecules such as collagen or fibrin possess intrinsic bioactive signaling cues, however, it can be challenging to engineer biopolymer scaffolds with precisely designed biochemical and biophysical surface cues to guide specific cell functions.^{15,20} Previous studies have primarily focused on the effects of scaffold compositions on cell and tissue responses such as myoblast proliferation, differentiation, and tissue regeneration. In contrast, few studies have systematically characterized the roles of scaffold degradation or growth factor elution on skeletal muscle regeneration.

Several studies have investigated the use of fibrin-based scaffolds to facilitate skeletal muscle regeneration. While its role as a provisional matrix makes fibrin an appealing material for tissue regeneration due to its ability to direct wound healing, it is highly susceptible to proteolytic degradation and remodeling in the presence of myoblasts.^{19,21} Various materials processing strategies have been investigated to increase the structural stability and the

persistence of fibrin-based scaffolds including chemical and physical crosslinking with agents such as transglutaminase/Factor XIII,^{22,23} ruthenium sodium persulfate,^{24,25} and ultraviolet (UV) light.²⁶ These crosslinking strategies demonstrated enhanced fibrin scaffold stiffness without affecting cell viability, but they did not show correlations between increases in stiffness with resistance to proteolytic degradation. One alternate approach to increasing the structural and mechanical stability of fibrin scaffolds has been to mix PLLA/PLGA into the fibrin scaffold.⁵ However, this method does not improve the intrinsic structural stability of fibrin, but it replaces it with a porous PLLA/PLGA scaffold. As such, there remains a need to develop fibrin based materials with increased resistance to proteolytic degradation for long term cell culture or implantation studies.

Our laboratory developed novel biomaterial constructs termed fibrin microthreads, which integrate the bioactivity of fibrin gel scaffolds with an aligned fiber matrix that directs cell alignment. We showed that the mechanical properties of these microthreads can be modulated by crosslinking with UV energy,²⁶ and that we could incorporate growth factors into these microthreads to direct cell proliferation and outgrowth on the surfaces of the scaffolds in a dose and time dependent manner.²⁷ When uncrosslinked fibrin microthreads were implanted in large muscle defects in a mouse model, we found that cell-populated microthreads enhanced the regenerative response of the host tissue, allowing for more complete endogenous muscle repair.⁴ While we observed a reduction in scar tissue deposition at later time points of the study (3-4 months), histological analyses of tissue harvested at early time points suggested that the microthreads were largely degraded within 2 weeks of implantation and many of the regenerated myofibers in the wound site at later time points exhibited misalignment with respect to the native muscle tissue. Other studies indicate that skeletal muscle tissue regeneration peaks 2 to 3 weeks post injury, suggesting that scaffold persistence in the wound site is critical for facilitating the regeneration of functional, organized skeletal muscle tissue.²⁸ From these findings, we hypothesize that myofiber formation and alignment as well as functional skeletal muscle regeneration will be enhanced by the persistence of fibrin microthreads that facilitate organized tissue deposition in the wound site.

This chapter reports on the results of the first study to investigate the use of 1-ethyl-3-(3-dimethylaminopropyl) carbodiimide (EDC) as a crosslinking strategy for fibrin

microthreads. While carbodiimide crosslinking is a robust approach to modulate the mechanical properties of collagen scaffolds,^{29,30} and to tether growth factors to the surface of scaffolds,^{31,32} it has not previously been used on fibrin-based materials. Previous studies showed that optimal carbodiimide-mediated crosslinking occurs in an acidic environment,³³ but previous unpublished studies from our lab suggest that this environment adversely affects the ultimate tensile strength (UTS) of fibrin microthreads during scaffold production. Here, we examined the effects of EDC crosslinking time and buffer pH on the structural and biochemical properties of fibrin microthreads. We hypothesized that the use of different buffer pH levels for the EDC crosslinking reaction would permit control of the degree of crosslinking and result in the ability to generate microthreads with tunable mechanical properties and plasmin degradation rates that might be more suitable for use as a scaffold to promote skeletal muscle regeneration.

3.2 MATERIALS and METHODS

3.2.1 Fibrin Microthread Preparation

3.2.1.1 Microthread Extrusion

Fibrin microthreads were co-extruded from solutions of fibrinogen and thrombin using extrusion techniques described previously.²⁶ Briefly, fibrinogen from bovine plasma (Sigma, St. Louis, MO; F8630) was dissolved in HEPES (N-[2-Hydroxyethyl]piperazine-N'-[2-ethanesulfonic acid]) buffered saline (HBS, 20 mM HEPES, 0.9% NaCl; pH 7.4) at 70 mg/mL and stored at -20 °C until use. Thrombin from bovine plasma (Sigma; T4648) was dissolved in HBS at 40 U/mL and stored at -20 °C until use.

To fabricate microthreads, fibrinogen and thrombin solutions were warmed to room temperature, and thrombin was mixed with a 40 mM CaCl₂ (Sigma) solution to form a working solution of 6 U/mL. Fibrinogen and thrombin/CaCl₂ solutions were loaded into 1 mL syringes which were inserted into a blending applicator tip (Micromedics Inc., St. Paul, MN; SA-3670). The solutions were combined in the blending applicator and extruded through polyethylene tubing (BD, Sparks, MD) with an inner diameter of 0.86 mm into a bath of 10 mM HEPES (pH 7.4) in a Teflon coated pan at a rate of 0.225 mL/min using a dual syringe pump. After 8-15 minutes, 25.4 cm, amorphous fibrin microthreads were removed from the buffer solution and stretched to form three-19-cm microthreads; these were air dried under the tension of their own

weight. Dry microthreads were placed in aluminum foil and stored in a desiccator until use.

3.2.1.2 EDC Crosslinking Procedure

Fibrin microthreads were affixed to vellum frames with a window size of 4 cm using medical-grade silicone adhesive (Factor II, Lakeside, AZ). Once the glue was cured, microthreads were hydrated in either acidic buffer (50 mM 2-(N-morpholino)ethanesulfonic acid (MES), Sigma, pH 5.0) or neutral buffer (100 mM NaH₂PO₄, Sigma, pH 7.4) for 30 minutes at room temperature. Hydrated fibrin microthreads were crosslinked at room temperature with either acidic (EDCa) or neutral (EDCn) buffer containing 16 mM N-hydroxysuccinimide (NHS, Sigma) and 28 mM EDC (Sigma) for 1, 2, 3, 4, 12, or 24 hours. Control microthreads were either not rehydrated (UNX), or hydrated with distilled water (UNXdi), acidic buffer (UNXa), or neutral buffer (UNXn) in the absence of EDC/NHS for two hours. After crosslinking, the buffered EDC/NHS solution was aspirated and the microthreads were rinsed three times in a DI (de-ionized) water bath for 5 minutes each rinse, air dried, and stored in a desiccator until use.

3.2.2 Mechanical Characterization of Crosslinked Microthreads

To facilitate uniaxial testing, individual microthreads were affixed with medical grade silicone adhesive to vellum paper frames with precut windows that defined the region of loading. An initial gage length of 2.0 cm was defined as the distance between adhesive spots at the edges of the precut window in the vellum frame. The microthreads on the vellum frames were hydrated in phosphate buffered saline (PBS) for at least 60 minutes prior to testing. Hydrated microthread diameters were measured using a calibrated reticule with a 10X objective, coupled to a Nikon Eclipse E600 upright microscope (Melville, NY). Microthreads were assumed to be cylindrical, and the average diameter calculated from 3 measurements taken along the length of each microthread defined the cross-sectional area. After hydration, microthreads were mounted in the grips of a uniaxial testing machine (ElectroPuls E1000; Instron, Norwood, MA) and a 1 N load cell, the edges of each vellum frame were cut, and the microthreads were uniaxially loaded until failure at a 50% strain rate (10 mm/min) relative to the initial gage length. Force and displacement were recorded continuously throughout each test at a frequency of 10 Hz. The mechanical failure load of each microthread was recorded as the point where a rapid (80%) drop

from the maximum load occurred. Engineering stress was calculated as the amount of force detected by the load cell divided by the initial cross-sectional area. Strain was calculated as the increased extension from the gage-length.

A MATLAB (MathWorks, Natick, MA) script was written to analyze the UTS, strain at failure (SAF), and load at failure for each sample. A script was created in Excel (Microsoft, Redmond, WA) to characterize the maximum tangent modulus (MTM), which was assessed by identifying the highest linear region of the stress-strain curve for each sample (over a range of time corresponding to 20% of the length of each test) and fitting it to a linear region of the stress-strain curve. Statistical analysis was used to identify and remove outliers as defined by microthreads whose wet diameters were 1.5 times greater than the inner quartile range (IQR) for each sample set (average wet diameter $\pm 1.5 * \text{IQR}$). To ensure this method was robust, we determined that the distribution of wet diameter measurements was normal using SigmaPlot 11.0 software (Systat Software, Inc., San Jose, CA) to validate our definition, and exclusion, of outliers. Data points falling outside of this range were excluded from later statistical analysis.

3.2.3 Structural Characterization of Crosslinked Microthreads

3.2.3.1 Microthread Swelling

Prior to mechanical testing, the diameters of dry crosslinked microthreads were recorded using a calibrated reticule with a 10X objective. The average diameter for each microthread was calculated from three measurements taken along the length. The wet diameter measurements taken during the mechanical testing procedure were also used to calculate the swelling ratio which was defined as the ratio of the wet diameter of a microthread to its dry diameter (wet/dry diameter).

3.2.3.2 Degradation Assay

Single crosslinked microthreads were cut into 0.8 cm fragments and secured to the bottom of 48-well plates using medical grade silicone adhesive (Figure 3.1A). Stock solutions of human plasmin (EMD Biosciences, San Diego, CA; 527621) were aliquoted and stored according to the manufacturer's instructions. Each experimental condition was run in triplicate. Microthreads were hydrated in 500 μL of tris buffered saline (TBS; 25 mM Tris-HCl (Sigma),

0.9% NaCl, pH 7.5) for 1 hour, and images were taken with a 10X objective on a Leica inverted microscope (Leica, Wetzlar, Germany) coupled with Leica imaging software to record diameter values at time 0 (d_0 , Figure 3.1B). The TBS was aspirated and replaced with 500 μ L of 0.1 U/mL of plasmin in TBS and samples were incubated at 37 °C until analysis for degradation by imaging. Microthreads were imaged every two hours for the first 6 hours, and subsequently every 12 hours, or until they were completely degraded (Figure 3.1C). Each image was processed with ImageJ (NIH) to measure the microthreads' diameter at three different positions along the length and plotted as a ratio to the initial diameter value (d/d_0).

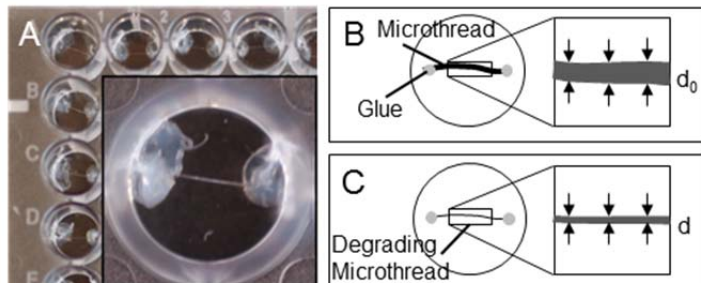


Figure 3.1. Experimental configuration of the degradation assay. Macroscopic view of degradation assay in a 48 well plate (A). Microthreads 0.8 cm in length were glued to the bottom of individual wells with medical grade silicone adhesive (inset). After initial hydration, the microthreads were visualized and the diameter measurements across three different areas of the microthread were averaged together to calculate the initial microthread diameter, d_0 (B). Images were periodically taken of each microthread to measure the diameter and quantify the amount of degradation as a function of time (C).

3.2.4 Cell Culture

Immortalized mouse myoblasts (ATCC, Manassas, VA; C2C12) were cultured in a 1:1 (v/v) ratio of high glucose Dulbecco's modified Eagle Medium (DMEM, Gibco BRL, Gaithersburg, MD) supplemented with 4 mM L-glutamine and Ham's F12 (Gibco) with 10% fetal bovine serum (FBS, HyClone, Logan, UT). Cells were incubated at 37 °C with 5% CO₂ and maintained at a density below 70% confluence using standard cell culture techniques. Routine cell passage was conducted using 0.25% trypsin-EDTA (CellGro, Manassas, VA).

3.2.5 Cell Attachment Assay

3.2.5.1 Microthread Bundling and Seeding

To facilitate cell seeding for cell attachment assays, microthreads were bundled together in groups of 10 and adhered to stainless steel rings (Seastrom Manufacturing, Twin Falls, ID; inner diameter, 0.750 inches; outer diameter, 1.188 inches; thickness, 0.005 inches) with medical

grade silicone adhesive. Individual washers were placed in wells of a standard six-well plate over an elevated 13 mm diameter circular Thermanox™ coverslip (Nalge Nunc International, Rochester, NY), as described previously.³⁴ Prior to cell seeding, microthread bundles were sterilized in 70% ethanol for 1 hour, rinsed in deionized (DI) water 3 times, air dried in a laminar flow hood, and stored in a desiccator until use.

Immediately prior to seeding, 150 μ L of sterile PBS was added to the coverslip to hydrate the microthreads for at least 1 hour. To attach C2C12 cells to the microthread bundles, the PBS was aspirated and replaced with 100 μ L of cell suspension (100,000 cells/mL) in complete culture medium. After a 4 hr incubation at 37 °C, cell-seeded microthread bundles were transferred into a new six-well plate with 2 mL of fresh medium and returned to the incubator. Each experimental treatment was run in duplicate and medium was changed every 2 days.

3.2.5.2 Analysis of Cell Viability

To characterize cell morphology and viability a viability assay was conducted after either 3 or 7 days of culture using a Live/Dead Stain Kit (Molecular Probes, Eugene, OR; L3224) according to the manufacturer's instructions. At each time point, the medium was aspirated and replaced with 2 mL of sterile PBS with 4 μ M ethidium homodimer-1 and 2 μ M calcein AM and plates were incubated at room temperature for 30 minutes. Calcein (green, Ex/em 495 nm/515 nm) is retained in the cytoplasm of living cells while ethidium (red, Ex/em 495 nm/635 nm) is excluded by intact cell membranes and enters damaged membranes where it binds nuclear DNA. Microthread bundles were visualized on a Leica inverted microscope using a 10X objective and dye-appropriate filter sets and photomicrographs were collected and processed using Leica imaging software.

3.2.5.3 Analysis of Cell Number

Quantification of the cell density of C2C12 cells on microthread bundles was determined after 1 or 3 days of culture. At each time point, cell-seeded microthread bundles were fixed in 10% neutral buffered formalin for 15 minutes and rinsed 3 times in DI water. Constructs were stained with Hoechst (1:6000, Molecular Probes) for 6 minutes and rinsed 3 times with DI water. Three regions of the cell-seeding area were visualized on a Leica inverted

microscope using a 10X objective and photomicrographs taken using Leica imaging software and images of nuclei were counted using ImageJ. To calculate cell density on the surface of the microthread bundles, it was assumed that images corresponded to one half of the surface area of the microthread bundle. Approximating a cylindrical geometry for each bundle, length (l) and diameter (d) measurements enabled calculation of the total surface area (SA) as: $SA = 0.5 * \pi * l * d$. Total cell number was divided by the SA of each image to calculate the cell surface density.

3.2.6 Statistical Analyses

Statistical analyses were performed using a one-way analysis of variance (ANOVA) with $p < 0.05$ indicating significant differences between groups using SigmaPlot 11.0 software. For post hoc analysis, a Holm-Sidak pairwise multiple comparison test was performed to determine significance between experimental groups using an overall significance level of $p < 0.05$. Where indicated, a paired Student's t-test was performed with $p < 0.05$ indicating significant differences between groups. The data are reported as means \pm standard deviation for the mechanical and structural characterization and as means \pm standard error for the cell density values (3 measurements were obtained per microthread bundle).

3.3 RESULTS

3.3.1 Crosslinking Enhances the Ultimate Tensile Strength of Fibrin Microthreads

Biopolymer microthreads designed as tissue engineering scaffolds are required to have mechanical properties comparable to the native tissues they are replacing. Fibrin microthreads were crosslinked in an acidic or a neutral pH buffer, mounted onto vellum test frames, and uniaxially loaded until failure to determine the mechanical properties of crosslinked microthreads. Characteristic stress-strain curves of uncrosslinked and EDC crosslinked microthreads showed initial toe regions of increasing elongation with little increase in stress (Figure 3.2A). However, the crosslinked microthreads displayed a much shorter toe region than uncrosslinked microthreads, followed by a much more rapid increase in stress until failure (Figure 3.2A). UTS values of microthreads crosslinked for 4 and 12 hours were significantly greater than UNX microthreads (Figure 3.2B). There were no significant differences between

the UTS values of crosslinked microthreads as a function of buffer pH or time, and the UTS values of EDCa 24hr microthreads were not significantly greater than UNX microthreads. Control microthreads incubated in acidic buffer without EDC for 24 hours were completely degraded (data not shown). To further characterize the effects of EDC crosslinking time and buffer pH on the mechanical properties of fibrin microthreads, we conducted an additional series of experiments that examined shorter crosslinking time points. The results of this study showed that all EDC crosslinked microthreads were significantly stronger than UNX microthreads (Figure 3.2C), independent of the crosslinking buffer.

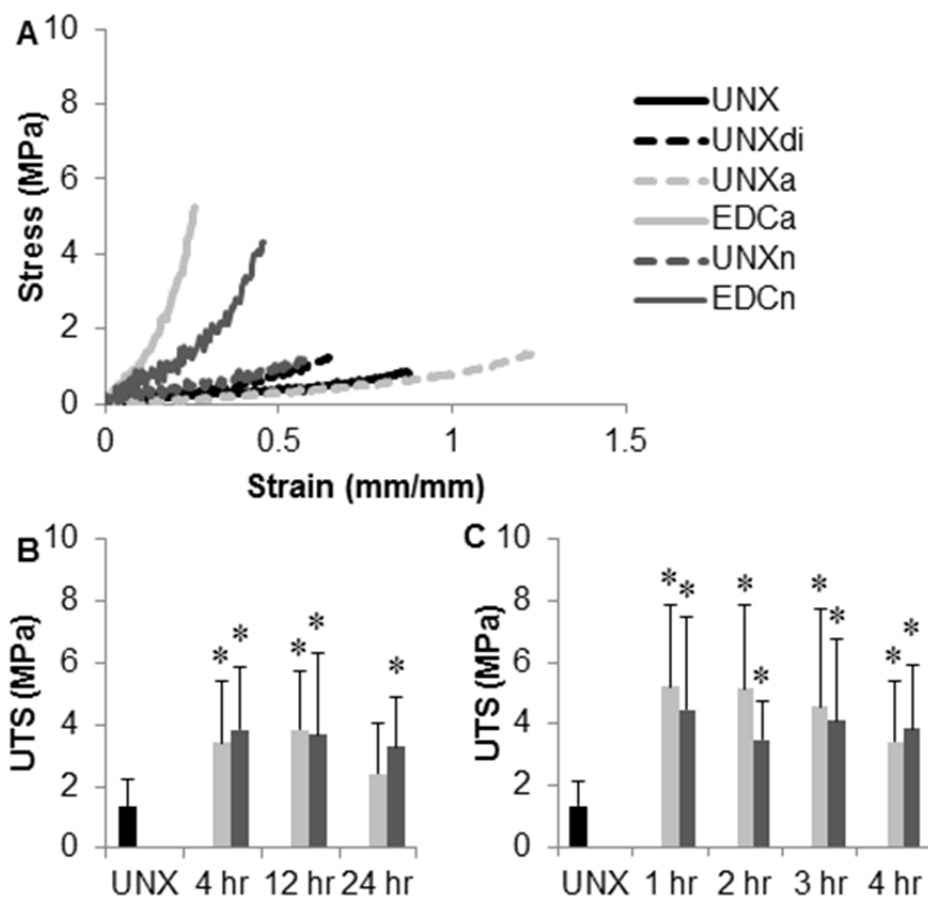


Figure 3.2. Mechanical properties of microthreads as a function of crosslinking time and buffer. Characteristic stress-strain curves for fibrin microthreads (A). Fibrin microthreads exhibited an initial toe region and in the case of the crosslinked microthreads, were followed by a rapid increase in stress until failure. Uncrosslinked microthreads displayed low stiffness and highly elastic toe regions, regardless of buffer treatment. UTS of fibrin microthreads crosslinked for 4, 12, or 24 hours (B; $n \geq 18$). UTS of fibrin microthreads crosslinked for 1, 2, 3 or 4 hours (C; $n \geq 30$). * indicates significant differences with respect to UNX microthreads by one-way ANOVA with Holm-Sidak post hoc analysis ($p < 0.05$).

To evaluate the effects of buffer pH conditions on the mechanical properties of fibrin microthreads, microthreads were incubated in crosslinking buffer solutions with or without EDC for 2 hours. The mean diameters, peak loads, UTS, SAF, and MTM of these microthreads are summarized in Table 3.1. The UTS of microthreads crosslinked for two hours were found to be dependent on crosslinking buffer pH, and all crosslinked microthreads (EDCn and EDCa) were significantly stronger than microthreads incubated in buffer conditions without the addition of EDC (Figure 3.3A). EDCa microthreads failed at significantly lower strains than UNXa and UNX microthreads (Figure 3.3B). EDCa microthreads had significantly higher moduli than EDCn, and all crosslinked microthreads were significantly stiffer than uncrosslinked controls (Figure 3.3C).

Table 3.1. The mechanical and structural properties of EDC crosslinked fibrin microthreads.

| | Sample Size (n) | Diameter (μm) | | Swelling Ratio | UTS (MPa) | MTM (MPa) | SAF (mm/mm) | Load (mN) |
|-------|-----------------|----------------------------|------------------|----------------|-----------------|-------------------|-------------------|-----------------|
| | | dry | wet | | | | | |
| UNX | 41 | 57.6 \pm 16.5 | 136.2 \pm 43.4 | 2.5 \pm 0.3 | 1.35 \pm 0.77 | 3.38 \pm 2.31 | 0.580 \pm 0.210 | 17.5 \pm 9.7 |
| UNXdi | 36 | 61.7 \pm 12.6 | 132.2 \pm 25.6 | 2.1 \pm 0.2 | 1.54 \pm 0.91 | 5.09 \pm 2.59 | 0.522 \pm 0.199 | 20.6 \pm 13.7 |
| UNXa | 33 | 61.8 \pm 18.7 | 143.3 \pm 48.9 | 2.4 \pm 0.2 | 1.86 \pm 2.35 | 4.22 \pm 3.71 | 0.652 \pm 0.313 | 21.4 \pm 13.2 |
| EDCa | 32 | 62.0 \pm 18.0 | 93.9 \pm 25.9 | 1.6 \pm 0.1 | 5.14 \pm 2.71 | 22.42 \pm 17.66 | 0.355 \pm 0.281 | 34.6 \pm 21.5 |
| UNXn | 42 | 60.0 \pm 14.7 | 124.8 \pm 35.6 | 2.3 \pm 0.2 | 1.81 \pm 0.95 | 5.09 \pm 4.98 | 0.507 \pm 0.257 | 20.4 \pm 11.5 |
| EDCn | 39 | 60.5 \pm 13.7 | 110.6 \pm 21.4 | 1.9 \pm 0.2 | 3.47 \pm 1.29 | 11.66 \pm 8.40 | 0.516 \pm 0.275 | 32.9 \pm 14.9 |

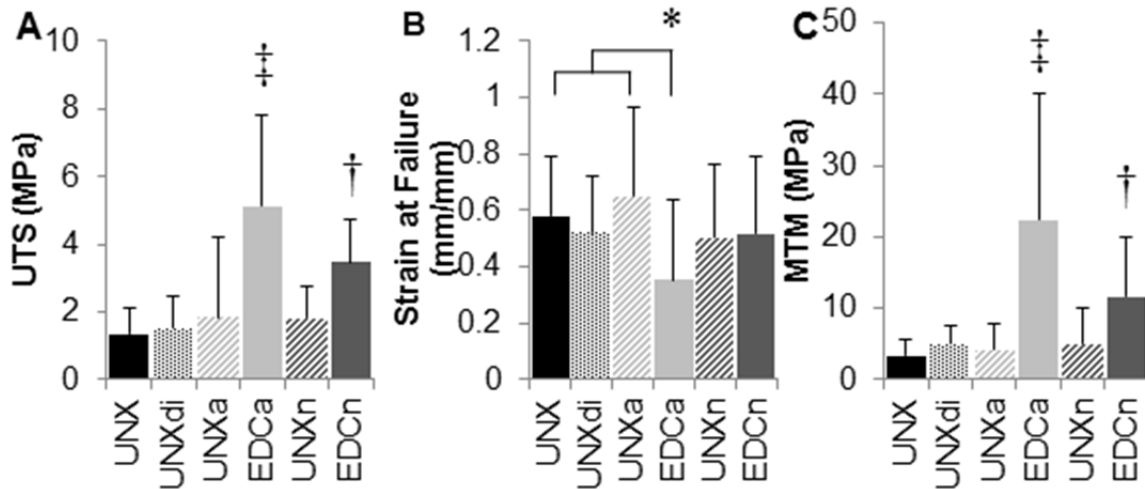


Figure 3.3. Mechanical properties of microthreads crosslinked for 2 hours. The UTS (A), SAF (B), and MTM (C) values of uncrosslinked and crosslinked microthreads. Crosslinking microthreads in either buffer exhibited significantly higher UTS values, including a difference between the two crosslinking buffers. EDCa microthreads failed at significantly lower strains than UNX or UNXa microthreads. † and ‡ indicate statistical significance with respect to all other conditions and * indicates statistical differences between indicated groups by one-way ANOVA with Holm-Sidak post hoc analysis ($p < 0.05$, $n \geq 23$ for all conditions).

3.3.2 Crosslinking Decreases the Swelling Ratio of Fibrin Microthreads

To predict the effect of the degree of crosslinking on the structural properties of fibrin microthreads, dried microthreads were rehydrated in PBS for at least 1 hour. Diameter measurements were taken before and after hydration of microthreads to calculate the swelling ratio as an approximation of crosslinking density within the microthreads.^{35,36} Swelling ratios for crosslinked microthreads (EDCa and EDCn) were significantly less than that for UNX microthreads and were independent of crosslinking time (Figure 3.4A). The swelling ratio was higher for EDCn microthreads than for EDCa microthreads, demonstrating a dependence of pH on the degree of crosslinking. UNXn and UNXdi microthreads were found to have significantly lower swelling ratios than UNX microthreads, which was still significantly higher than the swelling ratio of EDCa or EDCn microthreads (Figure 3.4B).

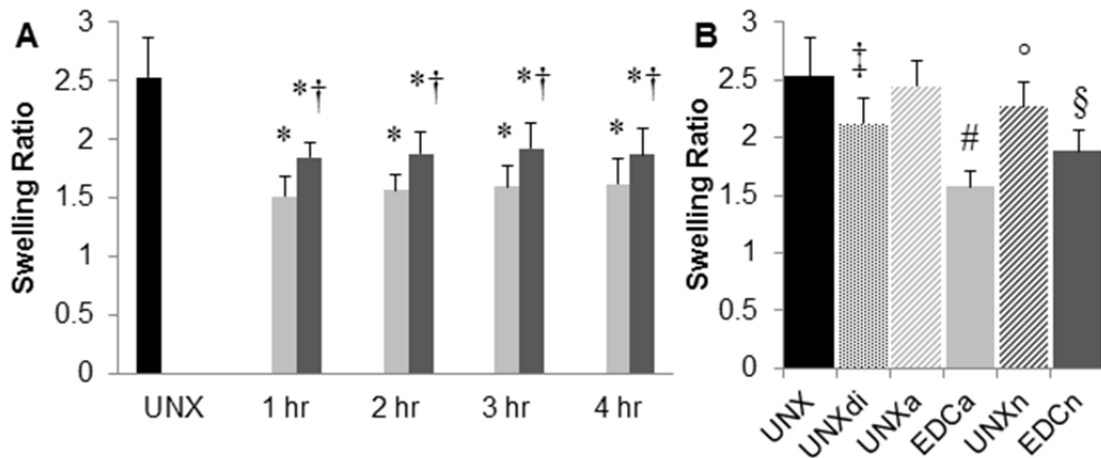


Figure 3.4. Swelling ratio of microthreads crosslinked as a function of time and buffer pH. Swelling ratio is significantly changed by the pH of the crosslinking buffer independent of crosslinking time (A). The swelling ratios of microthreads treated for 2 hours were statistically different between all experimental groups except for UNXa microthreads when compared to UNX microthreads (B). * indicates statistical significance with respect to UNX microthreads; † indicates significance with respect to all EDCa microthreads; and ‡, #, °, § indicates significance to all other groups by one-way ANOVA with Holm-Sidak post hoc analysis ($p < 0.05$, $n \geq 26$).

3.3.3 Crosslinking Increases Fibrin Microthread Resistance to Proteolytic Degradation

In vivo, fibrin is gradually degraded by tissue proteases, namely plasmin.²³ To evaluate whether the method or duration of crosslinking would enhance the structural integrity of fibrin microthreads and increase their persistence as a provisional scaffold, the sensitivity of microthreads to plasmin digestion was evaluated *in vitro*. No significant differences in the temporal degradation profile were noted with respect to crosslinking time for microthreads crosslinked for 1, 2, 3, or 4 hours (data not shown).

Representative phase contrast images of microthreads incubated in plasmin are shown at 0 and 12 hours of plasmin treatment (Figure 3.5). All uncrosslinked microthreads (UNX, UNXdi, UNXa, UNXn) were completely degraded at 12 hours (Figure 3.5 B, D, F, and J). EDCn microthreads showed extensive degradation (Figure 3.5L) at this time point, while EDCa and microthreads incubated without plasmin (negative control) showed no noticeable degradation (Figure 3.5 H and N). Uncrosslinked microthread controls completely degraded within four hours of plasmin incubation (Figure 3.6). EDCn microthreads persisted for approximately 24 hours, significantly slower than UNX microthreads. EDCa microthreads and microthreads incubated in TBS alone (no plasmin) showed no evidence of degradation throughout the duration of the assay (1 week) and, while not significantly different from each other, were significant with respect to EDCn and UNX microthreads, demonstrating three unique degradation profiles with our crosslinking treatments and uncrosslinked microthreads.

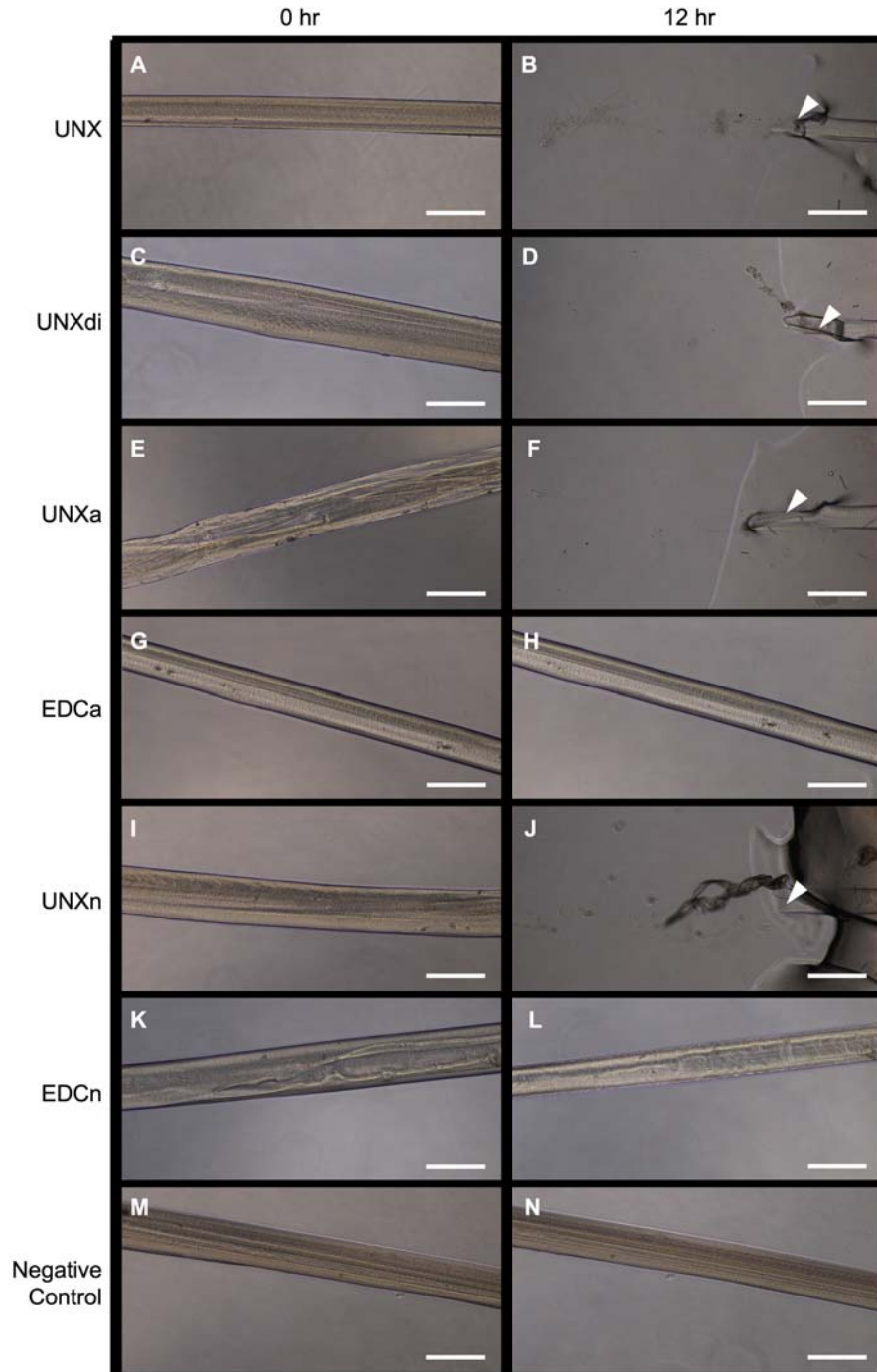


Figure 3.5. Representative images of microthreads in a degradation assay at 0 hours (A, C, E, G, I, K, and M) and at 12 hours (B, D, F, H, J, L, and N). Microthreads were incubated in 0.1 U/mL of plasmin in TBS (pH 7.5) and the diameter at each time point was measured. Uncrosslinked controls (UNX: A and B; UNXdi: C and D; UNXa: E and F; UNXn: I and J) all completely degraded before 12 hours, leaving no microthread at the glue interface (white arrow head). EDCn microthreads (K and L) persisted at 12 hours with approximately 50% of their initial diameter. Neither the EDCa microthreads (G and H) nor the no plasmin control (M and N) exhibited any degradation at 12 hours. Scale bar = 200 μm .

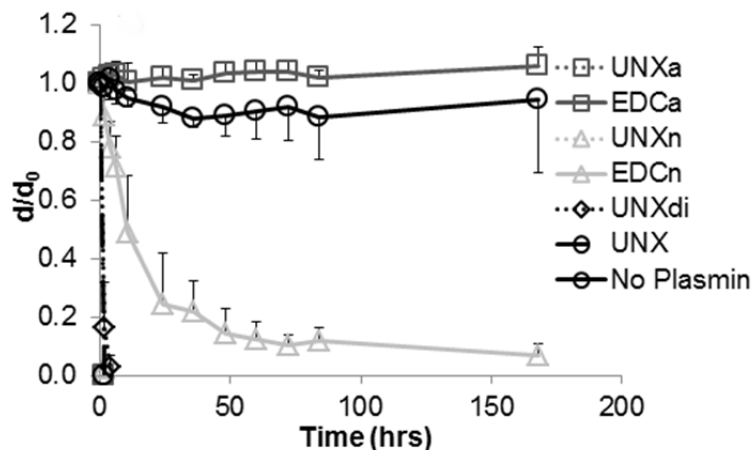


Figure 3.6. Degradation profiles of microthreads treated with plasmin. All control microthreads completely degraded within 4 hours, while EDCn microthreads persisted until 24 hours, after which only residual debris remained. Neither EDCa microthreads nor the no plasmin control exhibited any degradation within the assay period. EDCa and EDCn were statistically different than all controls and each other at all time points by one-way ANOVA with Holm-Sidak post hoc analysis ($p < 0.05$, $n=6$).

3.3.4 EDC Crosslinking Enhances Cell Attachment to Fibrin Microthreads

To determine whether our crosslinking strategy would alter cell functions such as cell adhesion and viability, EDC crosslinked and uncrosslinked microthreads were bundled in groups of ten, seeded with C2C12 cells and analyzed at 1 and 3 day time points following incubation. Cell attachment was measured, and quantified by measuring the cell density along the surface of the microthreads using Hoechst 33342 nuclear dye. When microthread bundles were hydrated for seeding, all of the constructs except for the EDCa microthread bundles compacted into a structure that exhibited a morphology approximating a large, single thread with the topography of each single microthread visible in its substructure; whereas EDCa microthread bundles remained discrete, individual microthreads. One day after seeding, cells readily attached to each bundle as visualized with Hoechst (Figure 3.7 A, C, E, G, I, and K). Significantly higher cell densities were observed on EDCa microthreads (Figure 3.7G) than UNX microthreads (Figure 3.7A and Figure 3.8). After 3 days of culture, the microthreads exhibited a significant increase in the number of C2C12 cells on the surface where the microthread surfaces appeared to be confluent at this time point (Figure 3.7 B, D, F, H, J, and L). All groups except for UNXdi microthreads had significantly higher cell densities at day 3 than that determined immediately after seeding (Figure 3.8). Interestingly, on EDCa crosslinked microthreads, which displayed discrete microthread structures, the cells created web-like structures between adjacent microthreads (Figure 3.7H, arrows). The cell densities of UNXn microthreads were significantly higher than UNX microthreads at 3 days of culture (Figure 3.8).

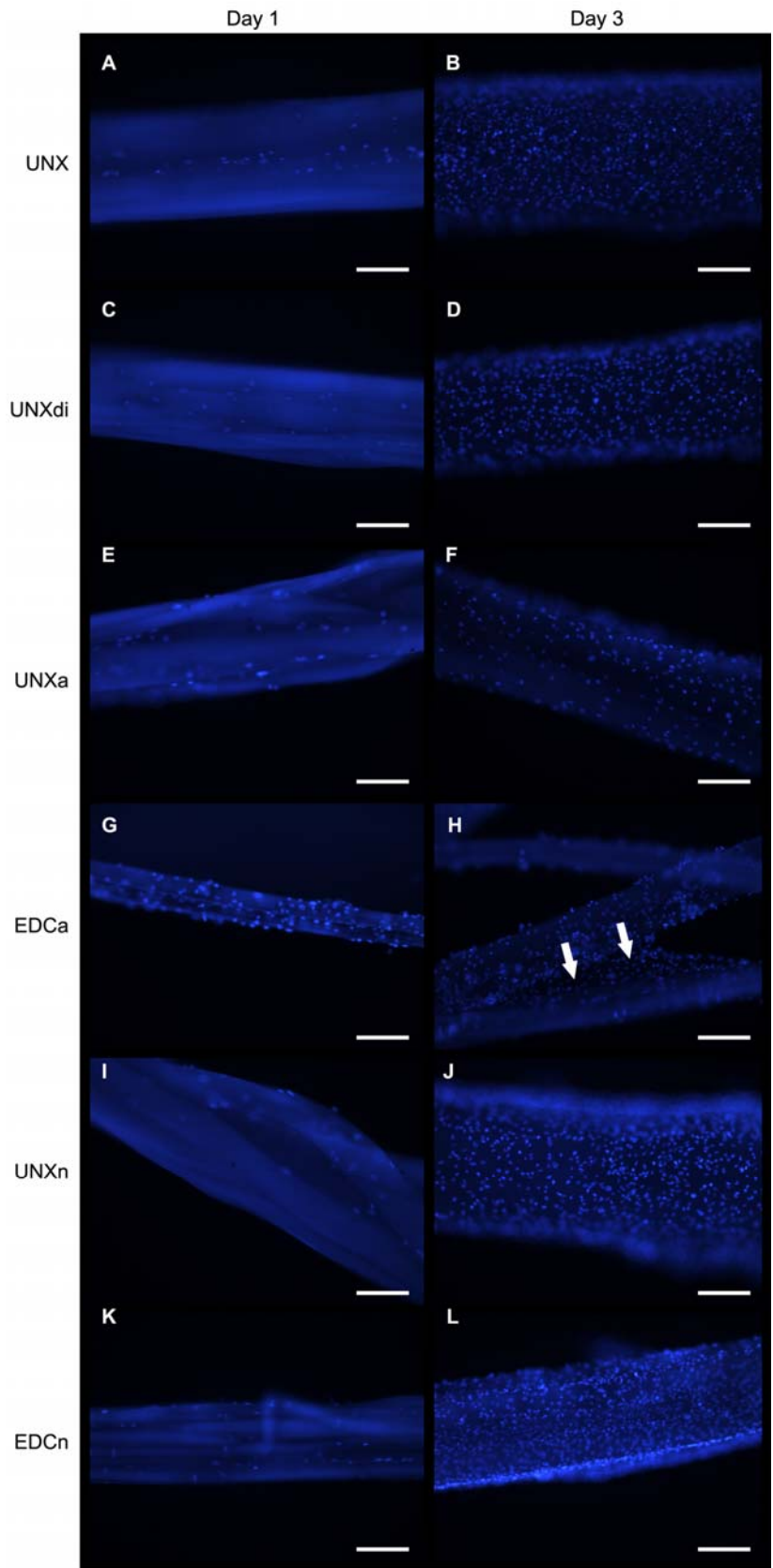


Figure 3.7. Representative images of microthreads seeded with 10,000 C2C12 cells for 1 day (A, C, E, G, I, and K) or for 3 days (B, D, F, H, J, and L). Microthreads were stained with 33342 Hoechst (blue) to quantify the cell attachment and density on each microthread. The density of cells on the microthreads appeared to increase with time, suggesting that the cells were proliferating. Uncrosslinked controls (UNX: A and B; UNXdi: C and D; UNXa: E and F; UNXn: I and J) showed moderate cell densities at day 1, while crosslinked microthreads (EDCn: K and L; EDCa: G and H) showed higher numbers of cells in similar regions of analysis. Cell densities appear to increase on the crosslinked microthreads compared to the uncrosslinked controls, and web-like structures of cells can be seen between different EDCa microthreads at 3 days (H, arrows). Scale bar = 200 μ m.

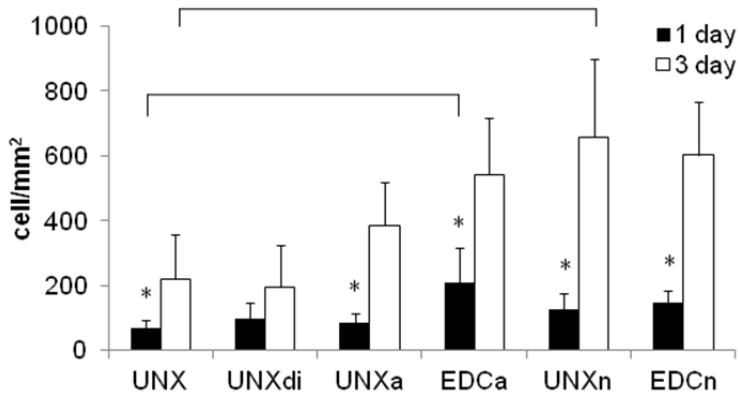


Figure 3.8. Density of C2C12 cells seeded on fibrin microthreads for 1 or 3 days. With the exception of UNXdi, all groups showed a significant increase in cell density from 1 to 3 days. At 1 day, EDCa microthreads had significantly higher cell densities than UNX microthreads. At 3 days, UNXn microthreads had significantly higher cell densities than UNX microthreads. Brackets indicate significance with indicated groups by one-way ANOVA with Holm-Sidak post hoc analysis ($p < 0.05$) * represent statistical significance between 1 and 3 days by a paired Student's t-test ($p < 0.05$, $n \geq 3$).

The increase in cell density that was observed with crosslinking did not correspond to an increase in cell death. Viability stains were performed at day 3 for all groups (Figure 3.9 A, C, E, G, I, and K). While there appeared to be differences in the number of live cells (green), the cells completely covered the microthreads and the number of dead cells (red) did not appear to increase. In all experimental cases, C2C12 cells tended to align along the longitudinal axis of the microthreads as well as within the grooves between the microthreads in the compacted bundles. Background autofluorescence in the red spectrum was observed for each treatment group which limited the ability to visually identify all of the nonviable cells on the microthreads (Figure 3.9 B, D, F, H, J, and L).

With increasing culture duration, cell-seeded microthreads became less morphologically distinct, possibly due to the activity of proteases secreted by the cells. By day 7, discrete microthread structure was observed only for EDCa microthreads. On these scaffolds, there was extensive cell growth on the surface and no indication of microthread degradation (Figure 3.9G, insert). EDCn microthreads persisted for 5 days, while UNX microthreads degraded between 3 and 4 days (data not shown).

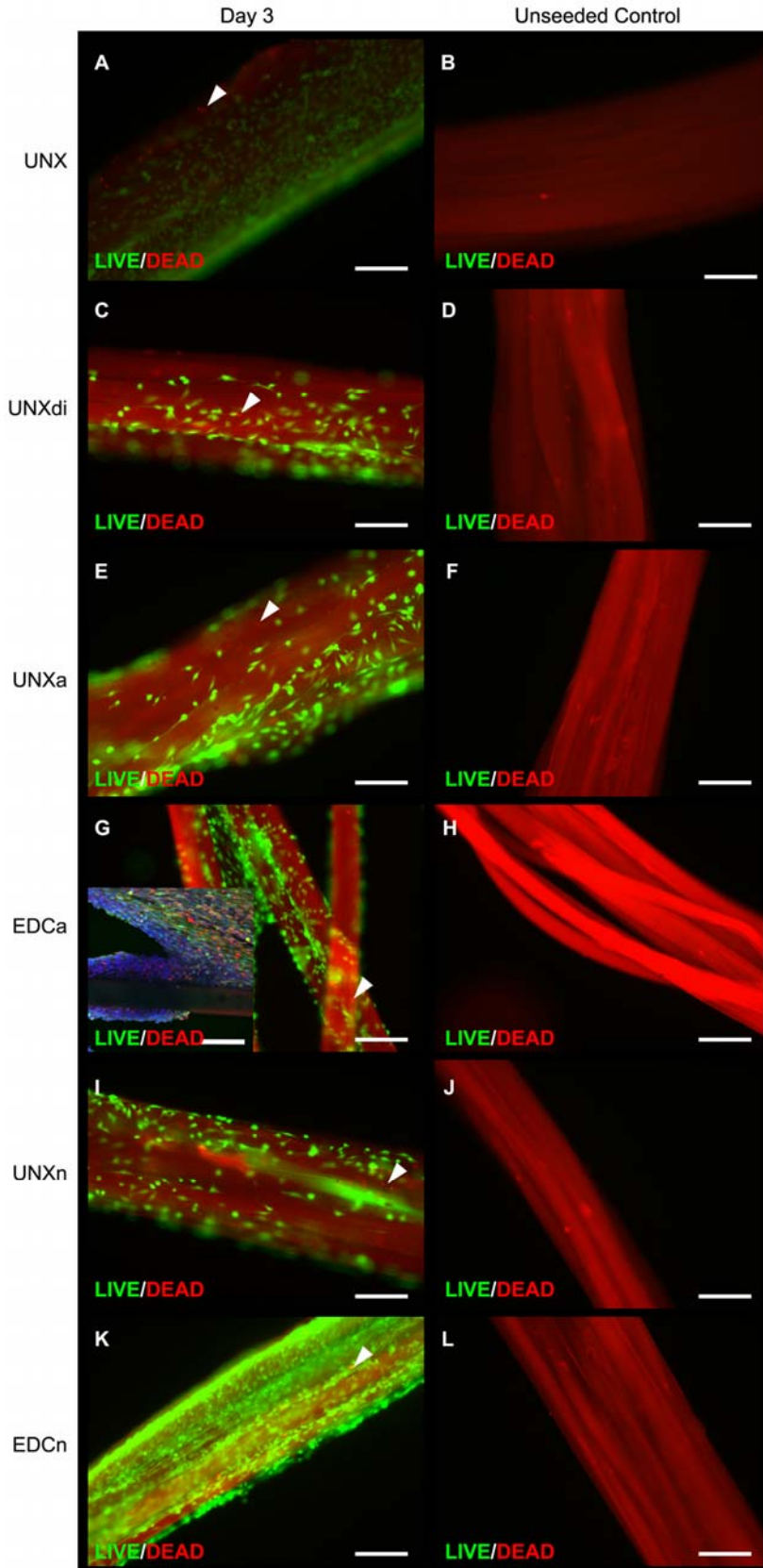


Figure 3.9. Representative images of C2C12 cell viability on crosslinked microthreads at 3 days (A, C, E, G, I, and K) and negative controls (B, D, F, H, J, and L). Microthreads were initially seeded with 10,000 C2C12 cells, cultured for 3 days, and stained with calcein (green, localized in cytoplasm of live cells), and ethidium homodimer-1 (EthD-1, red, binds to DNA of dead cells). Uncrosslinked controls (UNX: A; UNXdi: C; UNXa: E; UNXn: I) showed nearly complete cell coverage on all scaffolds, with few dead cells detected (white arrow heads). Crosslinked microthreads (EDCn: K; EDCa: G) showed higher density of live stained cells with similar numbers of dead cells, despite the increase in total cell number. In all cases, the negative acellular controls autofluoresced, limiting our ability to visually quantify the dead cells (B, D, F, H, J, and L). When C2C12 cells were cultured on microthreads for 7 days, all scaffolds except EDCa microthreads (G, insert) were completely degraded. Scale bar = 200 μm .

3.4 DISCUSSION

The goal of this study was to investigate the effect varying crosslinking times and pH on EDC crosslinking of fibrin microthreads to develop microthread scaffolds with tunable mechanical and structural properties to enhance skeletal muscle regeneration. Skeletal muscle is a load bearing tissue, so microthreads must be able to withstand considerable uniaxial loading to avoid mechanical failure in the injury site. Our early implantation studies demonstrated that UNX microthreads withstand sufficient loading *in situ* to persist in an injury site and facilitate tissue ingrowth.⁴ Interestingly, the stiffness of fibrin microthreads is in the MPa range, while skeletal muscle is reported to have a static stiffness of 12 kPa,³⁷ which can increase to 11.2 MPa in contracting muscle.³⁸ Mooney and colleagues have reported that softer substrates trigger a proliferative phenotype in myoblasts, while stiffer substrates trigger myoblast differentiation.^{8,37} Our uncrosslinked microthreads are stiffer than static muscle tissue, but more compliant than contracting muscle tissue, while EDCn microthreads are as stiff as contracting muscle, and EDCa microthreads are twice as stiff as contracting muscle. Despite being stiffer than static skeletal muscle, we observed healthy myoblasts that readily proliferated with limited cell death on all of our scaffolds. While it can be argued that a softer substrate would increase cell proliferation and better populate a wound site, evidence suggests that inhibiting early differentiation of myoblasts with growth factors will significantly impede muscle regeneration.³⁹ Downstream signaling induced by either growth factors or mechanical stimulation does not necessarily follow the same molecular pathways, however, these findings highlight the need to closely match both the mechanical and biochemical environment of the scaffold with native muscle tissue to promote tissue regeneration. While we have not investigated the differentiation capacity of myoblasts on our microthread scaffolds, studies suggest that scaffolds that are degradable will readily facilitate differentiation.⁸ In this study, we demonstrated that degradable, EDC-crosslinked scaffolds qualitatively improve cell attachment and therefore hold substantial promise for use in skeletal muscle regeneration.

The difference in swelling ratio observed with the crosslinking conditions indicates that acidic and neutral crosslinking environments greatly affect the internal structure of the fibrin microthreads. Water binding efficiency, or swelling ratio, has been used as a tool to estimate the degree of crosslinking in fiber-based biopolymer scaffolds.^{26,29,36} Acidic buffer facilitates

the higher availability of deprotonated carboxylic groups through the hydrolysis of amino acids asparagine or glutamine to their acidic counterparts aspartate and glutamate respectively,^{40,41} which are required to form EDC/NHS reactive intermediaries and, ultimately, the amide bonds that create the interfibrillar crosslinks within the microthreads. In our study, we hypothesize that the depletion of free carboxylic groups may alter the surface charge of the microfibrils within the microthreads, facilitating interfibrillar interactions, or crosslinks, which may explain the reduction in swelling ratio.³⁶ The differences in swelling ratios suggest that each condition differentially affects the crosslinking density within the microthreads. That is, the acidic buffer facilitated the formation of more interfibrillar crosslinks within the microthreads than the neutral buffer. In future studies, we will conduct a systematic series of experiments to validate these findings by detecting free amine groups as well as measuring the efficiency of biochemical interactions associated with the crosslinking reaction.

The hypothesis that EDCa and EDCn microthreads were crosslinked differentially was further supported by the results of our *in vitro* degradation assay. Uncrosslinked microthreads incubated in the presence of plasmin degraded within 4 hours, EDCn microthreads degraded within 24-48 hours, and EDCa microthreads did not show any degradation in our studies. These observations support the hypothesis that the decrease in swelling ratio is consistent with an increase in interfibrillar crosslinks within discrete microthreads. One possible explanation for the decreased degradation rate of the crosslinked microthreads is that these crosslinks inhibit enzyme access to cleavage sites. In studies evaluating the effects of Factor XIII crosslinking on fibrinolysis, it was found that increasing concentrations of Factor XIII decreased the rate of degradation, supporting the hypothesis that carbodiimide crosslinking may function similarly by hindering the access of plasmin to its cleavage sites and therefore increasing the persistence of fibrin in a proteolytic environment.²² Interestingly, when the culture time of C2C12 cells seeded on the microthreads was extended to 7 days, the cell-mediated temporal degradation trend was comparable to the plasmin degradation trend. The results of our recent implantation study suggest that the regenerative response of a large volume skeletal muscle defect might be enhanced with the inclusion of a scaffold with an increased persistence in the wound site.⁴ Together, these findings suggest that we would anticipate a more robust skeletal muscle regeneration response in a large muscle defect if our scaffolds were fabricated with EDCn or

EDCa crosslinked microthreads, since our *in vitro* studies demonstrate that these scaffold persist longer than the UNX microthreads that were used for our initial studies. We plan to pursue the effects of increased fibrin microthread degradation time due to controlled chemical crosslinking on skeletal muscle regeneration in future studies.

The initial increase in cell density observed on the surfaces of the EDCa microthreads may correlate to the increase in microthread stiffness observed from the tensile tests. Previous studies showed that the stiffness of a substrate may affect the presentation of specific integrin binding sites such as the RGD motif or the development of focal adhesion complexes, increasing the initial attachment of C2C12 cells onto stiffer substrates.⁴² Fibrin is known to interact with many integrins, including α_v and α_5 , which contribute to skeletal muscle precursor cell adhesion and maturation.^{42,43} We hypothesize that the interactions between these integrins and fibrin microthreads may be responsible for the initial, significant differences in cell density on EDCa crosslinked microthreads, relative to UNX microthreads after 1 day of culture. Further, the lack of a reduction in cell adhesion indeed suggests the binding sites remained intact through the crosslinking procedure. These findings suggest that this crosslinking strategy could enable the use of EDC as a conjugation agent to tether therapeutic molecules to the surface of the microthreads, increasing their bioactivity and regenerative potential without negatively impacting cell attachment. While the strategic conjugation of peptides, growth factors, or therapeutic agents to the surface of fibrin microthreads is not the goal of this dissertation, this ability could be used in future studies to further direct cell and tissue responses to fibrin microthreads in a precise manner.

3.5 CONCLUSIONS

In this study, we demonstrated that the mechanical and structural properties of fibrin microthreads can be modulated by varying the pH in the EDC crosslinking procedure. We showed that a physiological crosslinking pH resulted in the production of microthreads that are significantly stronger and stiffer as well as significantly more resistant to proteolytic degradation than UNX microthreads. We also showed that acidic crosslinking buffer further increases the strength and stiffness of microthreads as well as their resistance to proteolytic degradation compared to EDCn crosslinked microthreads. Further, these results suggest that cell adhesion

and proliferation on the surface of microthreads are not compromised by carbodiimide crosslinking. The ability to generate scaffolds with tunable mechanical and structural properties is essential to strategically develop scaffolds that match the mechanical and biochemical requirements of regenerating tissue. The tunable properties of EDC crosslinked microthreads in this study may be ideal to stimulate muscle regeneration due to their controllable resistance to proteolytic degradation, however, the biochemical properties of these microthreads may need to be tailored to facilitate the recruitment of myoblasts to a skeletal muscle injury site.

3.6 ACKNOWLEDGEMENTS

This research was funded in part by US Army (W81XWH-11-1-0631, GDP and RLP) and DSO/DARPA contract # W911NF09C0004 (CellThera, Inc.). The authors wish to acknowledge Lucy Vilner for her expert advice on cell culture and Stephen Greco for his assistance in the collection of the mechanical data.

3.7 REFERENCES

1. Reprinted from: *Acta Biomaterialia*, 8(11), Grasman JM, Page RL, Dominko T, Pins GD, "Crosslinking strategies facilitate tunable structural properties of fibrin microthreads", 4020-4030, Copyright (2012), with permission from Elsevier.
2. Liao H, Zhou GQ. Development and progress of engineering of skeletal muscle tissue. *Tissue Eng Part B Rev* 2009;15(3):319-31.
3. Koning M, Harmsen MC, van Luyn MJ, Werker PM. Current opportunities and challenges in skeletal muscle tissue engineering. *J Tissue Eng Regen Med* 2009;3(6):407-15.
4. Page RL, Malcuit C, Vilner L, Vojtic I, Shaw S, Hedblom E, Hu J, Pins GD, Rolle MW, Dominko T. Restoration of skeletal muscle defects with adult human cells delivered on fibrin microthreads. *Tissue engineering. Part A* 2011;17(21-22):2629-40.
5. Lesman A, Koffler J, Atlas R, Blinder YJ, Kam Z, Levenberg S. Engineering vessel-like networks within multicellular fibrin-based constructs. *Biomaterials* 2011;32(31):7856-69.
6. Choi JS, Lee SJ, Christ GJ, Atala A, Yoo JJ. The influence of electrospun aligned poly(epsilon-caprolactone)/collagen nanofiber meshes on the formation of self-aligned skeletal muscle myotubes. *Biomaterials* 2008;29(19):2899-906.
7. Williamson MR, Adams EF, Coombes AG. Gravity spun polycaprolactone fibres for soft tissue engineering: interaction with fibroblasts and myoblasts in cell culture. *Biomaterials* 2006;27(7):1019-26.
8. Boontheekul T, Hill EE, Kong HJ, Mooney DJ. Regulating myoblast phenotype through controlled gel stiffness and degradation. *Tissue Engineering* 2007;13(7):1431-42.
9. Borselli C, Storrle H, Benesch-Lee F, Shvartsman D, Cezar C, Lichtman JW, Vandenburgh HH, Mooney DJ. Functional muscle regeneration with combined delivery of angiogenesis and myogenesis factors. *Proc Natl Acad Sci U S A* 2010;107(8):3287-92.
10. Hinds S, Bian W, Dennis RG, Bursac N. The role of extracellular matrix composition in structure and function of bioengineered skeletal muscle. *Biomaterials* 2011;32(14):3575-83.
11. Turner NJ, Yates AJ, Jr., Weber DJ, Qureshi IR, Stolz DB, Gilbert TW, Badylak SF. Xenogeneic extracellular matrix as an inductive scaffold for regeneration of a functioning musculotendinous junction. *Tissue engineering. Part A* 2010;16(11):3309-17.

12. Valentin JE, Turner NJ, Gilbert TW, Badylak SF. Functional skeletal muscle formation with a biologic scaffold. *Biomaterials* 2010;31(29):7475-84.
13. Conconi MT, De Coppi P, Bellini S, Zara G, Sabatti M, Marzaro M, Zanon GF, Gamba PG, Parnigotto PP, Nussdorfer GG. Homologous muscle acellular matrix seeded with autologous myoblasts as a tissue-engineering approach to abdominal wall-defect repair. *Biomaterials* 2005;26(15):2567-74.
14. Engler AJ, Griffin MA, Sen S, Bonnemann CG, Sweeney HL, Discher DE. Myotubes differentiate optimally on substrates with tissue-like stiffness: pathological implications for soft or stiff microenvironments. *The Journal of Cell Biology* 2004;166(6):877-87.
15. Kroehne V, Heschel I, Schugner F, Lasrich D, Bartsch JW, Jockusch H. Use of a novel collagen matrix with oriented pore structure for muscle cell differentiation in cell culture and in grafts. *J Cell Mol Med* 2008;12(5A):1640-8.
16. Moon du G, Christ G, Stitzel JD, Atala A, Yoo JJ. Cyclic mechanical preconditioning improves engineered muscle contraction. *Tissue engineering. Part A* 2008;14(4):473-82.
17. Rhim C, Lowell DA, Reedy MC, Slentz DH, Zhang SJ, Kraus WE, Truskey GA. Morphology and ultrastructure of differentiating three-dimensional mammalian skeletal muscle in a collagen gel. *Muscle Nerve* 2007;36(1):71-80.
18. Beier JP, Stern-Straeter J, Foerster VT, Kneser U, Stark GB, Bach AD. Tissue engineering of injectable muscle: three-dimensional myoblast-fibrin injection in the syngeneic rat animal model. *Plast Reconstr Surg* 2006;118(5):1113-21; discussion 1122-4.
19. Huang YC, Dennis RG, Larkin L, Baar K. Rapid formation of functional muscle in vitro using fibrin gels. *Journal of Applied Physiology* 2005;98(2):706-713.
20. Norman JJ, Desai TA. Control of cellular organization in three dimensions using a microfabricated polydimethylsiloxane-collagen composite tissue scaffold. *Tissue Eng* 2005;11(3-4):378-86.
21. Clark RA. Fibrin and wound healing. *Ann N Y Acad Sci* 2001;936:355-67.
22. Siebenlist KR, Mosesson MW. Progressive crosslinking of fibrin gamma chains increases resistance to fibrinolysis. *The Journal of Biological Chemistry* 1994;269(45):28414-28419.
23. Mosesson MW. Fibrinogen and fibrin structure and functions. *J Thromb Haemost* 2005;3(8):1894-904.
24. Bjork JW, Johnson SL, Tranquillo RT. Ruthenium-catalyzed photo cross-linking of fibrin-based engineered tissue. *Biomaterials* 2011;32(10):2479-88.
25. Syedain ZH, Bjork J, Sando L, Tranquillo RT. Controlled compaction with ruthenium-catalyzed photochemical cross-linking of fibrin-based engineered connective tissue. *Biomaterials* 2009;30(35):6695-701.
26. Cornwell KG, Pins GD. Discrete crosslinked fibrin microthread scaffolds for tissue regeneration. *J Biomed Mater Res A* 2007;82(1):104-12.
27. Cornwell KG, Pins GD. Enhanced proliferation and migration of fibroblasts on the surface of fibroblast growth factor-2-loaded fibrin microthreads. *Tissue Eng Part A* 2010;16(12):3669-77.
28. Huard J, Li Y, Fu FH. Muscle injuries and repair: current trends in research. *J Bone Joint Surg Am* 2002;84-A(5):822-32.
29. Cornwell KG, Lei P, Andreadis ST, Pins GD. Crosslinking of discrete self-assembled collagen threads: Effects on mechanical strength and cell-matrix interactions. *J Biomed Mater Res A* 2007;80(2):362-71.
30. Kemp PD, Cavallaro JF, Hastings DH. Effects of carbodiimide crosslinking and load environment on the remodeling of collagen scaffolds. *Tissue Engineering* 1995;1(1):71-79.
31. Yang HS, Bhang SH, Hwang JW, Kim DI, Kim BS. Delivery of basic fibroblast growth factor using heparin-conjugated fibrin for therapeutic angiogenesis. *Tissue Eng Part A* 2010;16(6):2113-9.
32. Nillesen ST, Geutjes PJ, Wismans R, Schalkwijk J, Daamen WF, van Kuppevelt TH. Increased angiogenesis and blood vessel maturation in acellular collagen-heparin scaffolds containing both FGF2 and VEGF. *Biomaterials* 2007;28(6):1123-31.
33. Olde Damink LHH, Dijkstra PJ, van Luyn MJA, van Wachem PB, Nieuwenhuis P, Feijen J. Cross-linking of dermal sheep collagen using a water-soluble carbodiimide. *Biomaterials* 1996;17:765-773.
34. Proulx MK, Carey SP, Ditroia LM, Jones CM, Fakhrazadeh M, Guyette JP, Clement AL, Orr RG, Rolle MW, Pins GD and others. Fibrin microthreads support mesenchymal stem cell growth while maintaining differentiation potential. *J Biomed Mater Res A* 2011;96(2):301-12.
35. Pins GD, Christiansen DL, Patel R, Silver FH. Self-assembly of collagen fibers. Influence of fibrillar alignment and decorin on mechanical properties. *Biophysical Journal* 1997;73:2164-2172.

36. Zeugolis DI, Paul GR, Attenburrow G. Cross-linking of extruded collagen fibers--a biomimetic three-dimensional scaffold for tissue engineering applications. *Journal of biomedical materials research. Part A* 2009;89(4):895-908.
37. Gilbert PM, Havenstrite KL, Magnusson KE, Sacco A, Leonardi NA, Kraft P, Nguyen NK, Thrun S, Lutolf MP, Blau HM. Substrate elasticity regulates skeletal muscle stem cell self-renewal in culture. *Science* 2010;329(5995):1078-81.
38. Caiozzo VJ. Plasticity of skeletal muscle phenotype: mechanical consequences. *Muscle & nerve* 2002;26(6):740-68.
39. Miller KJ, Thaloor D, Matteson S, Pavlath GK. Hepatocyte growth factor affects satellite cell activation and differentiation in regenerating skeletal muscle. *Am J Physiol Cell Physiol* 2000;278(1):174-181.
40. Holt LA, Milligan B, Roxburgh CM. Aspartic acid, asparagine, glutamic acid, and glutamine contents of wool and two derived protein fractions. *Australian journal of biological sciences* 1971;24(3):509-14.
41. Cardamone JM. Keratin transamidation. *International journal of biological macromolecules* 2008;42(5):413-9.
42. Ren K, Fourel L, Rouviere CG, Albiges-Rizo C, Picart C. Manipulation of the adhesive behaviour of skeletal muscle cells on soft and stiff polyelectrolyte multilayers. *Acta biomaterialia* 2010;6(11):4238-48.
43. Sinanan AC, Machell JR, Wynne-Hughes GT, Hunt NP, Lewis MP. Alpha v beta 3 and alpha v beta 5 integrins and their role in muscle precursor cell adhesion. *Biology of the cell / under the auspices of the European Cell Biology Organization* 2008;100(8):465-77.

Chapter 4: Static Axial Stretching Enhances the Mechanical Properties and Cellular Responses of Fibrin Microthreads¹

4.1 INTRODUCTION

Biopolymer microthreads are a platform technology that can be used for several applications including scaffolds for tissue engineering, delivery vehicles for growth factors or cells, or as suture materials. These microthreads can be composed of a variety of materials, including collagen,²⁻⁴ silk,⁵⁻⁷ or fibrin.^{8,9} The structural requirements of these microthreads vary for each tissue or device application. For example, scaffolds implanted into load-bearing tissues such as skeletal muscle require that the constructs provide provisional mechanical stability to the tissue in the wound site until native tissue is regenerated.¹⁰ Conversely, a delivery vehicle for growth factors or cells may require relatively large initial mechanical loads to implant into the wound site, but require rapid degradation to facilitate controlled release of the specific growth factor or cell type. Skeletal muscle regeneration requires scaffolds that are capable of withstanding physiologic loading and can persist *in situ* for several weeks to guide the formation of nascent myofibers. Therefore, there is a significant need to tune or modulate the mechanical properties of these materials during the microthread fabrication process to enable the design of function-specific microthread scaffolds.

Fibrin has been used extensively as a scaffold material in tissue engineering because of its intrinsic bioactivity and its role as a provisional matrix during the initial stage of wound healing.^{11,12} Fibrin is a branched, microfibrillar polymer, formed when activated thrombin cleaves two small peptides from fibrinogen, allowing fibrinogen to self-assemble into a complex fibrillar network. Fibrin gels have been shown to increase cell production of extracellular matrix proteins when compared to extracellular matrix protein production in cell-seeded collagen gels.¹³ The molecular structure of fibrin enables individual microfibrils within the microfibrillar networks to undergo reorganization under tension, with strain at failure values in excess of 200%.¹⁴ Another study demonstrated that the increase in tensile strength of stretched bulk fibrin

scaffolds increased the alignment of the fibrin polymer network within the matrix.¹⁵ Together these findings support the hypothesis that stretching of microfibrillar fibrin networks during scaffold fabrication will increase the organization and alignment of the polymer-like network and enhance the mechanical strength of the scaffold.

Our laboratory developed a novel technique to extrude dense fibrin scaffolds into microthreads with average diameters between 100 and 150 μm .¹⁶ One advantage of these biopolymer microthreads is that their cylindrical shape facilitates cell alignment and new tissue deposition along the longitudinal axis of the microthread, enabling the guided regeneration of tissues with aligned fibrous tissue organization such as skeletal muscle, tendon, or ligament. Another advantage of creating microthreads from a dense fibrin matrix is to increase the mechanical strength of the overall fibrin scaffold.¹⁶ To further augment the mechanical properties of fibrin microthreads, we have investigated ultraviolet (UV),¹⁶ and carbodiimide,¹⁷ crosslinking methods to enhance the tensile strength of fibrin microthreads, and showed that carbodiimide crosslinking increased the tensile strength of microthreads as well as their resistance to proteolytic degradation *in vitro*. The current fibrin microthread fabrication process involves stretching microthreads immediately after fibrin polymerization, which generates uniform scaffolds with reproducible structural properties; however, we are not aware of any systematic studies that analyze the effects of static axial stretching on the structural or functional properties of fibrin scaffolds, including fibrin microthreads.

The goal of this chapter was to quantitatively characterize the effect of static axial stretching on the mechanical, structural, and biochemical properties of fibrin microthreads. We stretched fibrin microthreads 0-200% of their original lengths and evaluated their uniaxial strengths, rates of proteolytic degradation, and the degree with which C2C12 myoblasts aligned along the longitudinal axes of the microthreads. The results show that while stretching decreases the diameters of fibrin microthreads, it significantly increases the tensile strength and stiffness of the microthreads without affecting their rate of proteolytic degradation. The ability to tune the mechanical properties of fibrin microthreads without the use of crosslinking agents will create a more robust scaffold material that can be strategically employed as a regenerative matrix for tissues with varying mechanical and structural properties.

4.2 MATERIALS and METHODS

4.2.1 Fibrin Microthread Preparation

4.2.1.1 Microthread Extrusion

Fibrin microthreads were co-extruded from solutions of fibrinogen and thrombin using extrusion techniques described previously in section 3.2.1.1.^{16,17} Briefly, fibrinogen from bovine plasma (Sigma, St. Louis, MO; F8630) was dissolved in HEPES (N-[2-Hydroxyethyl]piperazine-N'-[2-ethanesulfonic acid]) buffered saline (HBS, 20 mM HEPES, 0.9% NaCl; pH 7.4) at 70 mg/mL and stored at -20 °C until use. Thrombin from bovine plasma (Sigma; T4648) was dissolved in HBS at 40 U/mL and stored at -20 °C until use.

To fabricate microthreads, fibrinogen and thrombin solutions were thawed and warmed to room temperature, and thrombin was mixed with a 40 mM CaCl₂ (Sigma) solution to form a working solution of 6 U/mL. Equal volumes of fibrinogen and thrombin/CaCl₂ solutions were loaded into separate 1 mL syringes which were inserted into a blending applicator tip (Micromedics Inc., St. Paul, MN; SA-3670). The solutions were combined in the blending applicator and extruded through polyethylene tubing (BD, Sparks, MD) with an inner diameter of 0.86 mm into a bath of 10 mM HEPES (pH 7.4) in a Teflon coated pan at a rate of 0.225 mL/min using a dual syringe pump.

4.2.1.2 Static Axial Stretching with and without a Drying Phase

Microthreads were incubated in 10 mM HEPES buffer for 10 minutes to facilitate fibrin polymerization, then the scaffolds were carefully removed from the bath solution without additional deformation and dried on a custom-made stretching device overnight (Figure 4.1A). After drying, microthreads were rehydrated in deionized (DI) water for one hour and static axially stretched to either 0, 50, 75, 100, 125, 150, 175 or 200 % of their initial length. To analyze the contribution of the drying phase on the mechanical properties of stretched microthreads, batches of microthreads were also stretched immediately after polymerization to the desired percentage (Figure 4.1B). After stretching, all microthreads were hung to dry under the tension of their own weight. Percent yield of microthreads was determined as the ratio of the number of stretched microthreads and the original number of microthreads mounted on the stretching device. Stretch percentages were reported as the ratio between the deformation (ΔL)

of the microthread and the starting length (L_0) of the microthread (stretch % = $\Delta L/L_0 * 100\%$). Microthreads were fabricated using previously reported methods, which included static axial stretching of approximately 150% immediately after polymerization to form three 19 cm microthreads.¹⁷ Hence these microthreads were designated as control microthreads. Dry, stretched microthreads were placed in aluminum foil and stored in a desiccator at room temperature until use.

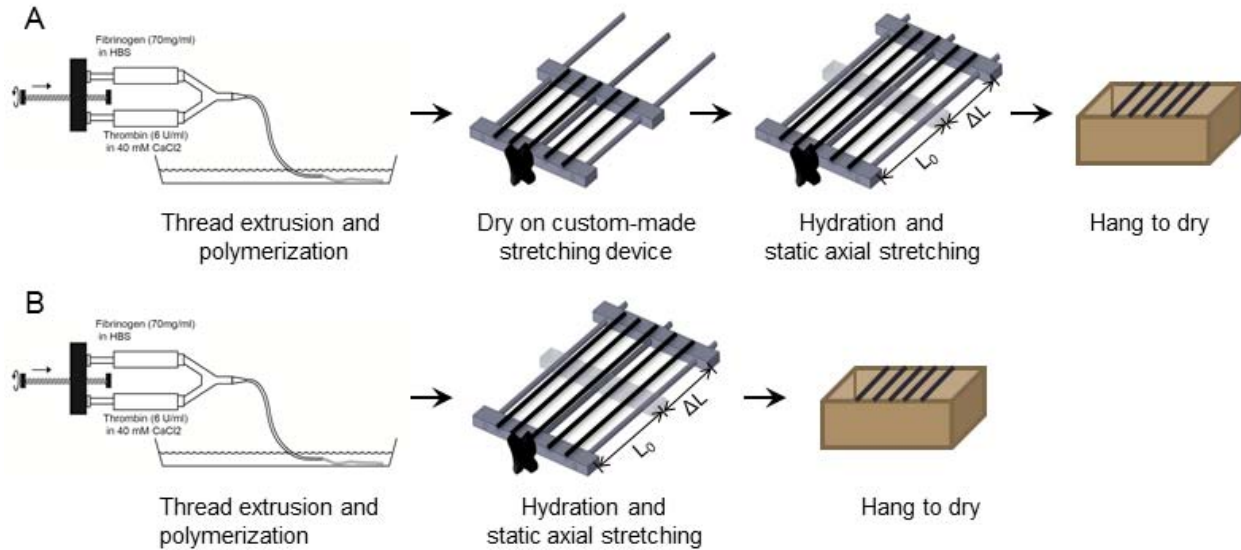


Figure 4.1. Flow-chart of the experimental setup for microthread fabrication with and without a drying phase. Microthreads were extruded into a pH controlled bath solution and incubated for 10 minutes at room temperature for microthread polymerization. After polymerization, microthreads were removed from the bath and dried overnight on a custom-made stretching device. The next day microthreads were rehydrated, static axially stretched to the desired percentage, and dried for immediate testing or storage (A). Control microthreads were stretched immediately after fibrin polymerization and dried overnight (B).

4.2.2 Mechanical Characterization of Stretched Fibrin Microthreads

Mechanical characterization of stretched fibrin microthreads was performed using techniques described previously in section 3.2.2.¹⁷ Briefly, individual microthreads were affixed with medical grade silicone adhesive to vellum paper frames with precut windows that defined the region of loading. An initial gage length of 2.0 cm was defined as the distance between adhesive spots at the edges of the precut window in the vellum frame. The microthreads on the vellum frames were hydrated in phosphate buffered saline (PBS) for at least 60 minutes prior to testing. Hydrated microthread diameters were measured using a calibrated reticule with a 10X objective, coupled to a Nikon Eclipse E600 upright microscope (Melville, NY). Microthreads

were assumed to be cylindrical, and the diameter was determined by averaging 3 measurements taken along the length of each microthread to define the cross-sectional area. After hydration, microthreads were securely mounted in the grips of a uniaxial testing machine (ElectroPuls E1000; Instron, Norwood, MA) and a 1 N load cell, the edges of each vellum frame were cut, and the microthreads were uniaxially loaded until failure at a 50% strain rate (10 mm/min) relative to the initial gage length. Force and displacement were recorded continuously throughout each test at a frequency of 10 Hz. The mechanical failure load of each microthread was recorded as the point where a rapid (80%) drop from the maximum load occurred. The grip-vellum paper interface was visually inspected during each test to ensure that no slippage occurred. Microthreads that slipped in the grips during testing were excluded from further analysis. Engineering stress was calculated as the amount of force detected by the load cell divided by the initial cross-sectional area. Strain was calculated as the increased extension from the gage-length.

A MATLAB (MathWorks, Natick, MA) script was written to analyze the ultimate tensile strength (UTS), initial microthread modulus, maximum tangent modulus (MTM), strain at failure (SAF), and load at failure for each sample (Figure 4.2). The initial modulus was defined as the

initial linear region of the stress-strain curve, typically within the toe region. The MTM was defined as the highest linear region in the stress-strain curve for each sample over a moving window length corresponding to 20% of the total length of each test) and fitted to a linear region of the stress-strain curve. The strain hardening ratio was defined as the ratio between the MTM and the initial modulus. In the event that there

was no change in the slope of the stress-strain curve (i.e. no visible toe region), the initial modulus was equal to the MTM and these values were not used to calculate strain hardening. Statistical analysis was used to identify and remove outliers as defined by microthreads whose wet diameters were 1.5 times greater than the inner quartile range (IQR) for each sample set (average wet diameter $\pm 1.5 * IQR$). To ensure this method was robust, we determined that the

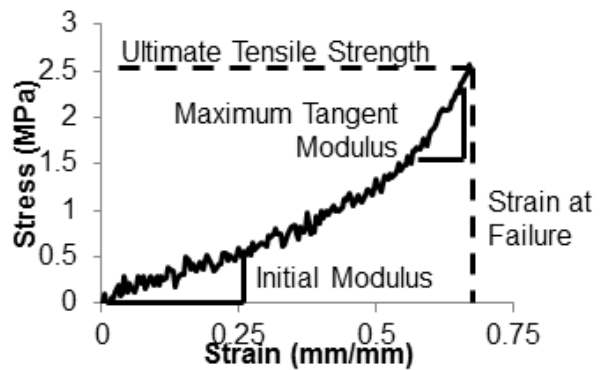


Figure 4.2. A representative stress-strain curve showing how each mechanical parameter was calculated in our MATLAB script.

distribution of wet diameter measurements was normal using SigmaPlot 11.0 software (Systat Software, Inc., San Jose, CA) to validate our definition, and exclusion, of outliers. Data points falling outside of this range were excluded from later statistical analysis.

4.2.3 Structural Characterization of Stretched Fibrin Microthreads

4.2.3.1 Scanning Electron Microscopy

Fibrin microthreads were imaged with a scanning electron microscope (SEM) to characterize microthread morphology and surface topography. Air-dried fibrin microthreads were mounted on aluminum stubs (Ted Pella, Redding, CA) coated with double-sided carbon tape and sputter coated with a thin layer of gold-palladium for 30 seconds at 45 mA using an EMS 550 (Electron Microscopy Sciences, Hatfield, PA). Images were acquired at 5 kV with a JSM-KLG SEM.

4.2.3.2 Microthread Swelling

Prior to mechanical testing, the diameters of dry crosslinked microthreads were recorded using a calibrated reticule with a 10X objective. In each case, the diameter for each microthread was averaged from three measurements taken along the length. The wet diameter measurements taken during the mechanical testing procedure were also used to calculate the swelling ratio which was defined as the ratio of the wet diameter of a microthread to its dry diameter (wet/dry diameter).

4.2.3.3 Transverse Strain and Poisson Ratio Calculations

Transverse strain (diameter strain) was calculated as the change in the mean wet diameter of each stretched microthread with respect to the mean diameter of the unstretched microthreads. Poisson's ratio was determined to be the negative of the ratio between the transverse strain and the axial strain of microthreads after stretching (Poisson = - transverse strain / axial strain).

4.2.3.4 Degradation Assay

Microthread degradation was performed on single fibers on the bottom of 48 well plates as previously described in Section 3.2.3.2.¹⁷ Briefly, stretched microthreads were cut into 0.8 cm

fragments and secured to the bottom of 48 well plates using medical grade silicone adhesive. Stock solutions of human plasmin (EMD Biosciences, San Diego, CA; 527621) were aliquoted and stored according to the manufacturer's instructions. Each experimental condition was run in triplicate. Microthreads were hydrated in 500 μ L of tris buffered saline (TBS, 25 mM Tris-HCl (Sigma), 0.9% NaCl, pH 7.5) for 1 hour, and images were taken with a 10X objective on a Leica inverted microscope (Leica, Wetzlar, Germany) coupled with Leica imaging software to record diameter values at time 0 (d_0). The TBS was aspirated and replaced with 500 μ L of 0.1 U/mL of plasmin in TBS and samples were incubated at room temperature. Microthreads were imaged every 30 minutes or until they were completely degraded. Each image was processed with ImageJ (NIH) to measure the microthreads' diameter at three different positions along the length and plotted as a ratio to the initial diameter value (d/d_0).

4.2.4 Cell Culture

Immortalized mouse myoblasts (CRL-1772, ATCC, Manassas, VA; C2C12) were cultured in a 1:1 (v/v) ratio of high glucose Dulbecco's modified Eagle Medium (DMEM, Gibco BRL, Gaithersburg, MD) and Ham's F12 (Gibco), supplemented with 4 mM L-glutamine and 10% fetal bovine serum (FBS, HyClone, Logan, UT). Cells were incubated at 37 °C with 5% CO₂ and maintained at a density below 70% confluence using standard cell culture techniques. Routine cell passage was conducted using 0.25% trypsin-EDTA (CellGro, Manassas, VA).

4.2.5 Cell Attachment and Alignment Assay

Two single microthreads from the same stretch group were adhered to stainless steel rings (Seastrom Manufacturing, Twin Falls ID; inner diameter 0.750 in.; outer diameter 1.188 in.; thickness 0.005 in.) with medical grade silicone adhesive. Each experimental condition was performed in duplicate. Individual rings were placed in wells of a standard six-well plate over an elevated 13 mm diameter circular ThermanoxTM coverslip (Nalge Nunc International, Rochester, NY), as described previously in section 3.2.5.1.^{17,18} Prior to cell seeding, microthreads were sterilized in 70% ethanol for 1 hour, rinsed in DI water 3 times, air dried in a laminar flow hood, and stored in a desiccator until use.

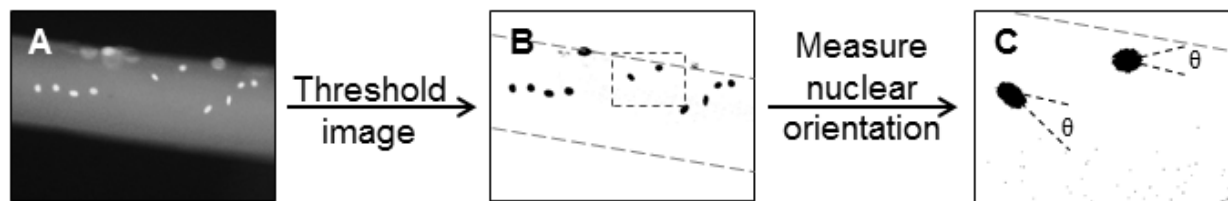


Figure 4.3. Method to determine nuclear alignment on fibrin microthreads. Grey scale images of nuclei on microthreads (A), were thresholded to remove background fluorescence and to visualize nuclei in ImageJ (B), and the ImageJ function analyze particles was used to identify individual nuclei and their orientation with respect to the long axis of the microthread (C).

Immediately prior to seeding, 150 μL of sterile PBS was added to the coverslip to hydrate the microthreads for at least 1 hour. To attach C2C12 cells to the microthread, the PBS was aspirated and replaced with 100 μL of cell suspension (100,000 cells/mL) in complete culture medium. After a 4 hour incubation, cell-seeded microthreads were transferred to a clean six-well plate with 2 mL of fresh medium and returned to the incubator. After 24 hours, microthreads were fixed in 4% paraformaldehyde and stained with Hoechst 33342 to visualize myoblast nuclei (Figure 4.3A). Fluorescent images were analyzed by thresholding the grey scale image in ImageJ (NIH) (Figure 4.3B), and performing the particle analysis function within the ImageJ software to obtain the orientation of the long axis of the nucleus with respect to the microthread (Figure 4.3C). Nuclei that were on the edge of the microthread, or in contact with another nucleus (cell-cell contact) were excluded from analysis, and the others were either binned in 15° increments and plotted into a histogram presenting the average frequency of each bin size, or averaged together to obtain total cell angle measurements.

4.2.6 Statistical Analyses

Statistical analyses were performed using a one-way analysis of variance (ANOVA) with $p < 0.05$ indicating significant differences between groups, using SigmaPlot 11.0 software. For post hoc analyses, Holm-Sidak pairwise multiple comparison tests were performed to determine significant differences between experimental groups using an overall significance level of $p < 0.05$. Where indicated, a Student's t-test was performed with $p < 0.05$ indicating significant differences between groups. The data are reported as means \pm standard deviation for the mechanical and structural characterization and as means \pm standard error for the degradation (3 discrete microthreads were analyzed for each of six experimental runs) and cell alignment

studies (4 discrete microthreads were analyzed for each condition for each of two experimental runs).

4.3 RESULTS

4.3.1 Stretching Increases the Ultimate Tensile Strength of Fibrin Microthreads

The mechanical properties of static axially stretched microthreads were investigated for the design of tissue-specific microthread scaffolds. Interestingly, while most static axially stretched microthreads were fabricated with similar percent yields, there was a reduction in the percent yield of microthreads stretched 200% of their initial length (Table 4.1). Characteristic stress-strain curves for stretched microthreads show that the 0, 50, and 75% stretch groups have an initial toe region of increasing elongation with little change in stress (Figure 4.4A). Interestingly, higher stretch percentages

Table 4.1. Percent yield for fabrication of static axially stretched microthreads.

| Stretch Percent | Yield (%) |
|-----------------|-----------|
| 0 | 100 ± 0 |
| 50 | 90 ± 9 |
| 75 | 95 ± 5 |
| 100 | 89 ± 11 |
| 125 | 80 ± 10 |
| 150 | 73 ± 28 |
| 175 | 86 ± 17 |
| 200 | 54 ± 15 |

decreased this toe region, becoming undetectable in microthreads stretched 100% of their initial length, and also decreased the SAF of the material twofold. Based on these mechanical results

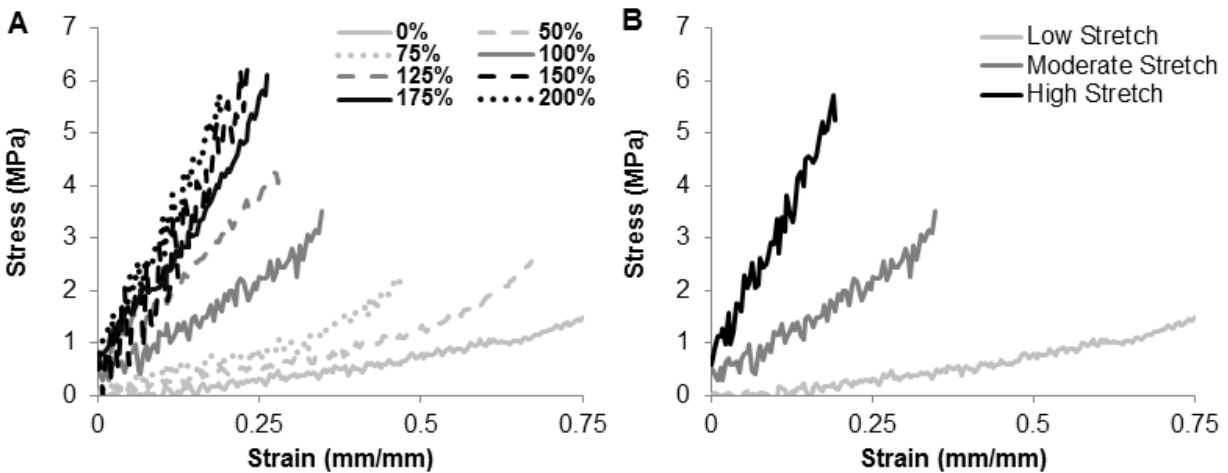


Figure 4.4. Characteristic stress-strain curves for fibrin microthreads fabricated with a drying phase. Microthreads were produced, dried, rehydrated in DI water, and stretched to the indicated percentage. Representative stress-strain curves showed three distinct stretch regimes: low stretch microthreads (stretched 0, 50, or 75% of their initial lengths), moderate stretch microthreads (stretched 100 or 125% of their initial lengths), and high stretch microthreads (stretched 150, 175, 200% of their initial lengths) (A). Low stretch microthreads displayed elastic toe regions and low stiffness. Middle and high stretch microthreads did not always have characteristic toe-regions, but they appeared to deform linearly until failure at higher stresses and at lower strain values (B).

we observed that the microthreads appear to exhibit 3 distinct structural morphologies that we are classifying as low stretch microthreads (microthreads stretched to 0, 50, or 75% of their initial length), moderate stretch microthreads (threads stretched to 100 or 125% of their initial length), or high stretch microthreads (microthreads stretched to 150, 175, or 200% of their initial length). Characteristic stress-strain curves of each of the low, moderate, and high stretch groups show the loss of the toe-region with the moderate and high stretch microthreads, as well as the increase in the MTM with increasing stretch (Figure 4.4B). The mean diameters, peak loads, UTS, MTM, and SAF of all microthreads loaded to failure in uniaxial tension are summarized in Table 4.2. UTS of high stretch microthreads were significantly higher than those of low stretch microthreads (Figure 4.5A). Additionally, moderate stretch microthreads displayed significantly lower UTS values than high stretch microthreads. The MTM values showed a similar trend where the high stretch microthreads were found to be stiffer than the low stretch microthreads (Figure 4.5B). High stretch microthreads also failed at significantly lower SAF values than low stretch microthreads (Figure 4.5C).

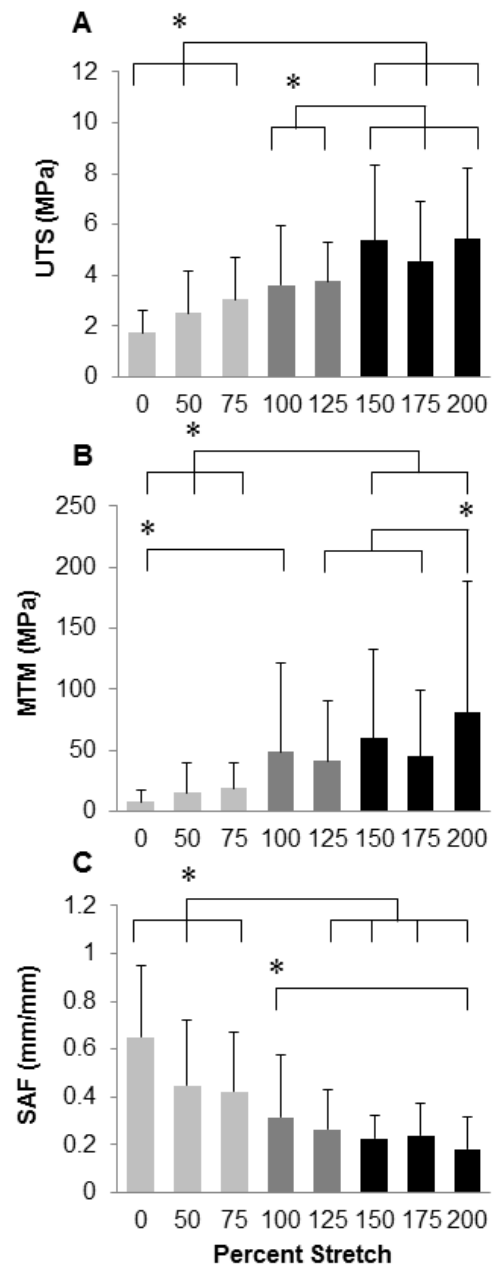


Figure 4.5. Mechanical properties of fibrin microthreads as a function of stretch percentage. Microthreads were fabricated, dried, rehydrated in DI water, stretched to the indicated percentage and dried in their stretched state. Microthreads were subsequently pulled to failure under uniaxial tension and the UTS (A), MTM (B), and SAF (C) were calculated. Low stretch microthreads failed at significantly lower UTS values, and were less stiff than high stretch microthreads. Low stretch microthreads also failed at significantly higher SAF values than high stretch microthreads. * indicates statistical significance between corresponding groups using one-way ANOVA with Holm-Sidak post hoc analysis ($p < 0.05$, $n \geq 41$).

To characterize the relationship between static axial stretching and the stiffness of the fibrin microthreads, we analyzed the strain hardening behavior of the stretched microthreads. Strain hardening refers to an increase in the tangent modulus with increasing strain (compare initial and maximum tangent modulus in Figure 4.2). Interestingly, static axial stretch was not found to affect the strain hardening ratio of fibrin microthreads (Table 4.3). Most stretching conditions demonstrated significantly higher MTM than the initial moduli in the toe regions of the stress-strain curves, showing that these fibrin microthreads are undergoing strain hardening. Additionally, the initial modulus of the high stretch microthreads was significantly greater than the initial modulus of low stretch microthreads. Combined with earlier observations about the effects of stretch on MTM values, these data suggest that high stretch microthreads are stiffer than the low stretch microthreads at all strain values during uniaxial loading. Taken together, these data support the observation that there are three discrete ranges of mechanical strength that correspond to the amount of stretching of fibrin microthreads.

Table 4.2. The mechanical and structural properties of fibrin microthreads stretched after a drying phase.

| Stretch Percent | Sample Size (n) | Diameter (μm) | | Swelling Ratio | UTS (MPa) | MTM (MPa) | SAF (mm/mm) | Load (mN) |
|-----------------|-----------------|----------------------------|--------------|----------------|---------------|------------------|-------------------|-------------|
| | | Dry | Wet | | | | | |
| 0 | 50 | 80 \pm 22 | 157 \pm 42 | 2.0 \pm 0.3 | 1.7 \pm 0.9 | 7.5 \pm 9.7 | 0.651 \pm 0.287 | 34 \pm 26 |
| 50 | 51 | 63 \pm 17 | 132 \pm 41 | 2.1 \pm 0.3 | 2.5 \pm 1.7 | 15.0 \pm 24.5 | 0.447 \pm 0.274 | 29 \pm 30 |
| 75 | 59 | 59 \pm 14 | 115 \pm 28 | 2.0 \pm 0.3 | 3.0 \pm 1.7 | 18.9 \pm 20.5 | 0.422 \pm 0.248 | 30 \pm 19 |
| 100 | 43 | 50 \pm 14 | 93 \pm 31 | 1.9 \pm 0.4 | 3.6 \pm 2.4 | 48.6 \pm 72.6 | 0.314 \pm 0.264 | 26 \pm 31 |
| 125 | 41 | 53 \pm 13 | 97 \pm 30 | 1.8 \pm 0.3 | 3.8 \pm 1.5 | 41.0 \pm 49.8 | 0.264 \pm 0.168 | 29 \pm 18 |
| 150 | 44 | 43 \pm 10 | 77 \pm 25 | 1.8 \pm 0.3 | 5.4 \pm 3.0 | 59.8 \pm 72.8 | 0.224 \pm 0.099 | 22 \pm 12 |
| 175 | 58 | 47 \pm 11 | 86 \pm 22 | 1.8 \pm 0.3 | 4.6 \pm 2.4 | 44.7 \pm 54.5 | 0.238 \pm 0.134 | 27 \pm 15 |
| 200 | 47 | 44 \pm 13 | 77 \pm 23 | 1.8 \pm 0.2 | 5.4 \pm 2.8 | 81.1 \pm 107.1 | 0.182 \pm 0.134 | 24 \pm 12 |

Table 4.3. Strain hardening behavior of static uniaxially stretched fibrin microthreads.

| Stretch Percent | Initial Modulus (MPa) | MTM (MPa) | Strain Hardening Ratio |
|-----------------|-------------------------------|------------------|------------------------|
| 0 | 2.2 \pm 1.6 [‡] | 7.5 \pm 9.7 | 3.9 \pm 4.6 |
| 50 | 7.6 \pm 9.0 [†] | 15.0 \pm 24.5 | 2.7 \pm 1.0 |
| 75 | 6.6 \pm 5.2 ^{††} | 18.9 \pm 20.5 | 3.0 \pm 1.3 |
| 100 | 22.3 \pm 33.9 [*] | 48.6 \pm 73.0 | 4.7 \pm 7.3 |
| 125 | 13.3 \pm 8.8 [‡] | 41.0 \pm 49.8 | 4.2 \pm 6.8 |
| 150 | 17.8 \pm 18.3 [‡] | 59.8 \pm 72.7 | 4.3 \pm 7.8 |
| 175 | 21.5 \pm 35.7 ^{**} | 44.7 \pm 54.5 | 3.8 \pm 4.9 |
| 200 | 30.9 \pm 22.4 ^{**} | 81.1 \pm 107.1 | 2.7 \pm 1.5 |

* indicates significance with the 0% stretch group and † indicates significance with the 200% stretch group as determined by one-way ANOVA with Holm-Sidak post hoc analysis, and ‡ indicates significance between initial modulus and MTM within a single percentage group as determined by Student's t-test ($p < 0.05$, $n \geq 41$).

4.3.2 Stretching Decreases the Diameters and Swelling Ratios of Fibrin Microthreads, but does not Affect Poisson's Ratio

To begin to understand the structural organization of fibrin fibrils within the microthreads, dried microthreads were imaged with a SEM and swelling ratios were calculated to estimate interfibrillar interactions, fibrillar packing and orientation, as well as crosslinking density. Scanning electron micrographs of the microthreads show an apparent decrease in diameter of the

microthreads with increased stretch (Figure 4.6). Low stretch microthreads (Figure 4.6, 0% and 75%) exhibited a smooth, rounded morphology with no evidence of surface topography. With increasing stretch, the microthread surfaces exhibit a more complex topography. There is evidence of longitudinal grooves present on high stretch microthreads

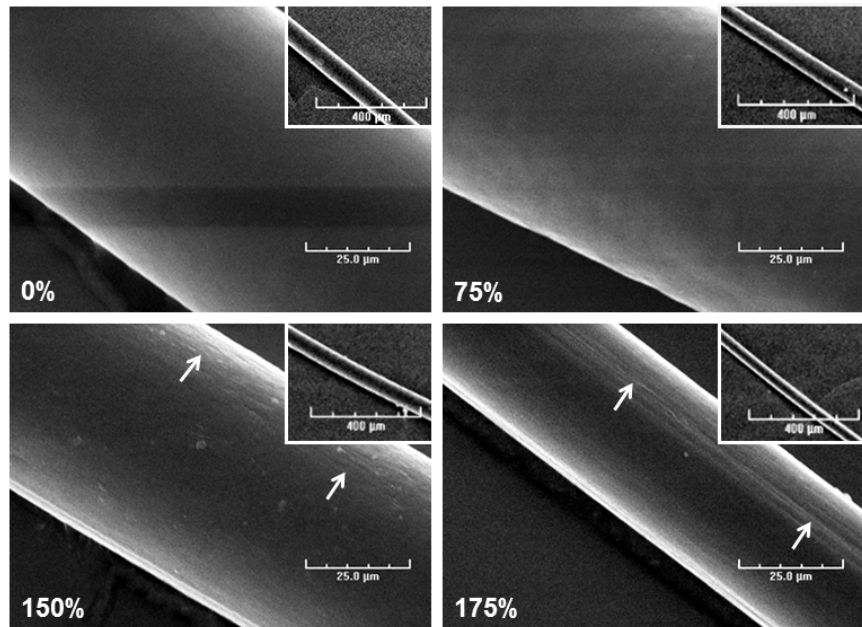


Figure 4.6. Scanning electron micrographs of stretched fibrin microthreads. Low (inset) and high magnification micrographs of fibrin microthreads stretched 0%, 75%, 150%, and 175% of their original lengths. As microthreads are stretched, their diameters decrease, and the topography changes from a smooth surface (0% and 75% stretch microthreads) to a surface with aligned grooves present at the 150% and 175% stretch groups (white arrows). Scale = 25 μm and inset image scale = 400 μm .

(Figure 4.6, 150% and 175%), suggesting that the uniaxial deformation generated by stretching of the microthreads may impart fibrillar reorganization on the surface of the microthreads (Figure 4.6, white arrows). Both the dry and wet diameters of microthreads were significantly higher in the low stretch microthread groups compared to the high stretch groups (Figure 4.7A). The swelling ratios of low stretch microthreads were also significantly higher than high stretch groups (Figure 4.7B), suggesting that stretching microthreads decreases both their mean diameters and their swelling ratio. The transverse strain increased with increasing stretch (Figure 4.7C). High stretch microthreads had the highest transverse strain, and the low stretch

microthreads had the lowest. Interestingly, Poisson's ratio was constant regardless of the amount of axial stretch applied to the microthreads (Figure 4.7D), suggesting that this material property is conserved through the stretch regimen applied in this study.

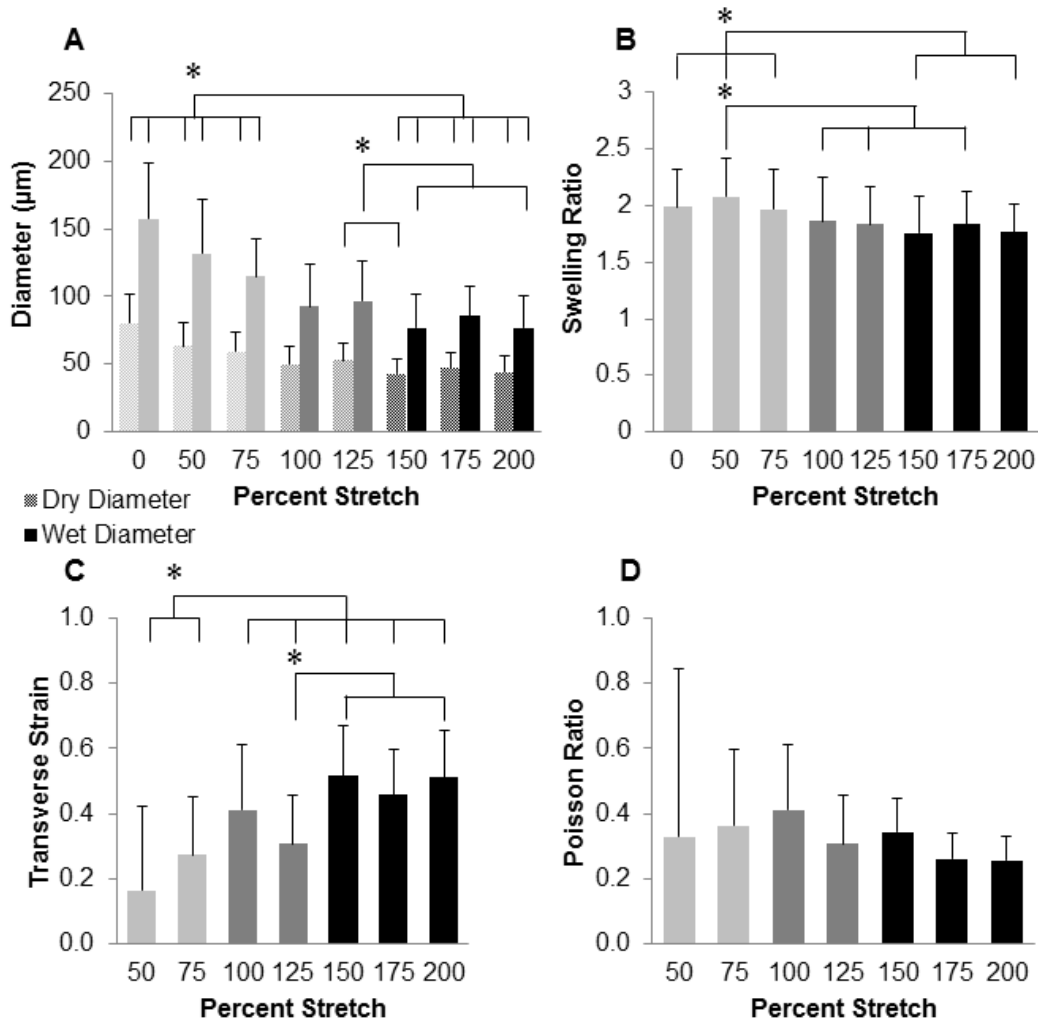


Figure 4.7. Structural properties of fibrin microthreads as a function of stretch. Plots showing changes of wet and dry diameters (A), changes in swelling ratio (B), transverse strain along the diameter of the stretched microthreads (C), and Poisson's ratio (D) as a function of static axial stretch. Low stretch microthreads had significantly larger diameters and higher swelling ratios than high stretch microthreads. Low stretch microthreads had transverse strain measurements that were significantly lower than all other microthreads. Poisson's ratio was found to be constant regardless of the amount of axial stretch applied to the microthreads. * and brackets indicates statistical significance between corresponding similar groups using one-way ANOVA with Holm-Sidak post hoc analysis ($p < 0.05$, $n \geq 41$).

4.3.3 A Drying Phase is Necessary for the Increase in Ultimate Tensile Strength of Stretched Fibrin Microthreads

To investigate whether the microthread drying phase affected the stretching-mediated changes in the mechanical and structural properties of fibrin microthreads, we stretched microthreads immediately after extrusion and polymerization in the HEPES bath (Figure 4.1B). These microthreads were compared to those used in the previous experiment, where a drying step was included after polymerization, but prior to the stretching of the fibrin microthreads (Figure 4.1A). When the UTS values of microthreads stretched immediately after polymerization were compared to corresponding microthreads that had undergone a drying phase prior to stretching, the groups with a drying phase had significantly higher UTS values (Figure 4.8). Additionally, microthreads stretched with a drying phase had smaller diameters than microthreads stretched immediately after polymerization, while 0% stretch microthreads had larger diameters than control microthreads (Table 4.4). Microthreads stretched immediately after polymerization also had comparable UTS values to the control microthreads. However, microthreads that were processed with a drying phase exhibited a fourfold increase in UTS with respect to control microthreads, demonstrating that the combination of a drying phase and stretching are necessary to enhance the mechanical strength of microthreads.

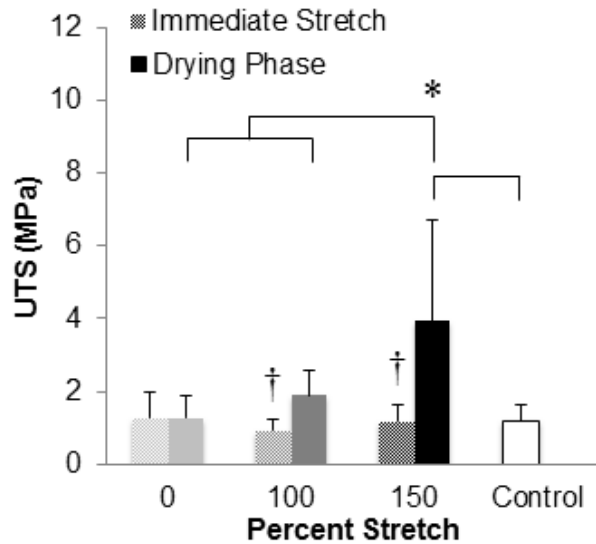


Figure 4.8. Comparison of the UTS of fibrin microthreads stretched with or without a drying phase. The UTS values of microthreads stretched with a drying phase were significantly higher than microthreads that were immediately stretched after polymerization. Additionally, microthreads stretched 150% with a drying phase had significantly higher UTS values than any other group, including the control. * and brackets indicates significance between corresponding groups as determined by one-way ANOVA with Holm-Sidak post hoc analysis and † indicates significance between immediate stretch and drying phase treatments within a single percentage group as determined by Student's t-test ($p < 0.05$, $n \geq 25$).

Table 4.4. The mechanical properties of fibrin microthreads stretched with and without a drying phase.

| Stretch Percent | Drying Phase | Sample Size (n) | Diameter (μm) | | UTS (MPa) | Load (mN) | SAF (mm/mm) |
|-----------------|--------------|-----------------|----------------------------|------------------------|-------------------------|----------------------|-----------------------------|
| | | | Dry | Wet | | | |
| Control | - | 33 | 54 ± 11 | 130 ± 22 | 1.2 ± 0.4 | 15 ± 4 | 0.492 ± 0.239 |
| 0% | + | 29 | $68 \pm 16^*$ | $156 \pm 33^*$ | 1.3 ± 0.6 | $23 \pm 11^*$ | $0.899 \pm 0.217^*$ |
| 0% | - | 34 | $69 \pm 10^*$ | $164 \pm 21^*$ | 1.3 ± 0.7 | $27 \pm 18^*$ | $0.755 \pm 0.318^*$ |
| 100% | + | 31 | $42 \pm 9^*$ | $97 \pm 17^*$ | 1.9 ± 0.7 | 13 ± 4 | 0.419 ± 0.136 |
| 100% | - | 31 | $48 \pm 8^{\dagger}$ | $132 \pm 13^{\dagger}$ | $0.9 \pm 0.3^{\dagger}$ | 12 ± 3 | $0.669 \pm 0.130^{\dagger}$ |
| 150% | + | 32 | $47 \pm 13^*$ | $100 \pm 37^*$ | $3.9 \pm 2.8^*$ | $23 \pm 9^*$ | 0.487 ± 0.235 |
| 150% | - | 25 | $47 \pm 9^*$ | $123 \pm 21^{\dagger}$ | $1.2 \pm 0.5^{\dagger}$ | $13 \pm 4^{\dagger}$ | 0.546 ± 0.141 |

\dagger indicates statistical significance from microthreads stretched with a drying phase determined with a Student's t-test ($p < 0.05$) and * indicates statistical significance from control microthreads using one-way ANOVA with Holm-Sidak post hoc analysis ($p < 0.05$).

4.3.4 Stretch Does Not Affect the Proteolytic Degradation of Fibrin Microthreads

To evaluate whether static axial stretching affects the rate of proteolytic degradation of fibrin microthreads, microthreads were incubated with plasmin and the degradation of the microthreads was observed over time as a function of the change in microthread diameter. Since results from Chapter 3 showed a rapid rate of degradation of uncrosslinked fibrin microthreads,¹⁷ the kinetics of proteolytic degradation were slowed by performing the assay at room temperature. There was a trend for moderate and high stretch microthreads to have smaller d/d_0 ratios than low stretch microthreads at any point in time (Figure 4.9), however, no significant differences were observed in the degradation rate of low, moderate, or high stretch fibrin microthreads, based on d/d_0 measurements.

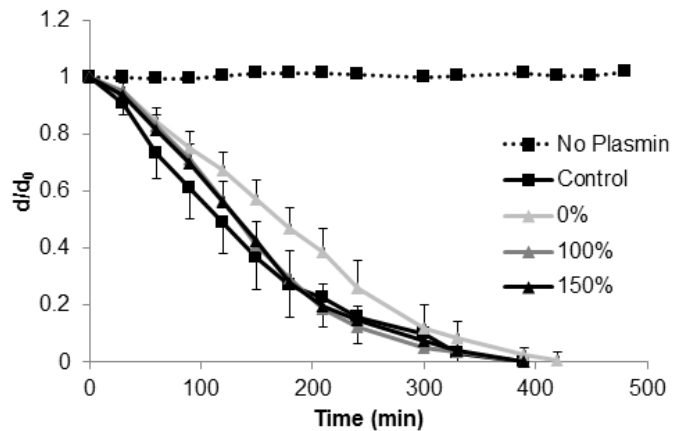


Figure 4.9. Degradation profiles of microthreads static axially stretched with a drying phase. Plots show changes in microthread diameter as a function of time and stretching regime. While 0% stretch microthreads exhibited a lag in the initial rate of degradation with respect to 100% and 150% stretch microthreads as indicated by a smaller negative slope of d/d_0 versus time, none of these degradation profiles are significantly different from one another or from control microthreads that were made with the current fabrication process ($n=6$).

4.3.5 Stretch Enhances Cell Alignment along the Longitudinal Axis of Fibrin Microthreads

We investigated how stretching fibrin microthreads affected cell alignment of C2C12 myoblasts after seeding. All stretch percentages facilitated a range of cell alignment with respect to the long axis of the microthread (Figure 4.10A). Cells tended to align more closely with the longitudinal axis of the microthreads with increasing levels of stretch, resulting in a 30% increase in myoblast nuclei oriented relative to low stretch microthreads (0-15° cell angle). The percentage of cells that showed no preferential orientation to the long axis of microthreads

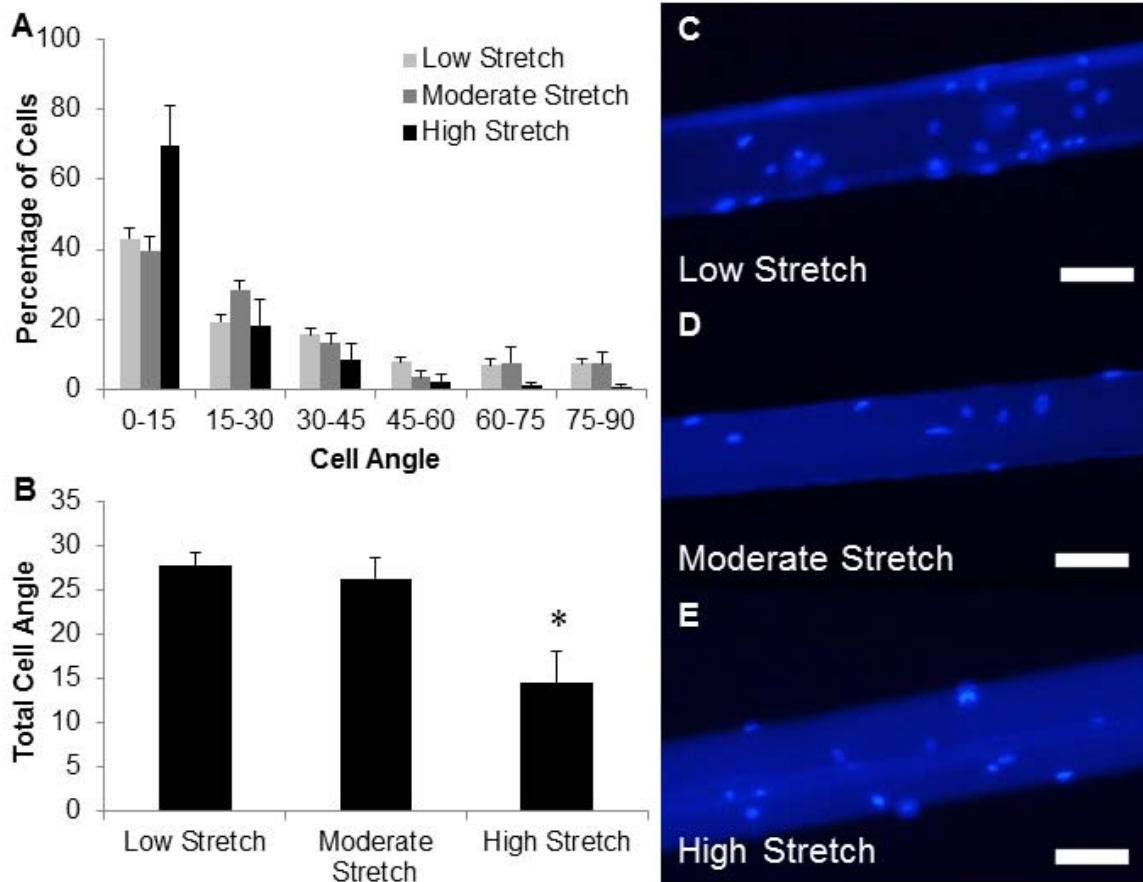


Figure 4.10. C2C12 myoblast alignment on static axially stretched fibrin microthreads. Results of the nuclear alignment analysis are presented as histograms of the average percentage of nuclei oriented along the long axis of the microthread in 15° increments (A). In all cases, most nuclei were aligned with the long axis of the microthread (0-15° orientation). There was no change in the amount of cells aligned with the long axis of the microthread between low and moderate stretch microthread groups; however, there was almost a twofold increase with high stretch microthreads. The average alignment angle of all nuclei along the microthreads shows that the average nuclear angle decreased twofold when cultured on high stretch microthreads (B). Representative fluorescent images of Hoechst stained nuclei on stretched microthreads show similar levels of attachment to microthreads regardless of their stretch regime (C-E). * indicates significance with all other groups as determined by one-way ANOVA with Holm-Sidak post hoc analysis ($p < 0.05$, $n \geq 150$ cells analyzed for each group, $n \geq 2$ experimental duplicates, scale = 100 μm).

(45-90° cell angle) also decreased with increased stretch regimes (22%, 18%, and 4% for low, moderate, and high stretch microthreads, respectively). When the alignment angles of all of the cells were averaged together, there was almost a twofold, statistically significant decrease in cell orientation with respect to the long axis of the microthread (Figure 4.10B). Taken together, these data show that the surfaces of moderate and high stretch microthreads direct increased alignment of myoblast nuclei along the long axis of microthreads. This trend was most evident with myoblasts analyzed in the high stretch group, where a majority of cells were aligned within 15 degrees of the microthread axis, and had the least amount of cells aligned towards the circumferential axis of the microthreads.

4.4 DISCUSSION

The goal of the present study was to characterize fibrin microthreads with tunable structural properties in the absence of exogenous crosslinking agents. Fibrin microthreads are a platform technology that can be used as scaffolds for tissue regeneration in a variety of tissue systems such as skeletal muscle, skin, tendon, ligament, or myocardium. Each of these tissue systems has distinct mechanical and structural requirements, suggesting that there is a significant need to create fibrin microthreads with tunable mechanical properties. In this study, we demonstrated that microthreads dried after polymerization, rehydrated, and then stretched to specific percentages produced three distinct stretch regimes (low, moderate or high stretch) that produce microthreads with specific mechanical properties. The tensile properties reported in this study for moderate and high stretch microthreads are comparable to those previously reported for carbodiimide crosslinked fibrin microthreads in Chapter 3.¹⁷ High stretch fibrin microthreads have tensile strengths comparable to carbodiimide crosslinked microthreads in an acidic buffer (EDCa), and moderate stretch microthreads are comparable to carbodiimide crosslinked microthreads in a neutral buffer (EDCn). While UTS values of stretched microthreads were comparable to carbodiimide crosslinked microthreads, the stiffness of these microthreads increased three to fourfold in comparison to carbodiimide crosslinked microthreads.

Our observations that the tensile strength of fibrin microthreads increased with the magnitude of microthread stretching are consistent with previous observations with collagen microthreads, where UTS and stiffness values of uncrosslinked collagen microthreads increased

with static axial stretching.¹⁹ Furthermore, when fibrin gels were stretched and imaged with atomic force microscopy, a significant increase in the interfibrillar alignment of fibrin fibrils was observed.¹⁵ Interestingly, we did not observe any changes in Poisson's ratio with increasing stretch, suggesting that these microthreads, composed of a dense fibrin matrix, demonstrated a consistent level of hydration within their fibrillar network, as was previously suggested with low concentration fibrin gels.²⁰ Together with the swelling ratio observations, we hypothesize that the combination of static axial stretching and drying are affecting the ability of the microthreads to swell independent of Poisson's ratio, resulting in decreased water content and subsequently increased packing density within the microthreads. These combined findings suggest that the increased tensile strength and stiffness of stretched microthreads is due to an increase in the interfibrillar orientation and interaction of fibrin fibrils within the microthread. An increase in the interfibrillar alignment could explain why no significant decreases in the load at failure were observed for stretched microthreads even when we observed decreases in the diameter of stretched fibrin microthreads.

When C2C12 myoblasts were seeded on the surfaces of stretched fibrin microthreads, we observed that cell orientation appeared to sense changes in the topography on the surfaces of the scaffold. Small cylindrical substrates, such as fibrin microthreads, have been previously shown to facilitate longitudinal alignment of cells.^{9,21} This phenomenon may explain why approximately 40% of the myoblast nuclei were oriented with the longitudinal axis of low stretch microthreads (0-15° orientation). In this study, we observed that there was a shift in the overall distribution of cell alignment towards the long axis of the scaffold when we applied a high stretch regimen to the microthreads and further, that the mean alignment angle of cells seeded on stretched microthreads significantly decreased twofold. Additionally, it has been shown that increasing the alignment of fibers on the surface of a scaffold will enhance myoblast alignment along the scaffold.²² Our SEM micrographs provide evidence of longitudinal topography on high stretch microthreads, further suggesting an alignment of the fibrils on the surface of the microthreads, similar to previous observations for stretched fibrin gels.^{15,23} Together, these findings support our hypothesis that static axial stretching of fibrin microthreads facilitates the reorganization and alignment of fibrin fibrils on the surfaces of scaffolds. To our knowledge, there has been little work on the design of scaffolds that concurrently mimic a tissue-like fibrous

architecture and also provide topographic instructive cues that direct cell function and orientation. In future studies, we will combine the findings presented here with an analysis on the topography of fibrin microthreads to assess the contribution of microthread topography to cell alignment, based on the hypothesis that the internal reorganization of fibrin fibrils within the microthread produces an aligned surface topography that facilitates enhanced cell alignment.

It is interesting to note that static axially stretched fibrin microthreads show strain hardening ratios of 2-4, similar to previously reported values for uncrosslinked, single fibrin fibers.¹⁴ Regardless of the amount of strain on the microthreads during uniaxial loading, there is a tenfold increase in stiffness between low and high stretch microthreads. Previous studies have shown that stiffer substrates stimulate myoblast proliferation, which may be important for delivering enough myoblasts to repair large muscle defects *in vivo* for skeletal muscle regeneration.^{24,25} In addition to increased alignment of fibrils on the surface of the scaffold, substrate stiffness has been suggested to enhance cell alignment, a critical step towards myoblast fusion.²⁶ While we have not characterized alignment-guided myoblast differentiation on static axially stretched fibrin microthreads as a function of scaffold rigidity, we hypothesize that there would be an increased ability of stretched microthreads to support myoblast differentiation.

Previous studies showed that fibrin clots stretched 200-300% of their original length degraded at a slower rate, suggesting that stretching fibrin fibrils somehow blocked access of proteases to their target sites in fibrin.²⁷ In this study, we showed that fibrin microthreads, stretched 0-200% of their original length, generated scaffolds with tunable mechanical and morphologic properties without significantly changing the rate of proteolytic degradation of the materials. In previous studies, the density of fibrin fibrils has also been found to influence fibrinolysis, where densely packed, larger fibrin fibrils were found to degrade at slower rates than less densely packed, or thinner, fibrin fibrils.^{28,29} It is important to note that in these previous studies, researchers examined physiologic concentrations of fibrinogen. In our study, fibrin microthreads are extruded with a fibrinogen concentration that is almost tenfold higher than physiologic levels. We hypothesize that stretching these fibrin microthreads plastically deforms the fibrin fibril network within the microthread rather than protect discrete degradation sites. This mechanism may explain why we did not observe a significant change in the degradation rate of stretched microthreads.

When uncrosslinked microthreads were implanted in a large skeletal muscle defect, microthreads were shown to degrade within 1-2 weeks.³⁰ It was hypothesized that microthreads would have to persist for a longer duration of time for use as a scaffold in a large muscle defect. Static axial stretching of fibrin microthreads has not been found to significantly affect proteolytic degradation, so *in vivo* applications for these microthreads may be limited to implantation times of 1-2 weeks. Another application for fibrin microthreads has been to use microthreads as suture material, as well as a cell delivery vehicle.³¹ We report here an efficient, and reproductive, method for increasing the mechanical strength of fibrin microthreads, which may aid in the use of these microthreads as a suture material due to their enhanced tensile strengths. The ability to stretch fibrin microthreads is also favorable from a manufacturing standpoint, as this method would increase the yield of usable microthreads per batch as well as standardize the microthread production process to reduce batch-to-batch variability. Further modifications of stretched microthreads, such as carbodiimide crosslinking, could generate microthreads with additional resistance to degradation as well as increased strength for use as a long-term scaffold for a variety of tissue regeneration applications. However, because of a lack of an increased resistance to proteolytic degradation, static axially stretched microthreads are not recommended for implantation into large muscle defects for skeletal muscle regeneration.

4.5 CONCLUSIONS

In this study, we present fibrin microthreads that are dried, rehydrated, and then static axially stretched with low (0-75%), moderate (100-125%), or high (150-200%) stretch regimes to generate tunable mechanical properties such as UTS and stiffness. The increase in UTS was attributed to the drying phase as well as the decrease in microthread diameter, as failure loads did not change. Increased strengths were comparable to those of carbodiimide crosslinked microthreads,¹⁷ demonstrating that crosslinking is not necessary to increase the mechanical strength of microthreads.

The fact that high stretch microthreads failed at the same load as low-stretch microthreads suggests that static axial stretching is reorganizing the fibrillar structure of fibrin fibrils within the microthreads. This hypothesis was supported by SEM micrographs and increased cell alignment on high-stretch microthreads. Interestingly, stretched microthreads with

increased mechanical strength did not have enhanced resistance to proteolytic degradation. Taken together, these findings suggest that we have developed a mechanism by which we can tune microthread structural properties without affecting their proteolytic degradation. Additionally, combining this process with crosslinking, or the incorporation of bioactive molecules, will significantly enhance the functional utility of these materials for the design of therapeutic delivery systems and scaffolds to promote functional tissue regeneration.

4.6 ACKNOWLEDGEMENTS

This research was funded in part by US Army (W81XWH-11-1-0631) and NIH R01-HL115282 (GDP) and NIH F31-DE023281 (JMG). The authors wish to thank Keith Gagnon for his technical assistance and Pat Flaherty for his help with the statistical analyses.

4.7 REFERENCES

1. Reprinted from: *Acta Biomaterialia*, 10(10), Grasman JM, Pumphrey LM, Dunphy M, Perez-Rogers J, Pins GD, "Static axial stretching enhances the mechanical properties and cellular responses of fibrin microthreads", 4367-4376, Copyright (2014), with permission from Elsevier.
2. Pins GD, Christiansen DL, Patel R, Silver FH. Self-assembly of collagen fibers. Influence of fibrillar alignment and decorin on mechanical properties. *Biophysical Journal* 1997;73:2164-2172.
3. Cornwell KG, Lei P, Andreadis ST, Pins GD. Crosslinking of discrete self-assembled collagen threads: Effects on mechanical strength and cell-matrix interactions. *J Biomed Mater Res A* 2007;80(2):362-71.
4. Zeugolis DI, Paul GR, Attenburrow G. Cross-linking of extruded collagen fibers--a biomimetic three-dimensional scaffold for tissue engineering applications. *Journal of biomedical materials research. Part A* 2009;89(4):895-908.
5. Chen J, Altman GH, Karageorgiou V, Horan R, Collette A, Volloch V, Colabro T, Kaplan DL. Human bone marrow stromal cell and ligament fibroblast responses on RGD-modified silk fibers. *J Biomed Mater Res A* 2003;67(2):559-70.
6. Horan RL, Antle K, Collette AL, Wang Y, Huang J, Moreau JE, Volloch V, Kaplan DL, Altman GH. In vitro degradation of silk fibroin. *Biomaterials* 2005;26(17):3385-93.
7. Horan RL, Collette AL, Lee C, Antle K, Chen J, Altman GH. Yarn design for functional tissue engineering. *Journal of biomechanics* 2006;39(12):2232-40.
8. Cornwell KG, Downing BR, Pins GD. Characterizing fibroblast migration on discrete collagen threads for applications in tissue regeneration. *J Biomed Mater Res A* 2004;71(1):55-62.
9. Cornwell KG, Pins GD. Enhanced proliferation and migration of fibroblasts on the surface of fibroblast growth factor-2-loaded fibrin microthreads. *Tissue Eng Part A* 2010;16(12):3669-77.
10. Turner NJ, Badylak SF. Regeneration of skeletal muscle. *Cell and tissue research* 2012;347(3):759-74.
11. Clark RA. Fibrin and wound healing. *Ann N Y Acad Sci* 2001;936:355-67.
12. Brown AC, Barker TH. Fibrin-based biomaterials: modulation of macroscopic properties through rational design at the molecular level. *Acta biomaterialia* 2014;10(4):1502-14.
13. Grassl ED, Oegema TR, Tranquillo RT. Fibrin as an alternative biopolymer to type-I collagen for the fabrication of a media equivalent. *Journal of Biomedical Materials Research* 2002;60(4):607-612.
14. Liu W, Carlisle CR, Sparks EA, Guthold M. The mechanical properties of single fibrin fibers. *Journal of thrombosis and haemostasis : JTH* 2010;8(5):1030-6.

15. Matsumoto T, Sasaki J, Alsberg E, Egusa H, Yatani H, Sohmura T. Three-dimensional cell and tissue patterning in a strained fibrin gel system. *PLoS ONE* 2007;2(11):e1211.
16. Cornwell KG, Pins GD. Discrete crosslinked fibrin microthread scaffolds for tissue regeneration. *J Biomed Mater Res A* 2007;82(1):104-12.
17. Grasman JM, Page RL, Dominko T, Pins GD. Crosslinking strategies facilitate tunable structural properties of fibrin microthreads. *Acta Biomaterialia* 2012;8(11):4020-30.
18. Proulx MK, Carey SP, Ditroia LM, Jones CM, Fakharzadeh M, Guyette JP, Clement AL, Orr RG, Rolle MW, Pins GD and others. Fibrin microthreads support mesenchymal stem cell growth while maintaining differentiation potential. *J Biomed Mater Res A* 2011;96(2):301-12.
19. Pins GD, Huang EK, Christiansen DL, Silver FH. Effects of static axial strain on the tensile properties and failure mechanisms of self-assembled collagen fibers. *Journal of Applied Polymer Science* 1997;63(11):1429-1440.
20. Lai VK, Lake SP, Frey CR, Tranquillo RT, Barocas VH. Mechanical behavior of collagen-fibrin co-gels reflects transition from series to parallel interactions with increasing collagen content. *Journal of Biomechanical Engineering* 2012;134(1):011004.
21. Rovinsky YA, Samoilo V. Morphogenetic response of cultured normal and transformed fibroblasts, and epitheliocytes, to a cylindrical substratum surface. *J of Cell Science* 1994;107:1255-1263.
22. Choi JS, Lee SJ, Christ GJ, Atala A, Yoo JJ. The influence of electrospun aligned poly(epsilon-caprolactone)/collagen nanofiber meshes on the formation of self-aligned skeletal muscle myotubes. *Biomaterials* 2008;29(19):2899-906.
23. Brown AE, Litvinov RI, Discher DE, Purohit PK, Weisel JW. Multiscale mechanics of fibrin polymer: gel stretching with protein unfolding and loss of water. *Science* 2009;325(5941):741-4.
24. Boontheekul T, Hill EE, Kong HJ, Mooney DJ. Regulating myoblast phenotype through controlled gel stiffness and degradation. *Tissue Engineering* 2007;13(7):1431-42.
25. Gilbert PM, Havenstrite KL, Magnusson KE, Sacco A, Leonardi NA, Kraft P, Nguyen NK, Thrun S, Lutolf MP, Blau HM. Substrate elasticity regulates skeletal muscle stem cell self-renewal in culture. *Science* 2010;329(5995):1078-81.
26. Engler AJ, Griffin MA, Sen S, Bonnemann CG, Sweeney HL, Discher DE. Myotubes differentiate optimally on substrates with tissue-like stiffness: pathological implications for soft or stiff microenvironments. *The Journal of Cell Biology* 2004;166(6):877-87.
27. Varju I, Sotonyi P, Machovich R, Szabo L, Tenekedjiev K, Silva MM, Longstaff C, Kolev K. Hindered dissolution of fibrin formed under mechanical stress. *J Thromb Haemost* 2011;9(5):979-86.
28. Collet JP, Lesty C, Montalescot G, Weisel JW. Dynamic changes of fibrin architecture during fibrin formation and intrinsic fibrinolysis of fibrin-rich clots. *J Biol Chem* 2003;278(24):21331-5.
29. Undas A, Zalewski J, Krochin M, Siudak Z, Sadowski M, Pregowski J, Dudek D, Janion M, Witkowski A, Zmudka K. Altered plasma fibrin clot properties are associated with in-stent thrombosis. *Arterioscler Thromb Vasc Biol* 2010;30(2):276-82.
30. Page RL, Malcuit C, Vilner L, Vojtic I, Shaw S, Hedblom E, Hu J, Pins GD, Rolle MW, Dominko T. Restoration of skeletal muscle defects with adult human cells delivered on fibrin microthreads. *Tissue engineering. Part A* 2011;17(21-22):2629-40.
31. Guyette JP, Fakharzadeh M, Burford EJ, Tao ZW, Pins GD, Rolle MW, Gaudette GR. A novel suture-based method for efficient transplantation of stem cells. *J Biomed Mater Res A* 2013;101(3):809-18.

Chapter 5: Adsorbed Hepatocyte Growth Factor on Crosslinked Fibrin Microthreads Enhances Cell Recruitment

5.1 INTRODUCTION

There are almost 100,000 reconstructive maxillofacial surgical procedures performed annually as a result of traumatic injury, cancer ablation, or cosmetic procedures, profoundly impacting the quality of life of patients.^{1,2} The excision or removal of muscle tissue may occur during these procedures, resulting in large scale muscle injuries termed volumetric muscle loss (VML) injuries, which cannot be repaired by skeletal muscle's innate repair mechanism.³ In small muscle wounds such as those from exercise, the basal lamina rapidly releases hepatocyte growth factor (HGF) upon injury to stimulate the activation, and recruitment, of satellite cells (SCs) to the wound site.⁴⁻⁷ These local progenitor cells reside between the sarcolemma and basal lamina of muscle fibers, and are responsible for the regeneration of skeletal muscle tissue.^{8,9} In VML injuries, this basal lamina has been completely destroyed or removed, and it is unclear what growth factors are present to promote SC migration (i.e. recruitment) into the injury site. The rapid release of HGF occurs in the first 48-72 hours of injury, as prolonged HGF signaling inhibits skeletal muscle regeneration,^{7,10} highlighting the importance of the temporal expression of growth factors in skeletal muscle regeneration. Thus, there is a need for biomimetic scaffolds to recapitulate early regenerative cues, such as HGF signaling, missing in VML injuries to stimulate the recruitment of SCs to the injury site.

To efficiently assess SC recruitment, a variety of *in vitro* chemotactic assays have been described to rapidly measure SC migration assays. Many chemotactic assays such as migration across membranes in Boyden chambers,¹¹ or over defined two-dimensional (2D) substrates,¹² do not accurately mimic the complex three-dimensional (3D) environment present in wound healing. To improve upon 2D migration studies, sophisticated cell tracking algorithms have been developed to track cell movement in 3D gel matrices.^{13,14} While the analysis of migration through gels remains a significant improvement to 2D migration, these models still do not mimic

the highly organized structure present in fibrillar tissues such as skeletal muscle, tendon, or ligament. Our laboratory developed a cell outgrowth assay designed to measure the importance of topographic cues in a model of 3D cell outgrowth along biopolymer microthread materials.^{15,16} Here, cells were seeded into type I collagen gels that mimic the provisional matrix at the wound margins. These collagen gels are cast around 3D biopolymer microthreads, and the rate of cell outgrowth on the microthreads was measured.¹⁵ This method of cell outgrowth, which is a combination of migration and proliferation, occurs in skeletal muscle regeneration, where minor wounds do not result in rupture of the basal lamina, resulting in the longitudinal recruitment of SCs along myofibers to the injury site.^{9,17} In skeletal muscle fibers, the basal lamina is composed of a combination of extracellular proteins such as type IV collagen and laminin-2, but not type I collagen.¹⁸ Furthermore, fibrin is rapidly deposited as a provisional matrix following injury in skeletal muscle as a provisional matrix to support wound healing.¹⁹ Therefore, we aim to modify this assay to generate a model system to predict SC recruitment for skeletal muscle regeneration in skeletal muscle injuries.

In this chapter, we describe an *in vitro* assay that can rapidly assess myoblast outgrowth onto fibrin microthreads as a predictor of *in vivo* recruitment to the injury site by adsorbing HGF to fibrin microthreads. Because HGF is present in the injury site for the first 3 days, our goal was to develop an HGF loading strategy to facilitate the rapid release of HGF. We hypothesized that passive adsorption could be employed as an HGF delivery mechanism to rapidly release HGF, and that HGF-adsorbed fibrin microthreads would enhance the rate of myoblast outgrowth. We demonstrate that HGF can be adsorbed to carbodiimide crosslinked fibrin microthreads in an active form to support 2D myoblast proliferation and migration, and cell outgrowth in a 3D environment. The release of adsorbed HGF from crosslinked microthreads corresponded to the time frame of HGF expression in skeletal muscle injuries.²⁰ HGF incorporation onto crosslinked microthreads could be essential for modulating skeletal muscle progenitor cell recruitment to wound sites such as those in VML, and could amplify the regenerative response of damaged tissues to scaffolds.

5.2 MATERIALS and METHODS

5.2.1 Fibrin Microthread Preparation

5.2.1.1 Microthread Extrusion

Fibrin microthreads were co-extruded from solutions of fibrinogen and thrombin using extrusion techniques described in section 3.2.1.1.^{21,22} Briefly, fibrinogen from bovine plasma (Sigma, St. Louis, MO; F8630) was dissolved in HEPES (N-[2-Hydroxyethyl]piperazine-N'-[2-ethanesulfonic acid]) buffered saline (HBS, 20 mM HEPES, 0.9% NaCl; pH 7.4) at 70 mg/mL and stored at -20 °C until use. Thrombin from bovine plasma (Sigma; T4648) was dissolved in HBS at 40 U/mL and stored at -20 °C until use.

To fabricate microthreads, fibrinogen and thrombin solutions were thawed and warmed to room temperature, and thrombin was mixed with a 40 mM CaCl₂ (Sigma) solution to form a working solution of 6 U/mL. Fibrinogen and thrombin/CaCl₂ solutions were loaded into 1 mL syringes which were inserted into a blending applicator tip (Micromedics Inc., St. Paul, MN; SA-3670). The solutions were combined in the blending applicator and extruded through polyethylene tubing (BD, Sparks, MD) with an inner diameter of 0.86 mm into a bath of 10 mM HEPES (pH 7.4) in a Teflon coated pan at a rate of 0.225 mL/min using a dual syringe pump. After 10 minutes, 25.4 cm, amorphous fibrin microthreads were removed from the buffer solution and stretched to form three-19-cm microthreads; these were air dried under the tension of their own weight. Dry microthreads were placed in aluminum foil and stored in a desiccator until use.

5.2.1.2 Fibrin Microthread Crosslinking

Fibrin microthreads were crosslinked using techniques described previously in section 3.2.1.2.²² Briefly, microthreads were hydrated in an acidic buffer of 50 mM 2-(N-morpholino)ethanesulfonic acid (MES, Sigma, pH 5.2) or a neutral buffer of 100 mM monosodium phosphate (NaH₂PO₄, Sigma, pH 7.4) for 30 minutes and then crosslinked in either acidic (EDCa) or neutral (EDCn) buffer containing 16 mM N-hydroxysuccinimide (NHS, Sigma) and 28 mM 1-ethyl-3-(3-dimethylaminopropyl)carbodiimide (EDC, Sigma) for 2 hours at room temperature. After crosslinking, the buffered EDC/NHS solution was aspirated and the

microthreads were rinsed three times in deionized (DI) water, air dried, and stored in a desiccator until use.

5.2.2 Adsorption of HGF to Microthreads

Three similarly treated microthreads (uncrosslinked (UNX), EDCn, or EDCa) 1.8 cm in length were attached onto polydimethylsiloxane (PDMS, 0.75 in. inner diameter, Dow Corning, Midland, MI) rings, sterilized with 70% ethanol for 90 minutes, rinsed in DI water 3 times, and air dried in a laminar flow hood overnight. Sterile microthread-PDMS constructs were hydrated in Dulbecco's phosphate buffered saline (DPBS) and the PDMS surfaces were blocked with 0.25% bovine serum albumin (BSA, Sigma) for 1 hour. These solutions were aspirated and replaced with 1 mL of varied concentrations of HGF (0, 5, 10, 20, 40 or 100 ng/mL, Peprotech, Rocky Hill, NJ) in DPBS and incubated at room temperature for 2 hours. The microthreads were rinsed five times in DPBS and immediately used for experiments. To estimate the amount of HGF adsorption, we loaded microthreads with 100 ng/mL fluorescein isothiocyanate (FITC)-labeled BSA (Sigma), rinsed the microthreads five times in DPBS, and imaged the microthreads with a Zeiss inverted microscope (Zeiss, Thornwood, NY).

5.2.3 Cell Culture

Immortalized mouse myoblasts (C2C12, ATCC, Manassas, VA) were cultured in a 1:1 (v/v) ratio of high glucose Dulbecco's modified Eagle Medium (DMEM, Gibco BRL, Gaithersburg, MD) supplemented with 4 mM L-glutamine and Ham's F12 (Gibco) with 10% fetal bovine serum (FBS, HyClone, Logan, UT). Cells were incubated at 37 °C with 5% CO₂ and maintained at a density below 70% confluence using standard cell culture techniques. Routine cell passage was conducted using 0.25% trypsin-EDTA (CellGro, Manassas, VA).

5.2.4 Quantifying Release of HGF from Microthreads

To quantify the active release of HGF, three HGF-loaded (0, 40, or 100 ng/mL HGF) microthreads attached to PDMS rings were incubated in 1 mL of serum-free medium (SFM, 1:1 v/v high glucose DMEM/F-12). At 24 hour increments, two 0.5 mL aliquots of conditioned-SFM (C-SFM) were replaced and incubated on C2C12 myoblasts to determine the ability of the

C-SFM to induce myoblast proliferation. Myoblasts were seeded in 24 well plates at a density of 10,000 cell/well and incubated in SFM for 4 hours prior to incubation with C-SFM to maintain a uniform cell population for each experiment. As a negative or positive control, myoblasts were cultured in SFM containing either 0 or 5 ng/mL of soluble HGF, respectively. Each experimental condition was run in triplicate. After an incubation time of 4 hours in C-SFM, cells were fixed with ice cold methanol, permeabilized with 0.1% Triton X-100 (Sigma), immunostained with a primary antibody against Ki67 (1:400, D3B5; Cell Signaling Technologies, Danvers, MA) and an Alexafluor 568 secondary (1:200, Life Technologies, Carlsbad, CA), then counterstained with Hoechst 33342 (1:6000, Molecular Probes). To determine the percentage of proliferating cells, five images were taken of each well with a Zeiss inverted microscope and the number of Ki67 positive nuclei were normalized to the total number of nuclei counted in each image.

5.2.5 Two-dimensional Motogenic Response from HGF-loaded Microthreads

To confirm that released HGF could stimulate myoblast migration, a dual-well PDMS device 5 mm thick was fabricated with two 1.9 cm diameter chambers and a 1 cm long, 3 mm wide, cell migration channel between the two chambers, which was initially sealed with a PDMS plug (Figure 5.1A). PDMS constructs were autoclave sterilized and secured to the bottom of P60 dishes (BD Falcon, Franklin Lakes, NJ) with sterile vacuum grease (Dow Corning). Three HGF-loaded microthreads were placed in the first chamber to serve as an HGF reservoir with 1 mL of medium, and the second chamber was seeded with 80,000 myoblasts in 1 mL of medium. As a negative or positive control, the first chamber was loaded with 0 or 100 ng/mL of soluble HGF, respectively. The cell seeding chamber was rinsed 4 hours after seeding to remove any non-adherent cells from the well, and then the plug separating the two chambers was removed (Figure 5.1B). Both chambers received equal volumes of medium to limit fluid flow after the removal of the plug. The cell front was immediately imaged and reimaged every 6 hours for 24 hours on a Leica inverted microscope (Leica, Wetzlar, Germany) coupled with Leica imaging software (Figure 5.1C). Each experimental condition was run in duplicate. To calculate migration rates, the position of the cells was determined at each time based on their distance from their starting

location in ImageJ (NIH), and a line of linear regression was fitted for each sample using Excel (Redmond, WA), where the slope is the migration rate ($\mu\text{m/hr}$) (Figure 5.1D).

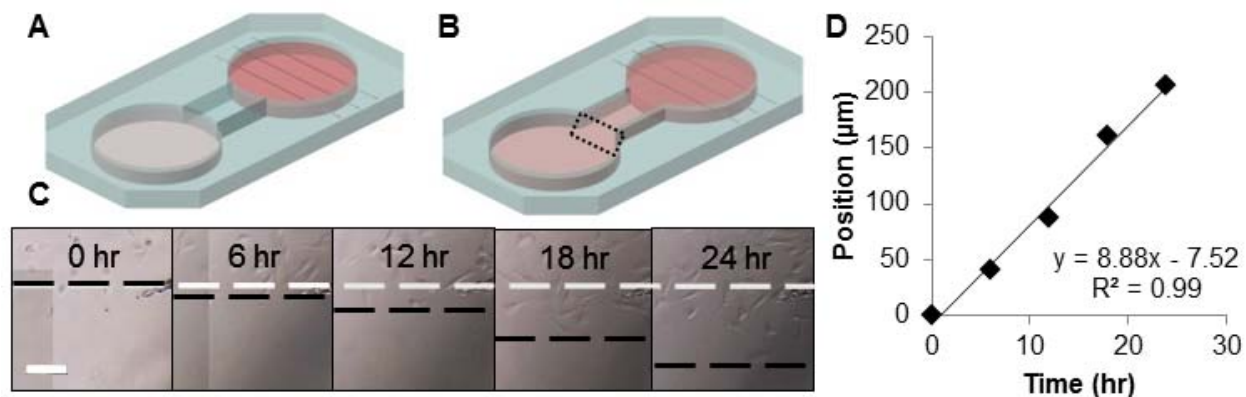


Figure 5.1. Two dimensional assay developed to quantify the migration of myoblasts towards HGF-loaded microthreads. Schematic of 2D migration assay. Three similarly crosslinked microthreads loaded with 0, 40, or 100 ng/mL of HGF were placed in one chamber, and C2C12 myoblasts were seeded into the second chamber (A). The two chambers were isolated with a PDMS block, which was removed to establish an HGF gradient at the start of the experiment (B). Brightfield images were taken where the cell front was present in the cell-seeded chamber every 6 hours (C), and the distance from their starting position (gray dashed line) was measured over time. The distance traveled at each time point was plotted in Excel, and was fit to a line of linear regression, where the slope of the regression line was the migration rate (D). Scale = 50 μm .

5.2.6 Three-dimensional Motogenic Outgrowth from HGF-loaded Microthreads

To measure cell outgrowth in a 3D model, we developed an outgrowth assay based upon a previously described outgrowth system.¹⁵ Here, the outgrowth assay was miniaturized to reduce medium volumes, and to isolate different microthread conditions from each other. Raised rectangular platforms of Thermanox[®] tissue culture plastic (3 x 13 mm) (Nalge Nunc, Rochester, NY) were elevated 2-3 mm above the surface of 6 well tissue culture dishes using molded PDMS plugs, and secured in place with medical-grade silicone adhesive (Factor II, Lakeside, AZ) (Figure 5.2A). The outgrowth assays were sterilized in 70% ethanol for at least 2 hours, rinsed in DI water 3 times, and then air dried in a laminar flow hood.

After 0, 5, 10, 20, or 40 ng/mL of HGF was adsorbed to fibrin microthreads, the PDMS rings were affixed to the outgrowth assay with four dots of sterile vacuum grease so that the microthreads were in contact with the central region of the raised platforms (Figure 5.2A). Each platform system had 6 microthread/platform interfaces, and each condition was done in duplicate.

To create cell outgrowth assays, 40 μL of myoblast-populated fibrin gels were placed on each platform. These fibrin gels were produced by generating a 1 mL aliquot of sterile fibrinogen (5.22 mg/mL), thrombin (2.35 U/mL), calcium chloride (31.25 mM), and cell solution (909,000 cell/mL) in a 8:1:1:2 ratio to produce a fibrin gel with a final fibrinogen concentration of 3.5 mg/mL and a final cell concentration of 150,000 cell/mL. Prior to mixing into the fibrin gel solution, myoblasts were loaded with DiO (Life Technologies) for twenty minutes, following the manufacturer's instructions. Myoblast-populated fibrin gels were incubated at 37 °C for 1 hour to facilitate complete gel formation, after which the wells were flooded with 4 mL of medium to completely cover the top of the gel.

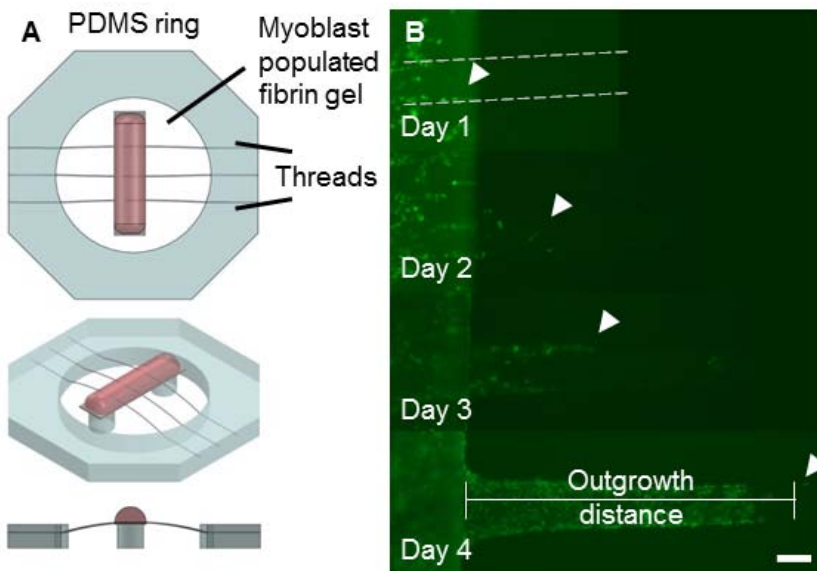


Figure 5.2. Myoblast outgrowth assay schematic. A top, isometric, and side projection of the outgrowth assay (A). Microthreads were suspended over an elevated Thermanox coverslip, upon which a myoblast populated fibrin gel was seeded. Representative images from the outgrowth assay (B). Dashed white lines highlight the thread edges, and the Thermanox coverslip is visible as the autofluorescent green rectangle on the left side of the images. Arrowheads indicated the furthest cell along the microthread, and the outgrowth distance at each time point was determined to be the distance to the leading cell (arrowhead) from the edge of the coverslip. Scale = 100 μm .

To study cell outgrowth on the fibrin microthreads, the microthread-coverslip interfaces were imaged daily to measure outgrowth, and the position of the leading cell was determined based on its distance from the edge of the coverslip (Figure 5.2B). To measure the effect of HGF on myoblast outgrowth, the outgrowth rate was determined as the slope of the line of linear regression from the first two days. After two days, the amount of dye present in migration cells was diminished due to cell division, so cells were redosed with DiO by adding 1 mL of medium supplemented with 5 μL of DiO solution. Microthreads were incubated in DiO-supplemented medium for 20 minutes, and then 3 mL of medium was removed from the wells and replaced

with 2 mL of fresh medium. The wells were gently agitated to mix the medium, and then an additional 2 mL was removed from each well and replaced with 2 mL of fresh medium.

After four days of culture, outgrowth assays were fixed in 4% paraformaldehyde and two microthreads per treatment group were permeabilized with 0.1% Triton X-100 and stained for Ki67, as described above in section 5.2.4. A single image from each microthread, focusing on the leading cell as well as the following confluent layer of cells, was imaged using a 20X long distance objective on an inverted Zeiss microscope, and the percentage of Ki67 positive nuclei were normalized to the total number of nuclei present the image.

5.2.7 Statistical Analyses

Statistical analyses were performed using a one-way analysis of variance (ANOVA) with $p < 0.05$ indicating significant differences between groups using SigmaPlot 11.0 software (Systat Software, Inc., San Jose, CA). For post hoc analysis, a Holm-Sidak pairwise multiple comparison test was performed to determine significance between experimental groups using an overall significance level of $p < 0.05$. The data are reported as means \pm standard error, where the sample size indicates the number of experimental replicates performed.

5.3 RESULTS

5.3.1 Adsorbed HGF is Rapidly Released from Fibrin Microthreads

To characterize the mechanism by which passively adsorbed HGF is released from fibrin microthreads, we developed several assays to study the release, and activity, of HGF. FITC-labeled BSA was used as a model molecule to confirm protein adsorption on UNX and crosslinked microthreads, based on its similar molecular weight to HGF. For UNX and EDCn microthreads, no FITC signal was detected with un-labeled BSA (Figure 5.3 A-B). When FITC-labeled BSA was adsorbed to UNX and EDCn microthreads, there was an increase in detectable FITC signal, with qualitatively more BSA adsorption observed on EDCn microthreads than on UNX microthreads (Figure 5.3 D-E). Interestingly, there was no notable evidence of BSA adsorption onto EDCa microthreads, relative to control samples (Figure 5.3 C and F). Together, these findings suggest that crosslinking the fibrin microthreads in a neutral environment affects the ability of molecules to bind to the surface of the microthreads.

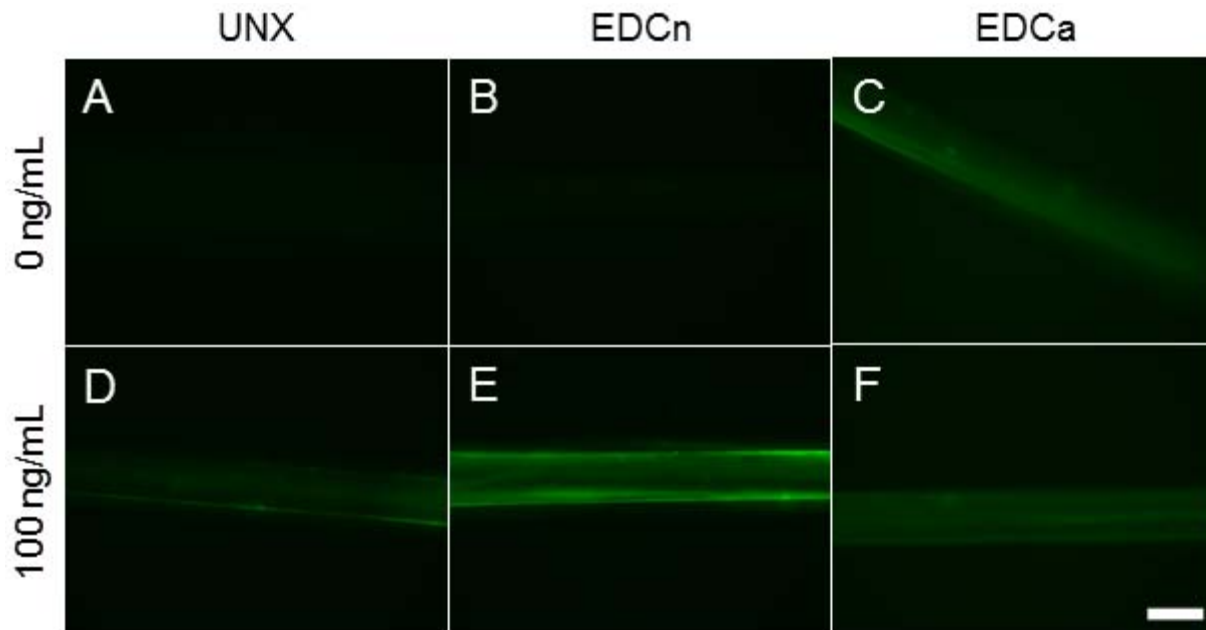


Figure 5.3. Representative images of microthreads loaded with FITC-labeled BSA. UNX (A, D), EDCn (B, E), or EDCa (C, F) microthreads were loaded with 0 ng/mL (A-C) or 100 ng/mL (D-F) FITC-BSA. UNX and EDCn microthread controls did not show evidence of fluorescence (A, B), and adsorbed FITC-BSA increased the detectable fluorescence of these microthreads (D, E). EDCa microthreads did not show any evidence of BSA adsorption (F), relative to controls (C). Scale = 100 μ m.

To quantitatively evaluate the temporal release activity of HGF from microthreads, myoblasts were incubated in medium conditioned by HGF-adsorbed microthreads and cells were assayed for increases in Ki67 expression. The percent of Ki67 positive myoblasts significantly increased with SFM conditioned with HGF coated EDCn microthreads at day one (Figure 5.4A). This level of stimulation was equivalent to that of 5 ng/mL of soluble HGF, which is in the range of HGF concentrations found in the literature to maximally stimulate proliferation in myoblast populations.²³ Active HGF was detected from UNX microthread C-SFM at day one, and no HGF-response was detected from EDCa microthreads (Figure 5.4A). Interestingly, EDCa microthread C-SFM stimulated myoblast proliferation regardless of the concentration of HGF adsorbed at one day. HGF coated, EDCn microthread C-SFM from day two also stimulated myoblast proliferation to values comparable to 5 ng/mL of soluble HGF (Figure 5.4B); however, by day four C-SFM was not found to have any effect on myoblast proliferation (Figure 5.4C).

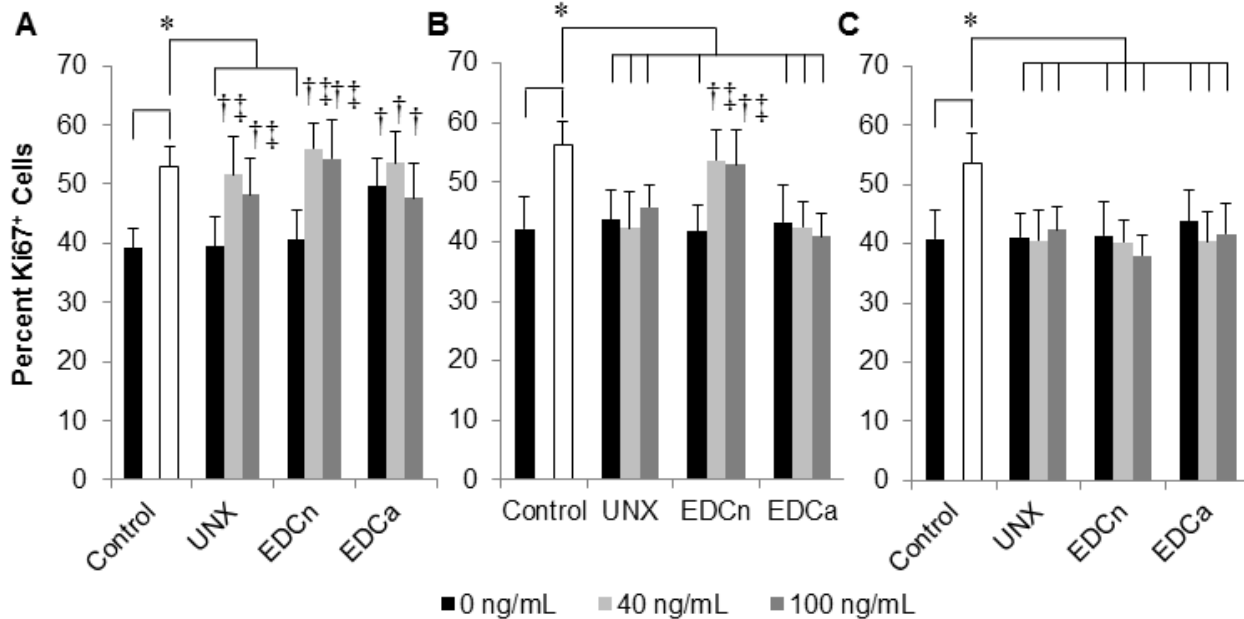


Figure 5.4. Percentage of C2C12 myoblasts expressing Ki67 stimulated from fibrin microthread C-SFM. Microthreads had increasing amounts of HGF adsorbed to their surfaces, and the ability of microthread C-SFM was compared to SFM with no exogenous HGF (negative control, black control bar) and SFM supplemented with 5 ng/mL HGF (positive control, white control bar). C-SFM from 24hrs (A), 48 hrs (B), and 96 hrs (C) were analyzed. EDCn microthread C-SFM from the first and second days were able to stimulate significantly higher amounts of myoblasts to express Ki67 compared to negative controls while releasate from the fourth day showed no increases in proliferation, suggesting that active HGF is released within the first two days of culture. † indicate statistical significance with the negative control, ‡ indicate statistical significance with the 0 ng/mL of the same microthread treatment group, and * represent statistical significance with the indicated groups as determined by one-way ANOVA with Holm-Sidak post hoc analysis ($p > 0.05$, $n \geq 2$).

5.3.2 HGF Released from Fibrin Microthreads is a Motogenic Factor for Myoblasts

To confirm that released HGF could stimulate myoblast migration, a dual-well PDMS device was fabricated where one reservoir had three HGF-loaded microthreads and the second chamber was seeded with C2C12 myoblasts (Fig 5.1A). The PDMS block separating the two channels was removed after 4 hours to allow for myoblast attachment (Fig 5.1B) to measure myoblast migration towards HGF-adsorbed microthreads in a 2D system. Migration was observed for 24 hours to limit the amount of proliferation in this system because the doubling time of C2C12 myoblasts is between 15-18 hours.²⁴⁻²⁶ There was a two-fold increase in the rate of myoblast migration stimulated by HGF-adsorbed EDCn microthreads independent of the amount of HGF adsorbed, suggesting that incubating microthreads with 40 ng/mL of HGF either saturates the surface of the microthreads, or that 40 ng/mL of HGF generates a similar cell response to the amount of HGF released from microthreads adsorbed with 100 ng/mL of HGF

(Figure 5.5). The migration rates stimulated by both HGF loading concentrations on EDCn microthreads were significantly higher than empty control reservoirs and they were comparable to experimental conditions that contained 100 ng/mL of soluble HGF; which was found to maximally stimulate migration of SCs along muscle fibers.²⁷ Despite measuring an increase in expression of Ki67 from myoblasts incubated in HGF-loaded UNX microthread C-SFM, we did not observe a motogenic response from UNX microthread C-SFM. There was no motogenic response towards EDCa microthreads regardless of the amount of HGF adsorbed.

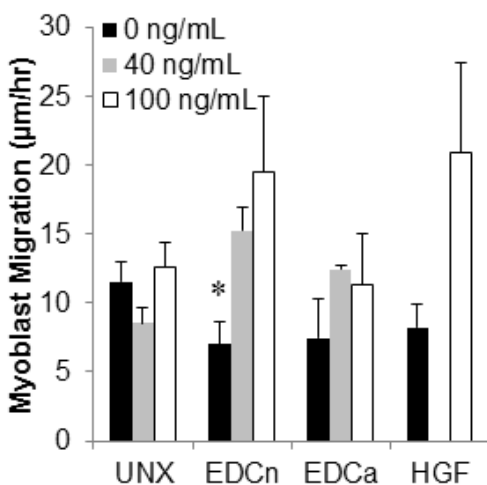


Figure 5.5. Two-dimensional myoblast migration towards HGF-loaded microthreads. Migration towards EDCn microthreads doubled between unloaded and HGF-loaded treatment groups. There was no significant increase in migration towards UNX or EDCa microthreads with increasing amounts of adsorbed HGF. As a control, 0 ng/mL of soluble HGF (HGF, black) or 100 ng/mL of soluble HGF (HGF, white) was added to microthread chambers. * indicate significant differences with migration rates from HGF-loaded microthreads of similar crosslinking type as determined by one-way ANOVA with Holm-Sidak post hoc analysis ($p < 0.05$, $n \geq 2$).

5.3.3 HGF Adsorbed onto Fibrin Microthreads Enhances Myoblast Outgrowth

To determine the effects of HGF-loading onto cell outgrowth along fibrin microthreads, we developed a miniature assay to quantify the rate of cell outgrowth onto fibrin microthreads in a 3D system. Because there were no detectable differences in 2D migration between 40 and 100 ng/mL of HGF, we adsorbed 0, 5, 10, 20, or 40 ng/mL of HGF to the surface of microthreads to evaluate the effect of lower concentrations of HGF on the 3D outgrowth of myoblasts. The HGF-loaded microthreads were positioned over raised Thermanox coverslips (Figure 5.2A), and C2C12 myoblasts were preloaded with the membrane dye tracker DiO to acquire daily images to visualize cell outgrowth (Figure 5.2B). The myoblast outgrowth rate was significantly higher on EDCn microthreads adsorbed with 40 ng/mL of HGF compared to untreated controls (Figure 5.6A). Interestingly, while there was no HGF-mediated outgrowth response on EDCa microthreads, myoblasts migrated along these microthreads at similar rates as UNX

microthreads. However, the total distance myoblasts traveled along EDCn microthreads after 4 days also significantly increased two- to three-fold with 10, 20, and 40 ng/mL of HGF compared to 0 ng/mL of HGF (Figure 5.6B). These elevated distances are similar to the distances traveled by myoblasts along UNX microthreads, again suggesting that adsorbing HGF to EDCn microthreads restores the bioactivity lost during crosslinking. These data suggest that preadsorption of 20 or 40 ng/mL of HGF to the surface of EDCn microthreads will maximize the outgrowth rate and distance these myoblasts will travel within 4 days.

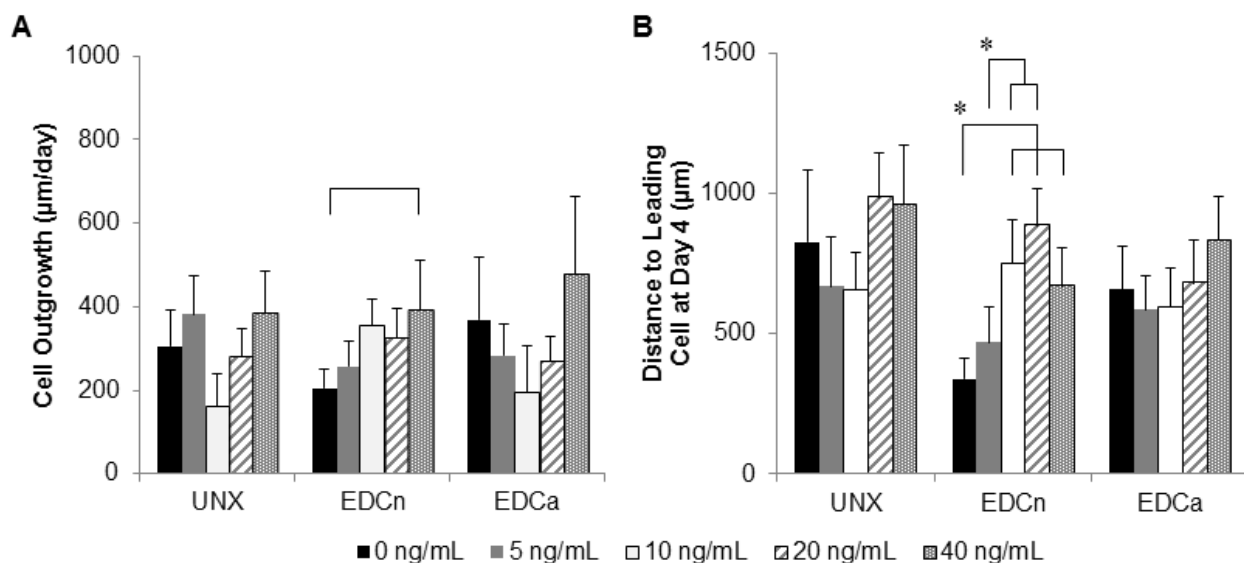


Figure 5.6. Cell outgrowth of C2C12 myoblasts from fibrin gels along fibrin microthreads with increasing concentrations of HGF preadsorbed to their surfaces. Outgrowth rate of myoblasts along microthreads during the first two days of HGF release (A). Cell outgrowth doubled on EDCn microthreads loaded with 40 ng/mL of HGF compared to unloaded EDCn microthreads. There was no observable effect of loading HGF to either UNX or EDCa microthreads. A graph displaying the total distance traveled in four days by myoblasts (B). The raw distance traveled on EDCn microthreads increased with larger amounts of preadsorbed HGF. * and brackets indicate statistical significance with indicated groups as determined by ANOVA with Holm-Sidak post hoc analysis ($p < 0.05$, $n=6$).

5.3.4 Fibrin Microthreads Enhance Myoblast Proliferation

Cell outgrowth is a phenomenon that incorporates both cell migration as well as cell proliferation. To understand what aspect of the measured outgrowth rates are due to proliferation, we quantified the amount of Ki67 positive cells present on the microthreads at day 4. In most cases, the cells were observed to be a confluent layer with several cells ahead of the migration front (Figure 5.7). Interestingly, Ki67 positive cells were evenly distributed among the

leading cells as well as within the layer of cells behind the migration front. There was a significant increase in the percentage of proliferating cells with EDCn and EDCa microthreads (Figure 5.8). There appeared to be qualitative increases in the number of Ki67 positive cells on crosslinked microthreads that had 20 ng/mL of HGF adsorbed to their surfaces; however, there were no significant increases in the percent of proliferating cells on microthreads with respect to HGF concentration, likely due to the absence of released HGF at this time point.

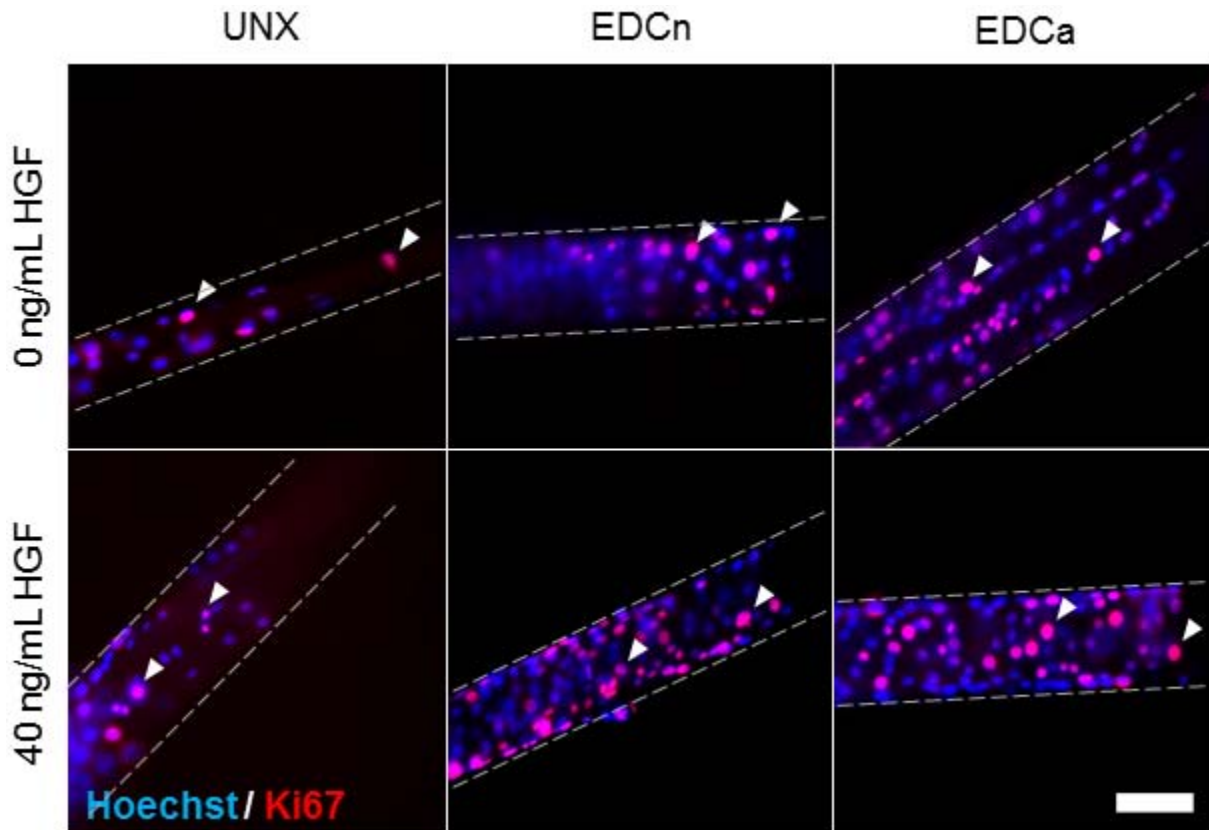


Figure 5.7. Representative images of the outgrowth assay at day 4 with Ki67 staining. In all cases, the myoblasts are migrating from the left of the image to the right. Single cells not surrounded by other cells are referred to as leading cells, while the subconfluent layer of cells behind the leading cell are the migration front. Proliferating cells, shown here as Ki67 positive nuclei, appear to be evenly distributed throughout the leading cells as well as within the layers of cells behind the migration front. Arrowheads indicate representative Ki67 positive cells and grey dotted lines indicate microthread edges. Scale = 100 μ m.

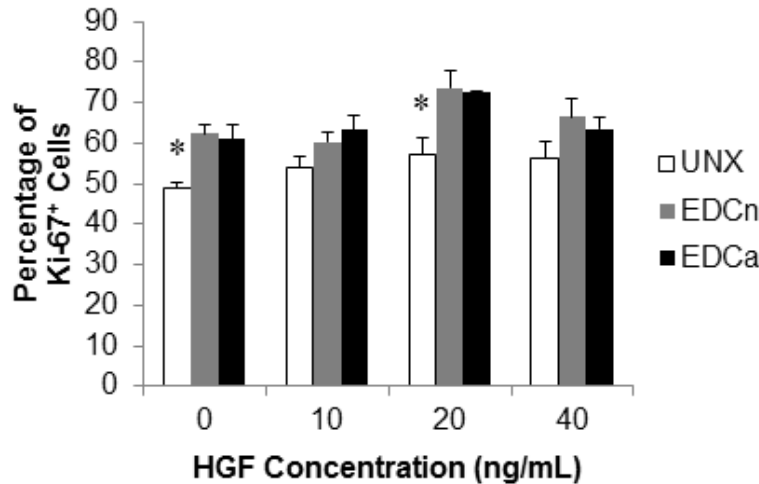


Figure 5.8. Percentage of Ki67 positive myoblasts in the migration front of the outgrowth assay at day 4. EDCn and EDCa microthreads consistently had an increased percentage of Ki67 positive cells, although there was no increase in proliferating cells with respect to HGF concentration. * indicate statistical significance with other microthread groups in the same HGF concentration as determined by ANOVA with Holm-Sidak post hoc analysis ($p < 0.05$, $n=4$).

5.4 DISCUSSION

Treatment of VML injuries remains a significant healthcare concern due to the inability of skeletal muscle to functionally regenerate these critically sized injuries. One reason that VML defects are difficult to regenerate via the endogenous skeletal muscle regenerative pathway is that the ECM is completely removed from these injury sites, eliminating essential cues that typically initiate regeneration. One of the first signals that is released from damaged skeletal muscle is HGF, which functions to activate, and recruit satellite cells to the wound site.^{28,29} We showed that HGF can adsorb to the surface of EDCn fibrin microthreads and rapidly release from the microthreads within 2-4 days, and that this release will facilitate enhanced myoblast outgrowth along fibrin microthreads in a 3D outgrowth assay. We hypothesize that HGF-loaded EDCn microthreads will enhance skeletal muscle regeneration due to this increased ability to recruit myoblasts.

To support the findings that cell outgrowth was only enhanced on HGF-loaded EDCn microthreads, results from our FITC-labeled BSA study indicated that a large increase in fluorescence was observed on EDCn microthreads, while no adsorption was detected on EDCa microthreads and small amounts of BSA-FITC were detected on UNX microthreads. Carbodiimide crosslinked surfaces have an increased amount of amide bonds due to the coupling of free amino and carboxyl groups, which may decrease the surface charge of the microthreads. In Chapter 3, we hypothesized that EDCa microthreads were composed of additional aspartate and glutamate amino acid residues due to the hydrolysis of the amine containing residues

asparagine and glutamine, respectively.²² The changes in the amino acid composition of EDCa microthreads compared to EDCn microthreads suggest that the surface chemistry of EDCa microthreads may be significantly altered, although further studies using Fourier transform infrared spectroscopy (FTIR) analysis are required to confirm these changes. Ultimately, these data suggest that because EDCa microthreads are not able to adsorb bioactive molecules such as BSA-FITC or HGF, they may not be able to direct SC recruitment to VML injuries.

It is interesting to note that while HGF adsorbed to EDCn microthreads stimulated proliferation and migration, HGF adsorbed to UNX microthreads only stimulated proliferation. HGF is a pleiotropic growth factor that stimulates a variety of cell functions including proliferation,³⁰ migration,^{31,32} and survival.³³ Regardless of which downstream pathway is activated, HGF signaling begins with its association with its tyrosine kinase receptor, c-met.^{34,35} Studies assessing the motogenic effects of HGF have found its effect to be maximized with concentrations at or below 100 ng/mL, and in general, higher concentrations elicit increased motility,^{27,36,37} while concentrations between 2 and 10 ng/mL have been found to stimulate myoblast proliferation.^{4,23,38} The ability of a growth factor to have several different functions based on its relative concentration to its receptor has been previously documented.^{23,39} Based on the size of HGF (100kDa), if we assume that the shape of HGF molecules is spherical, we can estimate the minimum size of the radius to be 3.06 nm, with a minimum surface area of 59 nm².⁴⁰ From Chapter 3, if we assume microthreads are approximately 130 μm in diameter, the surface area of each microthread is 4.08 mm² per cm of microthread. From these calculations, we can estimate the theoretical adsorption limit of HGF to microthreads, which is 11.5 ng of HGF per 1 cm of microthread. Since we adsorbed 1.8 cm lengths of microthreads, this yields an adsorption limit of 20.7 ng of HGF per microthread. Given that we are adsorbing HGF to three microthreads at a time, the maximum amount of HGF that could be adsorbed, and then released, would be 62.1 ng. If we continue to adsorb HGF onto microthreads in a volume of 1 mL and assume that all of the HGF adsorbed to the microthreads, this would require a loading concentration of at least 62.1 ng/mL to reach the adsorption limit. Because we did not observe any significant differences in myoblast proliferation or migration between adsorbing EDCn microthreads with a loading concentration of 40 ng/mL or 100 ng/mL, we assume that we did not reach this theoretical maximum. However, the minimum concentration of HGF that has been

reported to induce a chemotactic response on myoblasts is 10 ng/mL.³¹ Combined with previous literature, our data suggest that we are releasing at least 10 ng/mL of HGF per day from EDCn microthreads to enhance 2D and 3D migration. While we were unable to directly quantify the amount of HGF released to verify these calculations, we did make qualitative observations regarding BSA adsorption, which is approximately the same molecular weight as HGF, on the two different microthread scaffolds. We observed an increase in adsorption of FITC-labeled BSA on EDCn microthreads, further supporting the hypothesis that EDCn microthreads are facilitating the adsorption of more HGF than UNX microthreads.

In a similar system with collagen microthreads, fibroblasts were observed to migrate along EDC crosslinked materials at slower rates than uncrosslinked collagen microthreads.⁴¹ Interestingly, we did not observe a significant reduction in myoblast outgrowth on crosslinked fibrin microthreads. However, by adsorbing EDCn fibrin microthreads with 40 ng/mL of HGF, we have increased the outgrowth rate on EDCn microthreads twofold, slightly higher than the outgrowth rate on unloaded, control UNX microthreads. The total distance traveled along the microthreads followed the same trend: HGF loading increased the distance to the leading cell along EDCn microthreads to be comparable to the distances of myoblasts growing along UNX microthreads. For a scaffold to successfully regenerate skeletal muscle in VML defects, the material must recruit myoblasts to the wound site and persist for 2-4 weeks, long enough for the entire wound to regenerate.⁴² We hypothesize that the increased ability of EDCn microthreads to stimulate myoblast migration by the incorporation of HGF, combined with their increased resistance to proteolytic degradation,²² will enhance skeletal muscle regeneration.

While we did not observe any evidence of HGF adsorption to EDCa microthreads, it is interesting to note that SFM conditioned for 24 hours by EDCa microthreads stimulated an increase in myoblast proliferation, regardless of the concentration of HGF present for the adsorption process (0, 40, or 100 ng/mL). This effect was observed only when medium was conditioned by EDCa microthreads in the first 24 hours, and could be further evidence that the acidic conditions are supporting both the crosslinking, and degradation of fibrin microthreads. Fibrin degradation products have been shown in a variety of systems to direct cell functions such as proliferation and migration.⁴³⁻⁴⁶ In Chapter 3, we observed that prolonged incubation in the acidic buffer degraded the microthreads. These degradation products would have formed during

the hydration step, where microthreads were incubated in acidic buffer prior to crosslinking, and were loosely retained in the matrix of EDCa microthreads during the crosslinking reaction. These degradation products would then be released within a 24 hour period with the capacity to stimulate myoblast proliferation, but not migration. Future studies will analyze C-SFM from EDCa microthreads to identify the presence of any mitogens, specifically looking for fibrin degradation products.⁴⁴

We consistently observed several cells migrating ahead of what appeared to be a confluent cell layer along microthreads throughout the cell outgrowth study. This suggests that the migration of several cells along the microthread substrate precedes the proliferation of these cells to achieve a confluent layer. This phenomenon was observed each day that the microthreads were imaged (Fig 5.2B for a representative data set), suggesting that this is a continuous process, where several motile cells migrate ahead of a more confluent layer of cells that results from proliferation of other cells. This effect has been observed with endothelial cells, and migration was found to be diminished when cells were treated with mitomycin C, suggesting that both proliferation and migration are necessary for outgrowth.³⁶ Interestingly, when the percentage of Ki67 positive cells was quantified along microthreads at 4 days of culture, a substrate-dependent increase in proliferation was observed. Substrate stiffness has been reported to increase myoblast proliferation in other 2D studies,⁴⁷ and we have previously reported in Chapter 3 that EDCn and EDCa microthreads are significantly stiffer than UNX microthreads.²² Together, these observations suggest that while it is being released, HGF likely plays a role in enhancing the migration of motile cells along EDCn microthreads, while the cells are also proliferating to form confluent layers of cells behind these leading cells.

5.5 CONCLUSIONS

In this study, we passively adsorbed increasing amounts of HGF to the surface of crosslinked fibrin microthreads to ultimately enhance myoblast recruitment to skeletal muscle defects. Our immunofluorescence analyses suggest that the surface of EDCn microthreads facilitate the most HGF adsorption. We also showed that these substrates are capable of stimulating both myoblast proliferation and migration. These effects plateaued when 40 ng/mL of HGF were adsorbed to the surface. UNX microthreads supported some HGF adsorption,

which supported myoblast proliferation but not migration, possibly due to low concentrations of adsorbed HGF. We hypothesize that changes in the surface chemistry between UNX and EDCn microthreads are responsible for this difference in adsorption capacity for HGF. While EDCa microthreads did not facilitate the adsorption of HGF, medium conditioned from these microthreads stimulated myoblast proliferation, possibly due to the release of fibrin degradation products that resulted from the crosslinking procedure. Regardless of the adsorption of HGF, the proliferation of myoblasts 4 days after cells migrated along the microthreads was increased on crosslinked microthreads. The ability of EDCn microthreads to adsorb HGF in a way that facilitates its rapid, active release is ideal for VML injuries, and we hypothesize that these HGF-loaded EDCn microthreads will enhance skeletal muscle regeneration in these defects.

5.6 ACKNOWLEDGEMENTS

This research was funded in part by US Army (W81XWH-11-1-0631, GDP and RLP), NIH R01-HL115282 (GDP), and NIH F31-DE023281 (JMG). The authors wish to thank Michelle Zayas for creating the art used in this chapter and Laura Pumphrey and Brianna Sheldon for their assistance in making microthreads as well fabricating the outgrowth and migration assays.

5.7 REFERENCES

1. 2009 report of the 2008 statistics of plastic surgery statistics. American Society of Plastic Surgeons 2009.
2. Eckardt A. Microsurgical reconstruction in the head and neck region: an 18-year experience with 500 consecutive cases. *Journal of Cranio-Maxillofacial Surgery* 2003;31(4):197-201.
3. Heemskerk J, Kitslaar P. Acute compartment syndrome of the lower leg: retrospective study on prevalence, technique, and outcome of fasciotomies. *World Journal of Surgery* 2003;27(6):744-7.
4. Tatsumi R, Hattori A, Ikeuchi Y, Anderson JE, Allen RE. Release of hepatocyte growth factor from mechanically stretched skeletal muscle satellite cells and role of pH and nitric oxide. *Mol Biol Cell* 2002;13(8):2909-18.
5. Tatsumi R, Liu X, Pulido A, Morales M, Sakata T, Dial S, Hattori A, Ikeuchi Y, Allen RE. Satellite cell activation in stretched skeletal muscle and the role of nitric oxide and hepatocyte growth factor. *Am J Physiol Cell Physiol* 2006;290(6):C1487-94.
6. Tatsumi R, Sheehan SM, Iwasaki H, Hattori A, Allen RE. Mechanical stretch induces activation of skeletal muscle satellite cells in vitro. *Experimental Cell Research* 2001;267(1):107-14.
7. Gal-Levi R, Leshem Y, Aoki S, Nakamura T, Halevy O. Hepatocyte growth factor plays a dual role in regulating skeletal muscle satellite cell proliferation and differentiation. *Biochim Biophys Acta* 1998;1402(1):39-51.
8. Zammit PS, Partridge TA, Yablonka-Reuveni Z. The skeletal muscle satellite cell: the stem cell that came in from the cold. *The Journal of Histochemistry and Cytochemistry : Official Journal of the Histochemistry Society* 2006;54(11):1177-91.

9. Morgan JE, Partridge TA. Muscle satellite cells. *The International Journal of Biochemistry and Cell Biology* 2003;35:1151-1156.
10. Miller KJ, Thaloor D, Matteson S, Pavlath GK. Hepatocyte growth factor affects satellite cell activation and differentiation in regenerating skeletal muscle. *Am J Physiol Cell Physiol* 2000;278(1):174-181.
11. Allen DL, Teitelbaum DH, Kurachi K. Growth factor stimulation of matrix metalloproteinase expression and myoblast migration and invasion in vitro. *Am J Physiol Cell Physiol* 2003;284(4):C805-15.
12. Goetsch KP, Kallmeyer K, Niesler CU. Decorin modulates collagen I-stimulated, but not fibronectin-stimulated, migration of C2C12 myoblasts. *Matrix biology : journal of the International Society for Matrix Biology* 2011;30(2):109-17.
13. Kyburz KA, Anseth KS. Three-dimensional hMSC motility within peptide-functionalized PEG-based hydrogels of varying adhesivity and crosslinking density. *Acta biomaterialia* 2013;9(5):6381-92.
14. Meyer AS, Hughes-Alford SK, Kay JE, Castillo A, Wells A, Gertler FB, Lauffenburger DA. 2D protrusion but not motility predicts growth factor-induced cancer cell migration in 3D collagen. *J Cell Biol* 2012;197(6):721-9.
15. Cornwell KG, Downing BR, Pins GD. Characterizing fibroblast migration on discrete collagen threads for applications in tissue regeneration. *J Biomed Mater Res A* 2004;71(1):55-62.
16. Cornwell KG, Pins GD. Enhanced proliferation and migration of fibroblasts on the surface of fibroblast growth factor-2-loaded fibrin microthreads. *Tissue Eng Part A* 2010;16(12):3669-77.
17. Montarras D, Morgan J, Collins C, Relaix F, Zaffran S, Cumano A, Partridge T, Buckingham M. Direct isolation of satellite cells for skeletal muscle regeneration. *Science* 2005;309(5743):2064-7.
18. Sanes JR. The basement membrane/basal lamina of skeletal muscle. *The Journal of Biological Chemistry* 2003;278(15):12601-4.
19. Serrano AL, Munoz-Canoves P. Regulation and dysregulation of fibrosis in skeletal muscle. *Experimental Cell Research* 2010;316(18):3050-8.
20. O'Reilly C, McKay B, Phillips S, Tarnopolsky M, Parise G. Hepatocyte growth factor (HGF) and the satellite cell response following muscle lengthening contractions in humans. *Muscle Nerve* 2008;38(5):1434-42.
21. Cornwell KG, Pins GD. Discrete crosslinked fibrin microthread scaffolds for tissue regeneration. *J Biomed Mater Res A* 2007;82(1):104-12.
22. Grasman JM, Page RL, Dominko T, Pins GD. Crosslinking strategies facilitate tunable structural properties of fibrin microthreads. *Acta Biomaterialia* 2012;8(11):4020-30.
23. Yamada M, Tatsumi R, Yamanouchi K, Hosoyama T, Shiratsuchi S, Sato A, Mizunoya W, Ikeuchi Y, Furuse M, Allen RE. High concentrations of HGF inhibit skeletal muscle satellite cell proliferation in vitro by inducing expression of myostatin: a possible mechanism for reestablishing satellite cell quiescence in vivo. *Am J Physiol Cell Physiol* 2010;298(3):C465-76.
24. Kurth F, Franco-Obregon A, Bartschi CA, Dittrich PS. An adaptable stage perfusion incubator for the controlled cultivation of C2C12 myoblasts. *Analyst* 2014.
25. Forterre A, Jalabert A, Berger E, Baudet M, Chikh K, Errazuriz E, De Larichaudy J, Chanon S, Weiss-Gayet M, Hesse AM and others. Proteomic analysis of C2C12 myoblast and myotube exosome-like vesicles: a new paradigm for myoblast-myotube cross talk? *PLoS ONE* 2014;9(1):e84153.
26. Faralli H, Martin E, Core N, Liu QC, Filippi P, Dilworth FJ, Caubit X, Fasano L. Teashirt-3, a novel regulator of muscle differentiation, associates with BRG1-associated factor 57 (BAF57) to inhibit myogenin gene expression. *J Biol Chem* 2011;286(26):23498-510.
27. Ishido M, Kasuga N. In Vivo Real-Time Imaging of Exogenous HGF-Triggered Cell Migration in Rat Intact Soleus Muscles. *Acta Histochem Cytochem* 2012;45(3):193-9.
28. Tatsumi R, Allen RE. Active hepatocyte growth factor is present in skeletal muscle extracellular matrix. *Muscle Nerve* 2004;30(5):654-8.
29. Tatsumi R, Anderson JE, Nevoret CJ, Halevy O, Allen RE. HGF/SF is present in normal adult skeletal muscle and is capable of activating satellite cells. *Developmental biology* 1998;194(1):114-128.
30. Sheehan SM, Allen RE. Skeletal muscle satellite cell proliferation in response to members of the fibroblast growth factor family and hepatocyte growth factor. *J Cell Physiol* 1999;181(3):499-506.
31. Corti S, Salani S, Del Bo R, Sironi M, Strazzer S, D'Angelo MG, Comi GP, Bresolin N, Scarlato G. Chemotactic factors enhance myogenic cell migration across an endothelial monolayer. *Exp Cell Res* 2001;268(1):36-44.

32. Bladt F, Riethmacher D, Isenmann S, Aguzzi A, Birchmeier C. Essential Role for the C-Met Receptor in the Migration of Myogenic Precursor Cells into the Limb Bud. *Nature* 1995;376(6543):768-771.
33. Hill E, Boontheekul T, Mooney DJ. Designing scaffolds to enhance transplanted myoblast survival and migration. *Tissue Eng* 2006;12(5):1295-304.
34. Anastasi S, Giordano S, Sthandier O, Gambarotta G, Maione R, Comoglio P, Amati P. A natural hepatocyte growth factor/scatter factor autocrine loop in myoblast cells and the effect of the constitutive Met kinase activation on myogenic differentiation. *J Cell Biol* 1997;137(5):1057-68.
35. Matsumoto K, Nakamura T. Emerging multipotent aspects of hepatocyte growth factor. *J Biochem* 1996;119(4):591-600.
36. Bussolino F, Drenth MF, Ziche M, Bocchietto E, Olivero M, Naldini L, Gaudino G, Tamagnone L, Coffey A, Comoglio PM. Hepatocyte Growth-Factor Is a Potent Angiogenic Factor Which Stimulates Endothelial-Cell Motility and Growth. *Journal of Cell Biology* 1992;119(3):629-641.
37. Barbero A, Benelli R, Minghelli S, Tosetti F, Dorcaratto A, Ponzetto C, Wernig A, Cullen MJ, Albini A, Noonan DM. Growth factor supplemented matrigel improves ectopic skeletal muscle formation--a cell therapy approach. *J Cell Physiol* 2001;186(2):183-92.
38. Allen RE, Sheehan SM, Taylor RG, Kendall TL, Rice GM. Hepatocyte growth factor activates quiescent skeletal muscle satellite cells in vitro. *J Cell Physiol* 1995;165(2):307-12.
39. Coolican SA, Samuel DS, Ewton DZ, McWade FJ, Florini JR. The mitogenic and myogenic actions of insulin-like growth factors utilize distinct signaling pathways. *J Biol Chem* 1997;272(10):6653-62.
40. Erickson HP. Size and shape of protein molecules at the nanometer level determined by sedimentation, gel filtration, and electron microscopy. *Biol Proced Online* 2009;11:32-51.
41. Cornwell KG, Lei P, Andreadis ST, Pins GD. Crosslinking of discrete self-assembled collagen threads: Effects on mechanical strength and cell-matrix interactions. *J Biomed Mater Res A* 2007;80(2):362-71.
42. Chen XK, Walters TJ. Muscle-derived decellularised extracellular matrix improves functional recovery in a rat latissimus dorsi muscle defect model. *J Plast Reconstr Aesthet Surg* 2013;66(12):1750-8.
43. Gray AJ, Bishop JE, Reeves JT, Mecham RP, Laurent GJ. Partially degraded fibrin(ogen) stimulates fibroblast proliferation in vitro. *Am J Respir Cell Mol Biol* 1995;12(6):684-90.
44. Ahmann KA, Weinbaum JS, Johnson SL, Tranquillo RT. Fibrin degradation enhances vascular smooth muscle cell proliferation and matrix deposition in fibrin-based tissue constructs fabricated in vitro. *Tissue Eng Part A* 2010;16(10):3261-70.
45. Naito M, Stirk CM, Smith EB, Thompson WD. Smooth muscle cell outgrowth stimulated by fibrin degradation products. The potential role of fibrin fragment E in restenosis and atherogenesis. *Thromb Res* 2000;98(2):165-74.
46. Bootle-Wilbraham CA, Tazzyman S, Thompson WD, Stirk CM, Lewis CE. Fibrin fragment E stimulates the proliferation, migration and differentiation of human microvascular endothelial cells in vitro. *Angiogenesis* 2001;4(4):269-75.
47. Boontheekul T, Hill EE, Kong HJ, Mooney DJ. Regulating myoblast phenotype through controlled gel stiffness and degradation. *Tissue Engineering* 2007;13(7):1431-42.

Chapter 6: Hepatocyte Growth Factor Adsorbed onto EDC Crosslinked Microthreads Restores Mechanical Function in Mouse Model of VML

6.1 INTRODUCTION

Volumetric muscle loss (VML) typically results from traumatic incidents; such as those presented from combat missions, where soft tissue extremity injuries account for approximately 63% of diagnoses.^{1,2} These injuries not only cause cosmetic deformities, which may lead to the development of psychological conditions, but also lead to a devastating loss of function due to the complete removal of large amounts of tissue and its native basement membrane.³ While skeletal muscle has an innate repair mechanism that is largely directed by this native tissue architecture, it is unable to compensate for large-scale injuries due to the destruction of this regenerative template and growth factor reservoir. The current standard of care for large-scale skeletal muscle injury is an autologous tissue transfer from an uninjured site.⁴ This complicated surgical procedure yields limited restoration of muscle function and can result in complications such as donor site morbidity, infection, and graft failure due to necrosis.^{4,5} While muscle flaps may be a suitable treatment, as many as 10% of muscle flap surgeries develop complete graft failure, demonstrating the need for an alternative treatment.^{5,6} Thus, there is a need to develop an off-the-shelf, biomimetic scaffold that directs functional skeletal muscle tissue regeneration within large defect sites.

Skeletal muscle regeneration is mediated by local progenitor cells known as satellite cells (SCs), which reside between the sarcolemma and basal lamina of muscle fibers.^{7,8} In small muscle wounds such as those from exercise, the basal lamina rapidly releases hepatocyte growth factor (HGF) to stimulate the activation, and recruitment, of SCs to the wound site.⁹⁻¹² This immediate rapid release is important to gather enough progenitor cells to repair large defects.^{12,13} Importantly, reentry into the cell cycle has been found to be solely mediated by HGF.^{14,15} Because it inhibits SC differentiation, HGF will inhibit muscle regeneration if present for a

prolonged period, demonstrating that careful attention must be paid to the time scale that HGF is supplemented to a VML defect.^{12,16}

Acellular scaffolds engineered to direct the regeneration of VML injuries can be tuned via multiple design criteria to facilitate the recruitment of SCs to the injury site and create organized nascent myofibers. A simple method to increase the number of SCs at the injury site is to incorporate relevant growth factors within the scaffolding material such that they would be released upon implantation. Surprisingly, recent studies ignore the necessary goal of recruiting SCs to the defect, and rather focus on the revascularization of the tissue,¹⁷ or rely on the growth factors present in decellularized extracellular matrix (ECM) materials to direct regeneration.^{18,19} While some of these studies report improvements in mechanical function,²⁰ many studies using acellular ECM materials report that long term remodeling, between 3-6 months, is necessary for ECM scaffold mediated functional recovery.^{21,22} These data suggest that the addition of an exogenous factor capable of stimulating rapid SC recruitment may facilitate functional recovery at earlier time points, as this would recapitulate regenerative cues missing in VML injuries and expedite the remodeling of the defect site.

An additional limitation of previous acellular strategies is that regenerating myofibers are often not parallel to the remaining myofibers, limiting the functional efficiency of the newly formed tissue.²³⁻²⁵ This disorganized regeneration may be a result of the random protein network present in both decellularized ECM and the polymerization process involved in the formation of alginate or gelatin materials. To assist in the organized creation of myofibers within an injury site, we have developed biomimetic biopolymer microthreads that have a similar morphology to native tissue. By geometrically guiding the directional organization of the polymerization process of fibrinogen and thrombin, we developed an aligned fibrin microthread scaffold that is capable of directing cell alignment along the longitudinal axis of the microthread structure.²⁶ Results from early implantation studies investigating the use of fibrin microthreads in a mouse model of VML suggest that fibrin microthreads stimulate skeletal muscle regeneration; however, it was noted that a decreased rate of degradation of the microthreads could enhance the microthread-mediated regenerative response.²⁷ In Chapter 3, we showed that the mechanical and structural properties of carbodiimide crosslinked fibrin microthreads can be tuned by altering the buffer conditions of the crosslinking reaction without adversely affecting cell attachment,

proliferation, or viability.²⁸ When incubated in plasmin, the primary agent of fibrinolysis, these differentially crosslinked microthreads showed varying increases in resistance to proteolytic degradation, suggesting that these crosslinked materials might be ideal for skeletal muscle regeneration. In Chapter 5, we adsorbed HGF to uncrosslinked (UNX) microthreads and microthreads crosslinked with 1-ethyl-3-(3-dimethylaminopropyl)carbodiimide (EDC) in neutral (EDCn), or acidic (EDCa) buffers, and found that EDCn microthreads were able to adsorb HGF. Over the period of 2-4 days, HGF was released in an active form and was capable of stimulating myoblast proliferation and migration in two- and three-dimensions.

In this Chapter, we investigate the ability of HGF loaded EDCn (EDCn-HGF) microthreads to enhance regeneration of functional tissue in a mouse VML model. We hypothesize that EDCn-HGF microthreads will increase the functional recovery of VML injuries in the *tibialis anterior* (TA) muscle by increasing the number of SCs within the injury site. Interestingly, while there was not a significant increase in Pax7 positive SCs compared to injured controls two weeks post-injury, there was a significant increase in myogenin positive nuclei, suggesting that the recruitment of the majority of the SCs occurred before the two week time point. This increase in differentiating myoblasts led to a significant increase in mechanical function of the TA eight weeks post-injury; however, the EDCn microthreads were still present in the wound site. Together, these data suggest that by adsorbing HGF onto EDCn microthreads, we are recapitulating regenerative cues lost in VML injuries to ultimately enhance skeletal muscle regeneration.

6.2 MATERIALS and METHODS

6.2.1 Fibrin Microthread Preparation

6.2.1.1 Microthread Extrusion

Fibrin microthreads were co-extruded from solutions of fibrinogen and thrombin using extrusion techniques described previously in section 3.2.1.1.^{26,28} Briefly, fibrinogen from bovine plasma (MP Biomedical, Irvine, CA; Cat No. 08820224) was dissolved in HEPES (N-[2-Hydroxyethyl]piperazine-N'-[2-ethanesulfonic acid]) buffered saline (HBS, 20 mM HEPES, 0.9% NaCl; pH 7.4) at 70 mg/mL and stored at -20 °C until use. Thrombin from bovine plasma (Sigma; T4648) was dissolved in HBS at 40 U/mL and stored at -20 °C until use.

To fabricate microthreads, fibrinogen and thrombin solutions were thawed and warmed to room temperature, and thrombin was mixed with a 40 mM CaCl₂ (Sigma) solution to form a working solution of 6 U/mL. Fibrinogen and thrombin/CaCl₂ solutions were loaded into 1 mL syringes which were inserted into a blending applicator tip (Micromedics Inc., St. Paul, MN; SA-3670). The solutions were combined in the blending applicator and extruded through polyethylene tubing (BD, Sparks, MD) with an inner diameter of 0.86 mm into a bath of 10 mM HEPES (pH 7.4) in a Teflon coated pan at a rate of 0.225 mL/min using a dual syringe pump. After 10 minutes, 25.4 cm, amorphous fibrin microthreads were removed from the buffer solution and stretched to form three-19-cm microthreads; these were air dried under the tension of their own weight. Dry microthreads were placed in aluminum foil and stored in a desiccator until use.

6.2.1.2 Fibrin Microthread Crosslinking

Fibrin microthreads were crosslinked using techniques described in section 3.2.1.2.²⁸ Briefly, to create EDCn microthreads, microthreads were hydrated in monosodium phosphate buffer (100 mM NaH₂PO₄, Sigma, pH 7.4) for 30 minutes and then crosslinked in monosodium phosphate buffer containing 16 mM N-hydroxysuccinimide (NHS, Sigma) and 28 mM EDC (Sigma) for 2 hours at room temperature. After crosslinking, the buffered EDC/NHS solution was aspirated and the microthreads were rinsed three times in a deionized (DI) water bath, air dried, sterilized with ethylene oxide, and stored in a desiccator until use.

6.2.1.3 Adsorption of HGF to Microthreads

Three unsterilized EDCn microthreads were attached onto polydimethylsiloxane (PDMS, inner diameter 0.75 in., Dow Corning, Midland, MI) rings, sterilized with 70% ethanol for 90 minutes, rinsed with DI water three times, and air dried in a laminar flow hood overnight, as described in section 5.2.2. Sterile microthread-PDMS constructs were hydrated in Dulbecco's phosphate buffered saline (DPBS) and the PDMS surfaces were blocked with 0.25% bovine serum albumin (BSA, Sigma) for 1 hour. These solutions were aspirated and replaced with 1 mL of 40 ng/mL of HGF (Peprotech, Rocky Hill, NJ) in DPBS and incubated at room temperature

for 2 hours. The microthreads were rinsed three times in DPBS, twice in L-15 (Mediatech, Inc., Manassas, VA) and immediately used for implantation.

6.2.2 *Animals and Surgical Procedures*

All animal protocols were approved by the Institutional Animal Care and Use Committee (IACUC) at Worcester Polytechnic Institute. Female nude SCID hairless outbred (Strain SHO; Charles River Laboratories, Wilmington, MA) mice between 7 and 8 weeks of age were used to compare results to previous experiments within our lab.²⁷ Mice were anesthetized with an intraperitoneal (i.p.) injection of ketamine/xylazine (50/5 mg/kg), and all surgical procedures were performed under a stereo microscope as previously described.²⁷ The skin flap and fascia covering the TA muscle of the right hindleg were retracted (Figure 6.1A) and a critical sized defect was created in the central region of the muscle by resecting approximately 30 mg (4 x 2 x 2 mm) of tissue (Figure 6.1B). The severity of each injury was assessed by measuring a 50% reduction in the force produced by single electrical impulses (twitch force) compared to pre-injury values. At this point, one of five treatments were implanted into the injury site: no intervention (untreated), fibrin gel, UNX microthreads, EDCn microthreads, or EDCn-HGF microthreads. Fibrin gel implants were created by dropwise addition of sterile-filtered fibrinogen (70 mg/mL) into the injury site until it was full, followed by a single drop of sterile-filtered thrombin (6 U/mL). Fibrin microthreads were implanted in the injury site with sterile forceps and cut to the size of the injury, and were positioned such that the microthreads were parallel to the remaining myofibers. On average, 8-15 microthreads were used to fill the injury site. After implantation, microthreads were secured in the wound site using sequential drops of sterile fibrinogen and thrombin solutions. The muscle was kept hydrated during the procedure using sterile saline. The skin flap was replaced over the wound and secured with 8-0 Securo Orb suture with TG140-8 needles (Securos, Fiskdale, MA; Cat No. 008170). Animals were allowed to recover under a heat lamp and administered 0.05 mg/kg buprenorphine every 12 hours for 72 hours for post-op care. A total of three animals per treatment were used for analysis at 14 days post-injury, and six animals per treatment for analysis at 60 days post-injury.

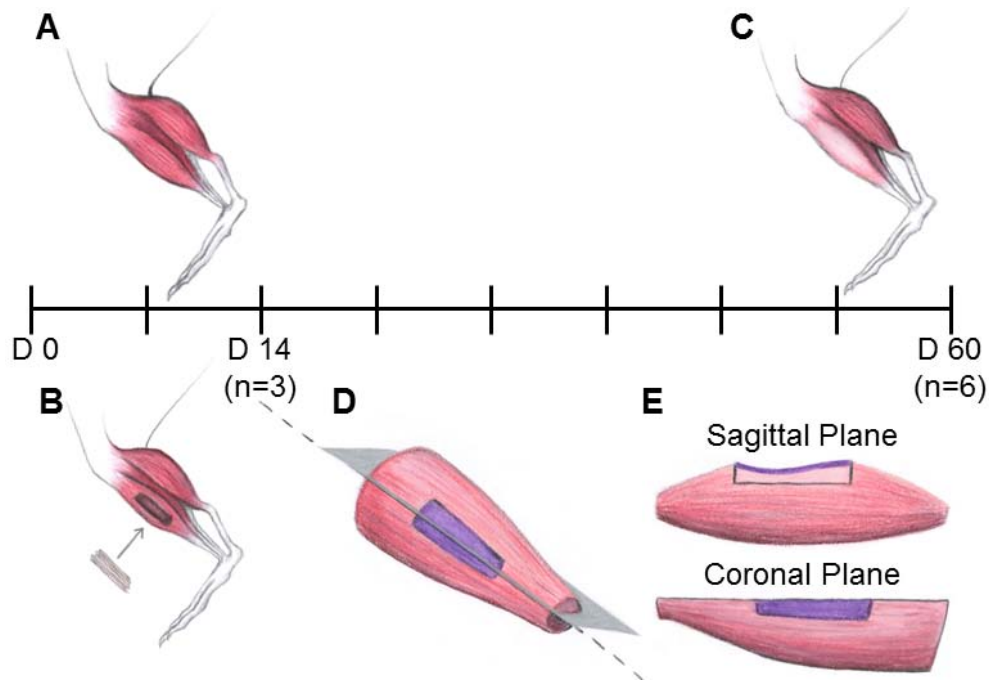


Figure 6.1. Schematic representation of study performed in Chapter 6. Healthy TA muscles were exposed and baseline force values were measured (A). A VML size injury was induced by resecting 4 x 2 x 2 mm of tissue, and one of five treatments was implanted (B). After 14 or 60 days, the TA was exposed, and observations were made on the gross morphology (C). After fixation, TA muscles were bisected (D) and observed either in the sagittal plane (longitudinal cross-section) or coronal plane (lateral top-down cross-section) (E). Images courtesy of M Zayas.

6.2.3 *Histological and Immunohistochemical Analysis*

Animals were euthanized at either 14 or 60 days post-injury and the TA muscle was exposed and dissected longitudinally away from the tibia leaving both ends affixed. The shape of the muscle as well as the gross morphology of the wound site was recorded, and the approximate wound site was marked with a histology marking pen (Figure 6.1C). The whole lower leg was placed in 4% paraformaldehyde in PBS for 1 hr, after which the TA muscle was removed from the rest of the lower leg and fixed for an additional 2 hr at room temperature. Tissue was rinsed in phosphate buffered saline (PBS) three times, bisected with a razor blade along the center of the wound site (Figure 6.1D), and stored in 70% ethanol until processing and paraffin embedding. Muscle sections were embedded in two orientations: a longitudinal cross-section of the sagittal plane of the muscle, which reveals regeneration in the defect site as a function of tissue depth, and a lateral top-down view of the coronal plane of the muscle, revealing regeneration events as a function of tissue width (Figure 6.1E). Serial 5 μm sections were cut from both tissue orientations, mounted on Superfrost Plus slides (VWR, West Chester,

PA), and used for histological and immunohistochemical (IHC) analyses. Slides stained with Masson's trichrome, which stains cytoplasm (muscle) and fibrin structures in red, collagen and connective tissue in blue, and nuclei in black, were prepared using at least two sections 50 μm apart per tissue orientation per animal using standard procedures. In all cases, histological and IHC data will be presented with a cartoon inset of the appropriate tissue orientation, and will denote the location within the injury site that is being analyzed (Figure 6.2).



Figure 6.2. Cartoon denoting location of proximal and distal ends of TA muscle.

Serial sagittal and coronal 5 μm sections were stained to visualize Pax7 positive nuclei (SCs), myogenin positive nuclei (myotubes), and platelet endothelial cell adhesion molecule (PECAM; CD-31; blood vessels), respectively. For all staining, sections were deparaffinized in xylenes and rehydrated through a series of graded alcohols. Antigen retrieval was conducted in a pressure cooker for 20 min using a citrate-based antigen retrieval solution (Vector Laboratories, Burlingame, CA; H-3300). The samples were allowed to cool to room temperature and rinsed with PBS. Each section was incubated for 30 min in a blocking solution of 2.5% horse serum in a humidified chamber. Sections were stained separately using antibodies targeting Pax7 (Developmental Studies Hybridoma Bank, Iowa City, IA) at a 1:15 dilution, myogenin (Abcam, Cambridge, MA; ab1835) at a 1:100 dilution, or PECAM (Abcam; ab28364) at a dilution of 1:50 in PBS/0.05% Tween for 45 min at room temperature. After 2 rinses of PBS/Tween, slides were incubated in 3% hydrogen peroxide for 30 min to inhibit endogenous peroxidase activity. The slides were rinsed twice in PBS and incubated in the appropriate Impress horseradish peroxidase-based secondary antibody (anti-mouse IgG (Vector, MP7402) for Pax7 and myogenin, anti-rabbit IgG for PECAM (Vector, MP7401)) for 30 min at room temperature. An Impact DAB kit (Vector, SK-4105) was used to develop positive staining due to the presence of the Impress secondary antibody. Slides were counterstained with hematoxylin, dehydrated through graded alcohols and xylenes, and cover-slipped for analysis. Histology and IHC images were observed on a Nikon Eclipse E400 microscope (Nikon, Inc., Melville, NY) coupled with a RT Color Spot camera (Spot Diagnostics, Sterling Heights, MI) with matching software.

6.2.3.1 Estimation of Wound Size

To approximate the change in the wound size over time, the defect width, length, and depth were measured from multiple images that were acquired from slides stained with

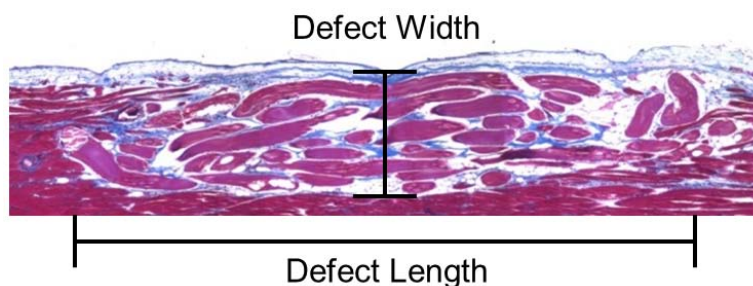


Figure 6.3 Definition of VML defect dimensions. The dimensions of defects stained with Masson's trichrome 14 and 60 days post-injury were measured to assess the change in defect size between these time points.

Masson's trichrome with a Nikon Eclipse E400 microscope using a 10X objective and stitched together using Adobe Photoshop CD5.1 (Adobe, San Jose, CA). Images were imported into ImageJ (NIH) and the length and width (coronal sections), and the depth and length (sagittal sections) of the defect region were measured (Figure 6.3). Wound margins were defined by identifying the implanted microthreads in UNX, EDCn, or EDCn-HGF microthread treatment groups, and by identifying disorganized myofibers surrounded by collagen fibers for untreated or fibrin gel treatment groups. In treatment groups where adipose tissue was observed, this was identified as part of the wound site and included in these measurements. Length measurements were combined between both tissue orientations, as they represent the same measurement in three-dimensional (3D) space.

6.2.3.2 Collagen Quantification

Collagen quantification was performed digitally by analyzing the entire defect site of Masson's trichrome stained tissue sections compiled in section 6.2.3.1 (Figure 6.4A). Collagen pixel red green blue (RGB) values were recorded at 4-6 points in each of 15 images to obtain an average pixel RGB value (59, 93, 199) to identify collagen deposition in Masson's trichrome images. Photoshop was used to select all blue pixels using this average RGB value (i.e. collagen content) in each image using the SELECT > COLOR RANGE function with a "fuzziness" value of 92 (Figure 6.4B). The fuzziness value was empirically selected by averaging the same value for 15 randomly selected images, and functions as a threshold value to include varying RGB values of collagen. The resulting image was imported into ImageJ, thresholded with a value of 214, and analyzed for percent of black pixels (i.e. collagen content) (Figure 6.4C). Parts of the image that

did not contain muscle tissue were also selected and removed from this percent area calculation to ensure that the analysis of percent area only considered muscle tissue.

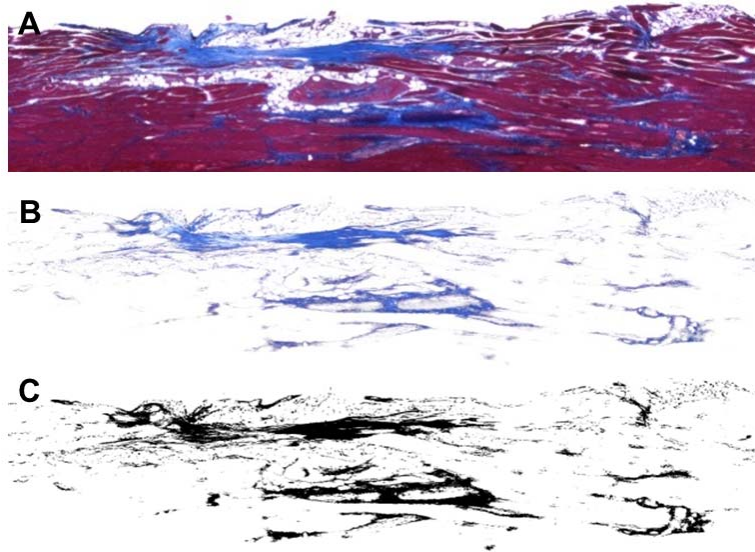


Figure 6.4. Collagen quantification method for VML defects. Composite images of the entire muscle defect, stained with Masson's trichrome, 60 days post-injury were prepared (A), and each blue pixel was selected in Photoshop (B). The resulting image was imported into ImageJ, thresholded, and the percent of black pixels was determined to be the collagen content (C).

6.2.4 Contractile Force Measurements

To measure the muscle strength recovered by the implants, the contractile force evaluated for animals before injury (baseline), after injury, and at the time of sacrifice *in situ*, as previously described.²⁷ Briefly, the right hindleg knee joint was anchored using a custom clamping system fixed to the base of the stereo microscope stand. A silk ligature was secured to the cleft between digits 1 and 2 of the mouse paw and it was anchored to a force transducer (Harvard Apparatus, Holliston, MA) on the other end. The exposed TA muscle was stimulated using 2 custom needle electrodes placed on the proximal surface of the muscle. Electrical stimulation was applied at 4 V with a 4 ms pulse duration at 500 ms intervals and the resultant twitch forces (g) were recorded at a rate of 200 Hz using a BioPac MP-100 (BIOPAC Systems, Inc., Goleta, CA) and accompanying software (AcknowledgeTM, BIOPAC Systems, Inc.). Maximum force produced at tetanus was measured by reducing the pulse intervals to 20 ms. As a control, the twitch force and maximum force at tetanus were measured for the contralateral leg 60 days post-injury. At least fifteen contraction measurements per animal per time point were made.

6.2.5 Statistical Analyses

Statistical analyses were performed using a one-way analysis of variance (ANOVA) with $p < 0.05$ indicating significant differences between groups using SigmaPlot 11.0 software (Systat Software, Inc., San Jose, CA). For post hoc analysis, a Holm-Sidak pairwise multiple comparison test was performed to determine significance between experimental groups using an overall significance level of $p < 0.05$. Where indicated, a paired Student's t-test was performed with $p < 0.05$ indicating significant differences between groups. The data are reported as means \pm standard error.

6.3 RESULTS

6.3.1 Gross Morphology of No Intervention and Fibrin Gel Implants Show Loss of Muscle Volume

To characterize how acellular fibrin microthread implants affect skeletal muscle regeneration, we implanted UNX, EDCn, and EDCn-HGF microthreads into VML injuries within the TA muscle of mice. As a material control, we implanted fibrin gels to the injury site to assess whether the fibrin biomaterial itself would induce muscle regeneration or whether the structural architecture of the microthreads was required for organized, functional regeneration. Throughout this study, no animals experienced any complications from the surgical procedures, and all survived to their designated time points. The body weight of each animal was recorded before surgery and before euthanization, and no significant changes in weight were noted at any time point (Table 6.1). Fourteen days post-injury, there was evidence of muscle volume loss in untreated and fibrin gel implant groups as shown by a loss of the convex shape of the surface of the muscle (black arrowheads, Figure 6.5 A-B). There appeared to be deformities in the shape of the muscles that were treated with UNX microthread implants (Figure 6.5C), although the general shape of the muscle was consistent with healthy tissue. EDCn and EDCn-HGF

Table 6.1. Animal weight at time of sacrifice.

| | No Intervention | | Fibrin Gel | | UNX Microthreads | | EDCn Microthreads | | EDCn-HGF Microthreads | |
|------------------------------|-----------------|----------------|----------------|----------------|------------------|----------------|-------------------|----------------|-----------------------|----------------|
| | 14 Days | 60 Days | 14 Days | 60 Days | 14 Days | 60 Days | 14 Days | 60 Days | 14 Days | 60 Days |
| Sample Size (n) | 3 | 6 | 3 | 6 | 3 | 6 | 3 | 6 | 3 | 6 |
| Body weight at surgery (g) | 25.2 \pm 0.5 | 25.2 \pm 0.5 | 24.9 \pm 0.6 | 24.9 \pm 0.6 | 24.7 \pm 0.4 | 24.7 \pm 0.4 | 24.3 \pm 0.6 | 24.3 \pm 0.6 | 24.0 \pm 0.7 | 24.0 \pm 0.7 |
| Body weight at sacrifice (g) | 26.3 \pm 1.2 | 27.0 \pm 1.1 | 24.3 \pm 0.7 | 27.0 \pm 0.7 | 24.7 \pm 0.3 | 27.3 \pm 0.8 | 25.3 \pm 0.9 | 27.3 \pm 0.8 | 25.7 \pm 0.7 | 26.2 \pm 0.9 |

microthreads remained visible 14 days post-injury, although the EDCn-HGF microthreads appeared to be covered by a layer of tissue (white arrowheads, Figure 6.5 D-E). Sixty days post-injury, the loss of muscle volume persisted in all animals treated with untreated control and fibrin gel implant groups (Figure 6.5 F-G). The shape of muscles 60 days post-injury with microthread implants exhibited a smooth, convex surface, showing no evidence of muscle loss (Figure 6.5 H-J). While microthreads were still visible in muscles treated with EDCn and EDCn-HGF implant groups, the area of the defect site seemed to decrease, and there appeared to be new muscle growth in and around the microthreads in these implant groups (Figure 6.5 I-J). Additionally, all mice that received EDCn-HGF implants 60 days post-injury were recorded to be highly active in their cages.

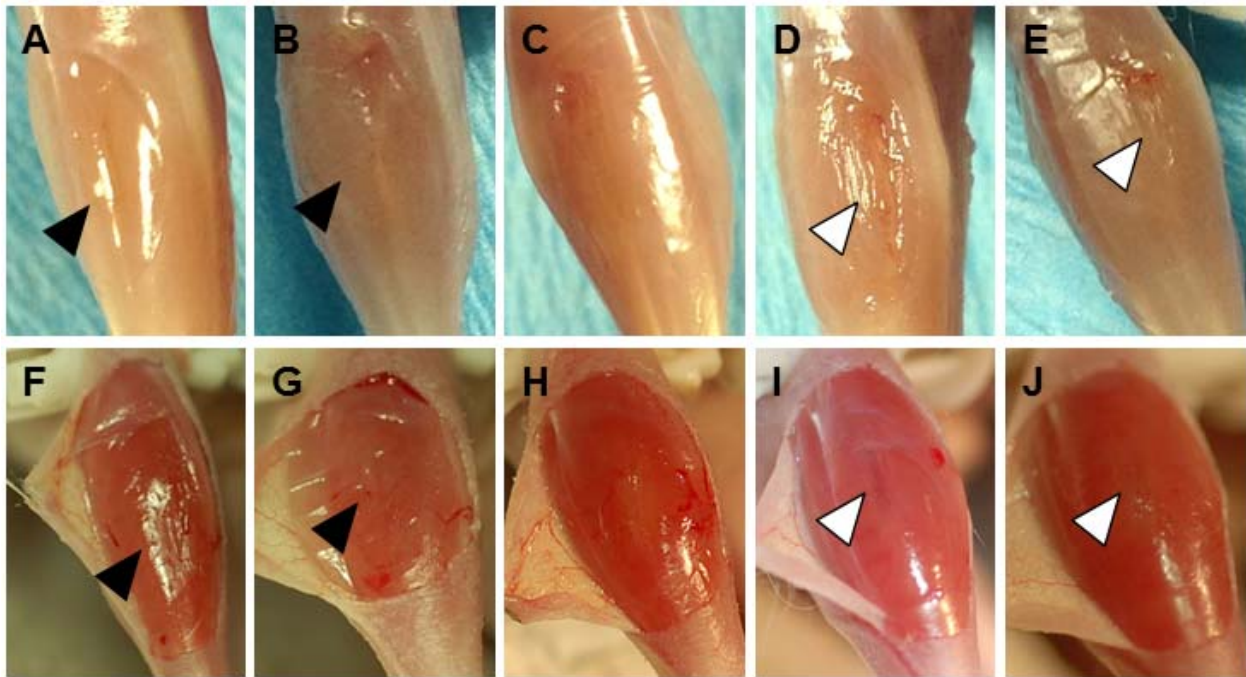


Figure 6.5. Gross morphology of TA muscle defects. VML injuries were created in each TA muscle, received no intervention (A,F), or fibrin gel (B,G), UNX microthread (C,H), EDCn microthread (D,I), or EDCn-HGF microthread (E,J) implants, and were allowed to recover to 14 days (A-E) or 60 days (F-J) post-injury. There was a loss of muscle volume evident by a loss in the convex shape of the surface of the muscle in untreated control and fibrin gel implant groups at both time points (black arrowheads). Additionally, some microthreads remain visible in EDCn (D,I) and EDCn-HGF (E,J) microthread implant groups at both time points (white arrowheads).

6.3.2 Fourteen Days Post-Injury, Microthread Implants Support Myoblast Infiltration

We analyzed the amount of muscle regeneration 14 days post-injury to determine the early regenerative response to fibrin microthread implants. There was a clear demarcation between healthy tissue, regenerating tissue, and the remaining injury site in each implant group in tissue sections stained with Masson's trichrome, where blue stains for collagen and connective tissue, black stains cell nuclei, and red stains cytoplasm (muscle) and fibrin structures. Regenerating tissue was defined as multinucleated cells (myofibers) with centrally positioned nuclei. With the exception of EDCn-HGF microthreads, all other treatment groups supported the deposition of connective tissue (Figure 6.6). All fibrin gel and microthread implants persisted 14 days post-injury and, interestingly, fibrin gel implants appeared to be heavily infiltrated with adipocytes (Figure 6.6B). There were fewer cells in the central region of the defect site of EDCn and EDCn-HGF microthreads than UNX microthreads (Figure 6.6 C-E).

The tissue morphology at the distal end of the muscle defects showed the integration of the host tissue with each of the implants (Figure 6.7). Untreated controls showed the most collagen fiber deposition (blue arrows), with few infiltrating myoblasts (Figure 6.7 A-B). Fibrin gel implants displayed poor integration with the host tissue, as evident by the lack of myoblast growth or myofiber formation within the implant itself. Instead of remaining an acellular space, there were a large number of adipocytes (white arrows) that infiltrated within the fibrin gel matrix (Figure 6.7 C-D). While there was more myoblast ingrowth (black arrows) into UNX microthread implants than fibrin gel implants, there was also adipocyte infiltration into the microthread structures, and connective tissue was deposited around the microthread implants (Figure 6.7 E-F). EDCn and EDCn-HGF microthread implant groups showed good tissue integration, as several myofibers were observed around, and between, discrete microthreads (Figure 6.7 G-J). EDCn-HGF microthread implants supported larger amounts of tissue ingrowth than EDCn microthread implants, and had less collagen deposition at this time point.

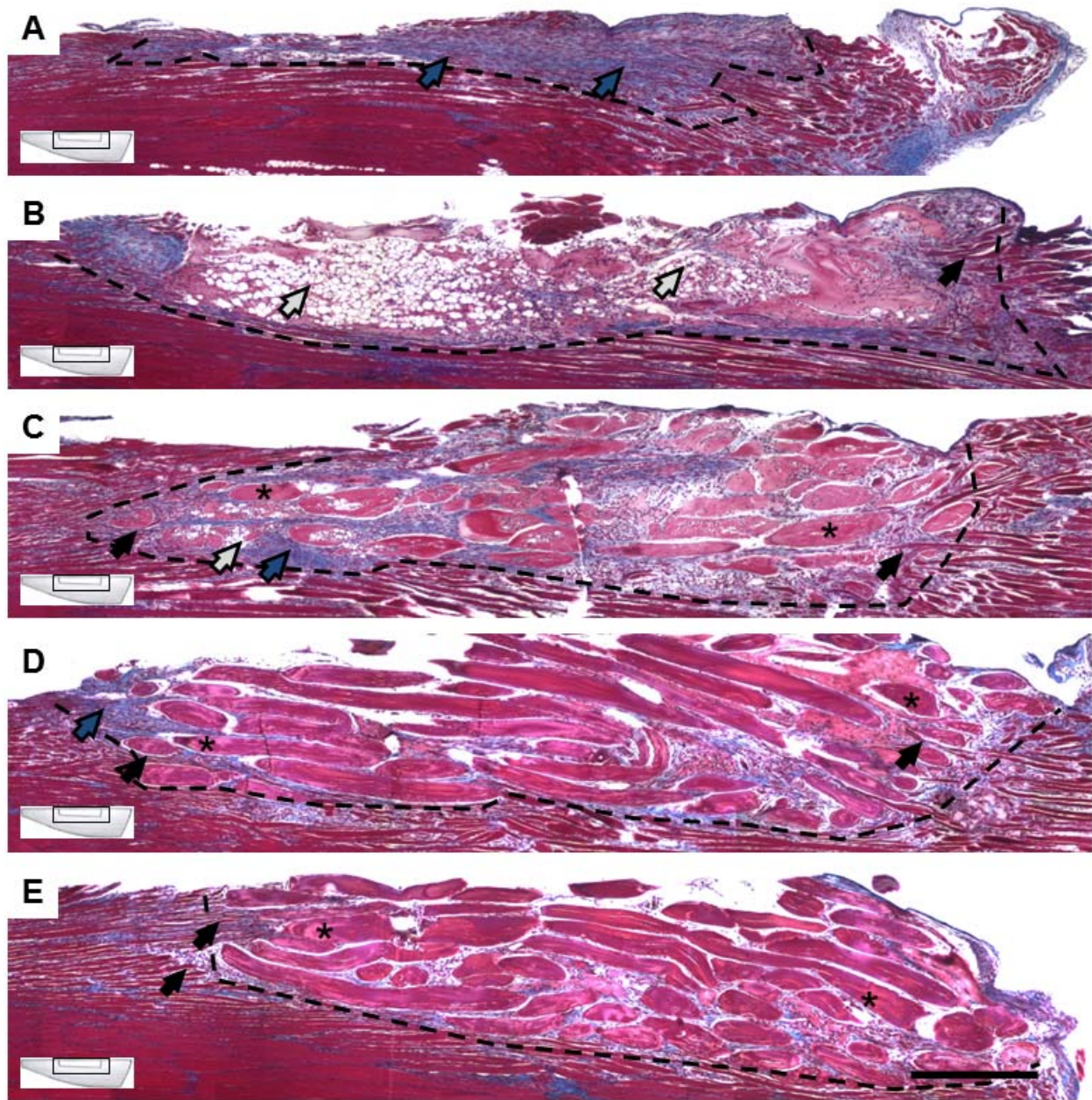


Figure 6.6. Low magnification images of entire VML defect sites 14 days post-injury. Masson's trichrome images of the coronal plane of VML defects with untreated controls (A), fibrin gel implants (B), or UNX (C), EDCn (D), or EDCn-HGF (E) microthread implants. All defect sites are indicated by the black dotted line, and are surrounded by healthy muscle tissue. Black arrows indicate muscle growth, blue arrows indicate connective tissue and collagen, white arrows indicate adipose tissue, and asterisks indicate microthreads within the defect. Varying amounts of muscle ingrowth are evident between treatment groups, with a large amount of adipocyte infiltration visible in fibrin gel implants. Inset shows tissue orientation and region of analysis with respect to distal and proximal ends of the injury site. Scale = 500 μm .

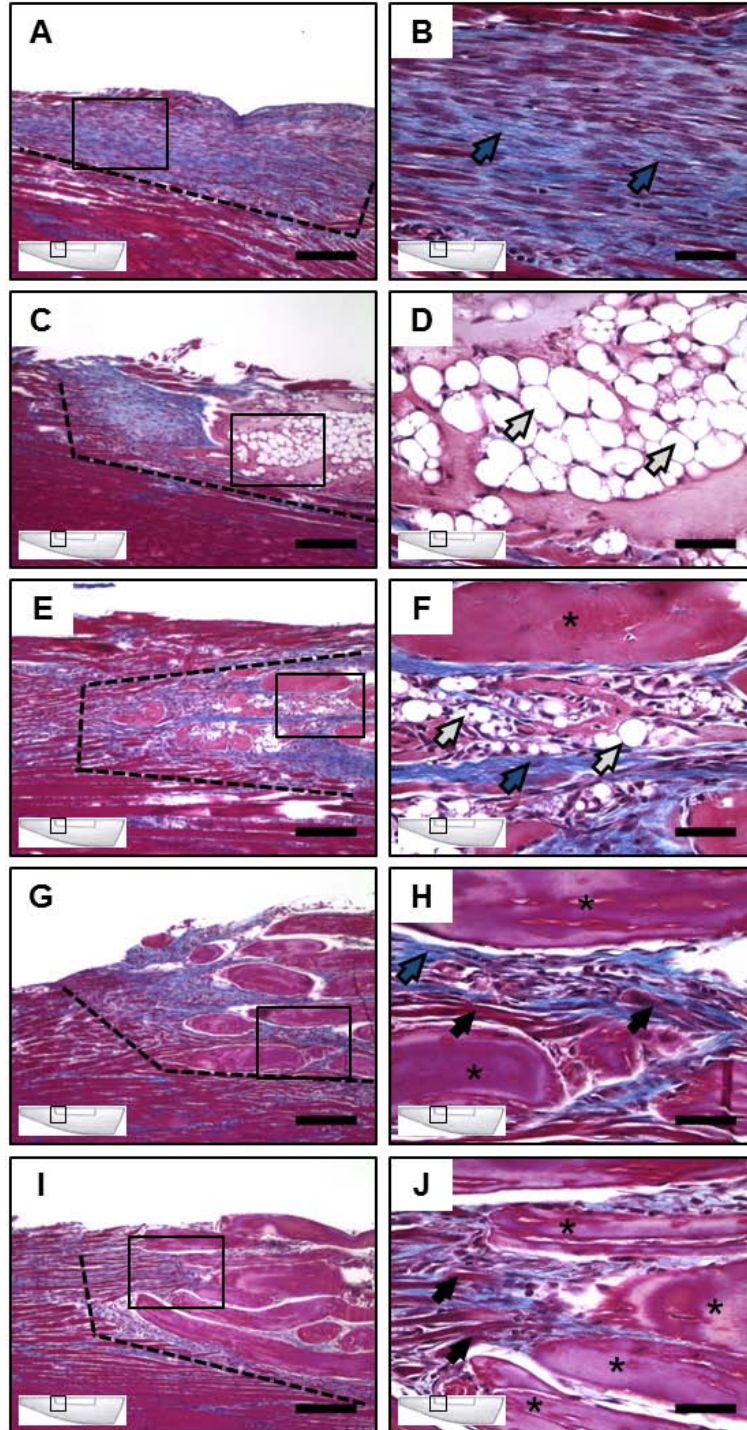


Figure 6.7. Morphology of the distal end of VML defect sites 14 days post-injury. Masson's trichrome images of the coronal plane of VML defects with untreated controls (A-B), fibrin gel implants (C-D), or UNX (E-F), EDCn (G-H), or EDCn-HGF (I-J) microthread implants at low (A,C,E,G,I) and high (B,D,F,H,J) magnification. All defect sites are indicated by the black dotted line, and are surrounded by healthy muscle tissue. Black arrows indicate muscle growth, blue arrows indicate connective tissue and collagen, white arrows indicate adipose tissue, and asterisks indicate microthreads within the defect. Inset shows tissue orientation and region of analysis with respect to distal and proximal ends of the injury site. Scale = 200 μm (A,C,E,G,I) and 50 μm (B,D,F,H,J).

6.3.3 Sixty Days Post-Injury, EDCn-HGF Microthreads Support Robust Regeneration of Muscular Tissue

A previous study suggested that scar tissue contributed to functional muscle recovery after the sixty day post-injury time point;¹⁹ therefore, to determine the amount of skeletal muscle regeneration due to fibrin microthreads, we analyzed the amount of tissue regeneration that occurred 60 days post-injury. While additional remodeling may occur over the next several months, we assumed that the majority of functional regeneration had occurred by this time point. There was a marked reduction in the number of mononuclear cells within the injury site 60 days post-injury, suggesting that the remodeling phase of skeletal muscle regeneration was complete (Figure 6.8). Remodeling without an implant resulted in disorganized myofibers that were surrounded by scar tissue (Figure 6.8A); while fibrin gel implants were completely remodeled into adipose tissue (Figure 6.8B). UNX microthread implants were mostly degraded at this time, although some small pieces of microthreads were observed. These microthreads were remodeled into a combination of adipose tissue, dense scar tissue, and somewhat organized myofibers (Figure 6.8C). EDCn microthreads persisted through 60 days post-injury (asterisks) with minimal adipose infiltration (Figure 6.8 D-E). Myofibers were observed in direct contact with microthreads, and this new tissue seems to be organized in plane with the surrounding healthy tissue (Figure 6.8E). Interestingly, the central regions of EDCn microthread implants appear to largely remain acellular at this time (Figure 6.8D).

The distal end of the muscle defect revealed that at least some muscle tissue ingrowth occurred into each defect site (Figure 6.9). Collagen tissue surrounded most of the regenerated myofibers present in the untreated control group (Figure 6.9 A-B). While both fibrin gel and UNX microthread implants supported extensive adipocyte infiltration (Figure 6.9 C-F), UNX microthreads also facilitated muscle tissue ingrowth, with small myofibers visible within the fatty tissue (Figure 6.9 E-F); however, these myofibers were not aligned with the surrounding healthy tissue. In contrast, myofibers completely surrounded several EDCn-HGF microthreads aligned with the surrounding tissue, showing a remarkable amount of tissue ingrowth (Figure 6.9 I-J).

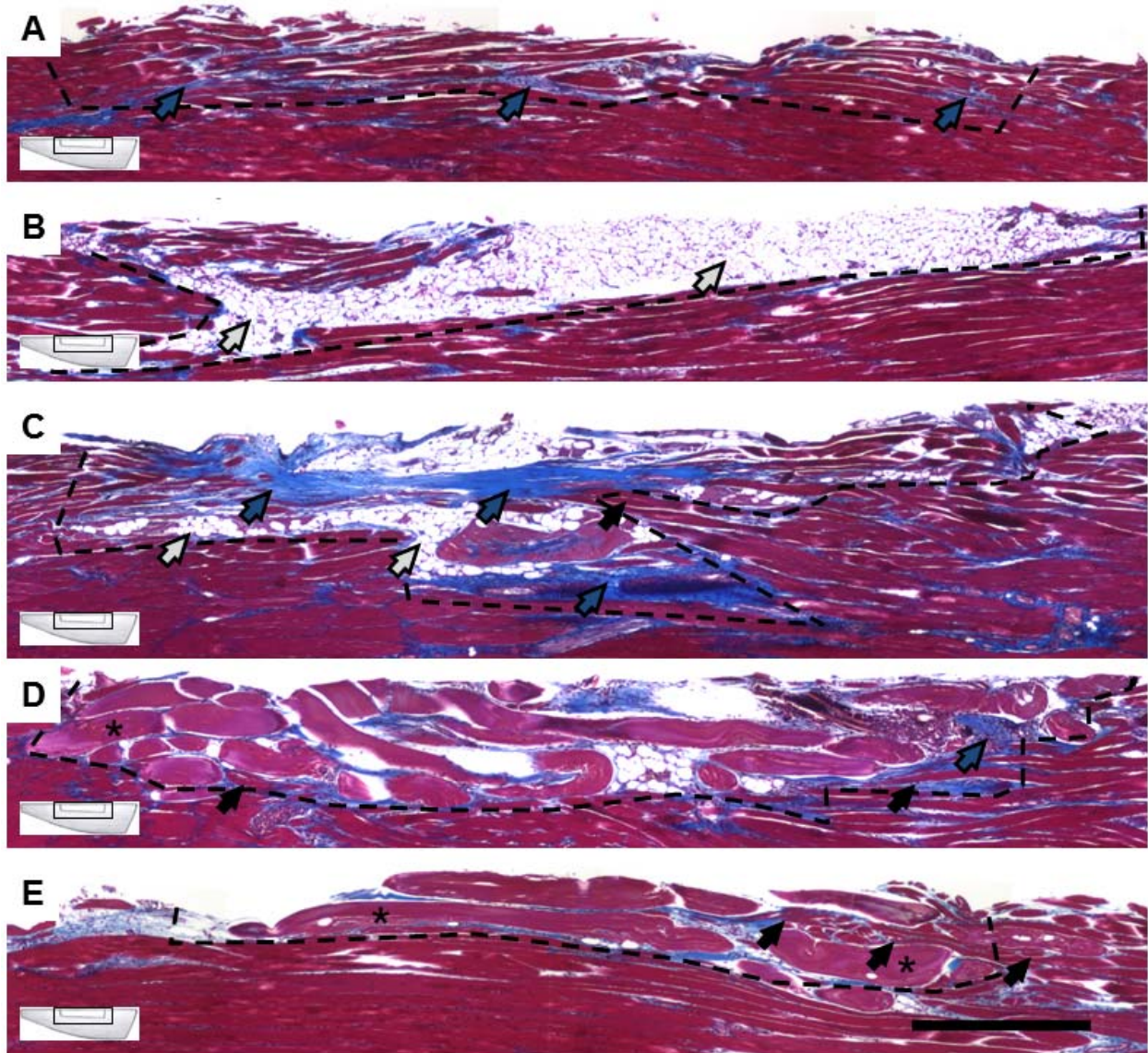


Figure 6.8 Low magnification images of entire VML defect sites 60 days post-injury. Masson's trichrome images of the coronal plane of VML defects with untreated controls (A), fibrin gel implants (B), or UNX (C), EDCn (D), or EDCn-HGF (E) microthread implants. All defect sites are indicated by the black dotted line, and are surrounded by healthy muscle tissue. Black arrows indicate muscle growth, blue arrows indicate connective tissue and collagen, white arrows indicate adipose tissue, and asterisks indicate microthreads within the defect. Fibrin gel implants were replaced with adipocytes, and UNX microthread implants were remodeled with adipocytes and collagen. Crosslinked microthreads persist at this time point with little cell infiltration, however it is apparent that much of the defect site was remodeled into muscle tissue. Inset shows tissue orientation and region of analysis with respect to distal and proximal ends of the injury site. Scale = 500 μm .

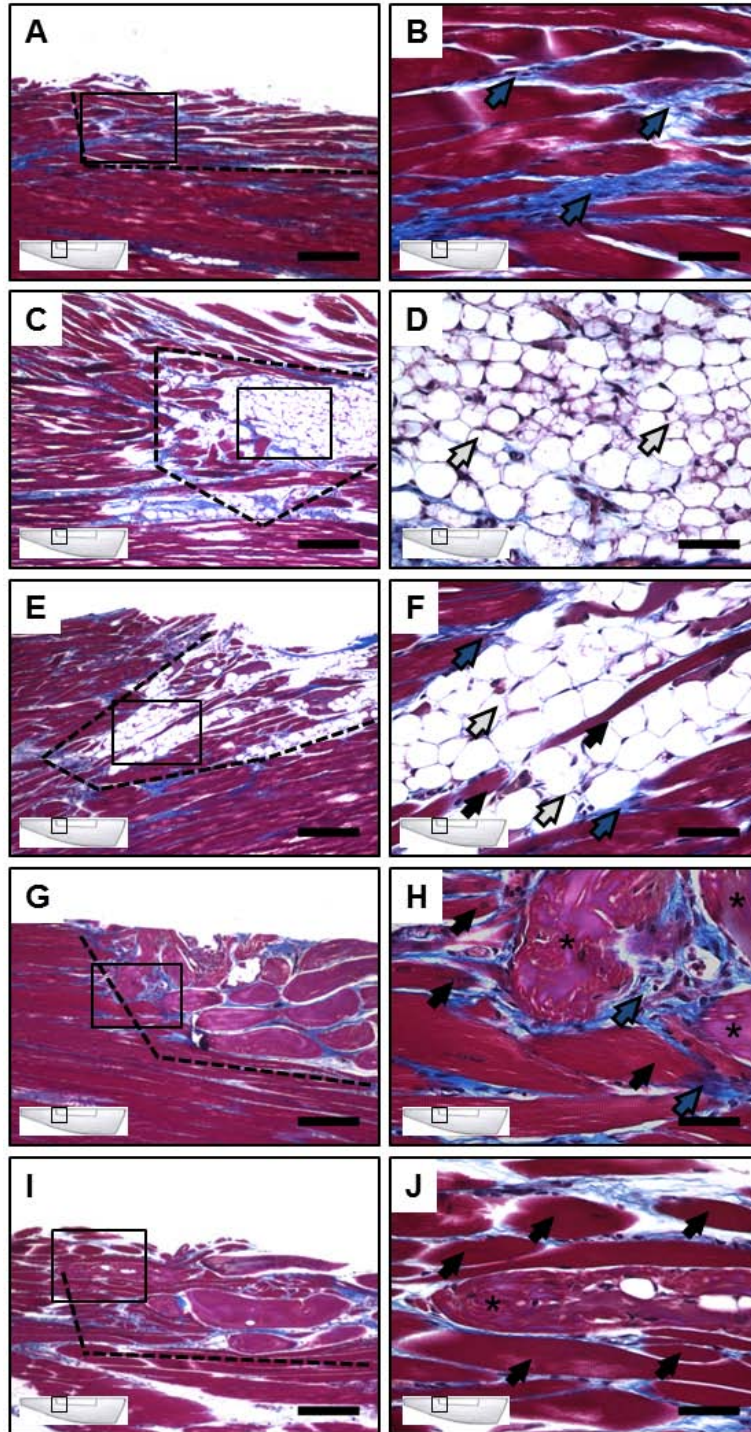


Figure 6.9. Morphology of the distal end of VML defect sites 60 days post-injury. Masson's trichrome images of the coronal plane of VML defects with untreated controls (A-B), fibrin gel implants (C-D), or UNX (E-F), EDCn (G-H), or EDCn-HGF (I-J) microthread implants at low (A,C,E,G,I) and high (B,D,F,H,J) magnification. All defect sites are indicated by the black dotted line, and are surrounded by healthy muscle tissue. Black arrows indicate muscle growth, blue arrows indicate connective tissue and collagen, white arrows indicate adipose tissue, and asterisks indicate microthreads within the defect. Inset shows tissue orientation and region of analysis with respect to distal and proximal ends of the injury site. Scale = 200 μm (A,C,E,G,I) and 50 μm (B,D,F,H,J).

6.3.4 Microthread Implants Reduce the Size of the Defect Site, but do not Affect Collagen Deposition

To quantify the observation that the defect size appeared smaller 60 days post-injury than 14 days post-injury, the length and width of defects were measured using coronal sections (Figure 6.3). The length and width of defects from untreated control and fibrin gel implant groups were qualitatively smaller than their respective measurements from microthread implant groups (UNX, EDCn, and EDCn-HGF microthreads) at 14 days post-injury; however, all of the measurements were similar at 60 days post-injury. Both the length and width of defects with microthread implants significantly decreased from 14 to 60 days post-injury (Table 6.2). Measurements taken 60 days post-injury were normalized against the measurements taken 14 days post-injury to obtain percent decreases in each of these dimensions over time. Interestingly, the percent of defect length from 14 days post-injury for each microthread implant group was significantly lower than the percent change for fibrin gel implants (Figure 6.10). Similarly, the percent of defect width remaining from 14 days post-injury for each microthread group was significantly lower than the percent change for both the untreated control and fibrin gel implant groups. These data suggest that microthread implant groups are facilitating an increase in tissue remodeling.

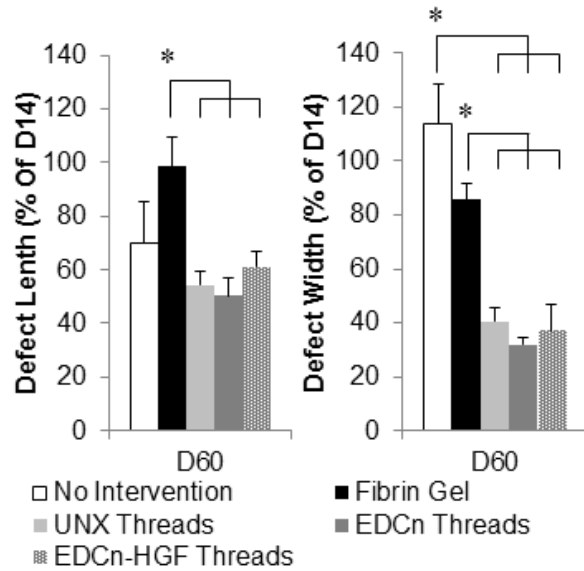


Figure 6.10. Change in muscle defect length and width from 14 to 60 days post-injury. Microthread implants decrease defect size, suggesting that the muscle may be remodeling the defect site into functional tissue. * indicate significance with indicated groups as determined by one-way ANOVA with Holm-Sidak post hoc analysis ($p < 0.05$, $n=6$).

Table 6.2. Length and width of VML defects 14 and 60 days post-injury.

| | No Intervention | | Fibrin Gel | | UNX Microthreads | | EDCn Microthreads | | EDCn-HGF Microthreads | |
|--------------------|-----------------|------------|------------|------------|------------------|-------------|-------------------|-------------|-----------------------|-------------|
| | 14 Days | 60 Days | 14 Days | 60 Days | 14 Days | 60 Days | 14 Days | 60 Days | 14 Days | 60 Days |
| Sample Size (n) | 3 | 6 | 3 | 6 | 3 | 6 | 3 | 6 | 3 | 6 |
| Defect Length (mm) | 2.0 ± 0.5 | 1.4 ± 0.2 | 2.1 ± 0.4 | 2.1 ± 0.2 | 3.8 ± 0.1 | 2.1 ± 0.2* | 3.7 ± 0.5 | 1.9 ± 0.2* | 3.5 ± 0.3 | 2.1 ± 0.2* |
| Defect Width (mm) | 0.2 ± 0.04 | 0.3 ± 0.03 | 0.3 ± 0.07 | 0.3 ± 0.02 | 0.7 ± 0.06 | 0.3 ± 0.04* | 0.7 ± 0.11 | 0.2 ± 0.02* | 0.5 ± 0.10 | 0.2 ± 0.05* |

* indicate significance with 14 day post-injury measurements as determined by Student's t-test ($p < 0.05$).

To determine the amount of scarring, a typical consequence of VML injuries, we used Photoshop to isolate all the blue pixels in low magnification composite images of the defect sites at 60 days post-injury (Figure 6.4). The number of pixels that were blue in the injury site were measured, and the total percent of the defect site that was comprised of these blue pixels was recorded. There was a qualitative increase in the percent of collagen tissue present in the defect site; however, there was no statistical significance between these measurements (Figure 6.11).

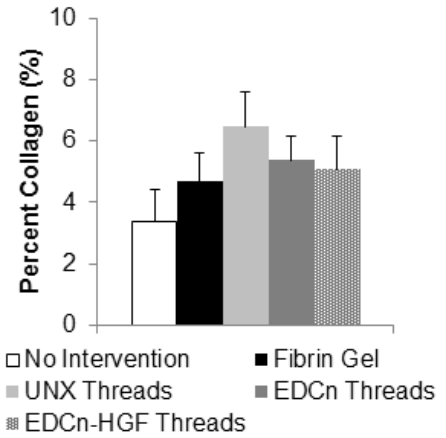


Figure 6.11. Percent collagen content within VML defect sites 60 days post-injury. No significant differences detected by one-way ANOVA with Holm-Sidak post hoc analysis ($p < 0.05$, $n=6$).

6.3.5 Crosslinked Microthreads Enhance Recruitment of Satellite Cells

To determine the amount of SCs in the area surrounding the VML defect, sections of VML defects were stained by IHC with an antibody recognizing Pax7 at 14 and 60 days post-injury. Positive nuclei were detected in all treatment groups 14 days post-injury, indicating that in all injuries SCs were being recruited to the injury site (Figure 6.12). Few SCs were observed within the injury sites of untreated control groups (Figure 6.12A) or fibrin gel implants (Figure 6.12B). SCs were observed to be in close proximity to microthread implants (Figure 6.12 C-E), and in all cases seemed to be located near newly forming myofibers. Sixty days post-injury, there were fewer SCs present in the defect site of all treatment groups (Figure 6.13). SCs were situated on the periphery of myofibers that were located near remaining EDCn and EDCn-HGF microthreads (Figure 6.13 D-E). Both EDCn and EDCn-HGF microthread implants recruited significantly more SCs than would typically be present in uninjured tissue, however, only EDCn microthread implants recruited significantly more SCs than untreated control and fibrin gel implant groups 14 days post-injury (Figure 6.14). While there was a significant reduction in the number of SCs present 60 days post-injury with respect to 14 days post-injury, there were no significant differences between treatment groups or uninjured controls, suggesting that no additional SC recruitment is occurring at this time, implying that SC-mediated regeneration is complete.

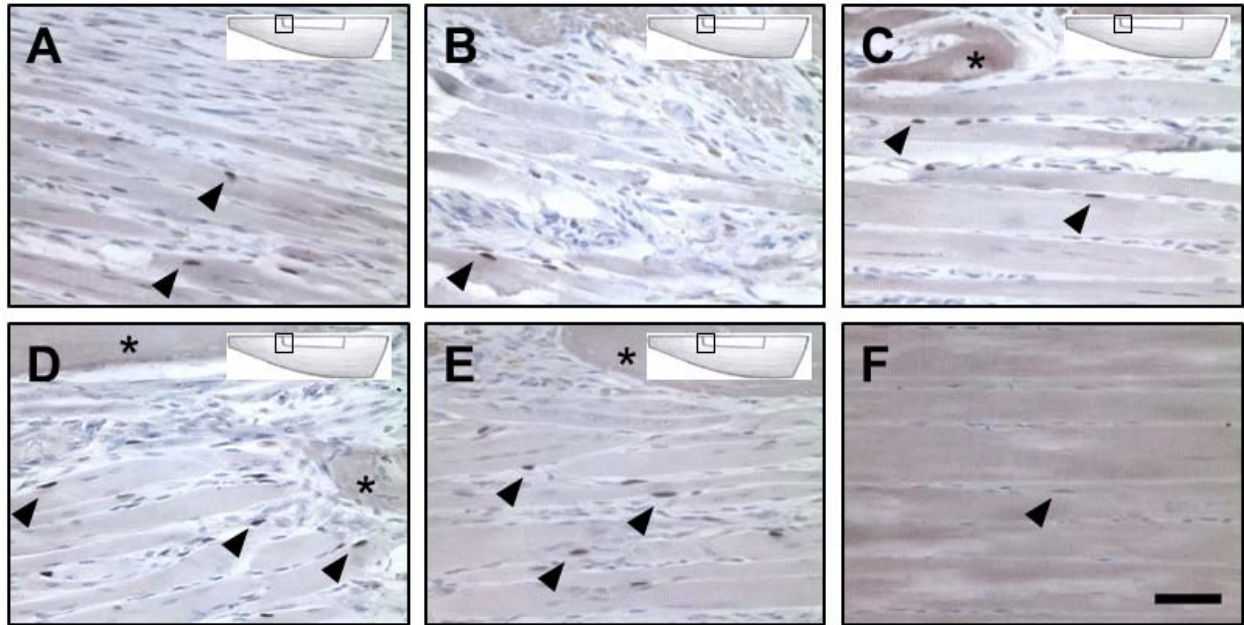


Figure 6.12. IHC staining of Pax7 positive cells in VML defects 14 days post-injury. IHC staining for Pax7 with a hematoxylin counterstain of VML defects with untreated controls (A), fibrin gel implants (B), or UNX (C), EDCn (D), or EDCn-HGF (E) microthreads, or un-injured muscle (F). SCs (Pax7 positive) were recruited towards the injury site, and appear in close proximity to microthreads. Asterisks indicate microthreads and black arrowheads denote representative Pax7 positive nuclei. Inset shows tissue orientation and region of analysis with respect to distal and proximal ends of the injury site. Scale = 50 μ m.

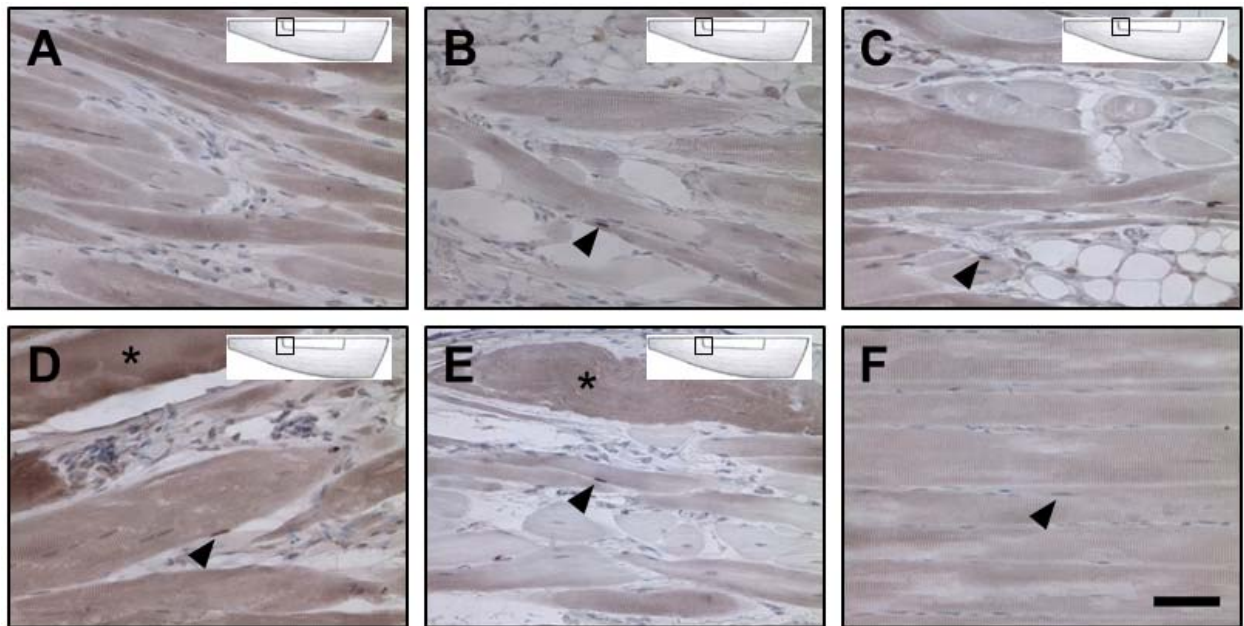


Figure 6.13. IHC staining of Pax7 positive cells in VML defects 60 days post-injury. IHC staining for Pax7 with a hematoxylin counterstain of VML defects with untreated controls (A), fibrin gel implants (B), or UNX (C), EDCn (D), or EDCn-HGF (E) microthreads, or un-injured muscle (F). SCs (Pax7 positive) were recruited towards the injury site, and appear in close proximity to microthreads. Asterisks indicate microthreads and black arrowheads denote representative Pax7 positive nuclei. Inset shows tissue orientation and region of analysis with respect to distal and proximal ends of the injury site. Scale = 50 μ m.

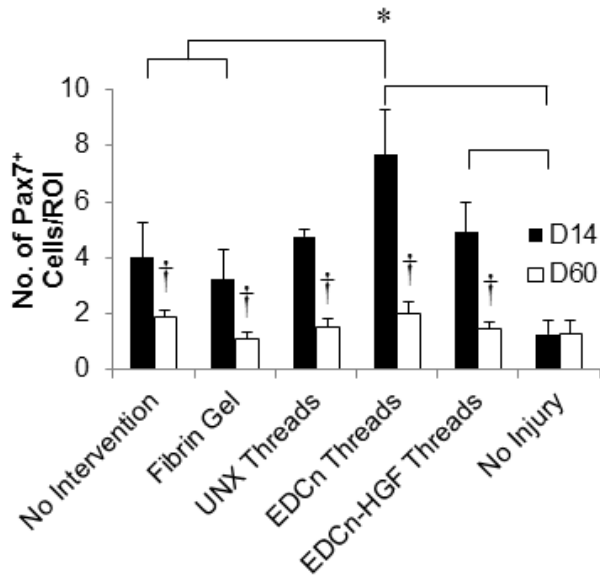


Figure 6.14. Number of Pax7 positive cells in VML defects. There were significantly more Pax7 positive SCs in crosslinked (EDCn and EDCn-HGF) implant groups than uninjured controls, however only EDCn microthread implants had elevated numbers of SCs present compared to the untreated control group. * and brackets indicate significant differences between indicated groups as determined by one-way ANOVA with Holm-Sidak post hoc analysis, † denote significance with D14 values as determined by Student's t-test ($p < 0.05$, $n=3$ for D14, $n=6$ for D60).

6.3.6 HGF Delivery Promotes Increased Number of Myogenin Positive Nuclei

To determine the amount of nascent myofibers forming within the VML defect, sections of VML defects were stained by IHC with an antibody recognizing myogenin at 14 and 60 days post-injury. Myogenin is a transcription factor that promotes myoblast fusion to become immature myofibers, and thus is considered a differentiation marker for myoblasts. Myogenin positive nuclei were found in all implant groups 14 days post-injury, however, the number of multinucleated myofibers increased with the presence of microthread implants (Figure 6.15). Myofibers were located immediately adjacent to several crosslinked microthreads, indicating that these scaffold materials successfully guided myoblast ingrowth into defect sites (Figure 6.15 D-E). Further, the myofibers adjacent to crosslinked microthreads appeared to have more nuclei present per multinucleated cell, suggesting an increase in the maturity of these nascent fibers. As expected, no positive nuclei were observed in uninjured controls (Figure 6.15F). Sixty days post-injury, there were almost no myogenin positive nuclei in any treatment group (Figure 6.16). All microthread implants supported significantly more myogenin positive nuclei than would typically be present in uninjured tissue 14 days post-injury, and EDCn-HGF microthreads supported significantly more myogenin positive nuclei than the untreated controls (Figure 6.17). The number of myogenin positive nuclei in fibrin gel implants and UNX, EDCn, and EDCn-HGF microthread implant groups 60 days post-injury significantly decreased with respect to 14 days post-injury (Figure 6.17). In fact, little to no myogenin positive nuclei were identified 60

days post-injury for any treatment group, suggesting that myoblasts were no longer fusing into myotubes at this time and that the differentiation phase of skeletal muscle regeneration had resolved at this time.

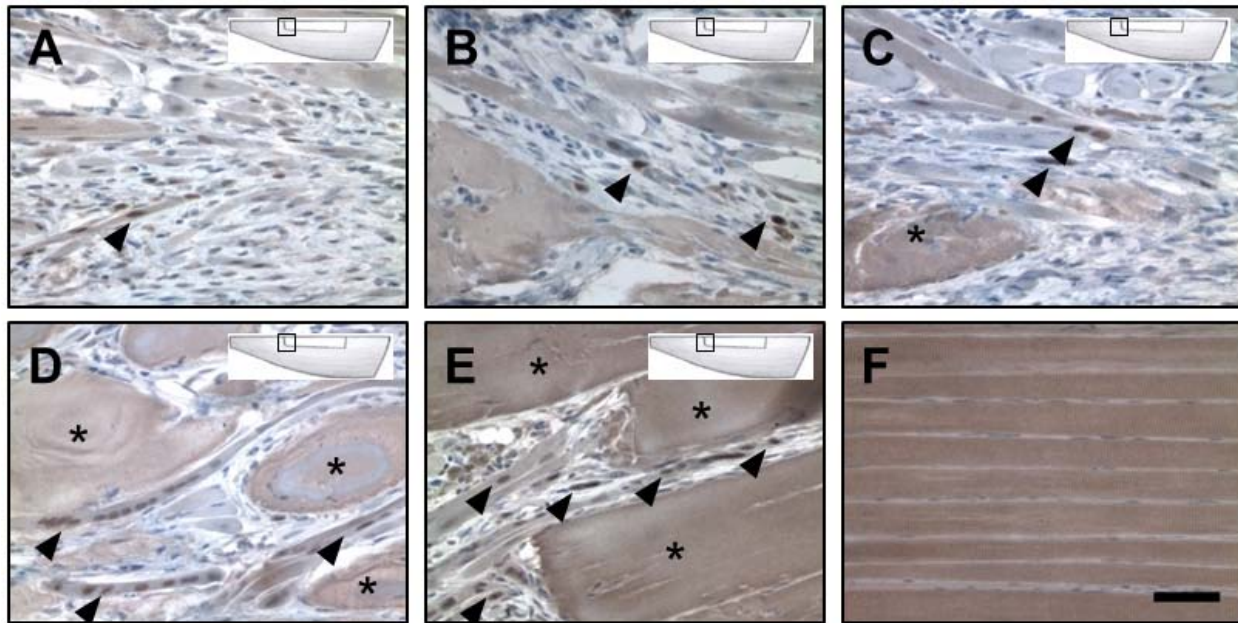


Figure 6.15. IHC staining of myogenin positive nuclei in VML defects 14 days post-injury. IHC staining for myogenin with a hematoxylin counterstain of VML defects with untreated controls (A), fibrin gel implants (B), or UNX (C), EDCn (D), or EDCn-HGF (E) microthreads, or un-injured muscle (F). Myoblasts were observed to be fusing around and between microthreads within the defect site. Asterisks indicate microthreads and black arrowheads denote representative myogenin positive nuclei. Inset shows tissue orientation and region of analysis with respect to distal and proximal ends of the injury site. Scale = 50 μ m.

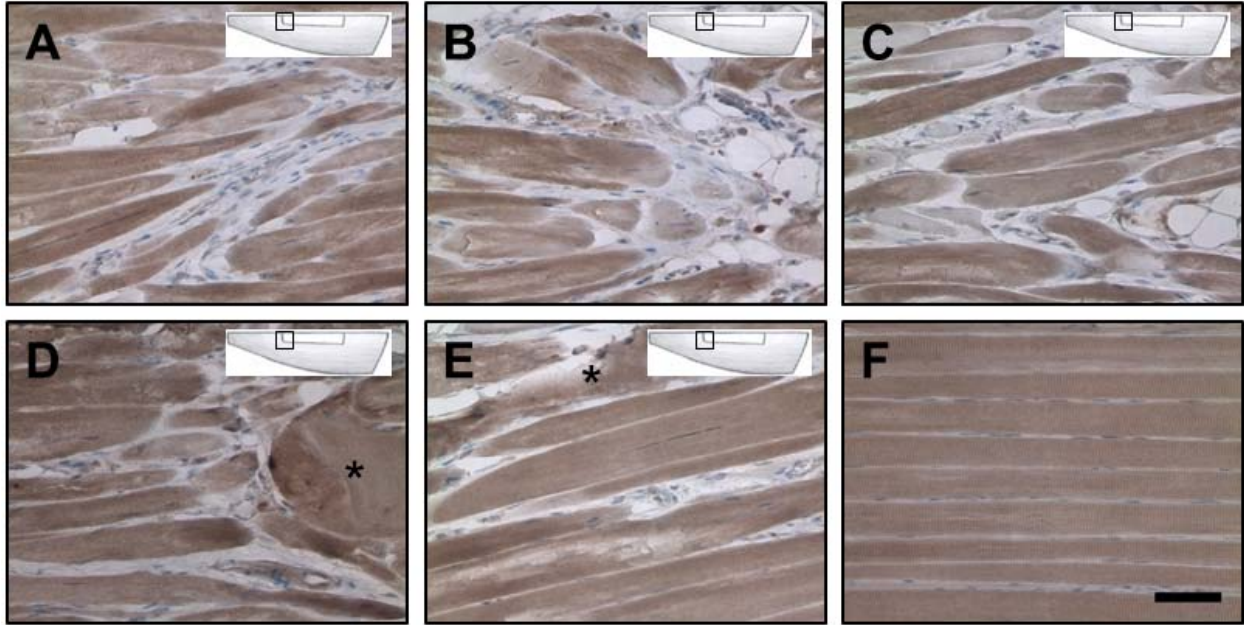


Figure 6.16. IHC staining of myogenin positive nuclei in VML defects 60 days post-injury. IHC staining for myogenin with a hemotoxylin counterstain of VML defects with untreated controls (A), fibrin gel implants (B), or UNIX (C), EDCn (D), or EDCn-HGF (E) microthreads, or un-injured muscle (F). Myoblasts were observed to be fusing around and between microthreads within the defect site. Asterisks indicate microthreads and black arrowheads denote representative myogenin positive nuclei. Inset shows tissue orientation and region of analysis with respect to distal and proximal ends of the injury site. Scale = 50 μm .

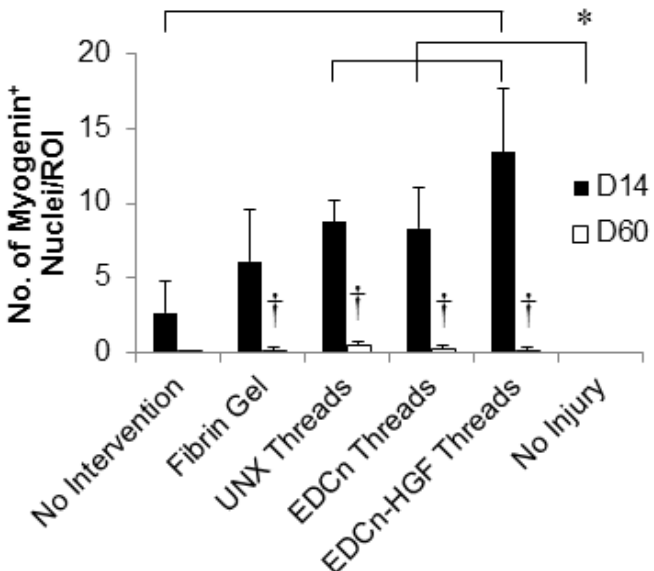


Figure 6.17. Number of myogenin positive nuclei in VML defects. There were significantly more myogenin positive nuclei in UNIX, EDCn, and EDCn-HGF microthread implant groups compared to un-injured controls, and EDCn-HGF microthreads supported significantly more myogenin positive nuclei than the untreated control group. * and brackets indicate significant differences between indicated groups as determined by one-way ANOVA with Holm-Sidak post hoc analysis, † denote significance with D14 values as determined by Student's t-test ($p < 0.05$, $n=3$ for D14, $n=6$ for D60).

6.3.7 *Microthread Implant Groups Support Early Angiogenesis in VML Defects*

To determine the number of blood vessels that infiltrated into the VML defect site over time, sections of VML defects were stained by IHC with an antibody recognizing PECAM (CD31). PECAM is a protein found on the surface of endothelial cells, and thus can be used to locate blood vessels within a defect site. Blood vessels were located in all defect sites 14 days post-injury (Figure 6.18), although there were few observed in the connective tissue within the injury site in the untreated controls (Figure 6.18A). Blood vessels surrounded the adipocytes that had infiltrated the fibrin gel implants (Figure 6.18B), and were adjacent to microthread implants in the injury site (Figure 6.18 C-E). Sixty days post-injury, there were fewer blood vessels present than 14 days post-injury in the defect site (Figure 6.19). The connective tissue present in untreated controls was largely avascular (Figure 6.19A), in contrast with the dense capillary network visible within adipose tissue present in fibrin gel and UNX microthread implant groups (Figure 6.19 B-C). Blood vessels continued to be adjacent to EDCn and EDCn-HGF microthread implant groups (Figure 6.19 D-E). Significantly more blood vessels formed in microthread implant injury sites than the untreated and uninjured skeletal muscle tissue controls 14 days post-injury. The fibrin gel implant group had significantly higher numbers of blood vessels in the injury site than uninjured controls as well (Figure 6.20). All microthread implants had significantly fewer blood vessels present in the defect site at 60 days post-injury with respect to 14 days post injury (Figure 6.20). There remained an elevated number of blood vessels within the wound sites of fibrin gel, UNX and EDCn-HGF microthread implant treatments with respect to the untreated and uninjured control groups (Figure 6.20).

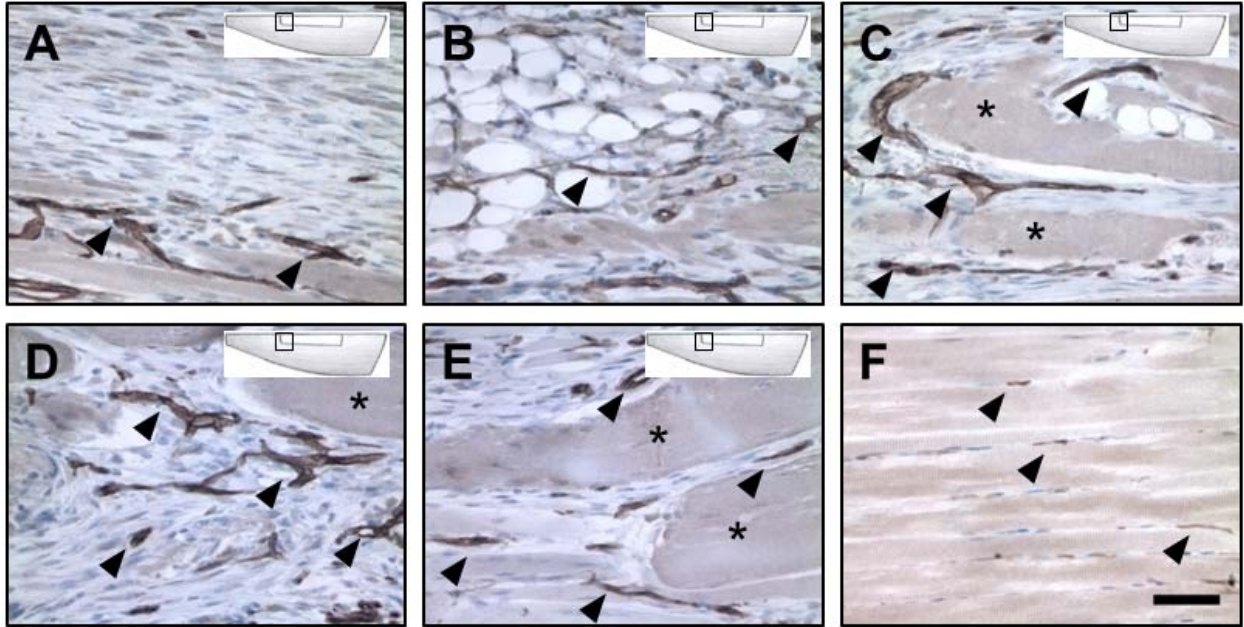


Figure 6.18. IHC staining of PECAM in VML defects 14 days post-injury. IHC staining for PECAM with a hemotoxylin counterstain of VML defects with untreated controls (A), fibrin gel implants (B), or UNX (C), EDCn (D), or EDCn-HGF (E) microthreads, or un-injured muscle (F). PECAM (CD31) is a marker of endothelial cells, revealing blood vessel formation with the defect site. Blood vessels were found to form in close proximity with microthreads, and between adipocytes. Asterisks indicate microthreads and black arrowheads denote representative blood vessels. Inset shows tissue orientation and region of analysis with respect to distal and proximal ends of the injury site. Scale = 50 μ m.

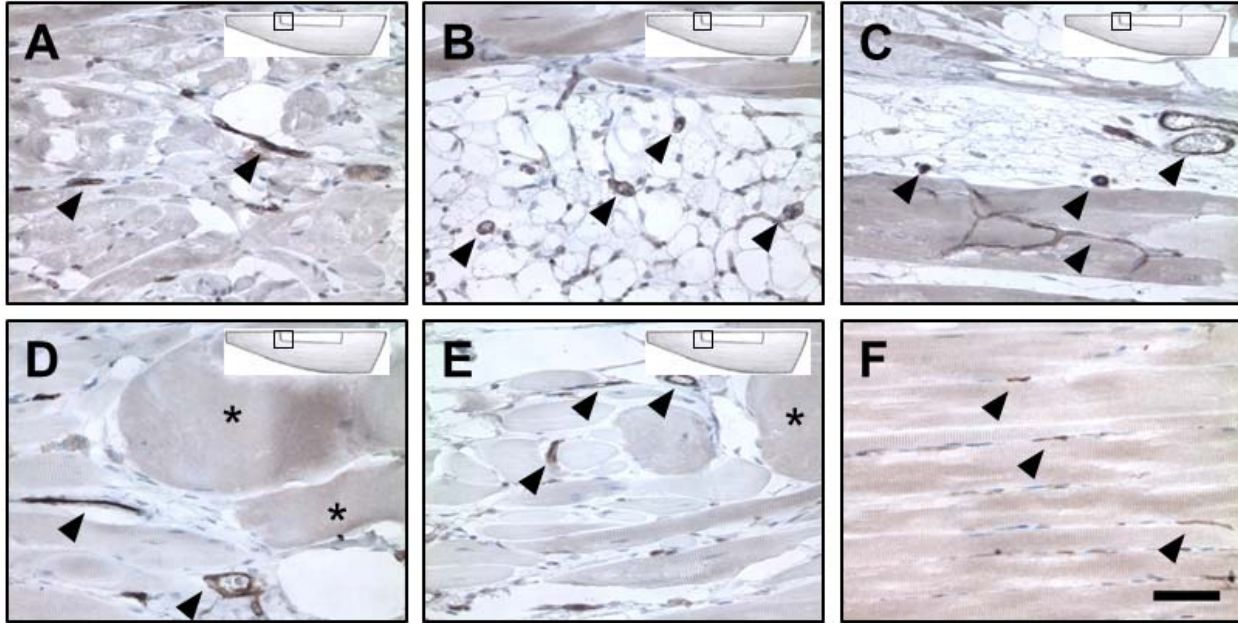


Figure 6.19. IHC staining of PECAM in VML defects 60 days post-injury. IHC staining for PECAM with a hemotoxylin counterstain of VML defects with untreated controls (A), fibrin gel implants (B), or UNX (C), EDCn (D), or EDCn-HGF (E) microthreads, or un-injured muscle (F). PECAM (CD31) is a marker of endothelial cells, revealing blood vessel formation with the defect site. Blood vessels were found to form in close proximity with microthreads, and between adipocytes. Asterisks indicate microthreads and black arrowheads denote representative blood vessels. Inset shows tissue orientation and region of analysis with respect to distal and proximal ends of the injury site. Scale = 50 μ m.

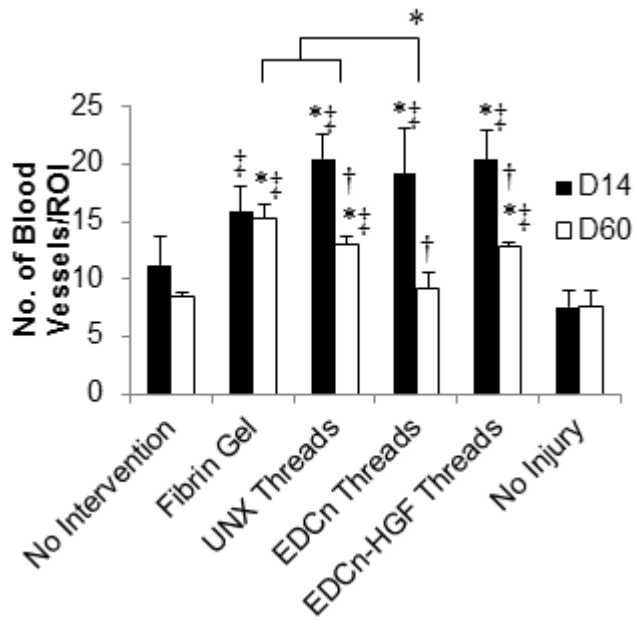


Figure 6.20. Number of blood vessels in VML defects. There were significantly more blood vessels in VML defects that received microthread implant groups after 14 days of recovery compared to untreated and uninjured controls. A significantly larger number of blood vessels remained in the fibrin gel, UNX, and EDCn-HGF implant groups 60 days post-injury compared to the untreated and uninjured controls. * indicate significant differences with untreated controls, † indicate significance with no injury values, and brackets indicate significant differences between indicated groups as determined by one-way ANOVA with Holm-Sidak post hoc analysis, ‡ denote significance with D14 values as determined by Student's t-test ($p < 0.05$, $n=3$ for D14, $n=6$ for D60).

6.3.8 EDCn-HGF Microthreads Restore Mechanical Function of TA Muscles after VML Injuries

To quantify the amount of functional recovery in mice that received VML defects, each injury was created such that there was approximately a 50% reduction in isometric twitch force from pre-injured, baseline values (Figure 6.21A). After the creation of each injury, each animal received one of five treatments and was allowed to recover for 60 days. At this time, the isometric twitch force was measured again to obtain recovered values. The recovery isometric twitch force was significantly greater than that of the twitch force generated immediately after injury for animals that received microthread implants (Figure 6.21A). The recovery forces resulting from fibrin gel or UNX microthread implants were still significantly lower than their original baseline values. Further, the recovered twitch force from EDCn-HGF microthread implants was significantly stronger than untreated control or fibrin gel implant groups, and the absolute value of this force is similar to the baseline twitch force recorded before the injury. To account for possible variations in injured force measurements between animals, the recovered force of each animal was normalized to its own after injury measurement. This shows a percent

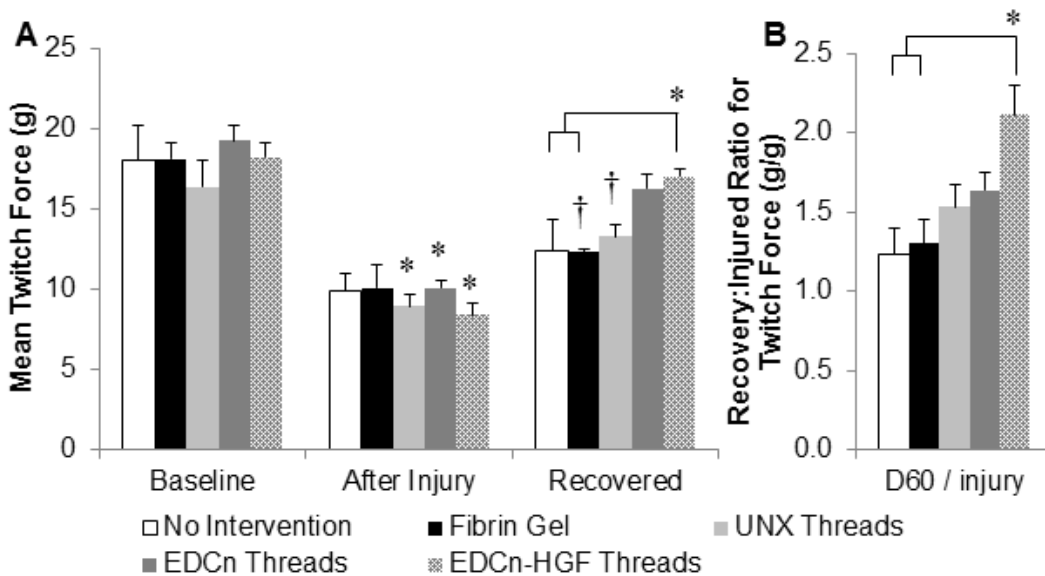


Figure 6.21. Isometric twitch force of TA muscles 60 days post-injury. The isometric twitch force of TA muscles before injury, immediately after injury, and 60 days post-injury (recovered) (A). EDCn-HGF microthread implants significantly increased the amount of force recovered compared to the untreated control and fibrin gel implant groups. To account for variation in the amount of regeneration between animals, the isometric twitch force was normalized to its individual after injury value (B). * indicate significance with recovered twitch forces, † indicate significance with baseline twitch forces, and brackets indicate significance with indicated groups as determined by one-way ANOVA with Holm-Sidak post hoc analysis ($p < 0.05$, $n=6$).

recovery based upon the injured values, where any ratio above 1 (100%) would indicate an increase in the amount of force based on the injury of each specific mouse. There was an approximate 150% increase in the twitch force production from injured values for UNX and EDCn microthread implant treatments, and there was an increase of over 200% in the twitch force production of animals that received EDCn-HGF microthread implants (Figure 6.21B).

To quantify the total strength of the muscle tissue before, after injury, and after recovery, the force produced at tetanus was also recorded. Tetanus was induced after a short period of rest after the isometric twitch forces were recorded. Force at tetanus values immediately after injury for EDCn-HGF microthread implants were qualitatively lower than all other treatment groups (Figure 6.22A). There was a significant improvement in the force at tetanus 60 days post-injury for all treatment groups except for the untreated controls, and the recovered force at tetanus for fibrin gel implants was still significantly lower than its baseline value. Force outputs for EDCn-HGF and EDCn microthread implants were qualitatively higher than all other treatment groups, and the absolute value of the tetanic force output from EDCn-HGF microthread implants was similar to the baseline force at tetanus initially recorded (Figure 6.22A). When the recovered

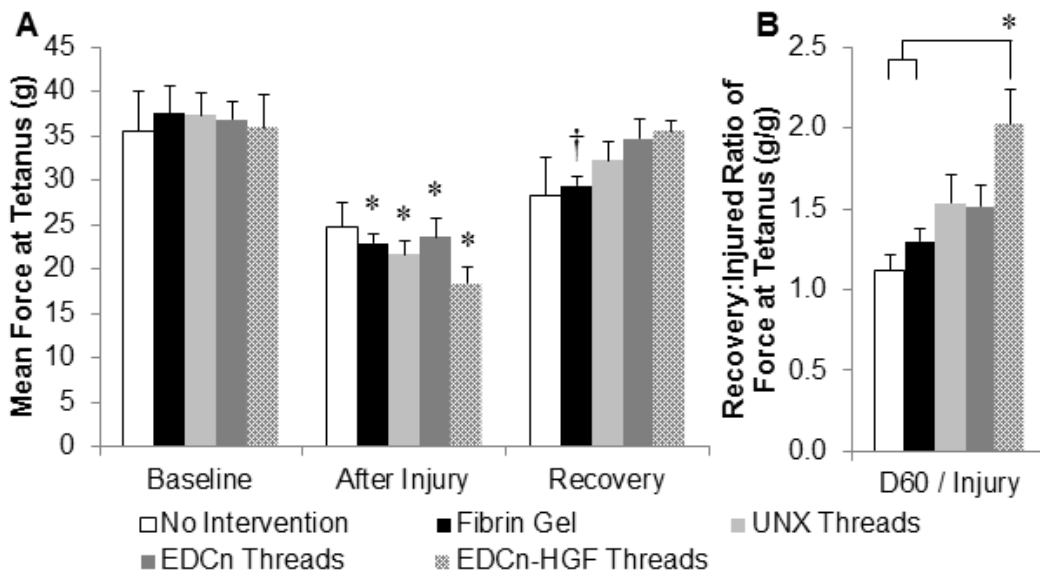


Figure 6.22. Force at tetanic contraction of TA muscles 60 days post-injury. The force at tetanus of TA muscles before injury, immediately after injury, and 60 days post-injury (recovered) (A). To account for variation in the amount of regeneration between animals, the force at tetanus was normalized to its individual after injury value (B). * indicate significance with recovered tetanic contractions, † indicate significance with baseline tetanic contractions, and brackets indicate significance with indicated groups as determined by one-way ANOVA with Holm-Sidak post hoc analysis ($p < 0.05$, $n=6$).

force of each animal was normalized to its own after injury measurement, there was an approximate 150% increase in the force production from injured values for animals that received UNX or EDCn microthread implants, while there was again an increase of over 200% in the force production of animals that received EDCn-HGF microthread implants (Figure 6.22B). A summary of the results from all of the force measurements is presented in Table 6.3.

Table 6.3. Summary of the functional characteristics of TA muscles before and immediately after the generation of a VML defect, and 60 days post-injury.

| | No Intervention | Fibrin Gel | UNX Microthreads | EDCn Microthreads | EDCn-HGF Microthreads |
|------------------------------------|---------------------------|--------------------------|--------------------------|-------------------|-----------------------|
| Sample Size (n) | 6 | 6 | 6 | 6 | 6 |
| Body weight at surgery (g) | 25.2 ± 0.5 | 24.9 ± 0.6 | 24.7 ± 0.4 | 24.3 ± 0.6 | 24.0 ± 0.7 |
| Body weight at sacrifice (g) | 27.0 ± 1.1 | 27.0 ± 0.7 | 27.3 ± 0.8 | 27.3 ± 0.8 | 26.2 ± 0.9 |
| Isometric twitch force | | | | | |
| Baseline (g) | 18.1 ± 2.2 | 18.3 ± 0.9 | 16.3 ± 1.6 | 19.2 ± 1.0 | 18.2 ± 0.9 |
| After Injury (g) | 9.9 ± 1.1 | 10.2 ± 1.4 | 8.9 ± 0.7* | 10.0 ± 0.5* | 8.3 ± 0.7* |
| Recovered (g) | 12.4 ± 2.0 ^a | 12.3 ± 0.2 ^a | 13.3 ± 0.8 [†] | 16.2 ± 0.9 | 17.0 ± 0.5 |
| Contralateral (g) | 17.8 ± 1.2 | 18.7 ± 0.8 | 18.4 ± 0.5 | 19.4 ± 1.4 | 18.7 ± 0.8 |
| Recovery/After injury (g/g) | 1.23 ± 0.18 ^a | 1.30 ± 0.15 ^a | 1.53 ± 0.14 | 1.64 ± 0.11 | 2.11 ± 0.19 |
| Recovery/Contralateral (g/g) | 0.70 ± 0.11 | 0.66 ± 0.02 ^a | 0.73 ± 0.05 | 0.85 ± 0.06 | 0.91 ± 0.03 |
| Recovery/Body weight (g/g body wt) | 0.45 ± 0.06 ^{ab} | 0.46 ± 0.01 ^a | 0.48 ± 0.02 ^a | 0.60 ± 0.04 | 0.65 ± 0.03 |
| Force at tetanic contraction | | | | | |
| Baseline (g) | 35.5 ± 4.6 | 37.5 ± 3.0 | 37.3 ± 2.4 | 36.8 ± 2.0 | 36.0 ± 3.5 |
| After Injury (g) | 24.7 ± 2.7 | 22.9 ± 1.1* | 21.7 ± 1.5* | 23.6 ± 2.1* | 18.4 ± 1.8* |
| Recovered (g) | 28.3 ± 4.2 | 29.4 ± 1.0 [†] | 32.2 ± 2.0 | 34.7 ± 2.3 | 35.6 ± 1.0 |
| Contralateral (g) | 38.8 ± 2.7 | 39.2 ± 1.1 | 35.7 ± 2.6 | 36.1 ± 3.5 | 36.0 ± 1.1 |
| Recovery/After injury (g/g) | 1.11 ± 0.10 ^a | 1.30 ± 0.08 ^a | 1.54 ± 0.18 | 1.51 ± 0.13 | 2.03 ± 0.21 |
| Recovery/Contralateral (g/g) | 0.72 ± 0.09 ^a | 0.75 ± 0.02 | 0.93 ± 0.09 | 0.98 ± 0.05 | 0.99 ± 0.03 |
| Recovery/Body weight (g/g body wt) | 1.03 ± 0.13 | 1.09 ± 0.04 | 1.19 ± 0.09 | 1.27 ± 0.06 | 1.37 ± 0.06 |

* indicate significance with recovered forces (60 days post-injury), [†] indicate significance with baseline forces, ^a indicate significance with EDCn-HGF microthread implants, and ^b indicate significance with EDCn microthread implants as determined by one-way ANOVA with Holm-Sidak post hoc analysis (p<0.05).

6.4 DISCUSSION

The goal of the present study was to investigate the ability of EDCn-HGF microthreads to enhance functional regeneration in a mouse model of VML. VML injuries typically result from traumatic incidents, often requiring immediate surgical intervention to stabilize patients. Acellular scaffold materials are ideal for these applications, because little to no preparation is required for implantation, while cell based skeletal muscle units can take several weeks to months to prepare, which does not fit the time table for immediate surgical intervention.^{29,30} However, previously characterized acellular scaffolds, such as decellularized ECM and gelatin gels, have not been shown to stimulate functional improvement of VML injuries.^{23,31,32} This could be due to the preparation of decellularized ECM materials, as the reagents used in the decellularization process can dramatically affect the activity of proteins or growth factors in the final product.³³ Our approach to the design and fabrication of scaffolding materials is a “bottom-up” approach, where materials are systematically added to a scaffold to instigate certain cell functions. Here, we adsorbed HGF because of its ability to activate and recruit SCs to localize to an injury site in small muscle injuries to the surface of EDCn microthreads to encourage SC recruitment to the defect site. Our results indicate that the combination of an EDC crosslinked microthread with rapid delivery of HGF to the injury site will direct significant tissue regeneration, and functional recovery of TA muscle defects.

All microthread implant groups increased the force production of the TA muscle by at least 150% from force measurements made immediately after injury. EDCn and EDCn-HGF microthread implants were the only treatment groups that consistently supported enough functional remodeling to produce forces comparable to baseline values measured before the induction of the VML injury. Further, EDCn-HGF microthreads increased the force production of TA muscles 200% from measurements taken immediately after injury. These significant findings support our hypothesis that HGF delivery to VML injury sites will enhance the functional recovery of VML injuries, by promoting significant functional recovery within 2 months post-injury. Our findings are inconsistent with the results of studies conducted with scaffold materials that were unable to produce any functional recovery within this time scale.^{18,23,31,34,35} Other studies indicate that acellular decellularized ECM materials promote functional recovery approximately 6 months post-injury, although it is not clear if this delay in

functional recovery was due to the creation of an injury site two- to three-fold larger than the one presented in this study due to the use of larger muscles.^{19,21,22,36} However, injuries of similar size as the one presented in this study also did not report significant functional recovery within 2 months post-injury.^{18,31} We attribute the successful functional regeneration of muscle tissue to the synergistic effects of the morphologic structure of our scaffolds, as well as the rapid delivery of HGF to the injury site.

One of the most critical functions of scaffolds in skeletal muscle regeneration is that they must direct myoblast differentiation in the same plane as the adjacent healthy skeletal muscle tissue. Fibrin microthreads have been shown to direct cell alignment along the length of the fibers,²⁶ and we showed in Chapter 5 that myoblasts will grow along their lengths over time. In Chapter 3, we hypothesized that microthreads with increased resistance to proteolytic degradation would enhance skeletal muscle regeneration observed in initial studies using fibrin microthreads in a mouse VML model.²⁷ Here, we report that these microthreads persist through 60 days post-injury and have a tremendously positive role in guiding skeletal muscle regeneration. Remarkably, myofibers were observed in direct contact with EDCn and EDCn-HGF microthreads, even completely surrounding EDCn-HGF microthreads, supporting our hypothesis that microthreads with increased resistance to proteolytic degradation would enhance skeletal muscle tissue regeneration.²⁸ However, it was unexpected to observe EDCn microthreads 60 days post-injury. While it was the initial aim of this project to have all scaffolding materials degrade before this time point, it remains unknown how long these materials will persist *in vivo*. Future studies will elucidate the degradation time of EDCn microthreads in skeletal muscle and define the results of long-term remodeling due to these materials, as others have indicated that long-term remodeling may be advantageous for the recovery of VML injuries.²¹

The delivery of HGF had a remarkable effect on the functional regeneration of mouse TA muscles. In native tissue, HGF is released from the ECM of muscle injuries to recruit and activate SCs, which proliferate within the injury site and eventually differentiate into myofibers, regenerating the injured tissue. Surprisingly, we observed the most SCs (Pax7 positive) in injury sites with EDCn microthreads, not EDCn-HGF microthreads, 14 days post-injury. In a rat TA model of VML, HGF-loaded gelatin scaffolds did not increase the number of SCs present in the

wound site; however, an increase in the number of regenerating muscle fibers was observed.³² These observations are consistent with our results, as we identified significantly more myogenin positive nuclei in the injury site of EDCn-HGF microthread implants than untreated or uninjured controls. Further, these nascent myofibers were in direct contact with EDCn and EDCn-HGF microthreads, validating much of our *in vitro* data in Chapters 3 and 5 that EDCn microthreads support robust myoblast attachment,²⁸ and that myoblasts will grow onto the surface of EDCn microthreads. These results suggest that the HGF-mediated recruitment in EDCn-HGF implants occurred earlier than 14 days post-injury, which fits with the HGF release profile from EDCn microthreads described in Chapter 5. We hypothesize that an earlier increase in the amount of SCs present in the injury site of EDCn-HGF microthread implants would facilitate a subsequent increase in the number of differentiating myoblasts, which would explain why there are more myogenin positive nuclei present near these implants than any other treatment group. Future studies will analyze earlier time points to fully understand how the release of HGF is enhancing SC recruitment and directing myoblast differentiation.

Interestingly, there was a lack of robust scarring in untreated VML injuries. Even still, there was scar tissue present between newly formed myofibers 60 days post-injury, which suggests that fibrosis is occurring, albeit at a smaller scale. Instead, we report a distinct loss of muscle volume from observations on the gross morphology of the shape of the TA muscle. This loss of volume is typical of VML injuries, and has been seen in clinical cases of VML, validating our animal model and wound size.³⁷⁻³⁹ Interestingly, while all of the injury sites were of the same size, only untreated control and fibrin gel implant groups resulted in this loss of volume. This implies that the microthreads were able to stabilize the injury site and serve as a space filling material to prevent the loss of muscle volume. It is unclear from our study whether this loss of volume was permanent. Recent human clinical trials treating VML defects with decellularized ECM suggest that the tissue loss may not be permanent, and might be recoverable with proper stimuli from biomaterials.³⁷ Future studies will assess the ability of EDCn-HGF loaded microthreads to restore muscle volume and function in existing VML injuries and will examine the volume and weight of each TA muscle.

Additional evidence of microthread implants preserving the size of the VML injury was evident with measurements of the defect size 14 days post-injury. The length and width of

defects with microthread implants were twice the size of their respective length and width measurements in untreated control and fibrin gel implant groups. This suggests that a decrease in muscle volume can occur in as little time as 14 days post-injury. In addition to the retention of the initial defect size, microthread implants supported a higher density of infiltrating myoblasts. Where noted, this infiltration appeared to be aligned with the longitudinal axis of the microthreads. Microthread implant groups were the only groups that showed a reduction in the defect size 60 days post-injury. Combined with the IHC and functional data, the reduction in wound size 60 days post-injury suggests that new tissue replaced the microthreads in parts of the defect site. Although it appears that much of the defect site in UNX microthread implants remodeled to adipose tissue, EDCn and EDCn-HGF microthread implants encouraged the growth of new muscle tissue. While the persistence of EDCn microthreads will be the subject of future studies, it is clear that these implants, especially EDCn-HGF microthreads, encouraged the formation of functional muscle tissue.

Another unexpected finding in this study was that UNX microthread and fibrin gel implants invoked a robust infiltration of adipocytes. This response is characteristic of a clinical pathology known as fatty degeneration, and has been observed in a variety of muscle wounds including rotator cuff tears.⁴⁰⁻⁴² Adipocyte infiltration has been observed in several other models of VML, showing that the environment presented by acellular scaffolds might encourage this pathological condition.^{21,22,43} While the origin of the adipocytes remains in question, some reports suggest they might arise from a population of pericytes, progenitor cells residing in skeletal muscle that are found in close proximity to blood vessels.^{40,44} Mesenchymal progenitors expressing platelet derived growth factor receptor α (PDGFR α) were also found to contribute to adipose formation in skeletal muscle; however the environment of healthy skeletal muscle tissue was able to reverse this adipogenesis.⁴⁵ An intriguing point is that 14 days post-injury, adipocytes were only found within the structure of the fibrin gel and UNX microthreads. This suggests that the unique biochemical and mechanical environment within the uncrosslinked fibrin may be facilitated the recruitment of adipocytes. While this might seem to suggest that recruited SCs would be transdifferentiating into adipocytes on UNX microthreads, recent studies demonstrate that SCs are committed to the myogenic lineage and do not spontaneously transdifferentiate.⁴⁶ Rather, it seems more likely that the mechanical and biochemical

environment within these fibrin matrices is somehow preventing infiltrating mesenchymal progenitor cells from receiving myogenic signals expressed at the margins of the injury site, thus ultimately supporting adipogenesis.⁴⁴ EDCn microthreads are twice as stiff as UNX microthreads, and are as stiff as contracting muscle.⁴⁷ It is possible that in this model of VML, fatty infiltration is mediated by a stiffness mismatch between the implanted material and skeletal muscle tissue; however, the mechanisms behind the cause and development of fatty infiltration or fatty degeneration are not known at this time. Future studies involving UNX microthread and fibrin gel implants may be able to reproducibly create a model for fatty infiltration or fatty degeneration in muscle tissue to answer these mechanistic questions.

6.5 CONCLUSIONS

In this chapter, we implanted HGF-loaded EDCn microthreads to improve the functional regeneration of a VML injury. EDCn-HGF microthread implants supported significant functional regeneration of the TA muscle that approached baseline values. All crosslinked microthreads persisted 60 days post-injury, and facilitated organized regeneration of myofibers as early as 14 days post-injury. EDCn-HGF microthreads supported significantly more myogenin positive nuclei than the untreated and uninjured controls 14 days post-injury, suggesting that an increased number of SCs were present before this time point to differentiate into nascent myotubes. Sixty days post-injury, the number of Pax7 positive cells and myogenin positive nuclei returned to the numbers present in the uninjured group, suggesting that much of the injury site had resolved at this time. Taken together, these data suggest that EDCn-HGF microthreads recapitulate some of the regenerative cues lost in VML injuries and are capable of restoring the mechanical function of the TA muscle in a mouse model.

6.6 ACKNOWLEDGEMENTS

This research was funded in part by US Army (W81XWH-11-1-0631, GDP and RLP), NIH R01-HL115282 (GDP), and NIH F31-DE023281 (JMG). The authors wish to thank Jason Forte, Jen Mologniano, and Amanda Clement for their assistance with the collection of the force data during the surgical procedures, and Michelle Zayas for her assistance with the artwork displayed in this manuscript.

6.7 REFERENCES

1. Masini BD, Waterman SM, Wenke JC, Owens BD, Hsu JR, Ficke JR. Resource utilization and disability outcome assessment of combat casualties from Operation Iraqi Freedom and Operation Enduring Freedom. *J Orthop Trauma* 2009;23(4):261-6.
2. Owens BD, Kragh JF, Jr., Macaitis J, Svoboda SJ, Wenke JC. Characterization of extremity wounds in Operation Iraqi Freedom and Operation Enduring Freedom. *J Orthop Trauma* 2007;21(4):254-7.
3. Heemskerk J, Kitslaar P. Acute compartment syndrome of the lower leg: retrospective study on prevalence, technique, and outcome of fasciotomies. *World Journal of Surgery* 2003;27(6):744-7.
4. Eckardt A. Microsurgical reconstruction in the head and neck region: an 18-year experience with 500 consecutive cases. *Journal of Cranio-Maxillofacial Surgery* 2003;31(4):197-201.
5. Bianchi B, Copelli C, Ferrari S, Ferri A, Sesenna E. Free flaps: outcomes and complications in head and neck reconstructions. *Journal of cranio-maxillo-facial surgery : official publication of the European Association for Cranio-Maxillo-Facial Surgery* 2009;37(8):438-42.
6. Floriano R, Peral B, Alvarez R, Verrier A. Microvascular free flaps in head and neck reconstruction. Report of 71 cases. *Journal of Cranio-Maxillofacial Surgery* 2006;34:90-90.
7. Zammit PS, Partridge TA, Yablonka-Reuveni Z. The skeletal muscle satellite cell: the stem cell that came in from the cold. *The journal of histochemistry and cytochemistry : official journal of the Histochemistry Society* 2006;54(11):1177-91.
8. Morgan JE, Partridge TA. Muscle satellite cells. *The International Journal of Biochemistry and Cell Biology* 2003;35:1151-1156.
9. Tatsumi R, Hattori A, Ikeuchi Y, Anderson JE, Allen RE. Release of hepatocyte growth factor from mechanically stretched skeletal muscle satellite cells and role of pH and nitric oxide. *Mol Biol Cell* 2002;13(8):2909-18.
10. Tatsumi R, Liu X, Pulido A, Morales M, Sakata T, Dial S, Hattori A, Ikeuchi Y, Allen RE. Satellite cell activation in stretched skeletal muscle and the role of nitric oxide and hepatocyte growth factor. *Am J Physiol Cell Physiol* 2006;290(6):C1487-94.
11. Tatsumi R, Sheehan SM, Iwasaki H, Hattori A, Allen RE. Mechanical stretch induces activation of skeletal muscle satellite cells in vitro. *Experimental Cell Research* 2001;267(1):107-14.
12. Gal-Levi R, Leshem Y, Aoki S, Nakamura T, Halevy O. Hepatocyte growth factor plays a dual role in regulating skeletal muscle satellite cell proliferation and differentiation. *Biochim Biophys Acta* 1998;1402(1):39-51.
13. Hayashi S, Aso H, Watanabe K, Nara H, Rose MT, Ohwada S, Yamaguchi T. Sequence of IGF-I, IGF-II, and HGF expression in regenerating skeletal muscle. *Histochemistry and cell biology* 2004;122(5):427-34.
14. Tatsumi R, Allen RE. Active hepatocyte growth factor is present in skeletal muscle extracellular matrix. *Muscle Nerve* 2004;30(5):654-8.
15. Tatsumi R, Anderson JE, Nevoret CJ, Halevy O, Allen RE. HGF/SF is present in normal adult skeletal muscle and is capable of activating satellite cells. *Developmental biology* 1998;194(1):114-128.
16. Miller KJ, Thaloor D, Matteson S, Pavlath GK. Hepatocyte growth factor affects satellite cell activation and differentiation in regenerating skeletal muscle. *Am J Physiol Cell Physiol* 2000;278(1):174-181.
17. Borselli C, Storrer H, Benesch-Lee F, Shvartsman D, Cezar C, Lichtman JW, Vandenberg HH, Mooney DJ. Functional muscle regeneration with combined delivery of angiogenesis and myogenesis factors. *Proc Natl Acad Sci U S A* 2010;107(8):3287-92.
18. Sicari BM, Agrawal V, Siu BF, Medberry CJ, Dearth CL, Turner NJ, Badylak SF. A murine model of volumetric muscle loss and a regenerative medicine approach for tissue replacement. *Tissue Eng Part A* 2012;18(19-20):1941-8.
19. Corona BT, Wu X, Ward CL, McDaniel JS, Rathbone CR, Walters TJ. The promotion of a functional fibrosis in skeletal muscle with volumetric muscle loss injury following the transplantation of muscle-ECM. *Biomaterials* 2013;34(13):3324-35.
20. Chen XK, Walters TJ. Muscle-derived decellularised extracellular matrix improves functional recovery in a rat latissimus dorsi muscle defect model. *J Plast Reconstr Aesthet Surg* 2013;66(12):1750-8.
21. Valentin JE, Turner NJ, Gilbert TW, Badylak SF. Functional skeletal muscle formation with a biologic scaffold. *Biomaterials* 2010;31(29):7475-84.

22. Corona BT, Ward CL, Baker HB, Walters TJ, Christ GJ. Implantation of in vitro tissue engineered muscle repair constructs and bladder acellular matrices partially restore in vivo skeletal muscle function in a rat model of volumetric muscle loss injury. *Tissue Eng Part A* 2014;20(3-4):705-15.
23. Merritt EK, Hammers DW, Tierney M, Suggs LJ, Walters TJ, Farrar RP. Functional assessment of skeletal muscle regeneration utilizing homologous extracellular matrix as scaffolding. *Tissue Eng Part A* 2010;16(4):1395-405.
24. Wolf MT, Daly KA, Brennan-Pierce EP, Johnson SA, Carruthers CA, D'Amore A, Nagarkar SP, Velankar SS, Badylak SF. A hydrogel derived from decellularized dermal extracellular matrix. *Biomaterials* 2012;33(29):7028-38.
25. Wolf MT, Daly KA, Reing JE, Badylak SF. Biologic scaffold composed of skeletal muscle extracellular matrix. *Biomaterials* 2012;33(10):2916-25.
26. Cornwell KG, Pins GD. Discrete crosslinked fibrin microthread scaffolds for tissue regeneration. *J Biomed Mater Res A* 2007;82(1):104-12.
27. Page RL, Malcuit C, Vilner L, Vojtic I, Shaw S, Hedblom E, Hu J, Pins GD, Rolle MW, Dominko T. Restoration of skeletal muscle defects with adult human cells delivered on fibrin microthreads. *Tissue engineering. Part A* 2011;17(21-22):2629-40.
28. Grasman JM, Page RL, Dominko T, Pins GD. Crosslinking strategies facilitate tunable structural properties of fibrin microthreads. *Acta Biomaterialia* 2012;8(11):4020-30.
29. Mertens JP, Suggs KB, Lee JD, Larkin LM. Engineering muscle constructs for the creation of functional engineered musculoskeletal tissue. *Regen Med* 2014;9(1):89-100.
30. VanDusen KW, Syverud BC, Williams ML, Lee JD, Larkin LM. Engineered Skeletal Muscle Units for Repair of Volumetric Muscle Loss in the Tibialis Anterior Muscle of a Rat. *Tissue Eng Part A* 2014;20(21-22):2920-2930.
31. Machingal MA, Corona BT, Walters TJ, Kesireddy V, Koval CN, Dannahower A, Zhao W, Yoo JJ, Christ GJ. A tissue-engineered muscle repair construct for functional restoration of an irrecoverable muscle injury in a murine model. *Tissue Eng Part A* 2011;17(17-18):2291-303.
32. Ju YM, Atala A, Yoo JJ, Lee SJ. In situ regeneration of skeletal muscle tissue through host cell recruitment. *Acta biomaterialia* 2014;10(10):4332-9.
33. Faulk DM, Carruthers CA, Warner HJ, Kramer CR, Reing JE, Zhang L, D'Amore A, Badylak SF. The effect of detergents on the basement membrane complex of a biologic scaffold material. *Acta biomaterialia* 2013.
34. Merritt EK, Cannon MV, Hammers DW, Le LN, Gokhale R, Sarathy A, Song TJ, Tierney MT, Suggs LJ, Walters TJ and others. Repair of traumatic skeletal muscle injury with bone-marrow-derived mesenchymal stem cells seeded on extracellular matrix. *Tissue Eng Part A* 2010;16(9):2871-81.
35. Gamba PG, Conconi MT, Lo Piccolo R, Zara G, Spinazzi R, Parnigotto PP. Experimental abdominal wall defect repaired with acellular matrix. *Pediatric surgery international* 2002;18(5-6):327-31.
36. Conconi MT, De Coppi P, Bellini S, Zara G, Sabatti M, Marzaro M, Zanon GF, Gamba PG, Parnigotto PP, Nussdorfer GG. Homologous muscle acellular matrix seeded with autologous myoblasts as a tissue-engineering approach to abdominal wall-defect repair. *Biomaterials* 2005;26(15):2567-74.
37. Sicari BM, Rubin JP, Dearth CL, Wolf MT, Ambrosio F, Boninger M, Turner NJ, Weber DJ, Simpson TW, Wyse A and others. An acellular biologic scaffold promotes skeletal muscle formation in mice and humans with volumetric muscle loss. *Science translational medicine* 2014;6(234):234ra58.
38. Mase VJ, Jr., Hsu JR, Wolf SE, Wenke JC, Baer DG, Owens J, Badylak SF, Walters TJ. Clinical application of an acellular biologic scaffold for surgical repair of a large, traumatic quadriceps femoris muscle defect. *Orthopedics* 2010;33(7):511.
39. Garg K, Ward CL, Hurtgen BJ, Wilken JM, Stinner DJ, Wenke JC, Owens JG, Corona BT. Volumetric muscle loss: Persistent functional deficits beyond frank loss of tissue. *Journal of orthopaedic research : official publication of the Orthopaedic Research Society* 2014.
40. Birbrair A, Zhang T, Wang ZM, Messi ML, Enikolopov GN, Mintz A, Delbono O. Role of pericytes in skeletal muscle regeneration and fat accumulation. *Stem Cells Dev* 2013;22(16):2298-314.
41. Itoigawa Y, Kishimoto KN, Sano H, Kaneko K, Itoi E. Molecular mechanism of fatty degeneration in rotator cuff muscle with tendon rupture. *Journal of orthopaedic research : official publication of the Orthopaedic Research Society* 2011;29(6):861-6.

42. Kim HM, Galatz LM, Lim C, Havlioglu N, Thomopoulos S. The effect of tear size and nerve injury on rotator cuff muscle fatty degeneration in a rodent animal model. *J Shoulder Elbow Surg* 2012;21(7):847-58.
43. Kin S, Hagiwara A, Nakase Y, Kuriu Y, Nakashima S, Yoshikawa T, Sakakura C, Otsuji E, Nakamura T, Yamagishi H. Regeneration of skeletal muscle using in situ tissue engineering on an acellular collagen sponge scaffold in a rabbit model. *ASAIO journal* 2007;53(4):506-13.
44. Joe AW, Yi L, Natarajan A, Le Grand F, So L, Wang J, Rudnicki MA, Rossi FM. Muscle injury activates resident fibro/adipogenic progenitors that facilitate myogenesis. *Nat Cell Biol* 2010;12(2):153-63.
45. Uezumi A, Fukada S, Yamamoto N, Takeda S, Tsuchida K. Mesenchymal progenitors distinct from satellite cells contribute to ectopic fat cell formation in skeletal muscle. *Nat Cell Biol* 2010;12(2):143-52.
46. Starkey JD, Yamamoto M, Yamamoto S, Goldhamer DJ. Skeletal muscle satellite cells are committed to myogenesis and do not spontaneously adopt nonmyogenic fates. *The journal of histochemistry and cytochemistry : official journal of the Histochemistry Society* 2011;59(1):33-46.
47. Caiozzo VJ. Plasticity of skeletal muscle phenotype: mechanical consequences. *Muscle & nerve* 2002;26(6):740-68.

Chapter 7: Conclusions and Future Work

7.1 OVERVIEW

The work in this thesis describes the development of a biomaterial scaffold that recapitulates regenerative cues found in the endogenous skeletal muscle regeneration pathway. The structural properties of fibrin microthreads were modulated with and without exogenous crosslinking agents, generating materials with tunable mechanical and structural properties. These properties were optimized for skeletal muscle regeneration, which requires scaffolds to persist at least 2-4 weeks to guide organized, functional regeneration. We developed loading strategies for hepatocyte growth factor (HGF) to ultimately guide regeneration of volumetric muscle loss (VML) injuries by recapitulating regenerative cues lost in the creation of VML injuries. Finally, these tailored microthreads were implanted into a mouse model of VML and it was determined that the addition of HGF to chemically crosslinked microthreads directed organized tissue regeneration that restored the functional capacity of the injured muscle.

7.2 RESULTS AND CONCLUSIONS

7.2.1 Specific Aim 1: Develop Microthreads with Tunable Structural Properties While Maintaining Cellular Viability

Based upon early implantation studies, we hypothesized that fibrin microthreads with an increased resistance to proteolytic degradation would increase the regenerative response of muscle tissue after VML injuries.¹ We decided to use two different methods to alter the structural properties of microthreads, chemical crosslinking and post-polymerization processing procedures, to develop alternative technologies designed to increase the strength and resistance to proteolytic degradation of fibrin microthread scaffolds. For chemical crosslinking, we employed carbodiimide chemistry to crosslink microthreads with 1-ethyl-3-(3-dimethylaminopropyl) carbodiimide (EDC). EDC was selected because it is a commonly used

crosslinking agent, and has also been repeatedly used as a conjugation agent to tether a variety of bioactive molecules to protein surfaces.²⁻⁵ To determine ideal conditions for fibrin microthread crosslinking, we assessed the structural and mechanical properties of microthreads after increasing durations of incubation with EDC and we varied the pH of the buffer environment. The optimal pH for EDC crosslinking has been determined to be acidic (pH ~5).⁶ In the course of this experiment, we observed that incubation in acidic buffer for prolonged time periods degraded fibrin microthreads, and so we also crosslinked in a neutral pH environment to both control the efficiency of the carbodiimide reaction chemistry as well as provide a stable environment for our scaffold material. In performing this optimization, we discovered that changing the buffer pH facilitated the differential crosslinking of fibrin materials. Microthreads crosslinked in acidic conditions (EDCa microthreads) were twice as strong as microthreads crosslinked in neutral conditions (EDCn microthreads), which were twice as strong as uncrosslinked (UNX) microthreads.

For post-polymerization enhancement of fibrin microthread mechanical and structural properties without the use of exogenous crosslinking agents, we took advantage of several unique properties of fibrin fibrils. Fibrin is a remarkable protein that is capable of stretching 200-300% of its original length,⁷ and has an affinity to a large number of growth factors and proteins.⁸ We investigated the effects of static axial stretching on fibrin microthreads and determined that there were three stretching regimes that generated tunable mechanical properties: low stretch microthreads, stretched 0-75% of their original length; moderate stretch microthreads, stretched 100-125% of their original length; and high stretch microthreads, stretched 150-200% of their original length. With increasing amounts of static axial stretch, fibrin microthreads increased their strength and stiffness similar to EDC crosslinking, such that moderate stretch microthreads had the same ultimate tensile strength (UTS) as EDCn microthreads, and high stretch microthreads had the same UTS as EDCa microthreads. Our results are consistent with previous observations with collagen microthreads and fibrin gels, where UTS and stiffness values increased with static axial stretching.^{9,10}

After identifying that both of our proposed methods increased the UTS and stiffness of fibrin microthreads, we correlated these increases in mechanical strength to resistance to proteolytic degradation. EDC crosslinking significantly increased the resistance to proteolytic

degradation: where UNX microthreads degraded within 2 hours, EDCn microthreads degraded in 24-48 hours, and EDCa microthreads did not degrade within the course of the 7 day experiment. Surprisingly, static axial stretching did not alter the degradation rate of fibrin microthreads, despite previous studies suggesting that stretching blocked access of proteases to their target sites in fibrin.¹¹ Our degradation assay utilized plasmin concentrations that were higher than those present in the wound site and served as a rough approximation of *in vivo* degradation. Through the use of this rapid, high throughput assay, we determined that EDCn microthreads would be an appropriate material for skeletal muscle regeneration, and that static axially stretched microthreads would be better suited for tissue engineering applications that required high tensile strength with relatively short persistence times *in vivo*.

To confirm that neither of our methodologies negatively impacted the cellular compatibility of our scaffolds, we seeded C2C12 myoblasts onto fibrin microthreads and observed the cell attachment and alignment on these materials. We observed a significant increase in the number of myoblasts that attached to EDCa microthreads, which we hypothesize could be explained by stiffness-mediated presentation and organization of integrin binding sites or the development of focal adhesion complexes.¹² While there were no significant differences, we qualitatively observed higher cell densities on crosslinked microthreads than UNX microthreads, suggesting that myoblast proliferation might have been increased by the stiffness of the crosslinked microthreads. This was confirmed in Chapter 5 (Specific Aim 2), where significantly more proliferative, Ki67 positive myoblasts on EDCn and EDCa microthreads than UNX microthreads. Static axial stretching did not appear to affect cell attachment; however, high stretch microthreads increased the cell alignment on the scaffold twofold. These results suggest that the fibrin fibrils on the surface of static axially stretched microthreads might be aligning, which is critical for aligning cell populations on the surfaces of biomaterials.¹³

In conclusion of Specific Aim 1: Develop Microthreads with Tunable Structural Properties While Maintaining Cellular Viability of this thesis, we determined that EDC crosslinking can be modulated by altering the pH environment of the reaction chemistry. This generates microthreads with discrete mechanical properties and distinct degradation profiles, without impacting cell viability. Further, there is evidence that EDCn and EDCa microthreads stimulate myoblast proliferation. Additionally, we showed that static axial stretching generates

tunable mechanical properties without changing the proteolytic degradation rate of fibrin microthreads. These stretched microthreads guide cell alignment along the longitudinal axis of the microthread to a higher degree than alternatively fabricated microthreads, creating scaffolds that are capable of being significantly stronger and guiding cell populations to be highly aligned to the longitudinal axis of the microthread. Taken together, these data suggest that EDCn and EDCa microthreads may enhance skeletal muscle regeneration due to their increased resistance to proteolytic degradation, and static axially stretched microthreads might be better suited to implantation models that require initial high tensile strengths without increased persistence in vivo.

7.2.2 Specific Aim 2: Quantify the Effects of Incorporating HGF onto Fibrin Microthreads to Increase Satellite Cell Recruitment

In this section of this thesis, we incorporated the findings from Specific Aim 1: Develop Microthreads with Tunable Structural Properties While Maintaining Cellular Viability, by seeking to enhance the ability of EDC crosslinked microthreads to recruit myoblasts in an *in vitro* model of myoblast recruitment. To do so, we made significant changes to an existing assay developed by our lab to predict fibroblast outgrowth along scaffolds for tendon/ligament regeneration.¹⁴ To account for differences in the composition of the extracellular matrix (ECM) of skeletal muscle,^{15,16} we altered the composition of the gel used in the cell outgrowth study from collagen to fibrin. Next, we miniaturized the experimental setup to minimize the amount of reagents required for the assay, using a single six-well instead of a one-well plate. This miniaturization not only reduced the amount of reagents necessary to run the experiment, it also allowed us to run multiple independent samples concurrently.

To determine the relative amount of protein that was adsorbed to UNX and crosslinked microthreads, we suspended microthreads using PDMS disks and incubated the microthreads in the presence of fluorescein isothiocyanate labeled bovine serum albumin (FITC-BSA) for two hours. We did not see any FITC-BSA adsorption onto EDCa microthreads, and while we saw some adsorption onto UNX microthreads, we saw a large increase in the amount of fluorescent signal detected from the EDCn microthreads. These results suggest that proteins of a similar size

to BSA (i.e. HGF) should readily adsorb to EDCn microthreads and some small amount of adsorption should occur on UNX microthreads.

To confirm these findings, we adsorbed HGF to the surface of these microthreads, allowed them to condition serum-free medium (C-SFM) for 24 hour increments, and then measured the release of HGF by measuring myoblast proliferation in response to microthread C-SFM. The hypothesis of this experiment was that if HGF was released into the C-SFM, it would stimulate myoblast proliferation, thereby allowing us to measure active HGF release by calculating the number of proliferating cells. UNX microthread C-SFM stimulated myoblast proliferation for 1 day while EDCn microthread C-SFM stimulated proliferation for at least 2 days. After 4 days of conditioning, C-SFM was not found to have any effect on myoblast proliferation. The rapid release profile of HGF from EDCn microthreads matched the release of HGF from injured skeletal muscle tissue, validating our proposed loading mechanism for this aim.

Additionally, we developed a purpose-built 2-dimensional (2D) assay to investigate myoblast migration in response to released, active HGF. Adsorbing either 40 ng/mL or 100 ng/mL of HGF to the surface of EDCn microthreads produced the same twofold increase in the rate of myoblast migration, suggesting that the surface of the EDCn microthreads may have been saturated at 40 ng/mL of HGF. Interestingly, HGF-loaded UNX and EDCa microthreads did not affect myoblast migration. Because these results did not show a difference in myoblast migration between 40 and 100 ng/mL of HGF adsorbed to the microthreads, we performed a second dose-response study, adsorbing 5, 10, 20, or 40 ng/mL of HGF to the microthreads, in our modified 3-dimensional (3D) cell outgrowth assay. Cell outgrowth was significantly increased with 40 ng/mL of HGF adsorbed to EDCn microthreads, while there was no HGF effect observed with UNX or EDCa microthreads. Together, these results demonstrate that the surfaces of EDCn microthreads adsorb concentrations of HGF that will release from the scaffolds for 2-4 days to stimulate myoblast migration and proliferation. This release is further capable of stimulating myoblast outgrowth in 2D and 3D models designed to mimic the complex environment found in VML injuries.

To attempt to parse out the contributions of myoblast migration and proliferation in our outgrowth assay, we analyzed the amount of proliferating cells present on the microthreads after

4 days in culture. This time point was chosen because there was no HGF release detected at this time in our release study, allowing us to isolate the contribution of proliferation to cell outgrowth without the presence of a mitogen. We determined that for all microthreads, at least half of the myoblasts growing on microthreads were proliferating, suggesting that proliferation is a major contributing factor to cell outgrowth.¹⁷ Further, there were consistently at least 10% more proliferating myoblasts on EDCn and EDCa microthreads than UNX microthreads, demonstrating that myoblasts may proliferate more readily on crosslinked microthreads.

In conclusion of Specific Aim 2: Quantify the Effects of Incorporating HGF onto Fibrin Microthreads to Increase Satellite Cell Recruitment, we determined that EDCn microthreads are capable of adsorbing sufficient quantities of HGF to stimulate myoblast proliferation and migration. We confirmed that the release of HGF adsorbed onto EDCn microthreads continued for 2-4 days, which is consistent with our expected release profile of HGF from skeletal muscle ECM after injury. We determined that adsorbing 40 ng/mL of HGF in the presence of EDCn microthreads deliver a sufficient concentration of HGF to myoblasts to significantly increase the outgrowth response in a 3D outgrowth assay. Additionally we conclude that proliferation and migration are equally important events in our cell outgrowth assay, and that proliferation is increased with EDCn and EDCa microthreads. Because EDCn microthreads adsorb HGF, we hypothesize that these microthreads loaded with 40 ng/mL of HGF will enhance skeletal muscle regeneration by recruiting additional SCs to the injury site, ultimately increasing the functional recovery of injured skeletal muscle tissue.

7.2.3 Specific Aim 3: Assess Microthreads' Enhancement of Skeletal Muscle Regeneration In Vivo

In the final section of this thesis, we incorporated the findings from Specific Aim 2: Quantify the Effects of Incorporating HGF onto Fibrin Microthreads to Increase Satellite Cell Recruitment into a mouse model of VML. A VML injury was created by resecting a large portion of the *tibialis anterior* (TA) muscle, and the severity of each injury was determined by measuring a 50% reduction in the twitch force of the TA from single electrical impulses compared to pre-injury values. One of five treatments was implanted into each injury site: no intervention, fibrin gel, UNX microthreads, EDCn microthreads, or EDCn microthreads

preloaded with 40 ng/mL of HGF (EDCn-HGF), and these sites were assessed histologically 14 and 60 days post-injury, and mechanically 60 days post-injury.

All implants persisted 14 days post-injury. Fibrin gel and UNX microthread implants supported adipogenic infiltration. This infiltration was confined to the implant material, suggesting that something unique to the environment within the uncrosslinked fibrin was supporting this infiltration. EDCn and EDCn-HGF microthreads supported the ingrowth of regenerating tissue, as shown by the presence of numerous multinucleated cells with centrally positioned nuclei. Microthread implants appeared to guide the early infiltration of regenerating tissue, as we have seen previously, demonstrating that microthread scaffolds facilitate aligned, and organized tissue ingrowth in addition to cell alignment.^{1,18}

Interestingly, EDCn microthreads persisted 60 days post-injury. Previous studies showed that biomaterials crosslinked with carbodiimides in acidic conditions have been shown to persist for 26 weeks.¹⁹ These findings are consistent with our *in vitro* data showing a lack of proteolytic degradation of EDCa microthreads. In this study, we subsequently developed a crosslinking procedure to generate materials that degraded at a slower rate than UNX microthreads (EDCn microthreads). These EDCn microthreads appeared to continue to guide regenerating tissue, which at times completely surrounded EDCn-HGF microthreads. Fibrin gel and UNX microthread implants continued to support the growth of adipose tissue, especially in the case of the fibrin gel implants where the entire injury site appeared to remodel into adipose tissue. In addition to the almost complete remodeling of UNX microthread injury sites into adipose tissue, there were some muscle fibers that regenerated into the injury site, although not always in plane with the surrounding healthy muscle. Untreated controls did not show much of a regenerative response, and new muscle fibers were often surrounded by fibrotic scar tissue, which is characteristic of large scale muscle injuries.²⁰ In general, remodeling events with fibrin gel and UNX microthread implants qualitatively seemed to result in increased scar tissue formation; however, there were no statistically significant increases or decreases in the amount of scar tissue deposited with any implant group. This finding is consistent with other published models of VML injuries, where scar tissue formation occurs between regenerating myofibers as opposed to a large amount of volume-filling scar tissue.^{21,22} Instead, these injuries resulted in a loss of skeletal muscle volume, which we also have observed in this Aim. Untreated control and fibrin

gel implant groups both were found to experience a loss of muscular volume, although we were unable to quantify how much volume was lost.

Remarkably, EDCn-HGF microthread implants facilitated almost complete functional recovery of the TA muscle, restoring the contractile strength of the tissue nearly to its baseline value. This functional regeneration was over a 200% increase from the force output of muscles immediately after injury. UNX and EDCn microthreads both supported a 150% increase from after injury force outputs, while untreated control and fibrin gel implant groups supported a 120-130% functional increase. These data suggest that the presence of the microthreads is facilitating some base amount of regeneration, and that the addition of HGF significantly enhances the ability of these materials to guide functional regeneration. Most acellular scaffolds do not result in significant increases in force output after a recovery time of 2 months,^{23,24} and instead recovery is observed after 6 months.^{19,25} The ability of EDCn-HGF microthreads to enhance skeletal muscle regeneration as early as 2 months post-injury is a significant finding, and is likely due to the early, targeted recruitment of satellite cells (SCs).

To quantify the amount of SC recruitment that occurred in our mouse model of VML, we performed immunohistochemistry (IHC) on tissue sections for molecular markers of SCs and differentiating myotubes. Surprisingly, while there were significantly more SCs present in EDCn-HGF microthread implant injury sites 14 days post-injury than uninjured controls, the EDCn implant injury sites had significantly more SCs than untreated and uninjured controls as well as fibrin gel implant groups. Rather, EDCn-HGF microthread implants supported significantly more myogenin positive nuclei than untreated and uninjured controls at this time point. Previous studies using HGF-loaded gelatin scaffolds showed that while SC recruitment was not increased 14 days post-injury, the amount of regenerating myofibers significantly increased.²⁶ Our data matches these findings, and suggests that EDCn-HGF microthreads recruited SCs earlier than 14 days post-injury, and that at this time they were supporting the fusion of myoblasts into nascent myotubes. This hypothesis is consistent with our histologic observations, where we noted more multinucleated myotubes within the injury site 14 days post-injury, and importantly many of these nascent myotubes were adjacent to microthreads. The increased amount of SCs near EDCn microthreads can also be explained by our findings in Chapter 5 that show myoblasts are more likely to proliferate on the stiffer EDCn microthreads,

and therefore some of the increase in SCs near EDCn microthread implants may be due to an increased amount of substrate-mediated proliferation of SCs.

In conclusion of Specific Aim 3: Assess Microthreads' Enhancement of Skeletal Muscle Regeneration In Vivo in this thesis, we developed a mouse model of VML as well as novel methods of analysis of the injury site and functional recovery by recording the mechanical strength of each individual animal before injury, after injury, and after recovery. We determined that EDCn-HGF microthreads appear to nearly completely restore mechanical strength to muscles subjected to VML injuries, and that this may be due to an increased recruitment in SCs. While we did not observe an increase in the number of SCs 14 days post-injury, we observed a significant increase in the number of differentiating myotubes, indicating that there was a larger pool of SCs present earlier than 14 days post-injury.

7.3 FUTURE WORK

The ultimate goal of this dissertation was to develop a biomaterial scaffold to enhance skeletal muscle regeneration. In accomplishing this goal, we created a variety of tools to generate microthreads with tunable mechanical, structural, and biochemical properties. To further develop fibrin microthread technology, work can be done to fully develop our animal model of VML injury, adopt other methods for post-modification of microthread properties, or increase the biochemical payload of fibrin microthreads for a more controlled delivery of a variety of growth factors. Further, the miniaturized 3D cell outgrowth assay developed in this thesis could be adapted into an *in vitro* model system for skeletal muscle formation.

7.3.1 Complete Analysis of our In Vivo Model to Assess Long-Term Remodeling

Results from this thesis validated our mouse model of VML injury. VML injuries are characterized by a loss of function and tissue volume, and scar formation within the injury site.²⁷ While we did not observe large amounts of scar tissue formation, we did observe scar tissue deposition between regenerating myofibers in the untreated control group. Matching baseline, after injury, and after recovery force values from individual animals is a novel idea that we reported upon previously,¹ and have refined here by normalization of force outputs after recovery to after injury values to address possible animal-to-animal variability within the experiment.

However, we were unable to characterize the loss of volume beyond making observations based on the gross appearance of the muscle at each time point. Quantitative methods to measure volume loss include comparing the weight of treated and uninjured muscles,^{25,28} and performing magnetic resonance imaging (MRI) of the muscle *in situ* to directly measure muscle volume.²⁹ Including one or both of these metrics could aid in the characterization of the regenerative response of skeletal muscle tissue in future investigations.

EDCn-HGF microthread implants regenerated sufficient amounts of skeletal muscle tissue to facilitate functional recovery of the TA muscle in SCID hairless outbred (SHO) mice. However, EDCn microthreads were still readily visible within the wound site and there were only a few infiltrating cells present within the microthread structure. Other carbodiimide crosslinked products have been shown to persist beyond 10-26 weeks,^{19,30} demonstrating that there is a need to follow these structurally stable materials *in vivo* for long term responses. Further, skeletal muscle regeneration has been shown to be significantly improved after long-term remodeling,¹⁹ and there have been some indications that scar tissue deposition may increase the functional output of damaged muscle over the course of several months.^{25,28} Later time points in future animal studies will determine the true persistence of EDCn microthreads *in situ*, and more importantly, will elucidate the effects of these microthreads on long term remodeling events in skeletal muscle tissue.

An interesting observation throughout the *in vivo* study was that the implanted microthreads were consistently larger than myofibers within both the healthy and regenerating skeletal muscle tissue. While these microthreads supported robust alignment of nascent myofibers, it is unclear if cell infiltration might have been limited by the larger size of the microthreads, creating less void space within the injury site, or if recruitment might be further enhanced if the diameter of the fibrin microthreads more closely resembled that of native, healthy myofibers. Analyzing the effect of smaller diameter microthreads, perhaps fabricated with an increase in static axial stretch as described in Chapter 4, may facilitate a further increase in the number of infiltrating myoblasts. We hypothesize that the ability to recruit additional SCs within the injury site along fibrin microthreads with diameters that more closely approximate the size of native myofibers will enhance the organized regeneration of skeletal muscle and will further align the regenerating myofibers with the remaining, healthy tissue.

The immune response of the host animal is incredibly important to the overall regeneration of skeletal muscle tissue.^{31,32} The effect of crosslinked microthreads on the immune response in skeletal muscle regeneration was beyond the scope of this dissertation, however, this remains a significant question to understand how biomaterials affect or even modulate the immune response in regeneration. There is a large body of literature linking macrophage phenotype to inflammatory (M1) or pro-regenerative (M2) environments within regenerating tissue.³¹⁻³⁵ Studying how these phenotypes may be effected by microthread scaffolds, and indeed designing future modifications to fibrin microthreads to modulate macrophages to an M2 phenotype, such as through delivery of interleukin-10 (IL-10),^{33,35} could become a powerful tool in the development of acellular scaffolding materials to direct functional tissue regeneration.

7.3.2 Next Generation of Fibrin Microthreads: Alternative Post-Modification Methods for Fibrin Microthreads

A variety of factors are involved in developing an optimized crosslinking methodology for biomaterials. In addition to controlling reaction efficiency of the EDC crosslinking reaction, the degree of substrate crosslinking can be modulated by the time of the reaction and the concentration of the crosslinking agent. In this thesis, we analyzed the effects of time and pH environment on EDC crosslinking. The shortest crosslinking time that we assessed was 1 hr, while others have assessed reaction times as little as 15 minutes.³⁶ Additionally, the concentration of EDC present with the scaffold material has been shown to affect the mechanical properties and tissue responses of scaffolds.^{3,37,38} A more in-depth characterization of EDC crosslinking may yield materials with further tuned structural properties that might be better suited for skeletal muscle regeneration, with *in vivo* degradation times under 2 months.

One advantage of biopolymer microthreads compared to bulk scaffolds made of similar materials is that the inherent architecture of microthreads will guide cell alignment.¹⁸ To achieve cell alignment in bulk materials, topographic cues are printed onto the surface of the materials.^{13,39,40} Interestingly, while we were analyzing the structural differences between UNX,

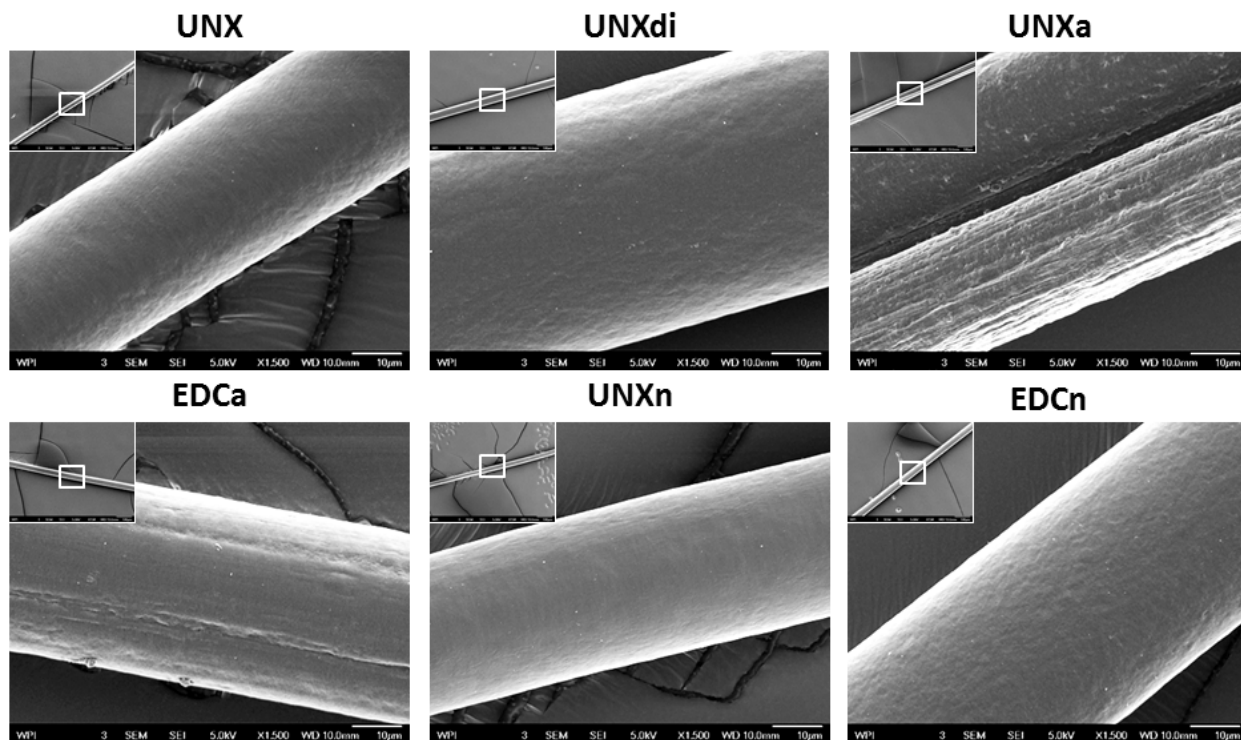


Figure 7.1. Scanning electron micrographs of EDC crosslinked microthreads. Scale = 10 μ m.

EDCa, and EDCn microthreads, we observed topographical features on the surface of uncrosslinked microthreads treated with acidic buffer (UNXa) and EDCa microthreads with scanning electron microscopy (SEM) micrographs (Figure 7.1). It is well known that micro and nanoscale structural features affect cell orientation, adhesion, and ingrowth.^{41,42} Topographic features were qualitatively characterized on polystyrene fibers with similar diameters as fibrin microthreads by changing solvent parameters in the fiber extrusion process, demonstrating that topographic cues can be spontaneously created on fibrous structures.⁴³ We hypothesize that the topographic features described on UNXa and EDCa microthreads are a result of interactions between the acidic buffer and the fibrin microthread surface, effectively etching topography into the microthreads. To test this hypothesis, scanning white confocal microscopy could be used to measure the surface topography of microthreads to characterize metrics such as surface roughness (R_a).⁴⁴ These findings in combination with results presented in this thesis regarding the effect of static axial stretch on cell alignment and mechanical properties of fibrin microthreads have the potential to create mechanically robust materials with topographic cues

designed to direct cell alignment to further facilitate organized cell ingrowth for *in vitro* characterization as well as *in vivo* tissue regeneration.

While the results presented in this thesis suggest that the rapid release of HGF significantly improves the functional regeneration of skeletal muscle in a VML injury, it is unclear if a more sustained release of this factor would result in a further increase in the amount of SC infiltration and tissue regeneration. A facile method to release HGF over a longer period of time is to coextrude it in the fibrin polymerization process. We showed that fibroblast growth factor 2 (FGF2) could be incorporated into fibrin microthreads by mixing it into fibrinogen aliquots prior to microthread fabrication.⁴⁵ FGF2 loading resulted in an increase in fibroblast migration and proliferation, demonstrating that this factor was released over time to direct cell function. Further, insulin-like growth factor 1 (IGF1) has been incorporated into fibrin gels to form *in vitro* skeletal muscle constructs.⁴⁶ Future studies could focus on analyzing the effects of prolonged HGF release on skeletal muscle regeneration to assess SC migration into the wound site at early time points and determine the functional recovery of VML injuries.

The most common method to crosslink fibrin materials is Factor XIII, which is responsible for crosslinking fibrin clots in the wound healing cascade.^{47,48} Factor XIII belongs to a family of enzymes known as transglutaminases, which have been investigated on a variety of materials including collagen⁴⁹ and fibrin clots.⁵⁰⁻⁵² In addition to serving as a crosslinking agent, several peptide sequences have been identified to facilitate the binding of bioactive agents within a scaffold by crosslinking them into the fibrin matrix by Factor XIII.^{53,54} In addition to a Factor XIII substrate, these fusion proteins contain degradation sequences that are cleaved in the presence of plasmin, the primary proteolytic enzyme of fibrin, releasing the bioactive payload.⁵⁵⁻⁵⁷ This delivery system is a powerful technology that delivers bioactive factors into the injury site as the scaffold material degrades, and could be used with insulin-like growth factor 1 (IGF1) to enhance skeletal muscle regeneration. IGF1 is a critical factor in skeletal muscle regeneration due to its ability to stimulate myoblast proliferation and subsequent differentiation.^{58,59} It is thought that IGF1 also has some motogenic activity with myoblasts, and therefore could serve as an additional method to recruit SCs into an injury site.^{26,60} In addition to our defined HGF delivery system, a dual release system, specifically with IGF1, would develop an incredibly

powerful biomimetic scaffold that would rapidly recruit SCs to the wound site and would stimulate the differentiation of myoblasts into myotubes as the microthreads degraded.

In addition to growth factor signaling, different protein surfaces have a substantial effect on cell fate. The SC niche is predominately composed of basement membrane proteins such as laminin-1, laminin-2 and type IV collagen, in addition to fibronectin.^{15,16} Laminin-1 injections into healthy muscle tissue significantly increased the number of SCs present in muscle tissue and these muscles were better suited to repair exercise-induced injuries.⁶¹ Further, laminin-1 injection into α_7 integrin-null animals also restored the regenerative response following a cardiotoxin-induced injury.⁶² Collagen IV seems to reduce myoblast differentiation, suggesting that this protein might stimulate SC attachment and proliferation rather than differentiation.⁶³ Fibronectin has been shown to increase myoblast migration and differentiation *in vitro*, suggesting that the deposition of this protein into the provisional matrix after injury is critical for SC recruitment.^{16,63,64} Fibronectin mediated migration is likely a result of the expression of α_v integrin in myoblasts, which is also attributed to stimulate myoblast fusion by organizing myoblasts into closer proximity with one another.^{64,65} These findings suggest that the addition of fibronectin to fibrin microthreads could increase SC alignment and organization on the surface of the microthreads, facilitating a more robust migratory and differentiation response. Additionally, fibronectin, as well as collagen IV, have been shown to interact with insulin-like binding proteins (IGFBPs), which serve to sequester, transport, and/or potentiate IGF signaling.⁶⁶⁻⁶⁸ The addition of any of these basement membrane proteins might improve our fibrin microthread system by directing cell functions such as migration, proliferation, or differentiation. Further, by including proteins that naturally bind to IGFBP/IGF complexes, we could create a powerful system that will physically direct cell motility and signal cells with paracrine factors.

7.3.3 Development of an In Vitro Model System for Skeletal Muscle Tissue

The development of a miniaturized cell outgrowth assay provides an excellent platform to create an *in vitro* model system to study skeletal muscle formation and repair mechanisms in minor injury models. Fibrin scaffolds have been used to generate skeletal muscle constructs in a variety of model systems due to their ability to be rapidly remodeled as well as favorable bioactivity.^{46,69,70} By conjugating specific proteins to fibrin microthreads as outlined above, we

can develop SC niche environments that will facilitate skeletal muscle growth in a complex 3D environment.^{71,72} We hypothesize that we can observe skeletal muscle formation in real-time with time lapse microscopy as has been performed on single cell migration along small fibers to provide information on how myofibers form *de novo*.⁷³ Using this system, we can investigate the interactions between a co-culture of fibroblasts and myoblasts in the generation of skeletal muscle constructs, as this has been shown to significantly impact the stability and performance of skeletal muscle constructs.^{74,75} Further, disease models could be developed by creating skeletal muscle constructs from patient cells with genetic diseases such as Duchenne muscular dystrophy.^{76,77} Additionally, this model system can also be used as an *in vitro* model of skeletal muscle injury by creating laceration-induced, strain-induced, or toxin-induced injuries, to investigate myofiber regeneration. Furthermore, we could also use our model system to study the interactions of skeletal muscle with other tissue systems such as blood vessels or nervous tissue to develop complex, 3D multi-tissue model systems.

7.4 FINAL CONCLUSIONS

In this thesis, we have developed a variety of tools to precisely modulate the mechanical and structural properties of fibrin microthreads. We investigated the effects of buffer pH on EDC crosslinking and found that EDCn microthreads were significantly stronger and stiffer than UNX microthreads with delayed degradation times. EDCa microthreads were more mechanically robust than EDCn microthreads and did not show evidence of any susceptibility to proteolytic degradation. Static axially stretched microthreads were significantly stronger and stiffer than unstretched microthreads, and this increase in stretch significantly enhanced cell alignment along the longitudinal axis of the microthreads. However, static axial stretching did not affect the proteolytic degradation of fibrin microthreads, and therefore while we generated two different methods to generate microthreads with tunable mechanical and structural properties, we moved forward with EDC crosslinking for skeletal muscle regeneration.

To create biomimetic scaffolds that recapitulate regenerative cues found in the endogenous skeletal muscle regeneration pathway, we developed a loading strategy for the adsorption of HGF to the surface of microthreads. EDCn microthreads adsorbed sufficient quantities of HGF to stimulate myoblast proliferation, migration, and outgrowth in a novel,

miniature 3D cell outgrowth assay. We hypothesize that our outgrowth assay could be adapted into an *in vitro* model system for skeletal muscle, and could be used to investigate skeletal muscle formation and complex interactions with other tissue systems.

Finally, we characterized the ability of HGF-loaded EDCn microthreads to direct tissue regeneration in a mouse model of VML, and demonstrated that these microthreads appeared to restore the functional output of injured muscles to their baseline values. These data suggest that by developing materials with increased resistance to proteolytic degradation and loading them with HGF, we have recapitulated regenerative cues lost in VML injuries to stimulate SC recruitment to the injury site. Further, the physical shape of the microthreads was able to guide this SC recruitment into organized, functional tissue. Fibrin microthreads are a promising acellular biomaterial for the regeneration of skeletal muscle, and future work should be performed to fully characterize the tissue response to EDCn microthreads. Lastly, the development of microthreads designed to deliver multiple growth factors to an injury site will be a significant improvement in microthread technology and will facilitate further site specific tissue regeneration.

7.5 REFERENCES

1. Page RL, Malcuit C, Vilner L, Vojtic I, Shaw S, Hedblom E, Hu J, Pins GD, Rolle MW, Dominko T. Restoration of skeletal muscle defects with adult human cells delivered on fibrin microthreads. *Tissue engineering. Part A* 2011;17(21-22):2629-40.
2. Pieper JS, Hafmans T, Veerkamp JH, van Kuppevelt TH. Development of tailor-made collagen-glycosaminoglycan matrices: EDC/NHS crosslinking, and ultrastructural aspects. *Biomaterials* 2000;21(6):581-93.
3. Wissink MJ, Beernink R, Pieper JS, Poot AA, Engbers GH, Beugeling T, van Aken WG, Feijen J. Immobilization of heparin to EDC/NHS-crosslinked collagen. Characterization and *in vitro* evaluation. *Biomaterials* 2001;22(2):151-63.
4. Bush KA, Pins GD. Carbodiimide conjugation of fibronectin on collagen basal lamina analogs enhances cellular binding domains and epithelialization. *Tissue Eng Part A* 2010;16(3):829-38.
5. Princz MA, Sheardown H. Heparin-modified dendrimer cross-linked collagen matrices for the delivery of basic fibroblast growth factor (FGF-2). *J Biomater Sci Polym Ed* 2008;19(9):1201-18.
6. Pieper JS, Oosterhof A, Dijkstra PJ, Veerkamp JH, van Kuppevelt TH. Preparation and characterization of porous crosslinked collagenous matrices containing bioavailable chondroitin sulphate. *Biomaterials* 1999;20(9):847-58.
7. Liu W, Carlisle CR, Sparks EA, Guthold M. The mechanical properties of single fibrin fibers. *Journal of thrombosis and haemostasis : JTH* 2010;8(5):1030-6.
8. Martino MM, Briquez PS, Ranga A, Lutolf MP, Hubbell JA. Heparin-binding domain of fibrin(ogen) binds growth factors and promotes tissue repair when incorporated within a synthetic matrix. *Proc Natl Acad Sci U S A* 2013;110(12):4563-8.
9. Matsumoto T, Sasaki J, Alsberg E, Egusa H, Yatani H, Sohmura T. Three-dimensional cell and tissue patterning in a strained fibrin gel system. *PLoS ONE* 2007;2(11):e1211.

10. Pins GD, Huang EK, Christiansen DL, Silver FH. Effects of static axial strain on the tensile properties and failure mechanisms of self-assembled collagen fibers. *Journal of Applied Polymer Science* 1997;63(11):1429-1440.
11. Varju I, Sotonyi P, Machovich R, Szabo L, Tenekedjiev K, Silva MM, Longstaff C, Kolev K. Hindered dissolution of fibrin formed under mechanical stress. *J Thromb Haemost* 2011;9(5):979-86.
12. Ren K, Fourel L, Rouviere CG, Albiges-Rizo C, Picart C. Manipulation of the adhesive behaviour of skeletal muscle cells on soft and stiff polyelectrolyte multilayers. *Acta biomaterialia* 2010;6(11):4238-48.
13. Lam MT, Sim S, Zhu X, Takayama S. The effect of continuous wavy micropatterns on silicone substrates on the alignment of skeletal muscle myoblasts and myotubes. *Biomaterials* 2006;27(24):4340-7.
14. Cornwell KG, Downing BR, Pins GD. Characterizing fibroblast migration on discrete collagen threads for applications in tissue regeneration. *J Biomed Mater Res A* 2004;71(1):55-62.
15. Sanes JR. The basement membrane/basal lamina of skeletal muscle. *The Journal of Biological Chemistry* 2003;278(15):12601-4.
16. Serrano AL, Munoz-Canoves P. Regulation and dysregulation of fibrosis in skeletal muscle. *Experimental Cell Research* 2010;316(18):3050-8.
17. Bussolino F, Direnzo MF, Ziche M, Bocchietto E, Olivero M, Naldini L, Gaudino G, Tamagnone L, Coffer A, Comoglio PM. Hepatocyte Growth-Factor Is a Potent Angiogenic Factor Which Stimulates Endothelial-Cell Motility and Growth. *Journal of Cell Biology* 1992;119(3):629-641.
18. Cornwell KG, Pins GD. Discrete crosslinked fibrin microthread scaffolds for tissue regeneration. *J Biomed Mater Res A* 2007;82(1):104-12.
19. Valentin JE, Turner NJ, Gilbert TW, Badylak SF. Functional skeletal muscle formation with a biologic scaffold. *Biomaterials* 2010;31(29):7475-84.
20. Jarvinen TA, Jarvinen TL, Kaariainen M, Kalimo H, Jarvinen M. Muscle injuries: biology and treatment. *Am J Sports Med* 2005;33(5):745-64.
21. Sicari BM, Agrawal V, Siu BF, Medberry CJ, Dearth CL, Turner NJ, Badylak SF. A murine model of volumetric muscle loss and a regenerative medicine approach for tissue replacement. *Tissue Eng Part A* 2012;18(19-20):1941-8.
22. Wu X, Corona BT, Chen X, Walters TJ. A Standardized Rat Model of Volumetric Muscle Loss Injury for the Development of Tissue Engineering Therapies. *BioResearch Open Access* 2012;1(6):280-290.
23. Merritt EK, Hammers DW, Tierney M, Suggs LJ, Walters TJ, Farrar RP. Functional assessment of skeletal muscle regeneration utilizing homologous extracellular matrix as scaffolding. *Tissue Eng Part A* 2010;16(4):1395-405.
24. Machingal MA, Corona BT, Walters TJ, Kesireddy V, Koval CN, Dannahower A, Zhao W, Yoo JJ, Christ GJ. A tissue-engineered muscle repair construct for functional restoration of an irrecoverable muscle injury in a murine model. *Tissue Eng Part A* 2011;17(17-18):2291-303.
25. Corona BT, Ward CL, Baker HB, Walters TJ, Christ GJ. Implantation of in vitro tissue engineered muscle repair constructs and bladder acellular matrices partially restore in vivo skeletal muscle function in a rat model of volumetric muscle loss injury. *Tissue Eng Part A* 2014;20(3-4):705-15.
26. Ju YM, Atala A, Yoo JJ, Lee SJ. In situ regeneration of skeletal muscle tissue through host cell recruitment. *Acta biomaterialia* 2014;10(10):4332-9.
27. Mase VJ, Jr., Hsu JR, Wolf SE, Wenke JC, Baer DG, Owens J, Badylak SF, Walters TJ. Clinical application of an acellular biologic scaffold for surgical repair of a large, traumatic quadriceps femoris muscle defect. *Orthopedics* 2010;33(7):511.
28. Corona BT, Wu X, Ward CL, McDaniel JS, Rathbone CR, Walters TJ. The promotion of a functional fibrosis in skeletal muscle with volumetric muscle loss injury following the transplantation of muscle-ECM. *Biomaterials* 2013;34(13):3324-35.
29. Li MT, Willett NJ, Uhrig BA, Guldborg RE, Warren GL. Functional analysis of limb recovery following autograft treatment of volumetric muscle loss in the quadriceps femoris. *Journal of biomechanics* 2014;47(9):2013-21.
30. Pieper JS, Hafmans T, van Wachem PB, van Luyn MJ, Brouwer LA, Veerkamp JH, van Kuppevelt TH. Loading of collagen-heparan sulfate matrices with bFGF promotes angiogenesis and tissue generation in rats. *J Biomed Mater Res* 2002;62(2):185-94.
31. Badylak SF, Valentin JE, Ravindra AK, McCabe GP, Stewart-Akers AM. Macrophage phenotype as a determinant of biologic scaffold remodeling. *Tissue Eng Part A* 2008;14(11):1835-42.

32. Tidball JG, Vallalta SA. Regulatory interactions between muscle and the immune system during muscle regeneration. *American journal of physiology. Regulatory, integrative and comparative physiology* 2010;298(5):R1173-87.
33. Deng B, Wehling-Henricks M, Vallalta SA, Wang Y, Tidball JG. IL-10 triggers changes in macrophage phenotype that promote muscle growth and regeneration. *J Immunol* 2012;189(7):3669-80.
34. Tidball JG. Mechanisms of muscle injury, repair, and regeneration. *Compr Physiol* 2011;1(4):2029-62.
35. Vallalta SA, Rinaldi C, Deng B, Liu G, Fedor B, Tidball JG. Interleukin-10 reduces the pathology of mdx muscular dystrophy by deactivating M1 macrophages and modulating macrophage phenotype. *Hum Mol Genet* 2011;20(4):790-805.
36. van Wachem PB, Plantinga JA, Wissink MJ, Beernink R, Poot AA, Engbers GH, Beugeling T, van Aken WG, Feijen J, van Luyn MJ. In vivo biocompatibility of carbodiimide-crosslinked collagen matrices: Effects of crosslink density, heparin immobilization, and bFGF loading. *J Biomed Mater Res* 2001;55(3):368-78.
37. Powell HM, Boyce ST. Wound closure with EDC cross-linked cultured skin substitutes grafted to athymic mice. *Biomaterials* 2007;28(6):1084-92.
38. Olde Damink LHH, Dijkstra PJ, van Luyn MJA, van Wachem PB, Nieuwenhuis P, Feijen J. Cross-linking of dermal sheep collagen using a water-soluble carbodiimide. *Biomaterials* 1996;17:765-773.
39. Choi JS, Lee SJ, Christ GJ, Atala A, Yoo JJ. The influence of electrospun aligned poly(epsilon-caprolactone)/collagen nanofiber meshes on the formation of self-aligned skeletal muscle myotubes. *Biomaterials* 2008;29(19):2899-906.
40. Aviss KJ, Gough JE, Downes S. Aligned electrospun polymer fibres for skeletal muscle regeneration. *Eur Cell Mater* 2010;19:193-204.
41. Desai TA. Micro- and nanoscale structures for tissue engineering constructs. *Med Eng Phys* 2000;22(9):595-606.
42. Norman JJ, Desai TA. Control of cellular organization in three dimensions using a microfabricated polydimethylsiloxane-collagen composite tissue scaffold. *Tissue Eng* 2005;11(3-4):378-86.
43. Megelski S, Stephens JS, Chase DB, Rabolt JF. Micro- and Nanostructured Surface Morphology on Electrospun Polymer Fibers. *Macromolecules* 2002;35(22):8456-8466.
44. Scott RS, Ungar PS, Bergstrom TS, Brown CA, Grine FE, Teaford MF, Walker A. Dental microwear texture analysis shows within-species diet variability in fossil hominins. *Nature* 2005;436(7051):693-5.
45. Cornwell KG, Pins GD. Enhanced proliferation and migration of fibroblasts on the surface of fibroblast growth factor-2-loaded fibrin microthreads. *Tissue Eng Part A* 2010;16(12):3669-77.
46. Huang YC, Dennis RG, Larkin L, Baar K. Rapid formation of functional muscle in vitro using fibrin gels. *Journal of Applied Physiology* 2005;98(2):706-713.
47. Mosesson MW. Fibrinogen and fibrin structure and functions. *J Thromb Haemost* 2005;3(8):1894-904.
48. Clark RA. Fibrin and wound healing. *Ann N Y Acad Sci* 2001;936:355-67.
49. Orban JM, Wilson LB, Kofroth JA, El-Kurdi MS, Maul TM, Vorp DA. Crosslinking of collagen gels by transglutaminase. *J Biomed Mater Res A* 2004;68(4):756-62.
50. Greenberg CS, Birckbichler PJ, Rice RH. Transglutaminases: multifunctional cross-linking enzymes that stabilize tissues. *FASEB J* 1991;5(15):3071-7.
51. Helms CC, Ariens RA, Uitte de Willige S, Standeven KF, Guthold M. alpha-alpha Cross-links increase fibrin fiber elasticity and stiffness. *Biophys J* 2012;102(1):168-75.
52. Hoppe B. Fibrinogen and factor XIII at the intersection of coagulation, fibrinolysis and inflammation. *Thromb Haemost* 2014;112(4).
53. Sakiyama SE, Schense JC, Hubbell JA. Incorporation of heparin-binding peptides into fibrin gels enhances neurite extension: an example of designer matrices in tissue engineering. *FASEB J* 1999;13(15):2214-24.
54. Sakiyama-Elbert SE, Hubbell JA. Controlled release of nerve growth factor from a heparin-containing fibrin-based cell ingrowth matrix. *J Control Release* 2000;69(1):149-58.
55. Sakiyama-Elbert SE, Panitch A, Hubbell JA. Development of growth factor fusion proteins for cell-triggered drug delivery. *FASEB J* 2001;15(7):1300-2.
56. Geer DJ, Swartz DD, Andreadis ST. Biomimetic delivery of keratinocyte growth factor upon cellular demand for accelerated wound healing in vitro and in vivo. *American Journal of Pathology* 2005;167(6):1575-1586.

57. Liang MS, Andreadis ST. Engineering fibrin-binding TGF-beta1 for sustained signaling and contractile function of MSC based vascular constructs. *Biomaterials* 2011;32(33):8684-93.
58. Engert JC, Berglund EB, Rosenthal N. Proliferation precedes differentiation in IGF-I-stimulated myogenesis. *J Cell Biol* 1996;135(2):431-40.
59. Florini JR, Ewton DZ, Coolican SA. Growth hormone and the insulin-like growth factor system in myogenesis. *Endocr Rev* 1996;17(5):481-517.
60. Borselli C, Storrie H, Benesch-Lee F, Shvartsman D, Cezar C, Lichtman JW, Vandenburgh HH, Mooney DJ. Functional muscle regeneration with combined delivery of angiogenesis and myogenesis factors. *Proc Natl Acad Sci U S A* 2010;107(8):3287-92.
61. Zou K, De Lisio M, Huntsman HD, Pincu Y, Mahmassani Z, Miller M, Olatunbosun D, Jensen T, Boppart MD. Laminin-111 improves skeletal muscle stem cell quantity and function following eccentric exercise. *Stem Cells Transl Med* 2014;3(9):1013-22.
62. Rooney JE, Gurpur PB, Yablonka-Reuveni Z, Burkin DJ. Laminin-111 restores regenerative capacity in a mouse model for alpha7 integrin congenital myopathy. *The American journal of pathology* 2009;174(1):256-64.
63. Maley MAL, Davies MJ, Grounds MD. Extracellular-Matrix, Growth-Factors, Genetics - Their Influence on Cell-Proliferation and Myotube Formation in Primary Cultures of Adult-Mouse Skeletal-Muscle. *Exp Cell Res* 1995;219(1):169-179.
64. Vaz R, Martins GG, Thorsteinsdottir S, Rodrigues G. Fibronectin promotes migration, alignment and fusion in an in vitro myoblast cell model. *Cell and tissue research* 2012;348(3):569-78.
65. Sinanan AC, Machell JR, Wynne-Hughes GT, Hunt NP, Lewis MP. Alpha v beta 3 and alpha v beta 5 integrins and their role in muscle precursor cell adhesion. *Biology of the cell / under the auspices of the European Cell Biology Organization* 2008;100(8):465-77.
66. Clemmons DR, Busby WH, Arai T, Nam TJ, Clarke JB, Jones JJ, Ankrapp DK. Role of insulin-like growth factor binding proteins in the control of IGF actions. *Prog Growth Factor Res* 1995;6(2-4):357-66.
67. Firth SM, Baxter RC. Cellular actions of the insulin-like growth factor binding proteins. *Endocr Rev* 2002;23(6):824-54.
68. Gui Y, Murphy LJ. Insulin-like growth factor (IGF)-binding protein-3 (IGFBP-3) binds to fibronectin (FN): demonstration of IGF-I/IGFBP-3/fn ternary complexes in human plasma. *J Clin Endocrinol Metab* 2001;86(5):2104-10.
69. Martin NR, Passey SL, Player DJ, Khodabakus A, Ferguson RA, Sharples AP, Mudera V, Baar K, Lewis MP. Factors affecting the structure and maturation of human tissue engineered skeletal muscle. *Biomaterials* 2013;34(23):5759-65.
70. Vandenburgh H. High-content drug screening with engineered musculoskeletal tissues. *Tissue Eng Part B Rev* 2010;16(1):55-64.
71. Neumann T, Hauschka SD, Sanders JE. Tissue engineering of skeletal muscle using polymer fiber arrays. *Tissue Eng* 2003;9(5):995-1003.
72. Ker ED, Nain AS, Weiss LE, Wang J, Suhan J, Amon CH, Campbell PG. Bioprinting of growth factors onto aligned sub-micron fibrous scaffolds for simultaneous control of cell differentiation and alignment. *Biomaterials* 2011;32(32):8097-107.
73. Sheets K, Wunsch S, Ng C, Nain AS. Shape-dependent cell migration and focal adhesion organization on suspended and aligned nanofiber scaffolds. *Acta biomaterialia* 2013.
74. Brady MA, Lewis MP, Mudera V. Synergy between myogenic and non-myogenic cells in a 3D tissue-engineered craniofacial skeletal muscle construct. *J Tissue Eng Regen Med* 2008;2(7):408-17.
75. Murphy MM, Lawson JA, Mathew SJ, Hutcheson DA, Kardon G. Satellite cells, connective tissue fibroblasts and their interactions are crucial for muscle regeneration. *Development* 2011;138(17):3625-37.
76. Vandenburgh H, Shansky J, Benesch-Lee F, Skelly K, Spinazzola JM, Saponjian Y, Tseng BS. Automated drug screening with contractile muscle tissue engineered from dystrophic myoblasts. *FASEB J* 2009;23(10):3325-34.
77. Zhu CH, Mouly V, Cooper RN, Mamchaoui K, Bigot A, Shay JW, Di Santo JP, Butler-Browne GS, Wright WE. Cellular senescence in human myoblasts is overcome by human telomerase reverse transcriptase and cyclin-dependent kinase 4: consequences in aging muscle and therapeutic strategies for muscular dystrophies. *Aging Cell* 2007;6(4):515-23.